



**Fluid mixing processes in enclosed shallow
water flows and applications**

Jingchun Wang

A thesis submitted for the degree of Doctor of Philosophy

Newcastle University
Faculty of Science, Agriculture and Engineering
School of Civil Engineering and Geosciences

March 2017

Abstract

This work develops a numerical modelling tool to investigate and better understand the fluid mixing processes in enclosed or semi-closed shallow water flows. The integrated fluid mixing modelling framework consists of two components, i.e. a shallow flow model for predicting hydrodynamics and a particle-tracking model for calculating the trajectories of passive particles released in the water bodies. The well-defined analysis method in dynamical system theory, Finite Time Lyapunov Exponent (FTLE), is used to extract the Lagrangian Coherent Structures (LCSs) to provide insight of the nonlinear particle dynamics in the time-dependant environmental shallow water flows under consideration.

The fluid mixing modelling and analysis framework is firstly used to study the mixing properties of an oscillating environmental flow driven by two inflows and one outflow in an idealised shallow basin. The Eulerian velocity field of the flow is first predicted using the shallow flow model, which is then used by the particle-tracking model to calculate the particle trajectories and describe the transport and mixing properties of the inflows/outflow driven shallow water flow. The particle dynamics is found to be controlled by a dimensionless parameter and fluid mixing changes from regular to chaotic when the magnitude of the parameter increases.

The integrated numerical modelling framework is then applied to reproduce the wind-driven flow hydrodynamics and investigate the corresponding fluid mixing in Taihu, one of the largest fresh water lakes in China, for continuous 12 months. The predicted flow field, which is used to drive the particle dynamics, compares favourably with the field measurements. The transport and mixing properties of the lake are analysed by calculating the FTLE and identifying the LCSs, clearly revealing the stagnant and well-mixing zones of the water body. The understanding of the underlying fluid mixing mechanism of the lake is also improved.

Through successful application to one idealised and one realistic case studies, the potential of the current integrated numerical modelling framework is confirmed for analysing fluid mixing in (semi-)enclosed water bodies.

Acknowledgements

First of all I would like to express my deepest gratitude to my supervisor, Professor Qiuhua Liang. He guided me into the research area of shallow flow modelling and dynamic system theories. Without his patience, encouragement and unrelenting help, I could never finish this thesis. I would also like to thank Professor Xijun Lai (Nanjing Institute of Geography & Limnology, Chinese Academy of Sciences), for the knowledge and experience about shallow lake modeling from him during my academic study in China and his visiting in Newcastle University. Finally I would like to thank Professor Yiping Li and his research group (Hohai University), for providing data of Lake Taihu and the management of Lake Taihu field work.

I am very grateful to ‘The Henry Lester Trust Limited’ and ‘The Great Britain-China Educational Trust’, for their financial supporting in the third and fourth year of my program.

I would also like to extend my thanks to peers, colleagues, and researchers including Xilin Xia, Reza Amouzgar, Hongbin Zhang, Jingming Hou, Xiaodong Ming, Samantha Mahaffey, Luke Smith and Ciprian Spatar for I could ask my questions, discuss and share our views. Also I would like to thank my dear friends, Xinxin Liang, Jingyi Zong, Miao Wang, Alexander Nicolson, Xiaohao Shi, Guang Gao, Jiajun Chen, Chen Yu and Zheng Wang for the help and happiness they provided in my life in Newcastle.

My thanks also go to the administrative staff in School of Civil Engineering and Geosciences, SAgE Faculty workshop organisers, librarians and computing technicians for the services they provided especially Melissa Ware, Hannah Lynn, Graham Patterson and Laura Hanson

Finally I would like to express my sincere gratitude to my parents for their continued love and support, I owe my achievements to them. Without their continuous help and support I could not be able to start and continue for my post graduate studies in overseas.

Abbreviations

1D	One-dimensional
2D	Two-dimensional
3D	Three-dimensional
ADI	Alternating Direction Implicit
ArcGIS	A GIS for working with maps and geographic information
BITT	Backward-in-time tracking
BOD	Biochemical oxygen demand
BV	Blink-vortex
CFL	Courant-Friedrichs-Lewy
COD	Chemical oxygen demand
Delft3D	An integrated hydrodynamic software by Deltares
DEM	Digital Elevation Model
DLM	Dynamic lake model
DPIV	Digital particle image velocimetry
DYRESM	Dynamics Reservoir Simulation Model
ECOM	A commercial version of POM
EFDC	Environmental Fluid Dynamic Code
ELCOM	Estuary, Lake and Coastal Ocean Model
FITT	Forward-in-time tracking
FTLE	Finite time Lyapunov exponent
FSLE	Finite size Lyapunov exponent
HLL	Harten, Lax, van Leer
HLLC	Harten, Lax, van Leer-Contact
FVCOM	Finite Volume Coastal Ocean Model
KAM	Kolmogorov-Arnold-Moser

LCS	Lagrangian coherent structure
LIMNMOD	A one-dimensional lake model
MATLAB	Matrix laboratory
MIKE21	A series of commercial models by the Danish Hydraulics Institute
MINLAKE	Minnesota Lake Water Quality Management Model
NW	Northwest
ODE	Ordinary differential equation
POM	Princeton Ocean model
PROBE	A compute code for lake water quality modeling
PTM	Particle tracking model
RK	Runge-kutta
RMA2	Resource Management Association-2
SS	Suspended substance
TN	Total nitrogen
TP	Total phosphorous
TRIM-3D	Tidal, Residual, and Inter-tidal Mudflat
TVD	Total variation diminishing

Table of Contents

Abstract.....	i
Acknowledgements.....	ii
Abbreviations	iv
List of figures.....	xi
List of tables.....	xix
Chapter 1. Introduction.....	1
1.1 Background of the research.....	1
1.2 Dynamical systems theory in environmental flows	3
1.3 Aims and Objectives	4
1.4 Thesis outline	4
Chapter 2. Literature review.....	7
2.1 Hydrodynamics modelling of (semi-) enclosed environmental shallow flows.....	7
2.1.1 One-dimensional versus two-dimensional models	8
2.1.2 Three-dimensional models.....	10
2.1.3 Multidimensional models.....	13
2.2 Lagrangian particle-tracking model	13
2.2.1 Numerical schemes for particle advection and diffusion.....	14
2.2.2 Forward tracking and backward tracking.....	15
2.3 Non-linear dynamical systems in fluid dynamics	17

2.3.1	Chaotic advection	17
2.3.2	Lagrangian coherent structure	19
2.4	The hydrodynamics and water quality of Lake Taihu	22
2.4.1	Hydrodynamic modelling	22
2.4.2	Water quality modelling	24
2.5	Concluding remarks.....	25
Chapter 3. Methodology		27
3.1	Full 2D Shallow Flow model	27
3.1.1	Shallow water equations	28
3.1.2	Second-order finite volume scheme	30
3.1.3	The HLLC approximate Riemann solver for inviscid flux calculation.....	31
3.1.4	Calculation of viscous flux terms	36
3.1.5	Discretisation of source terms	38
3.1.6	CFL criterion	40
3.1.7	Boundary conditions.....	40
3.2	Particle tracking model.....	41
3.2.1	Governing Equations and its relationship with dynamics system	41
3.2.2	Numerical algorithm for particle advection	42
3.2.3	Interpolation of velocity data from shallow water model.....	44
3.3	Relevant concepts in dynamics systems	45
3.3.1	Poincaré section.....	45
3.3.2	Stable/unstable manifolds of hyperbolic points in dynamic systems	46

3.3.3	Finite-time Lyapunov exponents and computation technique in 2D flows	47
3.3.4	Lagrangian coherent structures	50
3.4	Model validation	52
3.4.1	Jet-force flow	52
3.4.2	Backward step case	54
3.4.3	Wind-induced shallow lake.....	57
3.4.4	Blinking-vortex flow	59
3.4.5	Chaotic properties of Kranenburg's lake	62
3.5	Summary	68
Chapter 4. Inflows/outflow driven particle dynamics in an idealized lake.....		70
4.1	Introduction.....	70
4.2	The flow fields in the idealised model lake	71
4.3	Dimensionless parameter controlling particle dynamics	73
4.4	Lagrangian dynamics of the lake	74
4.4.1	FTLE distribution and local particle dynamics.....	74
4.4.2	Continuous particle dynamics and occupy rate.....	87
4.5	Conclusions.....	91
Chapter 5. Hydrodynamic modelling of Lake Taihu.....		92
5.1	Introduction about Lake Taihu.....	92
5.2	Eutrophication of Lake Taihu	93
5.3	Fresh water transfer and possible routes	94
5.4	The lake model.....	95

5.5	Model calibration and result discussion	99
5.5.1	Model calibration and validation.....	99
5.5.2	Wind-induced velocity fields at different seasons.....	104
5.6	Conclusions	106
Chapter 6.	Particle dynamics of Lake Taihu	108
6.1	Introduction of particle dynamics.....	108
6.2	FTLE distribution of Lake Tai	109
6.2.1	FTLE parameter setting	109
6.2.2	FTLE distribution of Lake Taihu in different months.....	113
6.3	Localized particle dynamics	117
6.4	Continuous particle dynamics	122
6.4.1	The Lagrangian dynamics of particles released from Wangyu Route.....	123
6.4.2	The Lagrangian dynamics of particles released from Xingou Route	129
6.4.3	The Lagrangian dynamics of particles released from Ximeng Route	135
6.4.4	The Lagrangian dynamics of particles released from Dongshao Route.....	141
6.4.5	Global occupy rates comparison of single route	146
6.4.6	The Lagrangian dynamics of particles released from two routes.....	148
6.4.7	The Lagrangian dynamics of particles released from three routes.....	151
6.5	Conclusions	154
Chapter 7.	Conclusions and future work	156
7.1	Conclusions	156
7.1.1	Full 2D Shallow water model.....	156

7.1.2	Particle tracking model	157
7.1.3	Horizontal mixing and transport processes in an inflows/outflow-induced idealised lake.....	157
7.1.4	Horizontal mixing and transport properties in a wind-induced natural lake.....	158
7.2	Future work	159
7.2.1	Diffusion effect in particle tracking process	159
7.2.2	Extraction of LCSs.....	160
7.2.3	Analysis of LCSs	160
7.2.4	Further Applications of this numerical work	161
References		162

List of figures

Figure 2.1 Illustration of two common vertical grid approaches: (a) a regular grid; (b) a “bottom-fitting” grid.....	11
Figure 2.2 Particle-tracking simulation in a natural lake.	16
Figure 3.1 The solution structure of the HLLC approximate Riemann solver.....	31
Figure 3.2 The predictor step of MUSCL-Hancock method.....	34
Figure 3.3 The corrector step of MUSCL-Hancock method.	35
Figure 3.4 Cells used for the calculation of viscosity term.	37
Figure 3.5 A fourth order RK method in space.	43
Figure 3.6 Bilinear interpolation for particle information.....	44
Figure 3.7 An example of Poincaré sections.	46
Figure 3.8 Stable/unstable manifolds and the corresponding hyperbolic point.	47
Figure 3.9 velocity distribution and streamlines of jet-force case: (a) $pvt = 0.85$; (b) $pvt = 1.7$; (c) $pvt = 3.4$; (d) Roger’s condition.	53
Figure 3.10 backward step geometry.....	54
Figure 3.11 velocity distribution and streamlines of backward step case: (a) $pvt = 0.135$; (b) $pvt = 0.27$; (c) $pvt = 0.54$; (d) Roger’s condition; (e) Fe’s experimental result.	55
Figure 3.12 Velocity component u in three different sections in the eddy zone: (a) $x=1.53\text{m}$; (b) $x=2.03\text{m}$; (c) $x=2.53\text{m}$	56
Figure 3.13 Velocity distribution and streamlines corresponding to constant northwest wind: (a) analytical solution; (b) numerical solution.....	58
Figure 3.14 Normalized depth-averaged velocity profile in the radial plane normal to the wind direction corresponding to constant northwest wind: (a) $pvt = 0.135$; (b) $pvt = 3.4$; (c) Roger’s condition.	58

Figure 3.15 Poincaré Sections of BV flows with different flow strength: (a) $\mu BV = 0.01$; (b) $\mu BV = 0.15$; (c) $\mu BV = 0.25$; (d) $\mu BV = 0.30$; (e) $\mu BV = 0.40$; (f) $\mu BV = 0.50$	60
Figure 3.16 Advection of a particle patch with $\mu BV = 0.25$ (a) $5T$; (b) $10T$; (c) $20T$; (d) $30T$	61
Figure 3.17 Advection of a particle patch with $\mu BV = 0.75$ (a) $5T$; (b) $10T$; (c) $20T$; (d) $30T$	61
Figure 3.18 Advection of a particle patch with $\mu BV = 2.25$ (a) $2T$; (b) $4T$; (c) $6T$; (d) $8T$	62
Figure 3.19 dynamics property of analytical solution when $\mu k = 0.14$ (a) Poincaré section; (b) backward FTLE; (c) forward FTLE.	64
Figure 3.20 dynamics property of analytical solution when $\mu k = 0.28$ (a) Poincaré section; (b) backward FTLE; (c) forward FTLE.	65
Figure 3.21 dynamics property of analytical solution when $\mu k = 0.42$ (a) Poincaré section; (b) backward FTLE; (c) forward FTLE.	65
Figure 3.22 dynamics property of analytical solution when $\mu k = 0.84$ (a) Poincaré section; (b) backward FTLE; (c) forward FTLE.	65
Figure 3.23 Advection of two particle circles in analytical solution (a) $8T$; (b) $16T$	66
Figure 3.24 Mean distance of two particle circles in analytical solution.	67
Figure 3.25 dynamics property of semi-numerical solution when $\mu k = 0.14$ (a) Poincaré section; (b) backward FTLE; (c) forward FTLE.	67
Figure 3.26 dynamics property of semi-numerical solution when $\mu k = 0.28$ (a) Poincaré section; (b) backward FTLE; (c) forward FTLE.	68
Figure 3.27 dynamics property of semi-numerical solution when $\mu k = 0.42$ (a) Poincaré section; (b) backward FTLE; (c) forward FTLE.	68
Figure 3.28 dynamics property of semi-numerical solution when $\mu k = 0.84$ (a) Poincaré section; (b) backward FTLE; (c) forward FTLE.	68

Figure 4.1 bathymetry (initial water depth) and inflow/outflow channels of the idealised lake.	71
Figure 4.2 Aerial view of the steady-state streamlines caused by (a) inflow from the northeast; (b) inflow from the northwest.	72
Figure 4.3 History of u of four gauge points.	73
Figure 4.4 FTLE distribution and evolution of three particle patches located in different mixing zones when $\mu i = 2.7$: (a) forward-tracked FTLE distribution; (b) backward-tracked FTLE distribution; (c) initial positions of the three particle patches; (d) snapshot of the particle patches at $t = 10T$; (e) $t = 20T$; (f) $t = 30T$; (g) $t = 40T$; (h) $t = 50T$	77
Figure 4.5 FTLE distribution and Evolution of three different particle patches with $\mu i = 5.4$: (a) forward FTLE distribution; (b) backward FTLE distribution; (c) initial position of patches; (d) snapshot of the particle patches at $t = 10T$; (e) $t = 20T$; (f) $t = 30T$; (g) $t = 40T$; (h) $t = 50T$	79
Figure 4.6 FTLE distribution and Evolution of three different particle patches with $\mu i = 10.8$: (a) forward FTLE distribution; (b) backward FTLE distribution; (c) initial position of patches; (d) snapshot of the particle patches at $t = 10T$; (e) $t = 20T$; (f) $t = 30T$; (g) $t = 40T$; (h) $t = 50T$	81
Figure 4.7 FTLE distribution and Evolution of three different particle patches with $\mu i = 21.6$: (a) forward FTLE distribution; (b) backward FTLE distribution; (c) initial position of patches; (d) snapshot of the particle patches at $t = 10T$; (e) $t = 20T$; (f) $t = 30T$; (g) $t = 40T$; (h) $t = 50T$	83
Figure 4.8 FTLE distribution and Evolution of three different particle patches with $\mu i = 43.2$: (a) forward FTLE distribution; (b) backward FTLE distribution; (c) initial position of patches; (d) snapshot of the particle patches at $t = 10T$; (e) $t = 20T$ (f) $t = 30T$; (g) $t = 40T$; (h) $t = 50T$	85
Figure 4.9 FTLE distribution and Evolution of three different particle patches with $\mu i = 86.4$: (a) forward FTLE distribution; (b) backward FTLE distribution; (c) initial position of patches; (d) snapshot of the particle patches at $t = 10T$; (e) $t = 20T$; (f) $t = 30T$; (g) $t = 40T$; (h) $t = 50T$	87

Figure 4.10 The lake area reached by continues particles from inflows with different μi condition (a) initial particle position in northeast inflow channel; (b) initial particle position in inflow northwest channel; (c) $\mu i = 2.7$; (d) $\mu i = 5.4$; (e) $\mu i = 10.8$; (f) $\mu i = 21.6$; (g) $\mu i = 43.2$; (h) $\mu i = 86.4$	90
Figure 5.1 Computational domain, gauge stations and inflow/outflow locations.	96
Figure 5.2 Annual time history of the water level in the Taipu River outlet.	96
Figure 5.3 Monthly-changed discharge of the 33 inflow channels surrounding Lake Taihu.	98
Figure 5.4 Bathymetry of computational domain: (a) original discrete point data; (b) transferred DEM at $125\text{m} \times 125\text{m}$	99
Figure 5.5 Annual time histories of water level at the four gauge stations: (a) Dapukou station; (b) Jiapu station; (c) Xiaomeikou station; (d) Xishan station.	102
Figure 5.6 Predicted flow fields of Lake Taihu at two different days: (a) Current predicted velocity field on 14 th March 2005; (b) Current predicted velocity field on 19 th August 2005; (c) Predicted velocity field and point-based velocities on 14 th March 2005 (from Li <i>et al.</i> (2011b)); (d) Predicted velocity field and point-based velocities on 19 th August 2005 (from Li <i>et al.</i> (2011b)).	103
Figure 5.7 Numerical velocity fields and corresponding streamlines in: (a) winter; (b) spring.	105
Figure 5.8 Numerical velocity fields and corresponding streamlines in (a) early-summer; (b) late-summer; (c) autumn.	106
Figure 6.1 FTLE distribution in Lake Taihu with integration time: (a) 10 days; (b) 20 days; (c) 30 days; (d) 40 days.	110
Figure 6.2 FTLE distribution in Lake Taihu with different grid size: (a) grid size of 250m; (b) grid size of 125m; (c) grid size of 62.5m; (d) grid size of 31.25m.	111
Figure 6.3 Average distance of neighboring particles during simulation progress with different particle tracking time steps.	112

Figure 6.4 FTLE distribution of Lake Taihu for 15 th January to 15 th February: (a) Forward FTLE; (b) Backward FTLE.	114
Figure 6.5 FTLE distribution of Lake Taihu for 15 th February to 15 th March: (a) Forward FTLE; (b) Backward FTLE.	114
Figure 6.6 FTLE distribution of Lake Taihu for 15 th March to 15 th April: (a) Forward FTLE; (b) Backward FTLE.....	115
Figure 6.7 FTLE distribution of Lake Taihu for 15 th March to 15 th April: (a) Forward FTLE; (b) Backward FTLE.....	115
Figure 6.8 FTLE distribution of Lake Taihu for 15 th May to 15 th June: (a) Forward FTLE; (b) Backward FTLE.....	116
Figure 6.9 FTLE distribution of Lake Taihu for 15 th July to 15 th August: (a) Forward FTLE; (b) Backward FTLE.....	116
Figure 6.10 FTLE distribution of Lake Taihu for 15 th August to 15 th September: (a) Forward FTLE; (b) Backward FTLE.	117
Figure 6.11 FTLE distribution of Lake Taihu for 15 th September to 15 th October: (a) Forward FTLE; (b) Backward FTLE.	117
Figure 6.12 Initial positions of localized particles released in lake areas: (a) Gonghu Bay; (b) West Zone.	118
Figure 6.13 Trajectories of Local particles patch initially located in Gonghu Bay: (a1) 20 days early summer; (b1) 20days of late summer; (a2) 40days of early summer; (b2) 40days of late summer; (a3) 60days of early summer; (b3) 60days of late summer.	120
Figure 6.14Trajectories of Local particles patch initially located in West Zone: (a1) 20days of early summer; (b1) 20days of late summer; (a2) 40days of early summer; (b2) 40days of late summer; (a3) 60days of early summer; (b3) 60days of late summer.	121
Figure 6.15 (a) locations of four routes for water transfer; (b) four highlighted areas for calculating the local occupy rates.	122

Figure 6.16 Particles continually released at Wangyu Route in winter: (a) particle trajectories on 5 th February; (b) particle trajectories on 25 th February; (c) particle trajectories on 15 th March.	124
Figure 6.17 Particles continually released at Wangyu Route in spring: (a) particle trajectories on 5 th April; (b) particle trajectories on 25 th April; (c) particle trajectories on 15 th May.	125
Figure 6.18 Particles continually released at Wangyu Route in summer: (a) particle trajectories on 25 th June; (b) particle trajectories on 5 th August; (c) particle trajectories on 15 th September.	126
Figure 6.19 Particles continually released at Wangyu Route in autumn: (a) particle trajectories on 5 th October; (b) particle trajectories on 25 th October; (c) particle trajectories on 15 th November.	127
Figure 6.20 Global Occupy rate of particles released at Wangyu Route for different seasons in year 2005: (a) winter; (b) spring; (c) summer; (d) autumn.	128
Figure 6.21 Particles continually released at Xingou Route in winter: (a) particle trajectories on 5 th February; (b) particle trajectories on 25 th February; (c) particle trajectories on 15 th March.	130
Figure 6.22 Particles continually released at Xingou Route in spring: (a) particle trajectories on 5 th April; (b) particle trajectories on 25 th April; (c) particle trajectories on 15 th May.	131
Figure 6.23 Particles continually released at Xingou Route in summer: (a) particle trajectories on 25 th June; (b) particle trajectories on 5 th August; (c) particle trajectories on 15 th September.	132
Figure 6.24 Particles continually released at Xingou Route in autumn: (a) particle trajectories on 5 th October; (b) particle trajectories on 25 th October; (c) particle trajectories on 15 th November.	133
Figure 6.25 Global occupy rate of particles released at Xingou Route for different seasons in year 2005: (a) winter; (b) spring; (c) summer; (d) autumn.	134

Figure 6.26 Particles continually released at Ximmeng Route in winter: (a) particle trajectories on 5 th February; (b) particle trajectories on 25 th February; (c) particle trajectories on 15 th March.....	136
Figure 6.27 Particles continually released at Ximmeng Route in spring: (a) particle trajectories on 5 th April; (b) particle trajectories on 25 th April; (c) particle trajectories on 15 th May.....	137
Figure 6.28 Particles continually released at Ximmeng Route in summer: (a) particle trajectories on 25 th June; (b) particle trajectories on 5 th August; (c) particle trajectories on 15 th September.....	138
Figure 6.29 Particles continually released at Ximmeng Route in autumn: (a) particle trajectories on 5 th October; (b) particle trajectories on 25 th October; (c) particle trajectories on 15 th November.....	139
Figure 6.30 Global occupy rate of particles released at Ximmeng Route for different seasons in year 2005: (a) winter; (b) spring; (c) summer; (d) autumn.....	140
Figure 6.31 Particles continually released at Dongshao Route in winter: (a) particle trajectories on 5 th February; (b) particle trajectories on 25 th February; (c) particle trajectories on 15 th March.....	141
Figure 6.32 Particles continually released at Dongshao Route in spring: (a) particle trajectories on 5 th April; (b) particle trajectories on 25 th April; (c) particle trajectories on 15 th May.....	142
Figure 6.33 Particles continually released at Dongshao Route in summer: (a) particle trajectories on 25 th June; (b) particle trajectories on 5 th August; (c) particle trajectories on 15 th September.....	143
Figure 6.34 Particles continually released at Dongshao Route in autumn: (a) particle trajectories on 5 th October; (b) particle trajectories on 25 th October; (c) particle trajectories on 15 th November.....	144
Figure 6.35 Global occupy rate of particles released at Dongshao Route for different seasons in year 2005: (a) winter; (b) spring; (c) summer; (d) autumn.....	145

Figure 6.36 Global occupy rate of particles released at different rivers for different seasons in year 2005: (a) winter; (a) spring; (a) summer; (a) autumn.	147
Figure 6.37 Particles released simultaneously at two different routes at early summer time (15 th May to 15 th July).....	149
Figure 6.38 Global occupy rate with simulation time from 15 th May to 15 th July: (a) single route; (b) multiple routes with two routes.....	150
Figure 6.39 Local occupy rate of highlighted areas with simulation time from 15 th May to 15 th July by multiple application with two routes.	151
Figure 6.40 Particles released simultaneously at three different routes at early summer time (15 th May to 15 th July).....	152
Figure 6.41 Global occupy rates with simulation time from 15 th May to 15 th July: (a) multiple application with two routes; (b) multiple application with three routes..	153
Figure 6.42 Local occupy rate of highlighted areas with simulation time from 15 th May to 15 th July by multiple application with three routes.	154

List of tables

Table 4.1 The highest occupy rates for different μ_i and the times required to achieve the corresponding rates.....	90
Table 6.1 Local occupy rates of particles released at Wangyu Route for different season	129
Table 6.2 Local occupy rates of particles released at Xingou Route for different seasons	135
Table 6.3 Local occupy rates of particles released at Xinmeng Route for different seasons	140
Table 6.4 Local occupy rates of particles released at Dongshao Route for different seasons	146

Chapter 1. Introduction

1.1 Background of the research

Enclosed/semi-enclosed environmental flows such as lakes and reservoirs are important to both natural ecosystems and human communities. For nature, these water bodies store freshwaters, provide habitat to aquatic and semiaquatic lives and moderate temperatures of the local land; for humans, they are used for supplying drinking water and other commercial purposes, including fishing, transportation, irrigation, industrial water supplies, and receiving waters for wastewater effluents (Deborah, 1996). However, due to the excessive and fallacious development and utilization by human beings, many reservoirs and lakes have undergone huge changes which lead to deterioration of water quality. The water quality degradation in lakes and reservoirs has become a fearful threat to both ecosystems and human lives.

The water quality of these enclosed/semi-enclosed environmental flows is highly related to the horizontal transport and mixing processes which have a significant influence on the relevant physical dynamics. The evolution and effects of environmental problems resulting from short-term accidental events (e.g. oil leaking) and long-term natural pollution disasters (e.g. eutrophication derived from organic pollutions) are both highly related to the horizontal mixing and transport process of materials. Therefore, a better understanding and accurate modelling of horizontal transport and mixing processes in environmental flows is important in order to support successful water quality management and engineering applications, such as interpreting water exchange mechanisms, predicting plankton movement, forecasting and controlling pollutant behaviours, planning and operating environmental engineering solutions.

One of the most popular ways to understand the horizontal transport and mixing in lakes/reservoirs is through numerical simulation of these flows using sophisticated hydrodynamics models. With the development of numerical models along with advancement of computing technologies, hydrodynamics simulation has been widely used nowadays to study complicated physical processes in these water bodies (Blumberg and Oey, 1985; Haidvogel *et al.*, 2000; Zhu *et al.*, 2001; Marchesiello *et al.*, 2003; Schimmelpfennig *et al.*, 2012). The simulation of flow hydrodynamics using an Eulerian transport model can provide substantial information about horizontal current and wave distribution driven by different prevailing winds, and the change of relevant flow variables such as pollution concentration or salinity in a water body. However, Eulerian-grid based hydrodynamics simulation can only provide frozen snapshots of discrete data but cannot describe the transient structures along with the temporal

variations. These pure Eulerian models are not sufficient to provide insight into the dynamics of environmental flows since transport processes are inherently a Lagrangian notion. A flow feature that is apparent via the instantaneous velocity field (e.g., in a streamline plot or a vorticity contour plot) may persist for only a short period of time compared to the unsteady timescale of the flow, and as such will have little impact on the actual flow transport. For example, using an Eulerian approach, if the concentration of pollutions at a selected location is found to increase or decrease, it is difficult, if not impossible, to tell where pollutions come from or where they will be heading. Other researchers (Huret *et al.*, 2007; Chen *et al.*, 2008; Miyake *et al.*, 2010; Wang *et al.*, 2010; Liu *et al.*, 2011; Postma *et al.*, 2013) have used more advanced hydrodynamic models incorporated with a particle-tracking model to simulate the motion of particles. But these studies only focused on trajectories of a limited number of advected particles and could not provide a sketch of transport and mixing properties of the whole flow field, when chaos impedes a meaningful direct comparison of simple particle trajectories. Also, they are not able to identify persistent coherent transport features which act as an intrinsic property of all manners in fluid flows and could quantify the integrated influence of time-varying velocity fields.

Haller and Yuan (2000) pointed out that the dynamical behaviors of particles are more dramatically affected by phase space geometry than the detailed history of the velocity field. This indicated that geometric structures arising from chaotic advection (Aref, 1984) might have relevance in describing transport and mixing properties of two-dimensional flows. In this regard, Lagrangian approaches (Haller, 2002; Shadden *et al.*, 2005) based on nonlinear dynamical theories have been recognized as a proper way to investigate the transport and mixing property in environmental flows. These approaches are objective tools for mapping the dynamical properties that environmental flows provide, including the identification of transport barriers, transport mechanisms, and regions of rapid dispersion. These Lagrangian approaches do not actually aim at predicting individual tracer trajectories, but at revealing the spatial structures known as Lagrangian coherent structures (LCSs), derived from the dynamical system theory to act as templates for the whole flow (Wiggins, 2013a). The key of dynamical system approaches is to establish frame-independent criteria that permit unambiguous definition of coherent structures based on their influence on flow transport. These approaches may be used in many engineering applications for the prediction of pollution transport and the discovery of contaminant sources.

1.2 Dynamical systems theory in environmental flows

A dynamical system deals with the analysis of different processes that evolve in time. The state of a system can be represented in the phase space given by the dynamic variables of the system. For the two-dimensional shallow flows that considered in this work, the phase space is equivalent to the two-dimensional real space, i.e., the dynamical variables are the spatial coordinates (x, y) denoting the position of a small fluid parcel (representing materials or passive particles) in the flow. Hence, the focus herein is to analyze the trajectories of small fluid parcels in the Lagrangian frame.

The mixing and transport properties in a time-dependent flow is investigated by identifying the coherent structures in the phase space, in particular, the hyperbolic points and the associated unstable and stable manifolds that control the motion of the fluid flow during certain time scales. These structures act as the transport barriers/paths in the fluid motion and regulate the flow into different regions corresponding to different dynamical behavior of the trajectories.

However, the study and application of the dynamical system theories to practical environmental flows as found in the natural water bodies are very complicated due to the lack of detailed velocity information and the complexity of these time-dependent flows. This means that comprehensive analytical methods used for idealized systems, where the associated vector fields are either known for whole time or having well-defined temporal behaviors (e.g. periodic, quasi-periodic) are no longer suitable for the situations of natural environmental flows. In recent years, with the latest nonlinear analysis techniques such as Finite time Lapunov exponent (FTLE) and Finite size Lapunov exponent (FSLE) developed to uncover LCS precisely in an aperiodic natural flow, dynamical theories have already been applied successfully to study the Lagrangian dynamics in oceanography and aerology (Kai *et al.*, 2009; Shadden *et al.*, 2009; Olascoaga and Haller, 2012; Peng and Peterson, 2012). However, little attention has been paid to the inland shallow water systems such as shallow lakes and reservoirs, where horizontal processes may dominate the transport and mixing of materials while vertical process might be largely ignored. Furthermore, because of their enclosed/semi-enclosed configurations, the characteristics of Lagrangian dynamics of these shallow water bodies are commonly different from that of the open flows (oceans and atmosphere). Hence, the purpose of this study is to develop a general and accurate numerical modelling framework to investigate the transport and mixing properties of inflow/outflow-induced or wind-induced enclosed/semi-enclosed shallow water flows through the application of nonlinear dynamical theories, and exploit the relevant properties for engineering applications.

1.3 Aims and Objectives

The aim of this research is to develop an integrated modelling tool, including a hydrodynamics model and a particle-tracking model, to study and comprehend the mixing and transport properties in time-dependant enclosed/semi-enclosed shallow water flows induced by inflows/outflow or winds. The aim will be achieved by accomplishing the following objectives:

- An existing depth-averaged shallow water model will be improved by adding a zero-equation turbulence model to estimate depth-averaged turbulent influence. Turbulence terms from zero-equation turbulence model will be involved in the governing shallow water equations. The improved shallow water model will be validated against benchmark test cases.
- The improved shallow water model will be set up to simulate the hydrodynamics of an idealized lake driven by inflows/outflow and a natural shallow lake (Lake Taihu) driven by winds.
- A particle-tracking model will be developed by solving the advection equations and validated against test cases for the computation of particle trajectories and FLTE.
- The particle-tracking model will be applied to predict particle trajectories, construct LCS and estimate particle occupy rates in both of the idealized lake and Lake Taihu.
- The integrated modelling tool will be developed by coupling the improved shallow water model with the particle-tracking model. Numerical velocity information obtained from shallow water model will be used to calculate Lagrangian particle trajectories in the particle tracking model. This tool will be used to evaluate the application of transferring fresh water to improve water quality in Lake Taihu through, e.g. calculating global occupy rate and local occupy rate.

1.4 Thesis outline

This work deals with the transport and mixing processes and its associated passive particle advection in enclosed/semi-enclosed shallow water flows induced by winds or inflows/outflow. Concepts and methods developed in the context of non-linear dynamics will be used to investigate these transport and mixing properties and the associated passive particle dynamics. A general introduction of the main concepts and methodology is given in Chapter 3, while the

detailed description of the respective characteristics of each of the case studies is specified at the beginning of the result chapters (Chapter 4, Chapter 5 and Chapter 6).

In the current chapter, i.e. Chapter 1, the horizontal transport and mixing processes in nature environmental flows are briefly introduced and the significant influence of transport and mixing to the local environment and ecosystem are highlighted.

In Chapter 2, a literature review is provided and organised in four parts: numerical modelling of enclosed/semi-enclosed environmental flows, methods for Lagrangian particle tracking, development and application of methods for non-linear dynamical systems in fluid dynamics and relevant studies on Lake Taihu including hydrodynamics and water quality modelling.

In Chapter 3, the methodology employed in this work will be introduced. An existing 2D depth-averaged shallow water model is improved by adding turbulent terms. A 2D particle-tracking model is developed to advect passive particles and calculate FTLE with velocity field predicted by the shallow water model. Five benchmark cases are considered and reproduced to validate the shallow water and particle-tracking models. For time-dependent velocity fields, analytical techniques (e.g. Poincaré section, advection of particle patch and FTLE) developed from dynamical systems theory are successfully applied to investigate the transport and mixing property that controls the Lagrangian motion of passive particles.

In Chapter 4, the transport and mixing property of the fluid flow in a semi-enclosed idealised lake which is driven by inflows/outflow will be studied. FTLE and LCS are calculated to detect the skeleton structures that organize the transport and mixing of passive tracers in this periodic dynamical system. A dimensionless parameter is derived to describe/control the Lagrangian mixing property and measure the magnitude of chaotic advection in the lake. Additionally, different inflow durations which are related to different cleaning efficiency of the lake with freshwater to identify the optimised inflow choice and its corresponding efficiency on lake cleaning are discussed.

In Chapter 5, a lake model will be set up to simulate the hydrodynamic processes of a natural wind-induced shallow lake, i.e. Lake Taihu. The lake model is validated by comparing water level and velocity fields with observed data or alternative numerical results from the literature. Also, the effects of change of wind direction on lake velocity fields and streamlines in different seasons are analysed.

In Chapter 6, the transport and mixing property of the fluid in Lake Taihu will be studied. Complex flow patterns, caused by the complicated bathymetry and time-dependant wind stress, are revealed through calculation of FTLE. Trajectories of localised particle patches are simulated to investigate the transport and mixing properties of different regions in Lake Taihu. Particles continuously released at the entrance of transfer routes are tracked and occupy rate by the fresh water particles in the lake are calculated to evaluate the performance of the existing and in-progress water transfer engineering projects.

In Chapter 7, brief conclusions are drawn from the current work and possible future work is suggested to continue research in this field.

Chapter 2. Literature review

This chapter first reviews the different types of hydrodynamics models used for modelling enclosed or semi-enclosed environmental flows, covering both original development of numerical schemes and application of existing numerical models. The advantages and disadvantages of these numerical models are highlighted and an appropriate modelling approach is then proposed for the current study.

The mixing and transport property of enclosed or semi-enclosed shallow water flows, which dominates the behaviours of nutrients, pollutants, zooplanktons and other suspended matters, has great influence on the water quality in these water bodies, and hence is a topic of great importance, both environmentally and ecologically. To simulate and predict the complicated motions of the aforementioned water quality parameters, Lagrangian particle tracking techniques are used in this work, which will be also reviewed and discussed, including the concepts and methods derived from the non-linear dynamic systems for investigating the mixing and transport property of enclosed or semi-enclosed shallow water flows.

Finally, existing studies related to hydrodynamics modelling and water quality assessments of Lake Taihu are also reviewed. Lake Taihu is the main case of this study.

2.1 Hydrodynamics modelling of (semi-) enclosed environmental shallow flows

Hydrodynamics modelling of enclosed/semi-enclosed shallow water flows provides insight into the spatial and temporal changes of physical processes taking place in lakes, reservoirs, and other natural/man-made shallow water bodies. Hydrodynamics modelling can reproduce the physical processes and provide relevant scalar fields (such as velocity and density) by solving the governing equations of continuity, momentum and energy derived based on the Newtonian continuum mechanics. Depending on the complexity of the hydrodynamics systems under consideration, these models may be 1D, 2D and 3D. Although the 3D models theoretically provide more comprehensive of underlying dynamic processes, it is not always necessary or even desirable to use 3D hydrodynamics models for environmental flows in enclosed/semi-enclosed water bodies due to the high demand in computational power and data requirement in model set up. Hydrodynamics models with low dimensions (1D and 2D) may achieve large-scale simulations with acceptable accuracy but less computational time and data required.

2.1.1 *One-dimensional versus two-dimensional models*

One-dimensional hydrodynamics models are primarily used for the simulation and calculation of vertical stratification, heat transport process and energy budget in water bodies. These models are obtained by averaging over horizontal planes. Generally speaking, 1D models may be classified into two groups: turbulent transport models and advection-diffusion transport models (Bonnet *et al.*, 2000). Turbulent transport models are based on turbulence closure schemes where the coefficients for vertical transport are highly relevant to the turbulent kinetic energy. Typical turbulent transport models used for lake and reservoirs modelling include DYRESM, DLM and PROBE (Imberger and Patterson, 1980; Casulli and Cattani, 1994; Kantha and Clayson, 1994; Goudsmit *et al.*, 1996; Hamilton and Schladow, 1997; Gal *et al.*, 2003). While advection-diffusion transport models are based on simple parameterization schemes or pre-given coefficients for vertical transport, and therefore are more empirical. Compared to turbulent transport models, these models are easier to develop and require less input data for simulations. Typical advection-diffusion transport models include MINLAKE and LIMNMOD (Riley and Stefan, 1988; Karagounis *et al.*, 1993; Omlin *et al.*, 2001).

Two-dimensional depth-averaged models (2D models) commonly solve the shallow water equations (i.e. the depth-averaged Navier-Stokes equations) and have been widely used to simulate the hydrodynamic of enclosed/semi-enclosed environmental flows, especially those shallow reservoirs and lakes where the flow fields show no significant variations in the vertical direction and the fluid density can be assumed to be constant. The prevailing 2D models solve the governing shallow water equations (representing the principals of mass and momentum conservation) using a variety of numerical schemes (i.e., finite difference, finite element and finite volume) and different mesh types (i.e., structured grids, unstructured grids and quadtree grids). In this study, enclosed/semi-enclosed environmental flows are mainly lakes and reservoirs in which the flows have relatively low velocities and slowly varying flow dynamics compared with the flows in rivers or channels. Hence the use of different numerical schemes to approximate the governing equations may not yield significantly different solutions. However, because of the complicated boundary geometries as found in these enclosed/ semi-enclosed environmental flows, the choice of numerical grids for simulations may be an important factor affecting solution accuracy and computational efficiency.

Many 2D models are developed with simple regular grid structure, e.g. the Cartesian grids, for studying the hydrodynamics of enclosed/semi-enclosed environmental flows (Millet and Guelorget, 1994; Tsanis and Saied, 2007; He *et al.*, 2008; Abd-el-Malek and Helal, 2009; Millet

et al., 2010). In 2D models developed on regular or structured grids, neighbouring information of an arbitrary cell is explicitly provided. For example, each of the cells inside the computational domain may be uniquely represented by a set of two indices, e.g. (i, j) , and its neighboring cells can be easily represented simply by increasing or decreasing the index in the respective dimension under consideration. 2D models with structured grid facilitate efficient computation because the explicit neighbour connectivity simplifies the programming procedure and the matrix of the algebraic equation system has a regular structure. However, the regular Cartesian grids are not suitable for approximating the complex boundaries of a domain with irregular shapes, which is a common case in environmental flows.

Models with a body-fitted curvilinear grid have been used to overcome the aforementioned problems. Horizontal curvilinear grid based numerical models have been reported for materials transport modelling (Sanderson, 2008; Li *et al.*, 2015), and wind/discharge-driven hydrodynamics simulation (Schimmelpfennig *et al.*, 2012). However, when the domain geometry is very complicated, curvilinear grids may contain highly distorted grids and highly uneven grid sizes.

Unstructured grids provide more a flexible and robust approach for approximating complex domain geometries. In two-dimensional cases, unstructured grids usually employ triangular elements to discretize the computational domain. Many well-known 2D models, such as Mike 21 and RMA2, are developed on unstructured grids and have been applied to simulate the hydrodynamics of enclosed/semi-enclosed environmental flows (Shrestha, 1996; Martin *et al.*, 2005; Hai *et al.*, 2008; Thompson *et al.*, 2008; Chittibabu and Rao, 2012). However, although unstructured-grid based 2D models have a proven capability to adapt to local flow features and fit better complex geometries, these models also have certain drawbacks. Unlike the structured grids, unstructured grids replace simple indexing by connectivity information and lookup tables for neighbor finding, and grid generation is typically a lengthy and complicated process. Furthermore, unstructured grids most commonly adopt triangular elements and the numerical schemes implemented on triangular grids are usually computationally much more expensive than those developed on Cartesian grids.

Quadtree-grids have also been widely reported for solving the two-dimensional shallow water equations to simulate the hydrodynamics of enclosed/semi-enclosed environmental flows. Quadtree grids discretise a computational domain using a recursive decomposition approach, which generates Cartesian cells of different size from an initial unit square and stores grid information in a hierarchical tree structure. Due to their efficiency and flexibility in performing

grid adaptation, adaptive Quadtree grid based models have been used widely on enclosed/semi-enclosed flow modelling, ranging from idealised cases to natural cases (Borthwick *et al.*, 2001; Sanmiguel-Rojas *et al.*, 2005; Liang *et al.*, 2006a; Liang *et al.*, 2006b; Krámer and Józsa, 2007).

2.1.2 Three-dimensional models

Since the mid-1980s, three-dimensional hydrodynamic models have also been developed and applied to support advanced sediment transport (Jin *et al.*, 2000), water quality (Spaulding and Mendelsohn, 1999), eutrophication (Park *et al.*, 2005) and contaminant transport (Andrejev *et al.*, 2011) modelling studies. Three-dimensional hydrodynamic modeling of enclosed/semi-enclosed environmental flows is typically performed using free-surface, hydrostatic, primitive equations solved on different computational grids (Brown, 2011). These models incorporate momentum, continuity, temperature, and salinity equations and employ a variety of physical and mathematical turbulence closure sub-models.

For three-dimensional models, grid structures in the horizontal dimensions are similar to those of 2D models which have already been discussed in the previous section. In the vertical dimension, water column are divided into layers to facilitate numerical simulations and there are mainly two types of grid structures to represent these layers: z -coordinate grids (regular grids) and σ -coordinate grids (bottom-fitting grids). In a z -coordinate grid based model, fixed depth is used for each layer. Such a model must impose boundary conditions for any of the bottom grid elements so that they do not have neighboring water elements. Since the flow within a river, lake or ocean is predominately horizontal, these boundary conditions must deal with the strong horizontal flow that “hits a wall” so that momentum is correctly conserved. Casulli and Cheng (1992) developed the first phase of the three-dimensional numerical model TRIM-3D (Tidal, Residual, and Inter-tidal Mudflat) that solves the depth-averaged Navier-Stokes equations with the hydrostatic assumption with a semi-implicit finite difference method. The non-conservative forms of vertically averaged horizontal and vertical momentum equations, free surface equation, and continuity equation were solved in conjugate with dry/flood conditions without coordinate transformations. An Eulerian-Lagrangian method was used to deal with the convective terms. Moreover, the horizontal diffusion terms were treated explicitly and vertical diffusion terms were treated implicitly. This model was used by Castellano *et al.* (2010) and Ambrosetti *et al.* (2012) to calculate the hydraulic paths and estimate the residence time of water in Lake Lago Maggiore. Using a similar numerical scheme, another z -coordinate grid model, named Estuary, Lake and Coastal Ocean Model (ELCOM), was developed in University of Western Australian (Hodges, 2000; Laval and Hodges, 2000; Hodges and

Dallimore, 2006). ELCOM can solve Navier-Stoke equations and scalar transport equations to simulate spatial and temporal velocity distribution and water temperature variation. ELCOM utilized a z -coordinate grid and resulted in a full, 3D Cartesian coordinate system for computational domain discretization. ELCOM has been known as one of the most important numerical models with wide range of applications for enclosed/semi-enclosed flow hydrodynamics modelling (Hodges *et al.*, 2000; Laval *et al.*, 2003; Romero and Imberger, 2003; León *et al.*, 2007; Chung *et al.*, 2009; Leon *et al.*, 2011).

In order to better approximate the complicated bottom topography, many 3D models adopt σ -coordinate grid systems. In these models, a fixed number of layers with variable depth are used. The models can better fit the bottom profile and avoid the boundary condition issue since every bottom grid has a water-column neighbor. The Finite Volume Coastal Ocean Model (FVCOM) developed by Chen *et al.* (2003a) solves the integral form of the governing equations for momentum, continuity, temperature, salinity and density on unstructured grids in horizontal dimensions and σ -coordinate grids in vertical dimension. The major advantages of FVCOM are the superior numerical efficiency and the capability of capturing irregular domain geometries provided by the unstructured-grid representation. The model is also implemented with a wetting-drying algorithm which is important for accurately simulating the hydrodynamics in estuarine environments with intertidal marshes and tidal flats. FVCOM has been widely applied to investigate the circulations and transport processes as presented in different types of lakes, estuaries, coastal waters and open ocean zones (Chen *et al.*, 2007; Huang *et al.*, 2008; Shore, 2009; Anderson *et al.*, 2010; Bek *et al.*, 2010; Bai *et al.*, 2013).

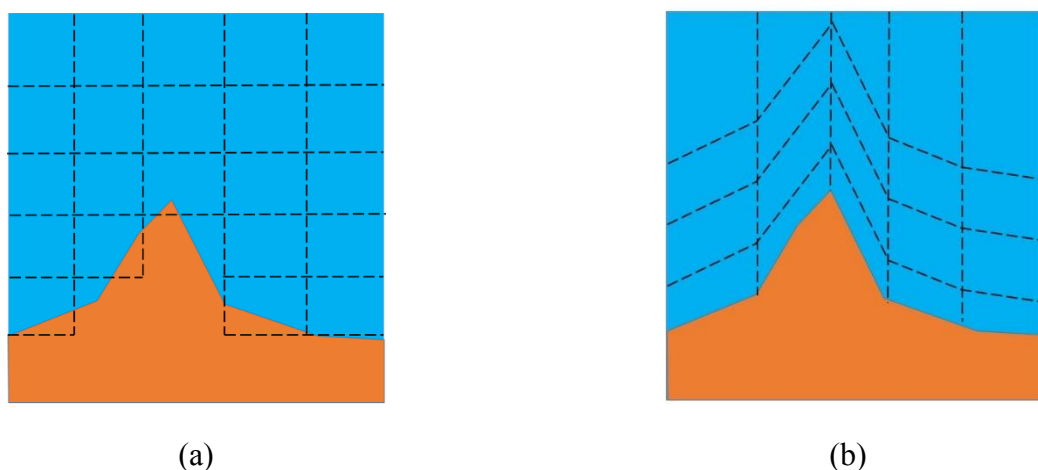


Figure 2.1 Illustration of two common vertical grid approaches: (a) a regular grid; (b) a “bottom-fitting” grid.

Hamrick (1992) developed the Environmental Fluid Dynamic Code, EFDC. Unlike FVCOM, EFDC can choose either Cartesian or orthogonal curvilinear grids in the horizontal dimensions. The internal state-variables included in the solution include turbulent kinetic energy, turbulent length scale, salinity and temperature. The model can also solve an arbitrary number of Eulerian transport-transformation equations for dissolved and suspended materials. A large number of research works on enclosed/semi-enclosed environmental flow modeling have been done using the EFDC model (Jin *et al.*, 2000; Jin *et al.*, 2002; Jin and Ji, 2005; Elçi *et al.*, 2007; Jin *et al.*, 2007).

Some hydrodynamic model such as ECOM (POM) and Delft3D adopt both of the aforementioned vertical grids. The Princeton Ocean Model (POM), also known as Estuary and Coastal ocean model (ECOM) for its commercial version, is a well-tested and extensively used three-dimensional hydrodynamic model originally developed by Blumberg and Mellor (1987). POM (ECOM) is a finite difference hydrodynamic model which was originally based on vertical sigma coordinate transformation. It solves the continuity equation, free surface equation, Reynolds-averaged momentum equations, and conservation equations of temperature and salinity. It incorporates the turbulent closure which was proposed by Mellor and Yamada (1982) to provide a realistic parameterization of vertical mixing. In the horizontal plane, a free surface flow is simulated to predict the changes of water level on a curvilinear coordinate system to better represent the complicated geometries. The original POM (ECOM) has been widely used to model major lakes all around the world (Chen *et al.*, 2001; Chen *et al.*, 2002; Schwab and Beletsky, 2003; Song *et al.*, 2004; Dabrowski and Berry, 2009; Huttula *et al.*, 2010). Ahsan and Blumberg (1999) modified the original ECOM by implanting a z-level vertical coordinate to replace the sigma vertical coordinate and named the modified model as ECOMsiz. The advantage of the z-level vertical grid based ECOMsiz is that it can better manage the regions with sharp bathymetric change where a sigma-grid coordinate may cause large error.

Delft3D-flow, developed by Deltares, is a multi-dimensional (2D or 3D) hydrodynamic and transport model that forms part of Delft3D, an integrated software suite including several modules (Hydraulics, 2006). In the horizontal dimensions, Delft3D-flow solves the continuity and momentum equations (Lesser *et al.* (2004) using an alternating direction implicit (ADI) method on a predefined Cartesian or a spherical grid. The model has been extensively applied to simulate non-steady environmental flows and transport phenomena resulting from tidal and meteorological forcing (Chanudet *et al.*, 2012; El-Adawy *et al.*, 2013; Kaçikoç and Beyhan, 2014; Razmi *et al.*, 2014).

This study focus on horizontal transport and mixing mechanism of enclosed/semi-enclosed environmental shallow flows and vertical stratification processes are not considered. To produce detailed velocity fields for particle tracking, high resolution hydrodynamics simulation which requires huge computational power is in demand. Therefore, a 2D hydrodynamic model will be more suitable to model the large scale horizontal environmental flows. In this work, an in-house shallow water model will be used for hydrodynamic modeling and the model will be introduced in Chapter 3.

2.1.3 Multidimensional models

In the case of actual environmental flows simulations, especially large-scale hydrodynamics simulation, the considered area may include several flow systems which have heterogeneous physical features. For example, an area both contains river/channel networks and lakes/estuaries. In these cases, a single hydrodynamics model maybe not suitable to handle the different kinds of physical feature simulations or simulate all the situations efficiently. Hence, one of the most popular way is coupling 1D-3D models which have been mentioned in previous sections to develop a multidimensional model for simulation (Bradford and Sanders, 2002; Miglio et al., 2005; Furman, 2008) . In the multidimensional model, the dimensionally different submodels will be used for specific portions of the computational domain to achieve both desirable solution accuracy and computational efficiency. According to the problem of concern, specific selection of submodels is also restricted by the availability of data.

There are mainly two categories to couple different submodles. Boundary-connected coupling is mostly used for connecting the boundaries of different flow systems such as river-lake system and river-estuary system (Steinebach *et al.*, 2004; Twigt *et al.*, 2009; Lai *et al.*, 2013; Van *et al.*, 2016). The most common multidimensional model for this category is 1D/2D model. Cross-section integrated 1D model will be used for simulating flow discharge along longitudinal rivers or streams and depth-integrated 2D model will used to simulate the hydrodynamics at horizontal plane in board areas such as lakes or estuaries (Wang *et al.*, 2011). Superpositinal coupling is usually adopted to get the details of flow patterns of specific positions by superimposing a local 2D zoom submodel while other positions are covered by a 1D global submodel (Gejadze and Monnier, 2007; Marin and Monnier, 2009).

2.2 Lagrangian particle-tracking model

Accurate prediction and better understanding of transport and mixing of water quality parameters are a crucial task in environmental engineering. Generally speaking, there are two

different approaches for material transport modelling, i.e. the Eulerian method and Lagrangian method. Eulerian method is included in the aforementioned two-dimensional and three-dimensional hydrodynamic models which simulate the transportation of some special flow variables (such as salinity and temperature). The transportation of these flow variables is described by an Eulerian approach on the internal finite volume representation of the computational domain with the application of the hydrodynamic models mentioned in the section 2.1.2.

Though an Eulerian approach is capable of computing mass fluxes at a given location, it is very difficult to directly be employed for tracing the transport of a parcel of mass from a given location. The transport process of mass such as pollutants, including oil spills (Ohshima and Simizu, 2008; Ollascoaga and Haller, 2012) or floating plastic debris (Lebreton *et al.*, 2012; Eriksen *et al.*, 2014), are often treated with a Lagrangian approach, usually using a particle-tracking model (PTM). The Lagrangian approach and its associated PTM have been used in a variety of applications ranging from rivers (Weitbrecht *et al.*, 2004), lakes (Li *et al.*, 2011c) to oceans (Ollascoaga *et al.*, 2013) for water quality modelling.

A PTM model provides a numerical tool to predict the fate of particles using the deterministic velocity fields obtained from a hydrodynamic model or observations for a period of time. Such a model may provide valuable, qualitative insights to the complex processes as presented in an environmental flow system. PTM models typically run ‘offline’, i.e. the hydrodynamic model is run first, followed by the PTM using the stored velocity fields output from the hydrodynamic model to compute the trajectory of particles released in the model domain (Liang *et al.*, 2006a). Fully dynamically coupled Eulerian-Lagrangian models are also possible (Soomere *et al.*, 2011) but are less commonly applied, potentially because of the greater computational requirements.

2.2.1 Numerical schemes for particle advection and diffusion

With the rapid development of computing technology and availability of the much increased computing power, the trajectories of relatively large numbers of particles can be simulated, overcoming statistical concerns relating to low sample sizes (Willis, 2011; Simons *et al.*, 2013). For some situations (e.g., large-scale transport simulation) in which the influence of diffusion is relatively small compared to advection, the motion of particles is simulated as a deterministic process by considering only the advection of the flow (Lee *et al.*, 2014a). Different numerical schemes have been used to solve the advection equation. The simplest scheme is the so-called ‘Forward Eulerian’ advection scheme that directly traces the trajectory of a particle using the

velocity information of the flow. While the Forward Eulerian method, being numerically first-order accurate, costs least computational power, some authors (Doglioli and Carlotti, 2011; Willis, 2011) pointed out that it is less reliable than other numerical schemes.

A number of particle-tracking models based on different numerical schemes have been developed and reported in the literature (Gräwe, 2011). Among these schemes, the fourth-order Runge-Kutta (RK4) integration method is well regarded and widely adopted. RK4 involves interpolating the velocity half way between a particle and the ‘destination’ (the point it would have been advected to under a Forward Eulerian scheme) four times per time step. Another promising advection scheme is based on the Adams-Bashforth-Moulton predictor-corrector scheme (Simons *et al.*, 2013) which is claimed to perform similarly to the RK4 scheme, but with somewhat reduced computational costs (Doglioli and Carlotti, 2011).

For certain situations both the deterministic advection and stochastic diffusion should be considered when modelling the motion of particles. In these situations the particle-tracking models are modified to include a small random displacement. This approximates the turbulent diffusion processes occurring below the grid scale of the model, and is often incorporated as a simple random walk process which first introduced by (Evans and Noye, 1995) based on the diffusivity of the medium being simulated. It is defined as the addition of a horizontal random increment, which is characterized by an arbitrary orientation, to the advection term. This result is an improvement of the reliability of PTMs (Willis, 2011), and some authors even contend that including this in models may remove the need for high-order RK4 integration (Ådlandsvik *et al.*, 2004). Other authors account for the effects of turbulent diffusion by explicitly including it within the particle advection scheme (Guizien *et al.*, 2006), or by explicit modelling of turbulence within the hydrodynamic model itself, though this can be extremely computationally demanding. In three-dimensional (or ‘pseudo-3D’) models, vertical diffusion may also need to be included in a similar fashion (Guizien *et al.*, 2006). Care must be taken when applying a random walk in a diffuse medium, since turbulent diffusion in the real world is non-uniform; this can lead to spurious modelling results if a random walk assumes uniform diffusivity. This can be compensated for by adjustment to the way in which a random walk is calculated and implemented (Visser, 1997).

2.2.2 Forward tracking and backward tracking

In a PTM model, there are usually two types of particle-tracking components, i.e. forward particle-tracking and backward particle-tracking, which both predict the location of a particle

as a function of time. The use of forward particle-tracking in time can be used for particle behaviour prediction or pollutions effects evaluation. The release of a statistically large number of particles in a flow field may be used to determine either the fraction of the particles from the releasing point (or region) that reaches a given point (or region) or the probability of the entire body of released particles reaching a given point or region. Fig. 2.1 shows an example of forward particle-tracking, in which the trajectories of a rectangular patch of particles released in Lake Poyang, China are marked using different colours. These particles may be used to represent the transport paths of pollutants (or any water-borne particles) and the paths these particles follow may be used to forecast affected regions and the possible concentration (based on relative particle density) of the pollutants.

Particle-tracking models have also been employed for backward-tracking, where particles are propagated backward in time to identify the possible sources of pollutants or other materials identified at a specific location (Chansheng and Croley, 2010; Olascoaga and Haller, 2012). Considering again the example in Figure 2.2, if pollutants are found at a location within lake, it is desirable to identify the region where the contaminants are originated from. The use of backward particle-tracking is one of the more efficient ways to identify these sources when a problem such as aggressive algal growth is discovered in a given region and the resource managers need to understand the sources contributing to the problem.

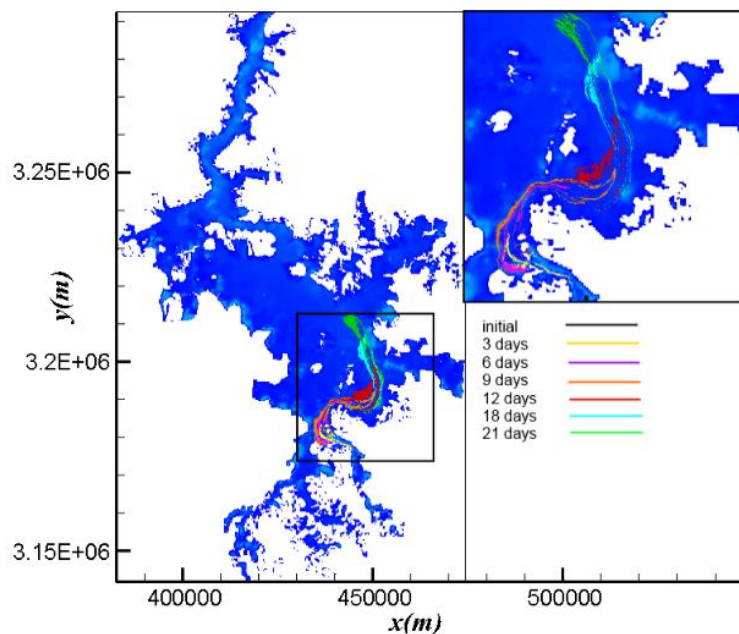


Figure 2.2 Particle-tracking simulation in a natural lake.

If diffusion is involved, the backward particle-tracking procedure will become more complicated because a random walk cannot be reversed in time, and particles that disperse from

a single point will not converge back to the same point in a reverse simulation (Thygesen, 2011). Statistical approaches must be used to deal with this problem, for example through running a series of BITT (backward-in-time tracking) and FITT (forward-in-time tracking) models in combination (Batchelder, 2006).

2.3 Non-linear dynamical systems in fluid dynamics

In recent years, the particle-tracking technique has been widely combined with theories and methods of nonlinear dynamics to detect significant structures which organize the transport and mixing process of particles in environmental flows (Aref, 1984; Kranenburg, 1992; Haller and Yuan, 2000). The application of these nonlinear theories (chaotic advection and Lagrangian coherent structure) has been proved to be very useful for understanding the transport and mixing properties in time-dependant (periodic and aperiodic) flows. In this section, relevant concepts and methods originated from nonlinear dynamics will be reviewed.

2.3.1 Chaotic advection

Applying the theory of chaos to fluid mixing, chaotic advection is a process by which Lagrangian particle dynamics driven by the simplified flows develops into complex fractal structures. The concept was first introduced by Aref (1984) when he investigated the particle paths of an important chaotic system: blinking-vortex system. He creatively linked fluid mechanics and non-linear dynamics by establishing the relationship of the flow domain and the phase space of dynamics system. The result of this work had two effects: 1) a great increase in the study of flows using dynamical systems, and 2) the key involvement of chaotic advection within the field of fluid mechanics and mixing. Also he found that the phenomenon of chaotic advection could occur even the velocity field of the flow is not complicated at all. Even though chaotic advection is possible in two-dimensional time dependent flows as well as in three dimensional flows, Saadjan and Leprevost (1998) sited that most experimental work has dealt with two-dimensional flows simply because the experimental apparatus is generally easier to build, cheaper to run, and the experiments are more straight forward to carry out. Also they proved that chaotic mixing and heat transfer enhancement are closely related, and they use two confocal elliptic cylinders to create chaotic motion to show the evidence of chaotic heat transfer.

Incompressible two-dimensional flows can be described through the stream function as a Hamiltonian system which makes the velocity field much easy to obtain. Khakhar *et al.* (1986) were among the first after Aref to capitalize on this technique. They revisited the ‘Aref-blinking-vortex’ flow and the ‘tendrill-whorl’ flow and attempted to find the supplying evidence

for the primary mechanisms responsible for mixing in two-dimensional deterministic flows by using mathematic methods. Chaiken *et al.* (1986) studied experimentally chaotic advection in time-periodic, stokes flow between two eccentric rotating cylinders. Their research provided the first experimental verification of chaotic advection and was detailed over extended flow parameters. Within the same year, Chien *et al.* (1986) performed an experimental study of laminar mixing in two-dimensional cavity flows. Their work elucidated the stretching of material lines and the complete blob deformation in chaotic and periodic areas. The alternate periodic motion of two bands in a cavity flow is an example of a laminar flow which might lead to chaotic mixing. The governing parameter is the dimensionless frequency of oscillation of the walls which, under the proper conditions, is able to produce horseshoe functions of various types. LEONG and Ottino (1989) presented a versatile cavity flow apparatus, capable of producing a variety of two-dimensional velocity fields, and use it to conduct a detailed experimental study of mixing in low-Reynolds-number flows and Swanson and Ottino (1990) develop techniques to predict the results of experiments involving chaotic dispersion of passive tracers in a journal bearing flow. This last experiment also provided numerical calculations and employed dynamical systems tools such as Poincare maps to verify and interpret the experimental results.

Solomon *et al.* (1994) studied the chaotic advection in an annular tank. In this work they found indication of anomalous diffusion, which quantifies the irregular growth of particle displacement with time. He proved that there is no chaotic mixing in time-independent flow while in a time-periodic flow the particle trajectories are typically chaotic. For a turbulence flow, mixing no longer appears super diffusive. Voth and Saint (2003) investigated an experimental setup in which the mixing rate is measured for a magnetically forced two-dimensional chaotic flow. He reported careful measurements of the rate at which an inhomogeneous scalar field becomes homogeneous in a two-dimensional flow exhibiting chaotic mixing.

The concept of chaotic mixing has already been used to study the transport and mixing property in a shallow environmental flow which is commonly driven by surface stress such as wind. Kranenburg (1992) gave examples on the importance of chaotic advection in inland surface water environment, namely wind-induced lake circulations. It was probably one of the first applications of the approach in such shallow conditions, developed decades ago in paint and food industry, where chaotic advection became an important issue to stir in an irreversible way substances being immiscible in the conventional diffusion sense. He used temporal change of average distance between neighbouring particles to indicate chaotic particle dynamics. Chaotic

advection and hence enhanced mixing are achieved if the averaged distance grows with time exponentially. Using the concept of chaotic advection, Kranenburg proposed a novel mean to investigate fluid mixing and hence control water quality in shallow water bodies. Liang *et al.* (2006a) have recently made further steps in evaluating and quantifying the above mentioned flows with the application of a numerical method. He found that particle motions gradually alter from regular to chaotic as the storm duration increases, which is in close qualitative agreement with Kranenburg's analytical solutions. Liang *et al.* (2006b) also studied the effect of irregular basin on wind-induced particle advection. In a rectangular basin and a mine tailing pond with complicated geometry, particle motions and mixing process shows a similar dynamics property as storm duration increases. However, global chaotic mixing could not be achieved due to the influence of flow geometry. The potential usefulness of these nonlinear system theory on water quality management was also discussed. Lee *et al.* (2014b) set up a two-layer Kranenburg's lake and investigated the particle dynamics in both the upper and lower layers which are subjected to alternating wind-induced circulation. Results show that particle advection becomes chaotic in parts of the flow in both layers where the effect of external forcing is concentrated primarily in the upper layer, with particles in the lower layer less mixed.

2.3.2 Lagrangian coherent structure

Typical fluid particle trajectories are sensitive to changes in their initial conditions. This makes the assessment of flow models and observations from individual tracer samples unreliable. Therefore direct interpretation of advection equation can be difficult. Locating robust, coherent patterns that dictate transport, such as separatrices that partition the flow, is often more enlightening. The theory on the knowledge that transport is strongly influenced by hyperbolicity. Hyperbolic structures in the flow are characterized by how particles behave in their vicinity. There are directions of significant stretching along which fluid moves away from the structure and directions of attraction where particles approach the structure. In the analysis of steady or periodic systems, hyperbolic stagnation points play a critical role. Such stagnation points have stable/unstable manifolds, which are composed of the same particles that asymptote the hyperbolic stagnation point in course of forward and backward time, respectively. These manifolds, which could be regarded as separatrices, separate the finite domain as different dynamics. For aperiodic systems, a complete theory of chaotic advection does not yet exist. But similar stretching and elongation of fluids parcels are frequently observed in ocean or lakes, and there are often analogous invariant manifolds that organise the transport structure. These invariant manifolds are usually regarded as Lagrangian coherent structure (LCS).

The LCS acronym are coined by Haller and Yuan (2000) to describe the most repelling, attracting and shearing structures that form the skeletons of Lagrangian particle dynamics. Haller refer these structures as material surfaces because of their capacity of organising scalars into different regions. Uncovering such surfaces from experimental and numerical flow data promises a simplified understanding of the overall flow geometry, an exact quantification of material transport, and a powerful opportunity to forecast, or even influence, large-scale flow features and mixing events. The definition was based firstly on the computation of the time interval during which a material surface would be stable or unstable, coherent structures being those that maximized this measure (the hyperbolicity time approach). The identification of Lagrangian coherent structure also could be achieved by another method. Shadden *et al.* (2005) define the finite-time Lyapounv exponents (FTLE) to develop the theory and reveal LCS. The ridges of FTLE field can be seen as finite-time templates. The definition of FTLE is applicable to flow with arbitrary time dependence and, in particular, to flows are only defined over a finite interval of time. The rationale for this criteria is that if LCS attract or repel particles for the longest in the flow, then, the net growth of a disturbance normal to them should be the largest during the time interval of interest (Haller, 2001). A third common approach is to use instead FSLE, which are a measure of the separation rate of fluid particles between two given distance thresholds to identify LCS (Aurell *et al.*, 1997). Although a rigorous connection between the FSLE and LCS has not been established, several works have shown that the ridges of the FSLE behave in a similar fashion as the ridges of the FTLE field (Joseph and Legras, 2002; d'Ovidio *et al.*, 2004; Branicki and Wiggins, 2009; d'Ovidio *et al.*, 2009). In additional there are some other methods serving similar purposes like, for instance, the leaking approach (Schneider and T'el, 2003; Schneider *et al.*, 2005).

Relevant applications of LCS approach as a powerful tool to uncover transport and mixing properties in two-dimensional flows has been illustrated integrally by an analytical or numerical approach. Haller and Yuan (2000) perform numerical simulations on a velocity field arising in a barotropic turbulence to validate their criterion for LCS identification. Koh and Legras (2002) use rigorous Lagrangian hyperbolicity criteria provided by Haller to detect hyperbolic lines and investigate the dynamics of the Antarctic stratospheric polar vortex. Lapeyre (2002) discuss the link between on tracer gradient dynamics and Lyapunov theory and provide the first description of the spatial distribution of FTLE in freely decaying turbulence. Shadden *et al.* (2006) employed FTLE to identify the structure of a piston-generated vortex ring and also captured the vortex ring wake structure of a jellyfish from two-dimensional DPIV data. Pattantyús-Ábrahám *et al.* (2008) use FSLE, the residence time and leaking method as mixing indicators to identify

the strong and weak shearing sub-regions in a simplified shallow lake whose hydrodynamic is driven by periodical wind forcing. Coherent structures as stable and unstable manifolds are also identified, playing the role of Lagrangian barriers that hinder local transversal material transfer, and avenues that significantly channel transport. Károlyi *et al.* (2010) study the transport and mixing properties of particles in a wind-induced shallow lake which is similar to Pattantyús-Ábrahám's lake.

In recent years, LCSs are able to be accurately identified from experimental techniques. Voth *et al.* (2002) use accurate experimental measurements to determine the stretching field in a magnetically forced two-dimensional time-periodic flow, thereby revealing the full time-dependent structure of the stable and unstable manifolds of the flow. Mathur *et al.* (2007) uncovers the Lagrangian building blocks of turbulence in a quasi-two-dimensional turbulent flow. The analysis identifies an intricate network of attracting and repelling material lines which act as Lagrangian skeleton of turbulence and show a level of complexity found previously only in theoretical and numerical examples. In an electromagnetically-driven weakly turbulent flow experiment, (Kelley *et al.*, 2013) finds that the LCSs tend to lie at zeros of the scale-to-scale energy flux and separate regions that have qualitatively different dynamics. He also suggests that the fluid on either side of an LCS is both kinematically and dynamically distinct. Raben *et al.* (2013) identify three-dimensional LCSs in three-dimensional multiphase flows by tracking inertial particles with an experimental method. The author points out that by using this method, it is possible to directly measure inertial particle FTLE fields and Lagrangian coherent structures without making assumptions about the underlying particle equations of motion.

The idea of LCS has been widely used to identify the key transport barriers, describe mixing dynamics of materials and forecast material motions in geophysical flows such as ocean and atmosphere. For ocean flows, the identification of the LCSs and the study of their influence on transport and mixing process are mainly focused on two-dimensional situations (d'Ovidio *et al.*, 2004; Lekien and Leonard, 2004; Beron-Vera *et al.*, 2008; Beron-Vera and Olascoaga, 2009; d'Ovidio *et al.*, 2009; Kai *et al.*, 2009; Beron-Vera *et al.*, 2010; Olascoaga and Haller, 2012; Olascoaga *et al.*, 2013). This is because: a) transport in horizontal plane is more important for spread of materials and pollutants forecasting compared to transport in vertical direction; and b) validation of LCS results rely on satellite data of any quantity (temperature, chlorophyll, altimetry for velocity, etc.) or drifter motions which are only available from the observation of the ocean surface. For atmospheric contexts, the relevance of the three-dimensional structure of LCSs are unveiled by many researchers (Du Toit and Marsden, 2010; Tallapragada *et al.*, 2011; Tang *et al.*, 2011b), although two-dimensional structure of LCSs are still available for

describing transport structures in atmospheric situations (Peng and Peterson, 2012; BozorgMagham and Ross, 2015; Garaboa *et al.*, 2015).

2.4 The hydrodynamics and water quality of Lake Taihu

Lake Taihu, located at one of the most economically developed areas in China, plays an important role of intense land and water use in the development of the region. Over the past 30 years, due to the increasing population and rapid economic growth in the basin, Lake Taihu has suffered dramatic environmental degradation. Hence, the numerical modelling of Lake Taihu including hydrodynamics modelling and ecological modelling has been carried out for several decades to illuminate the property of flow mechanisms, water quality, eutrophication and ecosystems of Lake Taihu.

2.4.1 Hydrodynamic modelling

Both two-dimensional and three-dimensional mathematical models have been employed to simulate hydrodynamic of Lake Taihu by researchers since 1980s. Because Lake Taihu is a typical shallow lake with huge areas, vertical physical processes such as seasonal stratification are less important compared to horizontal transport processes for many applications. Therefore, two-dimensional models are widely used to model horizontal water currents which are greatly driven by unstable wind forcing and lightly driven by inflow-outflow forcing.

Wang (1987) uses a two-dimensional finite difference model to simulate the wind-driven currents of Lake Taihu with constant wind conditions. Subsequently, Wu and Pu (1989) simulate the wind-induced currents and study the effect of wind on water levels in Lake Taihu by using an irregular-grid based model with an exact fit function for the lake shore and bottom topography. Thereafter, Wang *et al.* (1992) used a nested 2D hydrodynamic grid model to simulate wind-driven currents in Lake Taihu and accurately predicted flow direction. Liu (1993) simulated the currents in Meiliang Bay within a finite element method based model. Jiahu and Qun (1997) discuss application of the method of numerical inlay to set up an inlay-mesh model of the characteristics of East Taihu Lake's wind-driven currents in various wind regimes. Ma and Cai (1999) apply a two-dimensional upwinding finite element numerical model to investigate the distribution of total phosphorous in Lake Taihu. Xu and Liu (2009) shows that wind-induced currents in Taihu Lake are formed by the wind, the lake boundary and the landform of the lake bottom as well. There are obvious different laws of the current and hydrodynamics in different lake regions, and the reason caused the difference is analyzed with the fluid flow mechanism.

The aforementioned studies were all based on the hypothesis that there is no vertical shear stress and vertical variation of lake currents is excluded. However, in some areas of Lake Taihu, strong shear and mixing occur in the vertical direction and environmental factors such as dissolved oxygen, chlorophyll, light intensity and turbidity have an obvious vertical gradient. Thus, three-dimensional hydrodynamic models are required to model these vertical processes and gradients.

Pang *et al.* (1994) simulate the wind driven currents and wind-induced water setup with the influence of local wind field of Lake Taihu. He pointed out that the long narrow path between Xishan Island and Dongshan Island was most important for the formulation of global circulation flow in Lake Taihu. Zhu and Cai (1998b) developed a 3D hydrodynamic model for current simulation in Meiliang Bay. The lake was divided into five layers, and the differential equation was solved by the frog leap scheme (Zhu & Cai, 1998a). The results showed the horizontal current distribution in different layers, with the surface current being consistent with the wind direction, and the bottom current opposite to that at the surface.

Although these models separate lake currents into several layers, it is difficult for them to capture the vertical structure of the lake currents, because there are more layers in deep areas compared to shallow areas when water level changes dramatically and layer currents in deep areas cannot be computed. To deal with this issue, Liang and Zhong (1994) introduced a model with vertical σ -coordinate into the numerical simulation of Lake Taihu. Hu *et al.* (1998b) develop a three-dimensional model with multiple σ -layers and simulated the influence of No.3 Typhoon in 11th, Oct, 1997 on water level in Lake Taihu and water flow in the lake. (Hu *et al.*, 1998a) also analyzed the difference between the depth-mean current field and each individual depth current field and calculated the wind driven flow field with southeast, northeast and southwest wind. Li and Pang (2004) build a model with nested grids in horizontal dimension and σ -coordinate grid in vertical dimension to simulate the currents in Meiliang Bay and Gonghu Bay.

Change of relevant coefficients in three-dimensional models may greatly influence the accuracy of model outputs. The influence of the variation of vertical eddy viscosity coefficients on water depth, velocity profile and bed shear stresses are studied by Wang *et al.* (2001) and Song *et al.* (2003). Zhou *et al.* (2009) studied the effect of several proposed formulae of the drag coefficient varying with the wind speed on the numerical simulations of wind-induced flow.

2.4.2 Water quality modelling

The study of water quality by simulating the physical, geochemical and biological processes associated with the eco-environmental issues within the lake is regarded as a significant method to investigate the influence of eutrophication on local environment and ecological systems. Numerical modelling of water quality also could be applied to evaluate the efforts such as water transfer project have been made to control the process of eutrophication and water quality deterioration.

Many water quality models combine an advection-diffusion model with a lake hydrodynamic model to investigate transport of materials and concentration of objective chemical/biological variables such as total nitrogen (TN), total phosphorous (TP), suspended substance (SS), chemical oxygen demand (COD) and biochemical oxygen demand (BOD) in Lake Taihu (Ma and Cai, 1997; Zhu and Cai, 1998a; Hong and Pang, 2005; Pang *et al.*, 2006; Li *et al.*, 2011c). In addition to advection and diffusion, some models also consider the processes of sediments re-suspension and matter cycling (Pang *et al.*, 2008; Li *et al.*, 2009; Tang *et al.*, 2011a; Weiping *et al.*, 2011). Moreover, to study the changes in water quality and whole lake ecosystem, many ecological processes such as variation of aquatic animal, macrophytes, and phytoplankton are also required in some environmental applications. Thus, integrated water quality model like ecological models including more state variables are developed for lake environment control and research for examining the processes and determining the water quality (Rufeng, 1997; Li *et al.*, 2004; Hu *et al.*, 2006; Mao *et al.*, 2008; Han and Hu, 2012).

An integrated water transfer project named “Yin Jiang Ji Tai”, which is regarded as an emergency approach for pollutants dilution and lake water refreshment, has been utilized since the year 2002. This project introduces freshwater from Yangtze River into Lake Taihu to improve the water quality of the lake. The effects of “Yin Jiang Ji Tai” on water quality in Lake Taihu have been studied by many researchers. Hu *et al.* (2008) analyzed the environmental effect of water transfer in 2002 and 2003 by using both the observed data and estimated nutrient concentration with the elimination of effect from natural factors to evaluate the variations of space and time factors of water quality improvement induced by the two transfers. Zhai *et al.* (2010) use both ecological indicators and affiliated indicators to evaluate the water quality in Lake Taihu after water transfers from 2002 to 2007 with respect to the reference situation of years from 1998 to 2001 when the project of 'Yin Jiang Ji Tai' was not conducted. The conclusion showed the water transfers altered the ecosystem status and had positive effects on Lake Taihu and most of its sub-zones. Li *et al.* (2011c) used EFDC model to calculate water age and explored the time

required for the water flowing from Wangyu River into the lake to exchange. Later, Li *et al.* (2013a) test the effect of two pump stations set around Meiliang Bay using water age as indication and he also evaluate the effects of different transfer routes on water quality by using numerical simulation (Li *et al.*, 2013b). Ma *et al.* (2015) investigated the temporal and spatial distributions of water quality changes throughout the Lixia River watershed, by evaluating the effects of experimental water transfers from the Yangtze River on major water quality parameters. Notable improvements in water quality are found in the Lixia River watershed and the magnitude of water quality improvement was dependent on the quality of transferred water and associated flow rates, as well as subzones and fluctuations in transfer duration.

2.5 Concluding remarks

This chapter first reviewed multiple-dimensional (mainly two-dimension and three-dimension) mathematical models and their applications on enclosed/semi-enclosed environmental flow hydrodynamic modelling. Depth averaged two-dimensional models (2D model) based on various type of horizontal grid structures are popular to simulate horizontal physical processes which dominate the transport and mixing in environmental shallow flows. For relatively deep cases where vertical acceleration could not be ignored, three-dimensional models with vertical z-coordinate grid or σ -coordinate grid are applied. Unlike other environmental flows such as rivers, seas or oceans, the hydrodynamic of enclosed/semi-enclosed shallow flows such as lakes and reservoirs are usually dominated by wind-driven surface currents and are slightly influenced by inflows/outflows-driven surface currents. For the Lake Taihu case in this thesis, a hundred thousand level of grids will be used to discretize the computational domain. Proposed grid resolution is high enough to maintain the complicated geometry even with uniform Cartesian grids and what should be considered is the computational efficiency since the number of grids used for numerical simulation is so large. Uniform Cartesian grids allows a given point neighbours to be easily identified and efficiently accessed, which allows for speedy GPU-based codes. Hence, an in-house shallow water model based on horizontal Cartesian grid will be applied to simulate shallow flow hydrodynamics and predict wind-induced velocity fields.

Lagrangian particle tracking models have long been recognised as a useful technique to simulate the transport of passive particles and investigate water quality in environmental flows. Both the numerical scheme for advection process (deterministic process) and the random walk method for diffusion process (stochastic process) are reviewed. However in this study, due to

the applications of dynamic theories in which only the deterministic motion of particles are considered, only the advection process is focused.

In recent years, chaotic advection which derived from nonlinear dynamic theory has been proved to have great effects on transport and mixing in non-turbulent flows. Complicated particle motions caused by chaotic advection could be obtained from relatively simple velocity fields given by idealized analytical, numerical solutions or experimental data. However, for more complicated natural environmental flows, chaos theory could not be used directly since time is finite. In these cases, another new developed concept from nonlinear dynamic theory, Lagrangian coherent structures (LCSs), are used. LCSs identified by plotting Lagrangian-based measures of hyperbolicity are regarded as transport barriers which separate flows into different regions with different dynamic property and act as gallery for material transportation. LCSs computation arose as a means to compute effective stable and unstable manifolds of hyperbolic trajectories in temporally aperiodic flows, which was motivated by the previous study of chaotic advection that such manifolds organized transport in temporally periodic flows. Indeed, in both periodic and aperiodic flows, LCSs often govern the stretching, folding, and alignment mechanisms that control transport and mixing processes. Though applications of LCSs have widely ranged from ocean to atmosphere in geophysical flows, few attention have been paid to investigate mixing and transport properties in enclosed/semi-enclosed environmental flows such as lakes and reservoirs.

Lake Taihu, regarded as a semi-enclosed environmental flow system, is an important case in this research. Hence the development of studies on hydrodynamic modelling of Lake Taihu by a varieties of numerical models is reviewed. Water quality models which are used to study the different effects of physical, chemical and biological processes on lake water quality are also reviewed.

Next chapter introduces, a shallow water model which is capable to simulate the hydrodynamics of enclosed/semi-enclosed environmental flows and a Lagrangian particle tracking model which is capable to model passive particle trajectories. Recent developed dynamic approaches, Poincaré sections and FTLE, are explained. Five benchmark cases are used to validate the shallow water model and the particle tracking model.

Chapter 3. Methodology

Natural water bodies such as wide rivers, shallow lakes/reservoirs, coastal lagoons and estuaries could be recognized as environmental shallow water flows. This is because in these flows the horizontal dimensions are much larger than the vertical component (usually horizontal length is 20 times larger than vertical depth) and the water particle acceleration is negligible compared with the horizontal acceleration components so that the pressure variation can be assumed hydrostatic. Hence, horizontal mixing is of particular importance on water quality in environmental shallow water flows. Horizontal mixing has a great influence on the water exchange mechanisms, and have important implications when interpreting plankton movement or planning and operating pollutant outfalls. But the understanding of mixing and transport process still remains a major challenge in environmental shallow flows due to the complex flow hydrodynamics as involved. Understanding the mixing and transport processes in flow fields and predicting possible behaviours of water-born particles due to the change of hydrodynamics is crucial for many engineering applications.

The Lagrangian methods based on the theory of dynamical system have been well-developed in the last few decades to better understand a wide range of fluid mixing problems in geophysical shallow flows (Aref, 1984; Ottino, 1989; Wiggins, 1992; Aref, 2002; Koshel and Prants, 2006). These methods typically involve the use of passive particle tracking technique to investigate the mixing dynamics in environmental shallow flows.

This chapter first presents a finite volume model that solves numerically the 2D shallow water equations for predicting shallow flow hydrodynamics, followed by the introduction of a particle tracking model based on numerical integration of ordinary differential equations. Finally methods of analysing dynamical systems including Poincaré sections, finite-time Lyapunov Exponent (FTLE) are introduced to reveal the organizing structures that govern particle behaviours in shallow flow systems.

3.1 Full 2D Shallow Flow model

The hydrodynamics of shallow water flows will be simulated in this work by a 2D depth-integrated shallow flow model. The model solves the governing shallow water equations using a second-order Godunov-type finite volume numerical scheme on uniform Cartesian grids, with the inviscid fluxes through cell interfaces evaluated through solving local Riemann problems with the Harten-Lax-van Leer with Contact wave restored (HLLC) solver (Toro, 2001).

3.1.1 Shallow water equations

The current shallow flow hydrodynamic model is based on the 2D pre-balanced shallow water equations (SWEs) has been derived in Liang and Borthwick (2009), which automatically maintains the well-balanced numerical solutions for wet-bed applications. In a matrix form, the hyperbolic SWEs in conservative form can be expressed as:

$$\frac{\partial \mathbf{u}}{\partial t} + \frac{\partial \mathbf{f}}{\partial x} + \frac{\partial \mathbf{g}}{\partial y} = \mathbf{s} \quad (3.1)$$

where \mathbf{u} is the vector of conservative variables; \mathbf{f} and \mathbf{g} denote the vectors of fluxes in the x and y directions, respectively; \mathbf{s} is the vector of source terms; t is the time; and x and y are the Cartesian coordinates. The vectors are given by:

$$\mathbf{u} = \begin{bmatrix} \eta \\ uh \\ vh \end{bmatrix}, \mathbf{f} = \begin{bmatrix} uh \\ u^2h + \frac{1}{2}g(\eta^2 - 2\eta z_b) \\ uvh \end{bmatrix} \quad (3.2)$$

$$\mathbf{g} = \begin{bmatrix} vh \\ uvh \\ v^2h + \frac{1}{2}g(\eta^2 - 2\eta z_b) \end{bmatrix}, \mathbf{s} = \begin{bmatrix} 0 \\ (\tau_{wx} - \tau_{bx})/\rho - g\eta \frac{\partial z_b}{\partial x} + S_{vx} \\ (\tau_{wy} - \tau_{by})/\rho - g\eta \frac{\partial z_b}{\partial y} + S_{vy} \end{bmatrix}$$

where η and z_b are the water surface level and bed elevation above datum; h is the total water depth with $h = \eta - z_b$; u and v are the x and y -direction components of the depth-averaged velocity, respectively; g is the gravitational acceleration; ρ is the density of water; τ_{wx} and τ_{wy} are wind stresses in x and y directions and the magnitude of wind stresses are estimated as (Smith, 1988)

$$\tau_{wt} = \rho_{air} C_D U_h^2 \quad (3.3)$$

where τ_{wt} is the resultant vector of τ_{wx} and τ_{wy} ; ρ_{air} is the density of air; C_D is a drag coefficient; U_h is the mean velocity at a particular height over the water surface and the height is usually chosen to be 10 m (Smith, 1988).

τ_{bx} and τ_{by} are the bed friction stresses in the x and y directions which can be estimated from:

$$\tau_{bx} = \rho C_f u \sqrt{u^2 + v^2}, \tau_{by} = \rho C_f v \sqrt{u^2 + v^2} \quad (3.4)$$

The bed roughness coefficient C_f can be evaluated using $C_f = gn^2/h^{1/3}$ where n is the Manning coefficient, and C_f is set to be zero in dry areas with $h < 10^{-6}$ m. In these dry areas, local bed slope will be reconstructed to handle the zero flow conditions and avoid spurious flows (Liang and Borthwick, 2009). And finally, S_{vx} and S_{vy} are the second derivatives turbulent (viscous) terms:

$$\begin{aligned} S_{vx} &= \frac{\partial}{\partial x} \left(2hv_{mo} \frac{\partial u}{\partial x} \right) + \frac{\partial}{\partial y} \left(hv_{mo} \left[\frac{\partial v}{\partial x} + \frac{\partial u}{\partial y} \right] \right) \\ S_{vy} &= \frac{\partial}{\partial x} \left(hv_{mo} \left[\frac{\partial v}{\partial x} + \frac{\partial u}{\partial y} \right] \right) + \frac{\partial}{\partial y} \left(2hv_{mo} \frac{\partial v}{\partial y} \right) \end{aligned} \quad (3.5)$$

where v_{mo} represents the momentum diffusion coefficient. These terms are And we substitute (3.5) into (3.2) and obtain the full shallow water equations:

$$\begin{aligned} \mathbf{u} &= \begin{bmatrix} \eta \\ uh \\ vh \end{bmatrix}, \mathbf{f} = \begin{bmatrix} uh \\ u^2h + \frac{1}{2}g(\eta^2 - 2\eta z_b) \\ uvh \end{bmatrix} \\ \mathbf{g} &= \begin{bmatrix} vh \\ uvh \\ v^2h + \frac{1}{2}g(\eta^2 - 2\eta z_b) \end{bmatrix} \end{aligned} \quad (3.6)$$

$$\mathbf{s} = \begin{bmatrix} 0 \\ (\tau_{wx} - \tau_{bx})/\rho - g\eta \frac{\partial z_b}{\partial x} + \frac{\partial}{\partial x} \left(2hv_{mo} \frac{\partial u}{\partial x} \right) + \frac{\partial}{\partial y} \left(hv_{mo} \left[\frac{\partial v}{\partial x} + \frac{\partial u}{\partial y} \right] \right) \\ (\tau_{wy} - \tau_{by})/\rho - g\eta \frac{\partial z_b}{\partial y} + \frac{\partial}{\partial x} \left(hv_{mo} \left[\frac{\partial v}{\partial x} + \frac{\partial u}{\partial y} \right] \right) + \frac{\partial}{\partial y} \left(2hv_{mo} \frac{\partial v}{\partial y} \right) \end{bmatrix}$$

Herein the shallow water model, the viscosity terms are treated as viscosity fluxes to make the computation sample and convenient:

$$\frac{\partial \mathbf{u}}{\partial t} + \frac{\partial(\mathbf{f}_i + \mathbf{f}_v)}{\partial x} + \frac{\partial(\mathbf{g}_i + \mathbf{g}_v)}{\partial y} = \mathbf{s} \quad (3.7)$$

The viscosity fluxes \mathbf{f}_v and \mathbf{g}_v are not obtained by the HLLC Riemann solver so the calculation of \mathbf{f}_v and \mathbf{g}_v is different from that of the existing flux terms \mathbf{f} and \mathbf{g} . The inviscid flux \mathbf{f}_i and \mathbf{g}_i represent the flux of flow variables while the viscous flux \mathbf{f}_v and \mathbf{g}_v represent turbulence effect obtained from current flow variables. The two sets of flux terms are combined to become the total flux to update the flow states of each cell to next time step. After applying viscosity terms as viscosity fluxes, the final form of the shallow water equations used in this study could be derived:

$$\mathbf{u} = \begin{bmatrix} \eta \\ uh \\ vh \end{bmatrix}$$

$$\mathbf{f}_{total} = \mathbf{f}_i + \mathbf{f}_v = \begin{bmatrix} uh \\ u^2h + \frac{1}{2}g(\eta^2 - 2\eta z_b) \\ uvh \end{bmatrix} + \begin{bmatrix} 0 \\ 2hv_{mo} \frac{\partial u}{\partial x} \\ hv_{mo} \left(\frac{\partial v}{\partial x} + \frac{\partial u}{\partial y} \right) \end{bmatrix}$$

$$\mathbf{g}_{total} = \mathbf{g}_i + \mathbf{g}_v = \begin{bmatrix} vh \\ uvh \\ v^2h + \frac{1}{2}g(\eta^2 - 2\eta z_b) \end{bmatrix} + \begin{bmatrix} 0 \\ hv_{mo} \left(\frac{\partial v}{\partial x} + \frac{\partial u}{\partial y} \right) \\ 2hv_{mo} \frac{\partial v}{\partial y} \end{bmatrix} \quad (3.8)$$

$$\mathbf{s} = \begin{bmatrix} 0 \\ (\tau_{wx} - \tau_{bx})/\rho - g\eta \frac{\partial z_b}{\partial x} \\ (\tau_{wy} - \tau_{by})/\rho - g\eta \frac{\partial z_b}{\partial y} \end{bmatrix}$$

The shallow water equations (3.7) and (3.8) are solved by a second-order Godunov-type finite volume method. Inviscid flux are calculated by the HLLC approximate Riemann solver while viscous flux are calculated by central differencing method. Source terms including bed slope and friction are evaluated by different proper ways.

3.1.2 Second-order finite volume scheme

In the context of a finite volume scheme, the following time-marching formula (Toro, 2001) may be used to discretized equation (1) and update the flow variables to a new time step:

$$u_{i,j}^{k+1} = u_{i,j}^k - \frac{\Delta t}{\Delta x} (\mathbf{f}_{i+1/2,j} - \mathbf{f}_{i-1/2,j}) - \frac{\Delta t}{\Delta y} (\mathbf{g}_{i,j+1/2} - \mathbf{g}_{i,j-1/2}) + \Delta t \mathbf{s}_{i,j} \quad (3.9)$$

where the superscript k represents the present time level, the subscripts i and j are the cell indices, Δt , Δx and Δy are the time step and cell size in the x and y -directions, and $\mathbf{f}_{i-1/2,j}$, $\mathbf{f}_{i+1/2,j}$, $\mathbf{g}_{i,j-1/2}$, and $\mathbf{g}_{i,j+1/2}$ are the fluxes through the west, east, south and north cell interfaces.

3.1.3 The HLLC approximate Riemann solver for inviscid flux calculation

The HLLC approximate Riemann solver is used to calculate the interface inviscid fluxes since it has automatic entropy-fixed property and can be directly used to calculate wetting and drying situations. The solution structure of the HLLC Riemann solver is shown in Figure 3.1, where the four solution regions are defined according to left wave speed, middle wave speed and right wave speed, which are represented by S_L , S_M and S_R respectively.

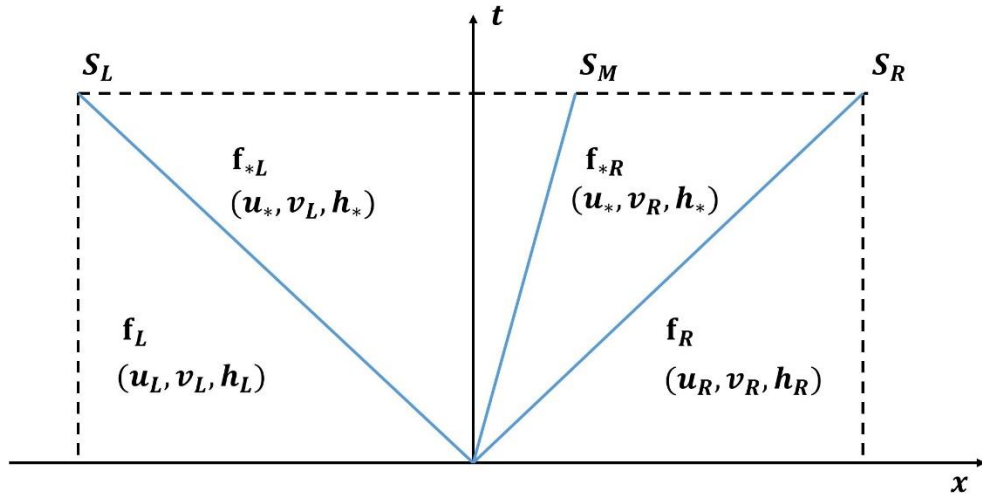


Figure 3.1 The solution structure of the HLLC approximate Riemann solver.

Taking $\mathbf{f}_{i+1/2,j}$ as an example:

$$\mathbf{f}_{i+1/2,j} = \begin{cases} \mathbf{f}_L & \text{if } 0 \leq S_L \\ \mathbf{f}_{*L} & \text{if } S_L \leq 0 \leq S_M \\ \mathbf{f}_{*R} & \text{if } S_M \leq 0 \leq S_R \\ \mathbf{f}_R & \text{if } 0 \geq S_R \end{cases} \quad (3.10)$$

where \mathbf{f}_L and \mathbf{f}_R are the fluxes defined at the left and right solution regions in Figure 3.1, which are directly evaluated using the left and right Riemann states that define the local Riemann

problem; \mathbf{f}_{*L} and \mathbf{f}_{*R} are the fluxes in the left and right middle region, which may be evaluated as follows (Toro, 2001)

$$\mathbf{f}_{*L} = \begin{bmatrix} \mathbf{f}_{1*} \\ \mathbf{f}_{2*} \\ \mathbf{f}_{1*} \cdot v_L \end{bmatrix}, \mathbf{f}_{*R} = \begin{bmatrix} \mathbf{f}_{1*} \\ \mathbf{f}_{2*} \\ \mathbf{f}_{1*} \cdot v_R \end{bmatrix} \quad (3.11)$$

in which v_L and v_R are the Riemann states of the left and right tangential velocity components; \mathbf{f}_{1*} and \mathbf{f}_{2*} are the first and second components of the flux vector \mathbf{f} in the middle region, which can be evaluated using the HLL flux formula (Harten *et al.*, 1983):

$$\mathbf{f}_* = \frac{S_R \mathbf{f}_L - S_L \mathbf{f}_R + S_L S_R (\mathbf{u}_R - \mathbf{u}_L)}{S_R - S_L} \quad (3.12)$$

In equation (3.12), \mathbf{u}_R and \mathbf{u}_L are right and left Riemann states defining the Riemann problem at each cell interface. S_L , S_M and S_R may be computed using the following formulas (Fraccarollo and Toro, 1995).

$$S_L = \begin{cases} u_R - 2\sqrt{gh_R} & \text{if } h_L = 0 \\ \min(u_L - \sqrt{gh_L}, u_* - \sqrt{gh_*}) & \text{if } h_L > 0 \end{cases} \quad (3.13)$$

$$S_R = \begin{cases} u_L - 2\sqrt{gh_L} & \text{if } h_R = 0 \\ \max(u_R - \sqrt{gh_R}, u_* - \sqrt{gh_*}) & \text{if } h_R > 0 \end{cases} \quad (3.14)$$

$$S_M = \frac{S_L h_R (u_R - S_R) - S_R h_L (u_L - S_L)}{h_R (u_R - S_R) - h_L (u_L - S_L)} \quad (3.15)$$

$$u_* = \frac{1}{2}(u_L + u_R) + \sqrt{gh_L} - \sqrt{gh_R} \quad (3.16)$$

$$h_* = \frac{1}{g} \left[\frac{1}{2}(\sqrt{gh_L} + \sqrt{gh_R}) + \frac{1}{4}(u_L - u_R) \right]^2 \quad (3.17)$$

A two-step unspilt MUSCL-Hancock method is implemented to extend the Godunov-type numerical scheme to second-order accuracy in time and space (Liang and Borthwick, 2009). The MUSCL-Hancock method contains two separate steps, i.e. a predictor step and a corrector step. The predictor step predicts inter-mediate cell-centre values over the half time step $\Delta t/2$ while the corrector step is then used to update the flow variables over a full time step with the interface fluxes evaluated through solving local Riemann problems. The predictor step is denoted

$$\begin{aligned} \bar{\mathbf{u}}_{i,j}^{k+1/2} = & \mathbf{u}_{i,j}^k - \frac{\Delta t}{2\Delta x} (\mathbf{f}(\mathbf{u}_{i+1/2,j}) - \mathbf{f}(\mathbf{u}_{i-1/2,j})) \\ & - \frac{\Delta t}{2\Delta y} (\mathbf{g}(\mathbf{u}_{i,j+1/2}) - \mathbf{g}(\mathbf{u}_{i,j-1/2})) + \frac{\Delta t}{2} \mathbf{s}_{i,j} \end{aligned} \quad (3.18)$$

where $\mathbf{f}(\mathbf{u}_{i+1/2,j})$, $\mathbf{f}(\mathbf{u}_{i-1/2,j})$, $\mathbf{g}(\mathbf{u}_{i,j+1/2})$ and $\mathbf{g}(\mathbf{u}_{i,j-1/2})$ are the fluxes which are evaluated within each cell directly using the face values of flow variables $\mathbf{u}_{i+1/2,j}$, $\mathbf{u}_{i-1/2,j}$, $\mathbf{u}_{i,j+1/2}$ and $\mathbf{u}_{i,j-1/2}$ reconstructed at the mid-points of the corresponding cell interfaces.

Face values of the flow variables are obtained by linearly interpolating the corresponding cell-centre values, commonly incorporated with a slope limiter to avoid the spurious oscillations appearing in the numerical solutions near the flow regions with sharp gradients or discontinuities and ensure a TVD high-order numerical solutions.

$$\mathbf{u}(x, y) = \mathbf{u}_{i,j} + \Psi(r) \mathbf{r} \nabla \mathbf{u}_{i,j} \quad (3.19)$$

in which the slope limiter $\Psi(r)$ is a function of \mathbf{r} , and $\mathbf{r} = \mathbf{r}[\mathbf{r}_1 \quad \mathbf{r}_2 \quad \mathbf{r}_3]^T$ is the ratio of gradients. Considering only the x -direction, \mathbf{r}_1 , \mathbf{r}_2 and \mathbf{r}_3 are the gradient component of the three conserved flow variables given by

$$\mathbf{r}_1 = \frac{\eta_{i+1,j} - \eta_{i,j}}{\eta_i - \eta_{i-1,j}}, \quad \mathbf{r}_2 = \frac{(uh)_{i+1,j} - (uh)_{i,j}}{(uh)_{i,j} - (uh)_{i-1,j}} \quad \text{and} \quad \mathbf{r}_3 = \frac{(vh)_{i+1,j} - (vh)_{i,j}}{(vh)_i - (vh)_{i-1,j}} \quad (3.20)$$

The slope limiter is then defined as (Hirsch, 2007):

$$\Psi(r) = \max[0, \min(\beta r, 1), \min(r, \beta)] \quad (3.21)$$

Here β ($1 \leq \beta \leq 2$) is the limiter parameter where $\beta = 1$ gives the minmod limiter and $\beta = 2$ defines the Roe's superbee limiter. Normally a minmod limiter is more diffusive and gives smoother results than the superbee limiter. In this thesis, a minmod limiter is chosen for more stable numerical simulations.

Finally the face values of cell (i, j) at the k time step in the x -direction may be obtained from:

$$\begin{aligned} \mathbf{u}_{i-1/2,j}^k &= \mathbf{u}_{i,j}^k - \frac{1}{2}\Psi(r)(\mathbf{u}_{i,j}^k - \mathbf{u}_{i-1,j}^k) \\ \mathbf{u}_{i+1/2,j}^k &= \mathbf{u}_{i,j}^k + \frac{1}{2}\Psi(r)(\mathbf{u}_{i,j}^k - \mathbf{u}_{i-1,j}^k) \end{aligned} \quad (3.22)$$

$\mathbf{u}_{i-1/2,j}^k$ and $\mathbf{u}_{i+1/2,j}^k$ are the face values only used in the predictor step to obtain $\bar{\mathbf{u}}_{i,j}^{k+1/2}$ by evaluating the fluxes which are not associated with the Riemann problems. The face values of cell i are calculated in a similar way.

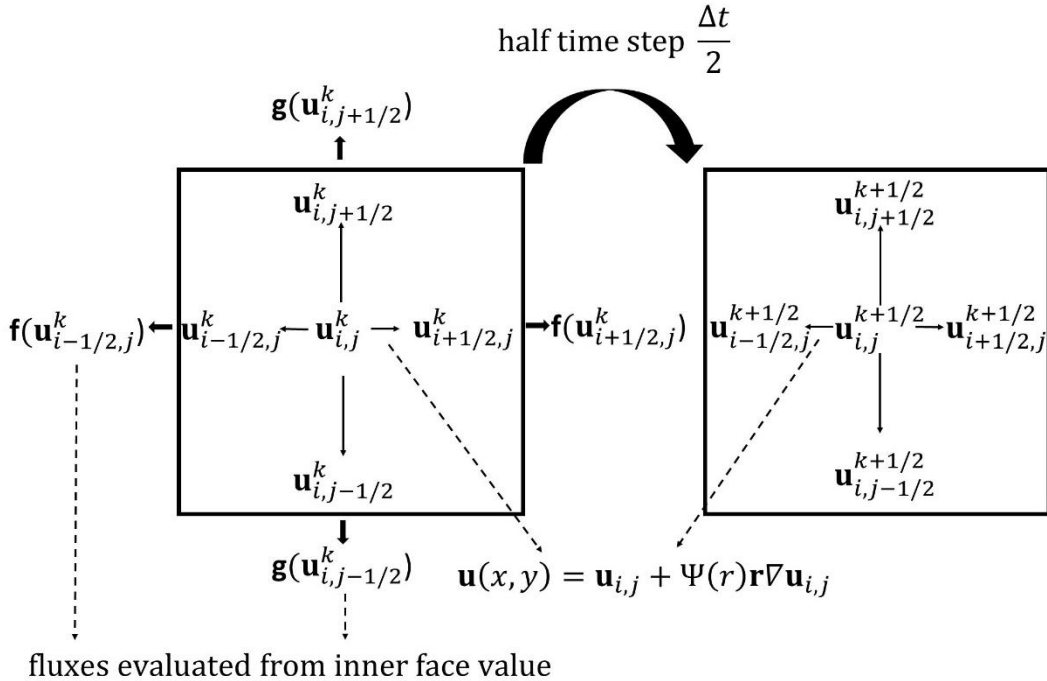


Figure 3.2 The predictor step of MUSCL-Hancock method.

In the corrector step, fluxes passing through the interfaces are evaluated by the HLLC approximate Riemann solver. Take the interface $(i + 1/2)$ for example, the left and right Riemann states are obtained from:

$$\mathbf{u}_{i+1/2,j}^L = \bar{\mathbf{u}}_{i,j}^{k+1/2} + \frac{1}{2}\Psi(r)(\mathbf{u}_{i,j}^k - \mathbf{u}_{i-1,j}^k)$$

$$\mathbf{u}_{i+1/2,j}^R = \bar{\mathbf{u}}_{i+1,j}^{k+1/2} - \frac{1}{2}\Psi(r)(\mathbf{u}_{i,j+1}^k - \mathbf{u}_{i,j}^k)$$
(3.23)

where $\bar{\mathbf{u}}_{i,j}^{k+1/2}$ and $\bar{\mathbf{u}}_{i+1,j}^{k+1/2}$ are the predicted cell-centre values at cell i and $i + 1$ obtained in the predictor step. When calculating the Riemann states, the application of the original flow variables $\mathbf{u}_{i,j}^k$ for the limiter and gradient vector terms $1/2\Psi(r)(\mathbf{u}_{i,j}^k - \mathbf{u}_{i-1,j}^k)$ and $1/2\Psi(r)(\mathbf{u}_{i,j+1}^k - \mathbf{u}_{i,j}^k)$ gets better results than the application of intermediate flow variables $\bar{\mathbf{u}}_{i,j}^{k+1/2}$ in the corrector step (Hu *et al.*, 2000). The Riemann states at the other three cell interfaces of cell i are given in a similar process.

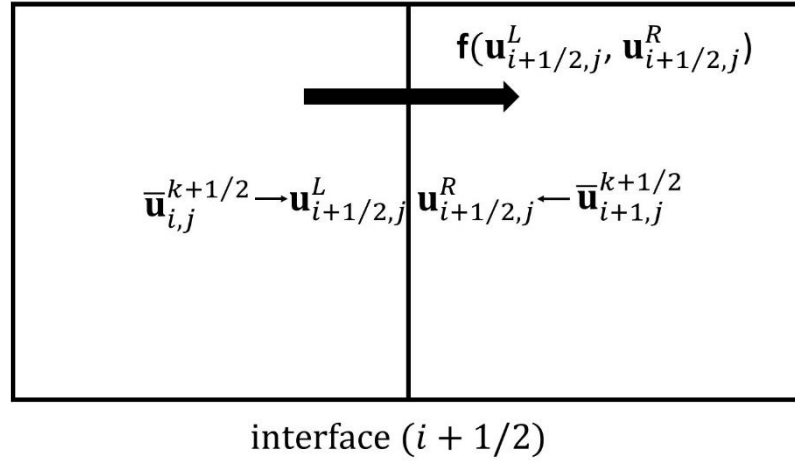


Figure 3.3 The corrector step of MUSCL-Hancock method.

The predictor step is non-conservative because the fluxes calculated by the flow states at the inner side and outer side of a cell interface are distinct and equation (3.18) only considers the fluxes at the inner side. However, the conservative property of the overall numerical scheme is not affected by the flux calculation in the predictor step as it is merely the intermediate step over the half time step $\Delta t/2$ to obtain temporary values of flow variables to facilitate the reconstruction of Riemann states in the corrector step. In the corrector step, equation (3.9) is used to update the flow variables over a full time step with the interface fluxes calculated using the HLLC approximate Riemann solver, making the numerical method fully conservative.

3.1.4 Calculation of viscous flux terms

In this work, the shallow water hydrodynamic model will be used to simulate environmental shallow flows in natural water bodies. The effects of viscosity and turbulence (leading to the flow structures of vortex and wakes) may not be negligible since the flows in nature are commonly random and chaotic due to the complicated situations. So the viscosity terms are considered and incorporated into the aforementioned shallow flow model to simulate the viscosity effects in the flows.

The calculation of \mathbf{f}_v and \mathbf{g}_v is based on central differencing of velocity values of six relevant cells, respectively. Here we just take x-direction for example. Then the viscosity effect is governed by \mathbf{f}_v since only \mathbf{f}_v pass through the interfaces perpendicular to x-direction. There are three partial differential parts in \mathbf{f}_v should be calculated:

$$\frac{\partial u}{\partial x} = \frac{u_{i+1,j} - u_{i,j}}{\Delta x}, \frac{\partial v}{\partial x} = \frac{v_{i+1,j} - v_{i,j}}{\Delta x} \quad (3.24)$$

$$\frac{\partial u}{\partial y} = \frac{(u_{i+1,j+1} + u_{i,j+1})/2 - (u_{i+1,j-1} + u_{i,j-1})/2}{2\Delta y}$$

So the \mathbf{f}_v could be rewritten as:

$$\mathbf{f}_v = \begin{bmatrix} 0 \\ 2h\nu_{mo} \left(\frac{u_{i+1,j} - u_{i,j}}{\Delta x} \right) \\ h\nu_{mo} \left(\frac{v_{i+1,j} - v_{i,j}}{\Delta x} + \frac{(u_{i+1,j+1} + u_{i,j+1})/2 - (u_{i+1,j-1} + u_{i,j-1})/2}{2\Delta y} \right) \end{bmatrix} \quad (3.25)$$

And the cells used to calculate \mathbf{f}_v are shown in Figure 3.4:

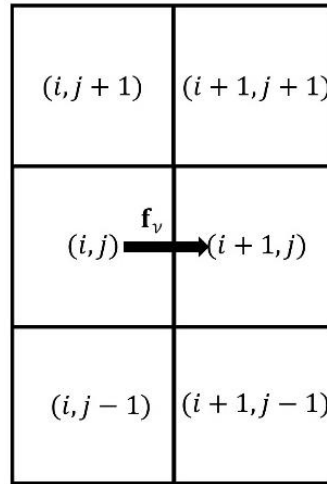


Figure 3.4 Cells used for the calculation of viscosity term.

The momentum coefficient ν_{mo} is consisted of molecule viscosity, eddy viscosity ν_t and the dispersion coefficient which is often ignored in numerical computation. Since the molecule viscosity is an intrinsic property of the flow, the value of the molecule viscosity is always regards as a constant (Wilcox, 1998). The eddy viscosity ν_t , demonstrated as the product of the Lagrangian length scale and the intensity of the turbulence, is defined as (Fischer *et al.*, 2013):

$$\nu_t = p_{\nu t} \sqrt{\frac{\tau}{\rho}} \quad (3.26)$$

where $p_{\nu t}$ is a parameter should be determined, τ is the shear velocity and ρ is the density of the fluid. The normal range of $p_{\nu t}$ is 0.09~0.25 in rectangular open channels with smooth sides and 0.3~3.4 in open channels with curves and irregular sides. And the eddy viscosity ν_t is evaluated as (Fischer *et al.*, 2013):

$$\nu_t = p_{\nu t} H \sqrt{C_f (u^2 + v^2)} \quad (3.27)$$

In this project, the value of $p_{\nu t}$ will be discussed based on the different situations. Since no differential equation is applied for calculating the eddy viscosity, the turbulence model is known as zero-equation model or algebraic model.

3.1.5 Discretisation of source terms

In order to maintain the stable and well-balanced numerical scheme with non-negative water depth in simulations involving wetting and drying, the non-zero source terms in two momentum equations expressed in equation (3.6) are spilt into two parts: bed slope terms and friction terms. The source terms in equation (3.6) are cell-centred and the bed slope term could be calculated simply by a central-differencing method. Take x -direction for example:

$$-g\eta \frac{\partial Z_b}{\partial x} = -g\bar{\eta} \left(\frac{Z_{b_{i+1/2}} - Z_{b_{i-1/2}}}{\Delta x} \right) \quad (3.28)$$

where $\bar{\eta} = (\eta_{i-1/2,j}^R + \eta_{i+1/2,j}^L)/2$ and the y -direction slope source term is treated in a similar way.

Since the shallow water model in this study will be used to simulate environmental shallow flows which are realistic flows in nature, bed friction is a non-negligible force influencing the hydrodynamics of these shallow flows. Due to the complex topography of these realistic flows, the simulations of this study will always be involved in wetting and drying conditions where the stability of a numerical scheme will be actually dominated by the friction terms due to the presence of water depth in denominator. If water depth is extremely (less than 0.01m) small, an overlarge force will be obtained by the application of Manning formula of friction and flow will even reverse the direction which is definitely physically incorrect. To avoid this problem and achieve better numerical stability, a splitting point-implicit scheme (Bussing and Murman, 1988; Fiedler and Ramirez, 2000) is used to evaluate the friction component of the source terms and the following ordinary differential equation (ODE) is solved:

$$\frac{d\mathbf{q}}{dt} = \mathbf{S}_f \quad (3.29)$$

where $\mathbf{S}_f = [0 \quad S_{fx} \quad S_{fy}]^T$ with $S_{fx} = -\tau_{bx}/\rho$ and $S_{fy} = -\tau_{by}/\rho$. In the x -direction momentum equation (3.8), the friction term could be isolated and expanded using a Taylor series as (Fiedler and Ramirez, 2000):

$$S_{fx}^{n+1} = S_{fx}^n + \left(\frac{\partial S_{fx}}{\partial q_x} \right)^n \Delta q_x + o(q_x^2) \quad (3.30)$$

where $\Delta q_x = q_x^{n+1} - q_x^n$. Then the flow variable q in a new time step could be obtained by ignoring the higher-order terms:

$$q_x^{n+1} = q_x^n + \Delta t \left(\frac{S_{fx}}{D_x} \right)^n = q_x^n + \Delta t F_x \quad (3.31)$$

where $D_x = 1 - \Delta t (\partial S_{fx} / \partial q_x)^n$ is the coefficient derived for a point implicit scheme in the x-direction and F_x is the friction source term including the implicit coefficient.

In order to maintain the stability of the numerical scheme when the computation is performed near to the wet-dry front where water depth is becoming extremely small, the value of implicit friction term should be bounded properly. Liang and Marche (2009) suggests that the value could be found by considering:

$$q_x^{n+1} q_x^n \geq 0 \quad (3.32)$$

i.e. the maximum effect of friction force is to stop the fluid. Then the limiting value of implicit friction term could be easily expressed as:

$$F_x = \begin{cases} -q_x^n / \Delta t & \text{if } q_x^n \geq 0 \text{ and } F_x < -q_x^n / \Delta t \\ -q_x^n / \Delta t & \text{if } q_x^n \leq 0 \text{ and } F_x > -q_x^n / \Delta t \end{cases} \quad (3.33)$$

The result of computed F_x will be replaced by the above critical one if it is beyond the limit value. For wet cells, the friction term is calculated at the beginning of each time step; for dry cells, the friction is set to zero since there is no flows. Liang and Marche (2009) pointed that although this splitting method is only first order accuracy, the overall accuracy of numerical scheme still remain as second order.

3.1.6 CFL criterion

Despite the implicit scheme to calculate the bed friction source terms, the overall numerical scheme is explicit and its numerical stability is controlled by the Courant-Friedrichs-Lewy (CFL) criterion (Courant *et al.*, 1967). The time step, Δt , may be determined according to

$$\Delta t = C_r \min(\Delta t_x, \Delta t_y) \quad (3.34)$$

with

$$\Delta t_x = \min_{i,j} \frac{\Delta x_{i,j}}{|u_{i,j}| + \sqrt{gh_{i,j}}}, \quad \Delta t_y = \min_{i,j} \frac{\Delta y_{i,j}}{|v_{i,j}| + \sqrt{gh_{i,j}}} \quad (3.35)$$

where the Courant number is specified in the range $0 < C_r \leq 1$.

3.1.7 Boundary conditions

Three types of simple boundary conditions are used herein, i.e. open boundary, slip boundary and no-slip boundary conditions (Liang and Borthwick, 2009). The water depth of ghost cell in three conditions is the same and the velocity is different with the change of boundary conditions.

At open boundaries: the velocity component of a ghost cell is just equal to the velocity of its neighbouring cell in both the direction tangential to the wall and the direction normal to the wall.

$$h_g = h_n, u_g = u_n, v_g = v_n \quad (3.36)$$

At slip boundaries: the velocity component normal to the wall is set to zero.

$$h_g = h_n, u_g = -u_n, v_g = v_n \quad (3.37)$$

At Non-slip boundaries: the velocity at the wall cells is set to zero.

$$h_g = h_n, u_g = -u_n, v_g = -v_n \quad (3.38)$$

Here, u_g is the velocity normal to the wall in the ghost cell; v_g is the velocity tangential to the wall in the ghost cell; u_n is the velocity normal to the wall in the cell next to the ghost cell; v_n is the velocity tangential to the wall in the cell next to the ghost cell.

3.2 Particle tracking model

A 2D particle tracking model is developed in this project for producing particle trajectories in flows. The numerical results, which is velocity field data here, from the shallow water model are used as the inputs of the particle tracking model. The motion of particles are achieved by integrating ordinary differential equations.

3.2.1 Governing Equations and its relationship with dynamics system

A dynamics system is a system evolving with the time and could be expressed by:

$$\frac{d\mathbf{x}}{dt} = \dot{\mathbf{x}} = \mathbf{v}(\mathbf{x}, t) \quad (3.39)$$

where \mathbf{x} a real variable representing the state of the system and could be regards as a point with position \mathbf{x} in phase space and $\mathbf{v}(\mathbf{x}, t)$ is the velocity field for the motion of the system with respect to its position and time. And particularly in a two-dimensional shallow water flow, the motion of a fluid particle is the trajectory of a dynamical system with given initial conditions governed by the velocity field and the equation (3.39) is regarded as the advection equation of passive particles in two-dimensional flows:

$$\frac{dx}{dt} = u(x, y, t), \quad \frac{dy}{dt} = v(x, y, t), \quad (3.40)$$

The trajectories of the particles may be obtained by numerically integrating these equations when the particle velocities are available. It is well known from the dynamical systems theory that solutions of (3.40) can be chaotic in the sense of exponential sensitivity to small variations in initial conditions and/or control parameters. This means that even a simple deterministic

velocity field may cause practically unpredictable particle trajectories, a phenomenon known as chaotic advection (Aref, 1984; Khakhar *et al.*, 1986).

In an analytical velocity method, velocity components u and v could be obtained from a stream function governing the whole domain with the current particle position. If the time step is suitable, the particle position of next time step is easily to be calculated with the application of stream function. So the position of this particle could keep updating during the process of chaotic mixing and the particle tracing model runs successfully. If we write down the positions of the particle every m time steps, a particle trajectory will appear to show the motions of this particle under the influence of chaotic advection.

3.2.2 Numerical algorithm for particle advection

The simplest method for particle advection mentioned above is first order Euler's method. And the advection equations (3.39) could be expressed as:

$$\frac{x_{n+1} - x_n}{\Delta t} = u, \quad \frac{y_{n+1} - y_n}{\Delta t} = v, \quad (3.41)$$

which may be then rearranged to update the position of the particle under consideration

$$x_{n+1} = x_n + u\Delta t, \quad y_{n+1} = y_n + v\Delta t, \quad (3.42)$$

where x_{n+1} and y_{n+1} denote the new position of the particle with x_n and y_n representing its position at the previous time step, Δt is the time step, u and v define the particle velocity in the x and y -direction, respectively.

It is a straight-forward method that estimates the next point based on the rate of change at the current point. This method is not commonly used for spatial discretization because it does not take into account the curvature of the solution which makes the estimated next step less accurate compared to an advanced methods, for example the Runge-kutta (RK) method (Press *et al.*, 1992).

The theory of a RK method is same as the Euler's method, but utilizes several predictor and corrector steps over a single time step Δt . A higher order RK method involves slope calculations at these steps at or between the current and next discrete time values. The next value of the dependent variable is calculated by taking a weighted average of these steps based

on a Taylor series approximation of the solution. The weights in this weighted average are derived by solving non-linear algebraic equations which are formed by requiring cancellation of error terms in the Taylor series. In our particle tracking model, the advection equation is solved with a 4th order RK method (Press *et al.*, 1992) and it is illustrated both in the following equations and Figure 3.5:

$$P_{n+1} = P_n + \frac{1}{6} \Delta t (u_1 + 2u_2 + 2u_3 + u_4)$$

$$t_{n+1} = t_n + \Delta t$$

$$u = f(t, P) \tag{3.43}$$

$$u_1 = f(t_n, P_n), u_2 = f(t_n + \frac{\Delta t}{2}, P_n + \frac{\Delta t}{2} u_1)$$

$$u_3 = f(t_n + \frac{\Delta t}{2}, P_n + \frac{\Delta t}{2} u_2), u_4 = f(t_n + \Delta t, P_n + \Delta t u_3)$$

$\mathbf{P}_n(x_n, y_n)$ is the particle position of the current time step and $\mathbf{P}_{n+1}(x_{n+1}, y_{n+1})$ is the particle position of the next time step. u_2, u_3 and u_4 are the predicted velocity vectors corresponding to three intermediate particle positions $\mathbf{P}_n + \frac{1}{2}\Delta t u_1, \mathbf{P}_n + \frac{1}{2}\Delta t u_2$ and $\mathbf{P}_n + \Delta t u_3$, respectively.

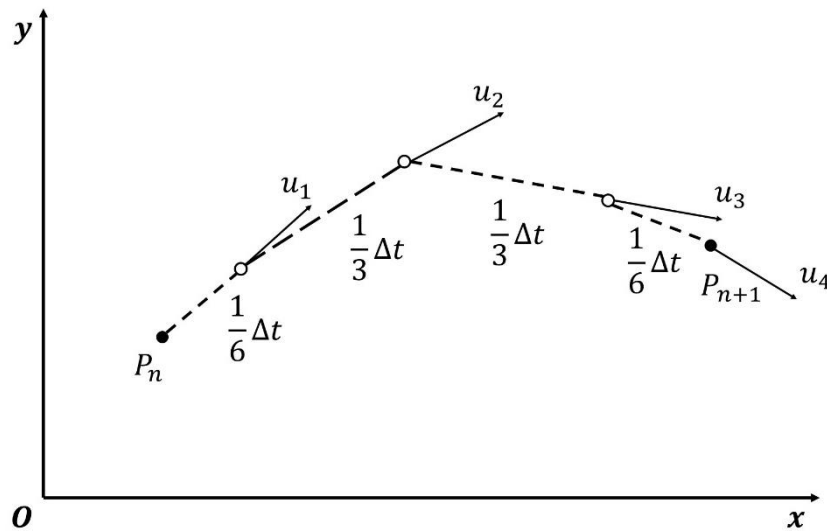


Figure 3.5 A fourth order RK method in space.

3.2.3 Interpolation of velocity data from shallow water model

The advection of a particle requires local velocity information of the point where the particle is located. This is not an obstacle in an analytical model because an analytical model is always governed by analytical equations and one can obtain the information anywhere by solving the analytical equations. While in the shallow water model, the velocity information is discrete due to the numerical solution. This means the velocity information is only located at the central of each hydrodynamic grid and there is no information at the rest of the domain. This situation is not suitable for particle tracking since particles could transport anywhere of domain during the tracking process and this requires the velocity information should cover the whole domain of interest rather than only discrete points. So in the particle tracking model, a bilinear interpolation in space is used to allow particle trajectories to be successfully integrated from the discrete velocity field. This interpolation method is illustrated in the Figure 3.6:

In the Figure 3.6, $C(x_i, y_j)$, $C(x_{i+1}, y_j)$, $C(x_i, y_{j+1})$ and $C(x_{i+1}, y_{j+1})$ represent the centrals of four hydrodynamics grids containing velocity information and $P(x, y)$ is the current position of the particle in an arbitrary time step. The idea of bilinear interpolation is the combine of several linear interpolations in different directions. Though each interpolation is linear, the bilinear interpolation as a whole is nonlinear.

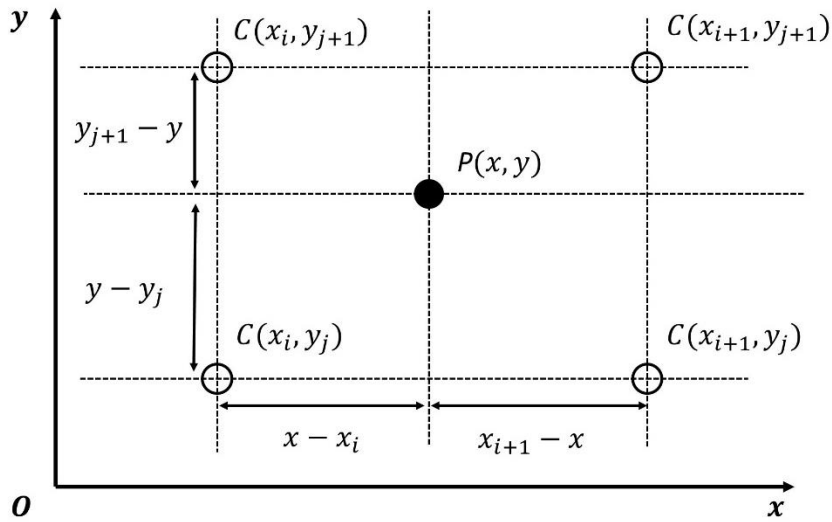


Figure 3.6 Bilinear interpolation for particle information.

A way to write down the solution of bilinear interpolation is

$$f(P(x, y)) \approx k_0 + k_1x + k_2y + k_3xy \quad (3.44)$$

Where the coefficients are obtained by solving the linear matrix system:

$$\begin{bmatrix} 1 & x_i & y_j & x_i y_j \\ 1 & x_i & y_{j+1} & x_i y_{j+1} \\ 1 & x_{i+1} & y_j & x_{i+1} y_j \\ 1 & x_{i+1} & y_{j+1} & x_{i+1} y_{j+1} \end{bmatrix} \begin{bmatrix} k_0 \\ k_1 \\ k_2 \\ k_3 \end{bmatrix} = \begin{bmatrix} f(C(x_i, y_j)) \\ f(C(x_i, y_{j+1})) \\ f(C(x_{i+1}, y_j)) \\ f(C(x_{i+1}, y_{j+1})) \end{bmatrix} \quad (3.45)$$

3.3 Relevant concepts in dynamics systems

3.3.1 Poincaré section

A Poincaré section is a technique invented by Henri Poincaré as a means of simplifying phase space diagrams of complicated systems. The main idea of this technique is to reduce the study of continuous time systems (flows) to the study of an associated discrete time system. It is constructed by viewing the phase space diagram stroboscopically in such a way that the motion is observed periodically. More precisely, one considers a periodic orbit with initial conditions within a section of the space, which leaves that section afterwards, and observes the point at which this orbit first returns to the section. One then creates a map to send the first point to the second, hence the name first recurrence map. The transversely of the Poincaré section means that periodic orbits starting on the subspace flow through it and not parallel to it.

Poincaré section provides two significant properties for the investigation of a dynamical system. First property is the reduction of dimension of the dynamic problem. The construction of a Poincaré section involves the elimination of variables of problem resulting in the study of a lower dimensional problem; second one is the reveal of global property of the dynamic system. Poincaré section provide an insightful and striking display of the global dynamics of a system especially in lower dimensional problems.

In a chaotic mixing flow, the periodic forcing term is time-period flows. And Poincaré sections are produced by plotting the intersections of particle trajectories with the time plane.

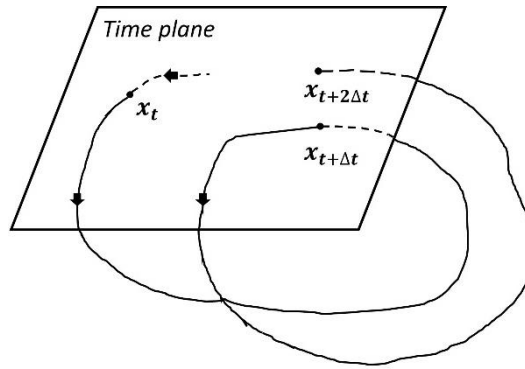


Figure 3.7 An example of Poincaré sections.

3.3.2 Stable/unstable manifolds of hyperbolic points in dynamic systems

Now we consider the dynamic system described by the equation (3.39) again. If a point in the system has the property:

$$v(\mathbf{x}_0, t) = 0 \quad (3.46)$$

Then the state of the system is equilibrium at this point and the point is a fixed point \mathbf{x}_f . A flow or a mapping f could be defined to describe the evolution of a dynamic system:

$$\mathbf{x} = f_t(\mathbf{x}_0) \quad (3.47)$$

Where \mathbf{x} denotes the position of the particle after time t with the initial location \mathbf{x}_0 . And if a particle returns to its initial position \mathbf{x}_0 after k times mapping, we say that the point where the particle initially located is a period point \mathbf{x}_p of period k of a mapping

$$\begin{aligned} f: \mathbf{x} &\longrightarrow f(\mathbf{x}) \\ \mathbf{x}_p &= f^k(\mathbf{x}_p) \end{aligned} \quad (3.48)$$

A periodic point and its associated stable/unstable manifolds are the fatal structures governing the behaviour of a dynamic system (Wiggins, 2013b).

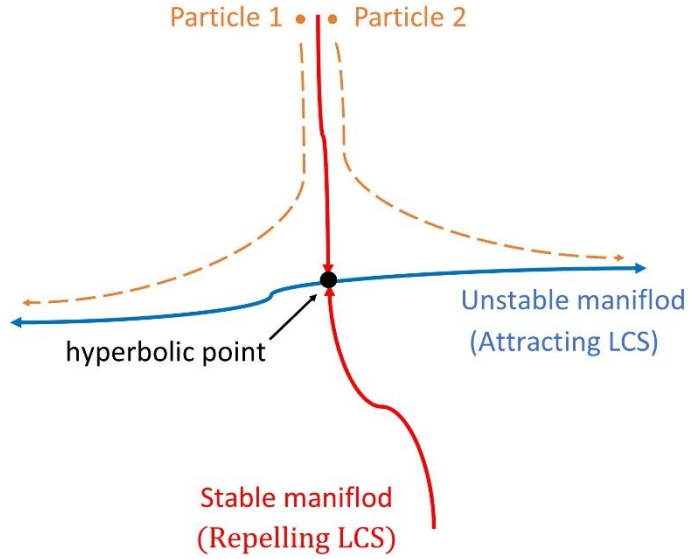


Figure 3.8 Stable/unstable manifolds and the corresponding hyperbolic point.

The transverse intersection of a hyperbolic periodic point is sufficient to produce chaotic behaviour. If the Jacobian of the k times iterated mapping f evaluated at x_p has eigenvalues with non-zero real part, x_p^k is called a k -period hyperbolic point. Now we come to the definition of stable and unstable manifolds of a k -period hyperbolic point (Khakhar *et al.*, 1986):

$$M_k^S(x_p^k) = \{f^{nk}(x) \rightarrow x_p^k \text{ as } k \rightarrow \infty\} \quad (3.49)$$

$$M_k^U(x_p^k) = \{f^{nk}(x) \rightarrow x_p^k \text{ as } k \rightarrow -\infty\}$$

So that if a point belongs to a manifold all its forward and reverse images iterated n times also belong to the manifold. A transverse intersection between the stable and unstable manifold of a periodic point is referred to as a transverse homoclinic point. Transverse intersections between the manifolds of different periodic points are known as transverse heteroclinic points, and we refer to the wild behaviour of the manifolds that results as heteroclinic or homoclinic behaviour. In the case of regular flows, the manifolds join smoothly and none of the above behaviour occurs.

3.3.3 Finite-time Lyapunov exponents and computation technique in 2D flows

Lyapunov exponents are a mathematical tool to describe the characteristics of trajectories dispersion. They are widely used to analysis the chaos in a dynamical system because one of the most important symptoms of chaos is sensitive dependence on initial conditions. The

Lyapunov exponents are positive in a chaotic system where initial close trajectories separate exponentially fast. A simple definition of Lyapunov exponents σ is:

$$\sigma = \lim_{t \rightarrow \infty} \lim_{\delta \mathbf{x}(0) \rightarrow 0} \frac{1}{t} \ln \frac{\delta \mathbf{x}(0)}{\delta \mathbf{x}(t)} \quad (3.50)$$

where $\delta \mathbf{x}(0)$ is the initial perturbation of a trajectory $\mathbf{x}(t; t_0, \mathbf{x}_0)$ and $\delta \mathbf{x}(t)$ is the grown perturbation over the time interval $[0, t]$. The concept of Lyapunov exponents is based on one important assumption that the evolution time of the dynamical system is infinite. This is impossible in the real applications. In other words, the velocity field in fluid dynamics is limited within a finite time interval no matter it is simulated in numerical models or measured in experiments. The Lyapunov exponents could not be defined directly in these situations.

The finite-time Lyapunov exponents (Shadden *et al.*, 2005), which is denoted by $\sigma_t^T(\mathbf{x})$ is a scalar measurement which describes the amount of stretching of the trajectory of point $\mathbf{x}_0 \in D$ from t_0 to t_0+t . Here the open set $D \subset R^2$ since the domain of interest is two-dimensional actual flows. We define a time-dependent velocity field $\mathbf{v}(\mathbf{x}, t)$ on D and a trajectory $\mathbf{x}(t; t_0, \mathbf{x}_0)$ starting at point $\mathbf{x}_0 \in D$. Then the solution of the trajectory is:

$$\frac{d\mathbf{x}(t; t_0, \mathbf{x}_0)}{dt} = \mathbf{v}(\mathbf{x}(t; t_0, \mathbf{x}_0)) \quad (3.51)$$

With the corresponding initial condition:

$$\mathbf{x}(t_0; t_0, \mathbf{x}_0) = \mathbf{x}_0 \quad (3.52)$$

The solution of the dynamical system represented by Eq. can be treated as a flow map which map the particles from initial position \mathbf{x}_0 to final position \mathbf{x}_n over the time interval $[t_0, t_0 + T]$. So the flow map is defined:

$$\phi_{t_0}^t: D \rightarrow D: \mathbf{x}_0 \mapsto \phi_{t_0}^t(\mathbf{x}_0) = \mathbf{x}(t; t_0, \mathbf{x}_0) \quad (3.53)$$

To analysis the amount of perturbation about the trajectories, two points $\mathbf{x}, \mathbf{y} \in D$ are considered and point $\mathbf{y} = \mathbf{x} + \delta \mathbf{x}(0)$ is defined as the perturbed point where $\delta \mathbf{x}(0)$ is the

infinitesimal perturbation and arbitrarily oriented. So the growth of $\delta\mathbf{x}(0)$ in a finite time period T is:

$$\begin{aligned}\delta\mathbf{x}(T) &= \phi_{t_0}^{t+T}(\mathbf{x} + \delta\mathbf{x}(0)) - \phi_{t_0}^{t+T}(\mathbf{x}) \\ &= \frac{d\phi_{t_0}^{t+T}(\mathbf{x})}{d\mathbf{x}} \delta\mathbf{x}(0) + \mathcal{O}(|\delta\mathbf{x}(0)|^2)\end{aligned}\tag{3.54}$$

Where $\frac{d\phi_{t_0}^{t+T}(\mathbf{x})}{d\mathbf{x}}$ is the deformation gradient or Jacobian of the flow map and by ignoring the higher order term, the magnitude of the perturbation is given by

$$\|\delta\mathbf{x}(T)\| = \sqrt{\langle \delta\mathbf{x}(0), \frac{d\phi_{t_0}^{t+T}(\mathbf{x})^*}{d\mathbf{x}} \frac{d\phi_{t_0}^{t+T}(\mathbf{x})}{d\mathbf{x}} \delta\mathbf{x}(0) \rangle}\tag{3.55}$$

Where A^* indicates the transpose of the matrix A and the right Cauchy-Green deformation tensor Δ is defined as:

$$\Delta = \frac{d\phi_{t_0}^{t+T}(\mathbf{x})^*}{d\mathbf{x}} \frac{d\phi_{t_0}^{t+T}(\mathbf{x})}{d\mathbf{x}}\tag{3.56}$$

It should be mentioned that Δ is a time-dependent 2×2 matrix and it is a real symmetric matrix therefore has real eigenvalues. Since the magnitude of linearized stretching is governed by this deformation tensor, the largest eigenvalue of Δ implies the largest stretching in the flow and the corresponding eigenvector shows the direction that this stretching will follow. As it has mentioned above, the eigenvalues of Δ measure the amount of stretching. Finally we define the finite-time Lyapunov exponents using the maximum eigenvalue of the tensor Δ

$$\sigma_{t_0}^T(\mathbf{x}) = \frac{1}{|T|} \ln \sqrt{\lambda_{max}(\Delta)}\tag{3.57}$$

The algorithm for FTLE computation in 2D flows is derived from the advection of passive particles in a finite time interval. Grid with a proper resolution of cells (referred to as the FTLE grid) is used to define the initial locations of passive particles (each cell contains a particle at

its centre). Similar to the discrete velocity data from the shallow water model, FTLE distribution from the particle-tracking model is also discrete, with the resolution determined by the FTLE grid. The particles are advected and the deformation gradient of particles is used to compute the values of FTLEs. To calculate the FTLE field, trajectory of each particle obtained by the particle-tracking model is needed. The discrete numerical velocity field is interpolated in space and time by bilinear interpolation to provide necessary information. To calculate the particle trajectory, a 4th-order Runge-Kutta integration method is used to advect each particle in the FTLE grid. If the initial positions and final positions of particles are defined as $\mathbf{x}_{ij}(t_0)$ and $\mathbf{x}_{ij}(t_1)$ respectively, then the deformation gradient for each particle in FTLE grid can be approximated using central differencing:

$$\left. \frac{d\phi_{t_0}^{t+T}(\mathbf{x})}{d\mathbf{x}} \right|_{\mathbf{x}_{ij}} \approx \begin{bmatrix} \frac{x_{(i+1)j}(t_1) - x_{(i-1)j}(t_1)}{x_{(i+1)j}(t_0) - x_{(i-1)j}(t_0)} & \frac{x_{i(j+1)}(t_1) - x_{i(j-1)}(t_1)}{y_{i(j+1)}(t_0) - y_{i(j-1)}(t_0)} \\ \frac{y_{(i+1)j}(t_1) - y_{(i-1)j}(t_1)}{x_{(i+1)j}(t_0) - x_{(i-1)j}(t_0)} & \frac{y_{i(j+1)}(t_1) - y_{i(j-1)}(t_1)}{y_{i(j+1)}(t_0) - y_{i(j-1)}(t_0)} \end{bmatrix} \quad (3.58)$$

The deformation gradients at all four directions are calculated and the largest singular value (the maximum deformation within the four different directions) is chosen as the FTLE value at $\mathbf{x}_{ij}(t_0)$. This is the algorithm for calculating FTLE in 2D flows. Based on this algorithm, we can obtain FTLE distribution for dynamic flow in 2D cases at a given time instant t_0 .

Since the FTLE method is a Lagrangian approach, the FTLE usually varies as a function of time and space. In the shallow geophysical flow, one typically is interested in the FTLE field, especially how it varies over time and space. The most advantage of FTLE field compared to an instantaneous field such as the velocity field is that the FTLE field measures the average or integrated separation between trajectories. This distinction is important because in time-dependant flow like shallow geophysical flow, an instantaneous field usually is not able to reveal the fake of actual trajectories, that is, instantaneous streamline can quickly diverge from actual particle trajectories. However the FTLE field shows the integrated effect of the flow because it is derived from the Lagrangian approach, and this Lagrangian property makes the FTLE field more indicative in particle behaviour predication and investigation.

3.3.4 *Lagrangian coherent structures*

The concept of Lagrangian coherent structures (LCSs) is derived from the dynamical systems perspective (Haller and Yuan, 2000). So before define the LCSs directly, one should consider

a dynamical system like equation (3.39). It is a time-dependent system and the trajectories in this system are inherently chaotic which means direct integration of particle trajectories is impossible. The key point to investigate the transport and behaviours of trajectories in such systems is hyperbolicity (Mancho *et al.*, 2006; Shadden *et al.*, 2009). Hyperbolic fixed points and their associated stable and unstable manifolds are considered as the organizing structures to describe the mechanics in dynamical systems. Trajectories asymptote to the hyperbolic fixed points by following the stable and unstable manifolds in forward and backward time, respectively. Hence these structures of hyperbolic points separate the regions of different dynamics and behave as the skeletons of the flow systems.

For a 2D steady flow, there is no chaos because the flow is integrable. The hyperbolic point is a stagnation point and no homoclinic tangle (the interaction of stable and unstable manifolds of the same hyperbolic point) exists. If a small periodic perturbation is added to the 2D steady flow, then the flow becomes a time-periodic system, for example, the blinking-vortex flow. Hyperbolic points start to move periodically since the change of velocity and hyperbolic trajectories appears. The stable and unstable manifolds of the new hyperbolic trajectories begin to interact with each other and create homoclinic tangle, which is the core of chaos (Schuster and Grigoriev, 2012). Although the flow velocity is simple and deterministic, the effect of homoclinic tangle tear apart nearby trajectories to have very complicated behaviours (Khakhar *et al.*, 1986).

In practical applications such as geophysical flows, the systems are always more complicated and it is very difficult to identify those invariant manifolds mentioned above in temporally aperiodic systems. Although it is a still challenge to define hyperbolic points and their stable and unstable manifolds in such aperiodic systems, special structures, always revealed by fluid parcels in nature or experiments, which have the ability to attracting or repelling particles like invariant manifolds do exist in these systems. These special structures, or special material surfaces (Haller, 2011), are regarded as Lagrangian coherent structures. In other words, LCSs are often locally the most strongly attracting or repelling material surfaces in the flow. In two-dimensional flows, LCSs are material lines depicting the hyperbolic regions in these flows and referred as the transport barriers.

A more quantitative and mathematical definition of LCS is given by Shadden *et al.* (2005) with the application of the FTLE scalar field $\sigma_{t_0}^T(\mathbf{x})$. A Lagrangian Coherent Structure (LCS) is a local maximizing ridge of $\sigma_{t_0}^T(\mathbf{x})$. To make this definition more clearly, the curvature of the field $\sigma_{t_0}^T(\mathbf{x})$ is introduced by using the Hessian matrix Σ :

$$\Sigma = \nabla^2 \sigma_{t_0}^T(\mathbf{x}) \quad (3.59)$$

Here Σ is a real symmetric matrix and has real eigenvalues and orthogonal eigenvectors. Let λ_n be the smallest eigenvalue and \mathbf{n} be the corresponding eigenvector. Then the LCS is defined to be the set of all points in the field satisfying the following conditions:

$$\begin{aligned} \mathbf{C1.} \lambda_n < 0 \\ \mathbf{C2.} \nabla \sigma_{t_0}^T(\mathbf{x}) \cdot \mathbf{n} = 0 \end{aligned} \quad (3.60)$$

It is clear that LCSs defined in this way can reveal an underlying flow structure in two-dimensional time-dependent flows which is not typical evident from the Eulerian version of velocity field. Also the LCSs derived from this definition will be very sharp in the following examples which indicate that the mechanics of separation in these systems is the concentration to LCSs rather than a randomly diffusion.

3.4 Model validation

There are two models requiring validation here—the shallow water model and particle tracking model. For the shallow water model, the turbulent term and wind term need to be validated. For the particle tracking model, the RK method, bilinear interpolation and the method of FTLE computation need to be validated.

Three different cases are used for the validation of shallow water model. Jet-force flow case and backward step case are used for validating the turbulence term and its eddy viscosity parameter. The third case, wind induced shallow lake, validate both the wind term and turbulent term since wind is the driven force of the lake. Two benchmark cases are used for the validation of particle tracking model. Blink-vortex flow is used for validate whether the model is reasonable to describe the chaotic system. The Kranenbugh's lake is used to validate the method of FTLE computation.

3.4.1 *Jet-force flow*

A useful case to test the performance of the turbulence model is Jet-force flow in a circular reservoir. The key point of this case is that the boundary of the whole domain including two conditions—rectangular and curved condition. It is very complicated to discretize the

computational domain with uniform meshes. The same test has already been studied other researchers (Anastasiou and Chan, 1997; Rogers *et al.*, 2001). The bed friction is set to be zero and choose eddy viscosity coefficient ν_t to be 0.00078 directly. While in our jet-force flow case, the Manning coefficient of the bed is 0.025 and ν_t is calculated from equation (3.27) in which p_{ν_t} should be validated with different values. 24000 uniform rectangular cells are used for this computational domain. The velocity distribution and streamlines of steady flow are shown in Figure 3.9. As suggested by Fisher, the range of p_{ν_t} for curved or irregular boundaries should from 0.85 to 3.4. Hence the values of p_{ν_t} here are chosen as 0.85, 1.7 and 3.4. When $p_{\nu_t} = 0.85$, the separation of flow from the inlet is not obvious and the through-flow which from inlet towards outlet by passing the whole reservoir is splinted by two symmetric water drop-shaped vortices. As p_{ν_t} increases, in other words, the effect of eddy viscosity increases, vortices begin to separate to north and south bound of the reservoir, respectively and the centres of vortices move to the rest of the reservoir. When $p_{\nu_t} = 3.4$, the velocity distribution and streamlines are almost the same as those produced by other researchers.

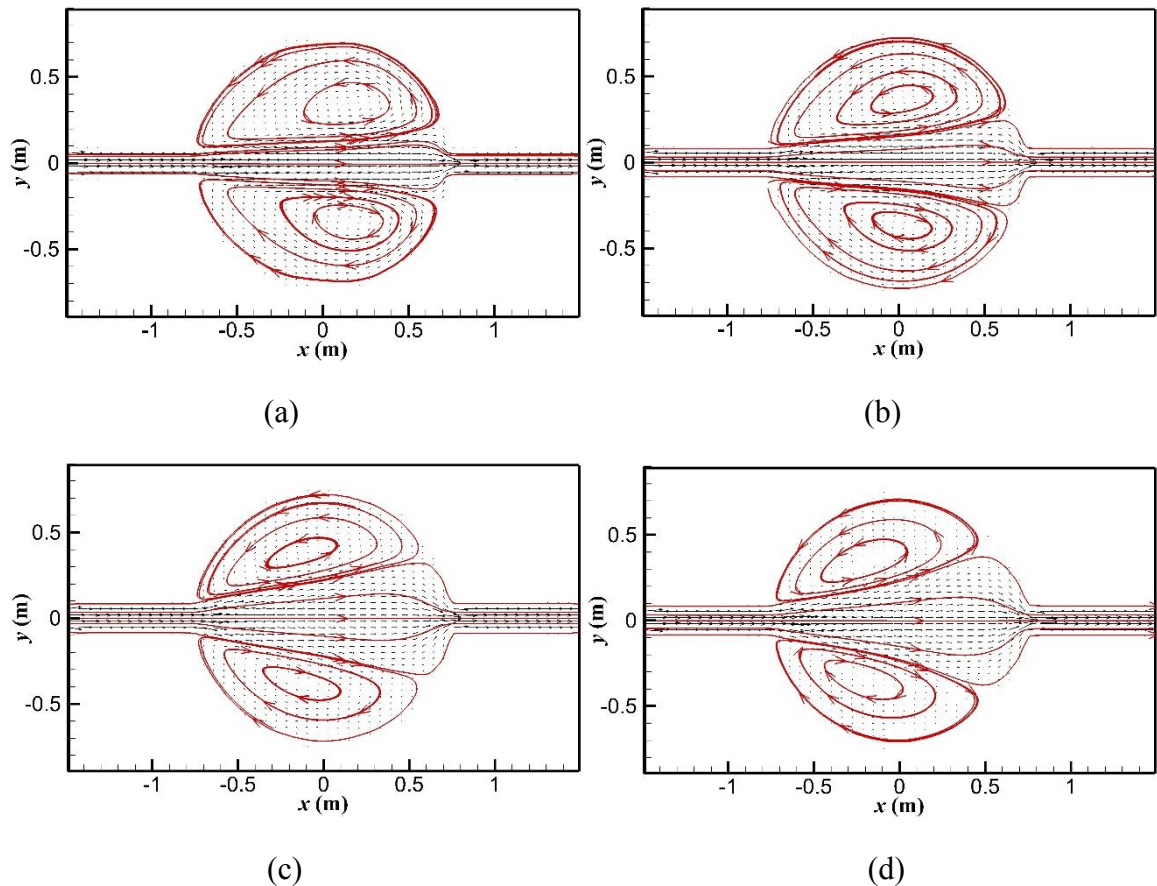


Figure 3.9 velocity distribution and streamlines of jet-force case: (a) $p_{\nu_t} = 0.85$; (b) $p_{\nu_t} = 1.7$; (c) $p_{\nu_t} = 3.4$; (d) Roger's condition.

3.4.2 Backward step case

The backward step case is made up by two horizontal flat channels. A narrow channel is connected to a wide channel directly and this forms an abrupt expansion. The geometry of the case is shown in Figure 3.10. For numerical modelling, the input/output conditions are same as those applied by Fe *et al.* (2009) and no-slip wall condition is used. The Manning coefficient is 0.01 and grid cell is 0.02012m. The total computational domain consist of 5625 cells.

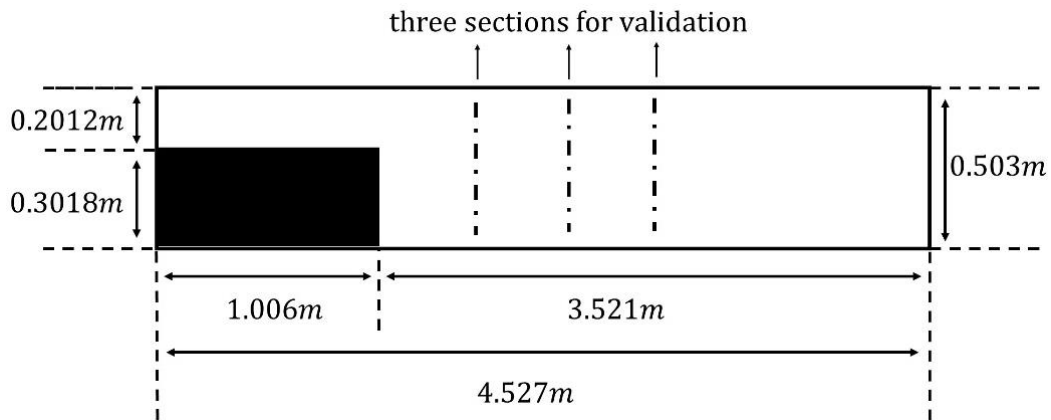
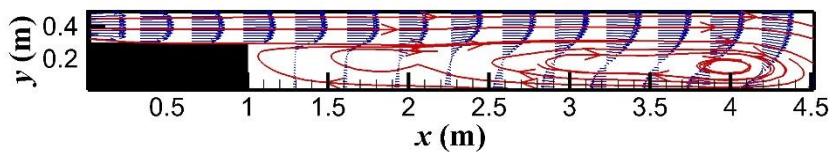
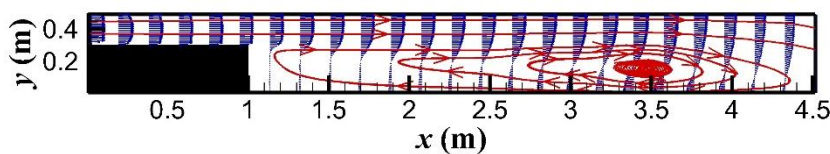


Figure 3.10 backward step geometry.

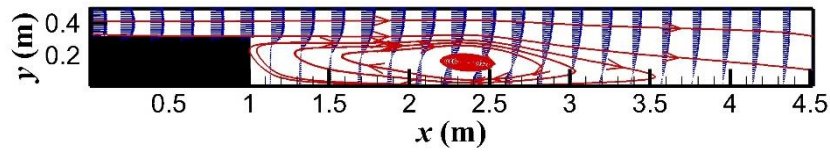
From Figure 3.11(a), it is obvious that although the eddy is reproduced after the step in a steady situation, the length of the eddy is too long compared to the experimental results. And the eddy contains two small clockwise vortices while there is only one bigger vortex in the experiments. In Figure 3.11(b), the results become better as p_{vt} increases. Two vortices get close to each other and partly merge to create a larger one. And the position of the centre of the vortex is moving upstream towards the step. When $p_{vt} = 0.54$ as shown in Figure 3.11(c), only one vortex exist and the streamlines are already very close to the experimental results. Roger's approximation of eddy viscosity coefficient value is still reasonable in this case as shown in Figure 3.11(d). For comparison purpose, Fe's experimental results is shown in Figure 3.11(e).



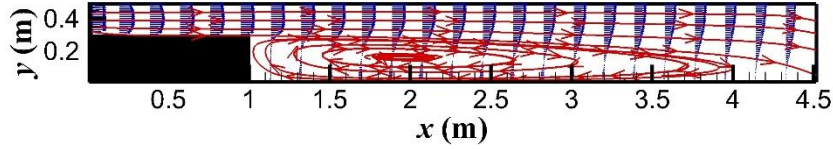
(a)



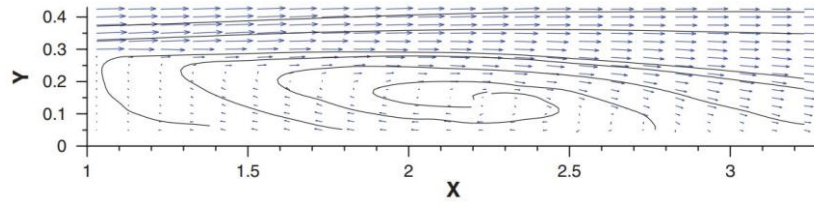
(b)



(c)



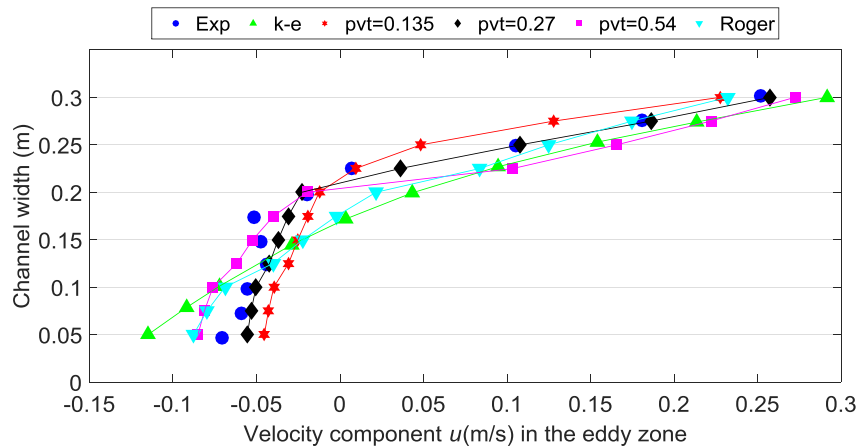
(d)



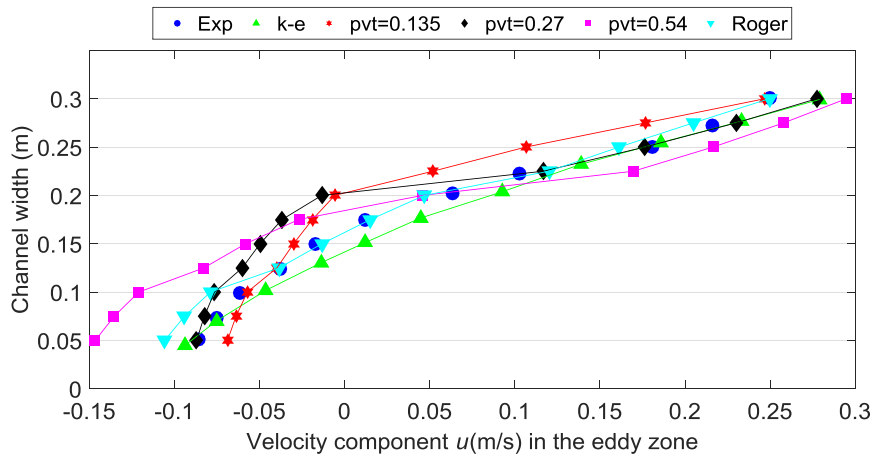
(e)

Figure 3.11 velocity distribution and streamlines of backward step case: (a) $p_{vt} = 0.135$; (b) $p_{vt} = 0.27$; (c) $p_{vt} = 0.54$; (d) Roger's condition; (e) Fe's experimental result.

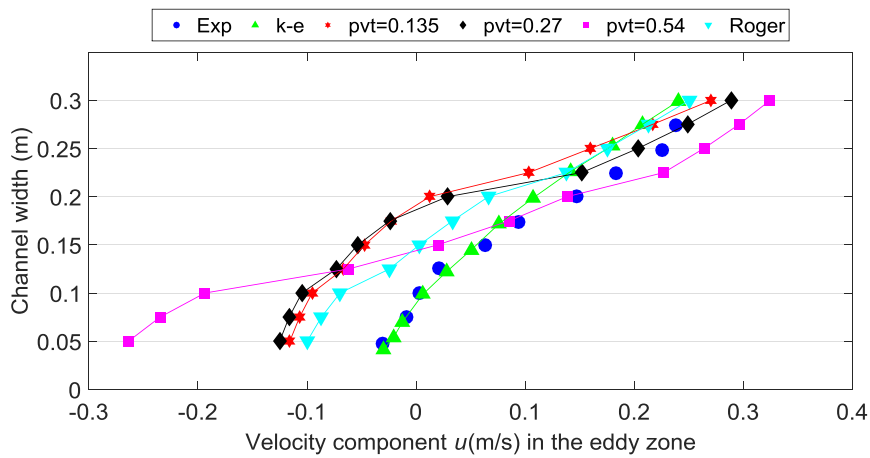
Figure 3.12(a-c) compares the velocity component u from Fe's experimental data with the numerical results from the algebraic turbulent model and a more advanced model-- $k-\varepsilon$ model at three different sections in the eddy zone. At the first section $x=1.53\text{m}$, the results from the algebraic turbulent model using small value of p_{vt} is much more similar with the experimental measurements than those from the $k-\varepsilon$ model. Both the result from the algebraic turbulent models and the $k-\varepsilon$ model is lower than experimental results at the centre of the eddy. It seems that these turbulence models are not able to wonderfully simulate the complicated situation at the centre of the eddy.



(a)



(b)



(c)

Figure 3.12 Velocity component u in three different sections in the eddy zone: (a) $x=1.53\text{m}$; (b) $x=2.03\text{m}$; (c) $x=2.53\text{m}$.

At the section $x = 2.03\text{m}$ and $x = 2.53\text{m}$, the absolute value of simulated velocity from algebraic turbulent model near the lower wall boundary are slightly larger than that from $k-\varepsilon$ model and experimental measures. Because the wall boundary conditions are different in the algebraic turbulent model and $k-\varepsilon$ model. The sample boundary conditions used by algebraic turbulent model are not very suitable for flows close to a solid wall. Also as y increases, the results of algebraic turbulent model are lower than the experimental data while those results from the $k-\varepsilon$ model are higher than the experimental ones. This may be because the left side of the eddy is more influenced by the main flow which make this area is more difficult to be predicted by numerical methods. Consider the results shown in Figure 3.11 and Figure 3.12, the most appropriate value of p_{vt} for this simulation is 0.54.

3.4.3 Wind-induced shallow lake

Surface stress such as wind could be the major source of momentum in lakes. Here a shallow lake is chosen to test the wind stress term in the shallow water model. To compare the numerical solutions with the analytical solutions obtained by Kranenburg (1992), the bathymetry of this shallow lake is set to be the same as Kranenburg's lake in which the still water depth h_k is a function of radial distance from the centre of the lake:

$$h_k = H(1/2 + \sqrt{(1/2 - 1/2 * (r/R))}) \quad (3.61)$$

where H is a weighted mean water depth and set to 0.5m; R is the radius of the lake and set to 120m; r is the distance from the centre of the lake.

The computational domain of the shallow lake is consisted of 176400 uniform cells with cell size is 0.6m. Water is initially rest in the lake and water depth is given by equation (3.61). Wind stress τ_w with a magnitude of 0.002N/m^2 is uniformly distributed all over the domain and starts its action at $t = 0\text{s}$. Gravitational acceleration g is set to 9.81m/s^2 and water density ρ is set to 1000kg/m^3 . Bed stresses are obtained from equation (3.4) and the bed roughness coefficient C_f can be evaluated by (Liang *et al.*, 2006a)

$$C_f = \left[\frac{\kappa}{1 + \ln(z_0/h)} \right]^2 \quad (3.62)$$

where $\kappa = 0.4$ is the Von Karman constant and $z_0 = 0.0028\text{m}$ is the roughness height of the bed. Wind stress is added from north-west direction and the streamlines of two gyres as a symbol of steady situation is obtained after eight hours simulation. The velocity field and streamlines are illustrated in Figure 3.13. The numerical solution of wind-induced shallow lake is very close to the analytical solution. Since the wind stress is uniformly working all over the lake surface, the depth-averaged velocities are directed against the wind force in deep parts of the lake, and with the wind in shallow parts. The main difference of these two solutions is the position of the gyre centres. Two gyre fully are symmetric in analytical solution while they are not in the numerical solution. In numerical solution, the gyre slightly separate towards the lake boundary at north-west area where the wind comes from.

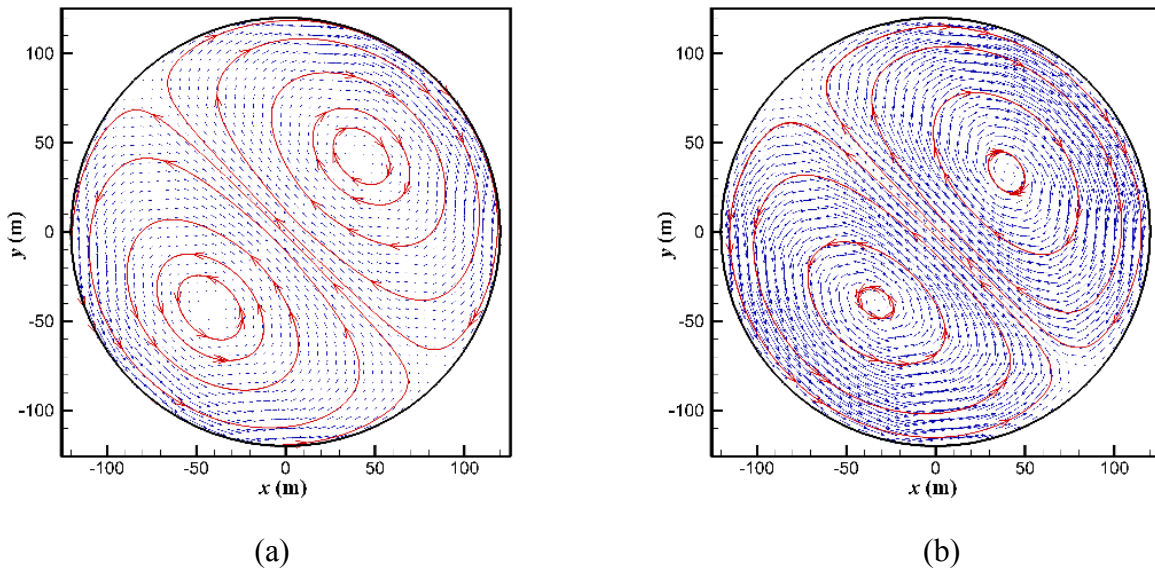


Figure 3.13 Velocity distribution and streamlines corresponding to constant northwest wind: (a) analytical solution; (b) numerical solution.

The parameter of eddy viscosity coefficient p_{vt} is chosen differently to analysis the effect of turbulence on the magnitude of velocity profile. The normalized depth-averaged velocity profile is given by $v_{pro} = \kappa U / ((u_* \ln(H/z_0)))$ where $U = (u + v) / \sqrt{2}$, u_* is the friction velocity and the analytical solution of $U = u_*(h/H - 1) \ln(H/z_0) / \kappa$.

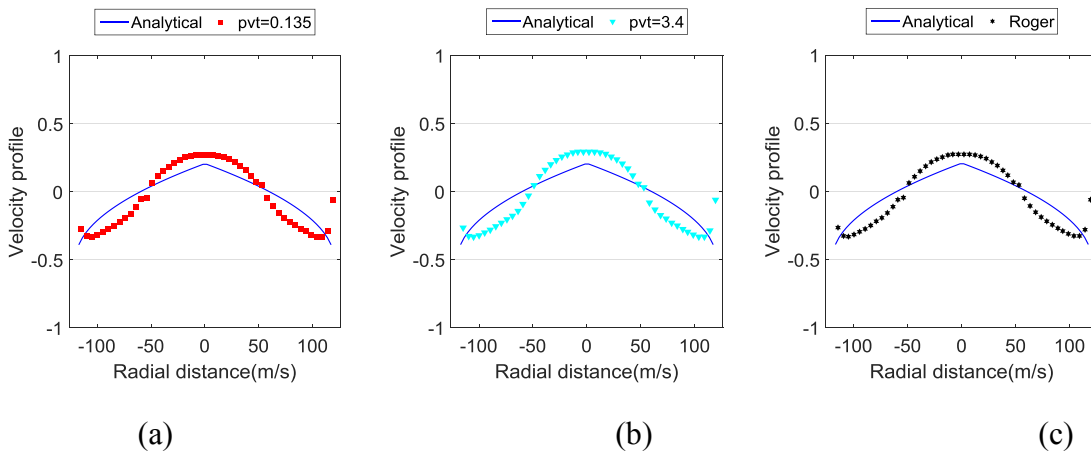


Figure 3.14 Normalized depth-averaged velocity profile in the radial plane normal to the wind direction corresponding to constant northwest wind: (a) $p_{vt} = 0.135$; (b) $p_{vt} = 3.4$; (c) Roger's condition.

Figure 3.14 illustrates that the change of p_{vt} value does not have obvious influence on the distribution of numerical velocity profile in the radial plane which is normal to wind direction. Even the eddy viscosity coefficient regard as a simple constant all over the lake, the result remains the same. This means the effect of turbulence on velocity could be ignored compared to the effect of wind force in this shallow lake. The numerical velocity profile is in close agreement with the analytical velocity profile (Liang *et al.*, 2006a). However, due to the poor

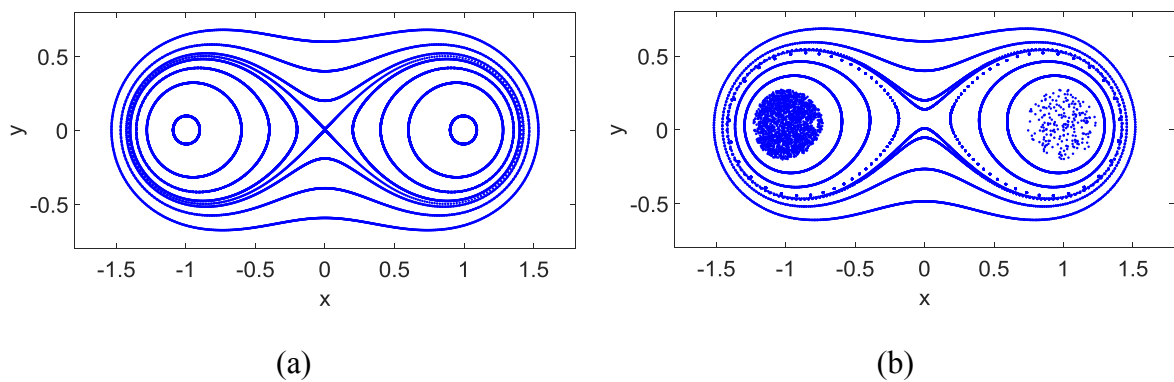
performance of uniform grids on curved boundary, the numerical velocity profile increase abruptly and irregularly near the lake boundary.

3.4.4 *Blinking-vortex flow*

BV flow involves two agitators located in a suitable distance to represent two point vortices that are turned “on” and “off” respectively with a fixed period “ T ” (Aref, 1984). Although the flows created by the agitators are essentially very simple and not turbulent, the particles trajectories became very complicated and unpredictable and showed the existence of chaotic advection. Herein μ_{BV} is parameter representing the flow strength and could be described as:

$$\mu_{BV} = \frac{\Gamma T}{4\pi a^2} \quad (3.63)$$

where Γ denotes the strength of the vortex and T is the period, a represents the half distance between the two vortices. Twelve particles initially locating at the different positions of x -axis are tracked for 2000 periods to make Poincaré Sections. The chaotic properties of Blinking-vortex systems with different μ is shown in Figure 3.15. The flow strength μ_{BV} starts with the value of 0.01 as shown in Figure 3.15(a). There is no chaos in the flow and all particles travel regularly around the two vortices. At $\mu_{BV} = 0.15$, only the point vortices area is chaotic while other particles show regular trajectories. With the increasing of μ , the chaotic region becomes larger and larger from the centres of each vortex to the boundary of the domain. When $\mu_{BV} = 0.40$, only the particles locating at outmost still remains regular behaviours and it can predicate that the chaotic mixing area will continue to grow with the influence of a stronger flow strength μ_{BV} . The results from the particle tracking model are extremely similar with those from other researchers (Aref, 1984; Ottino, 1989).



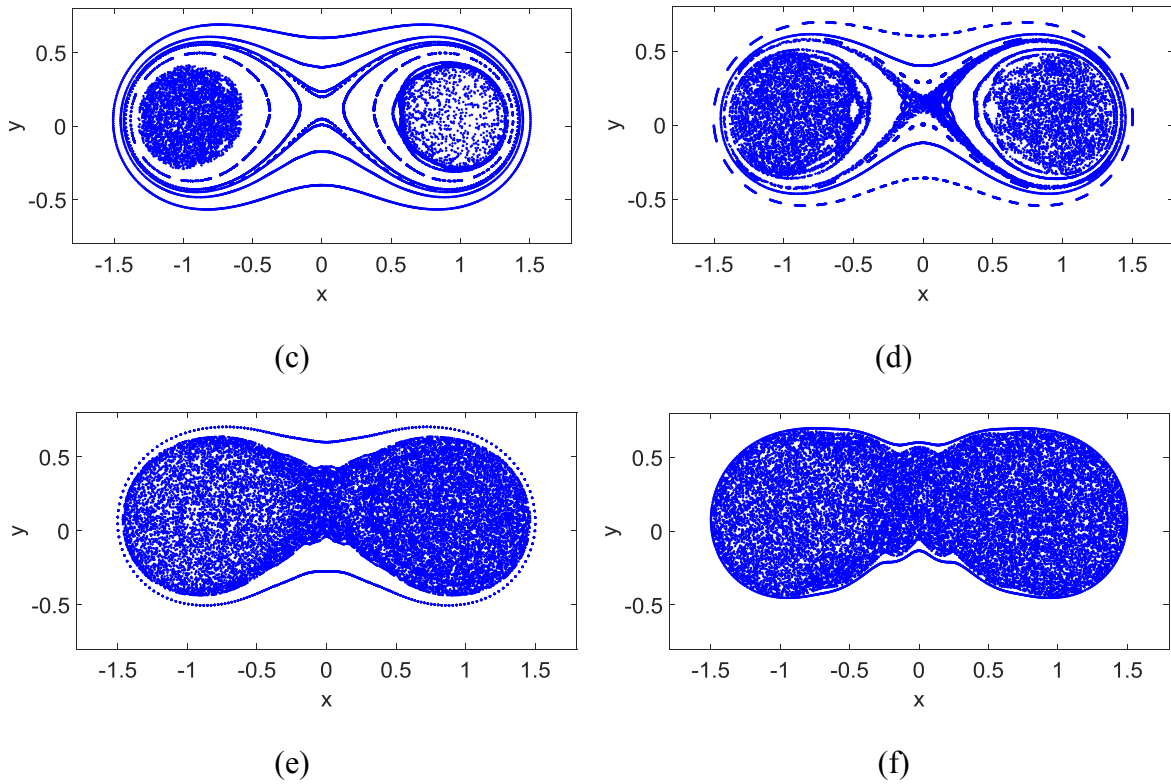
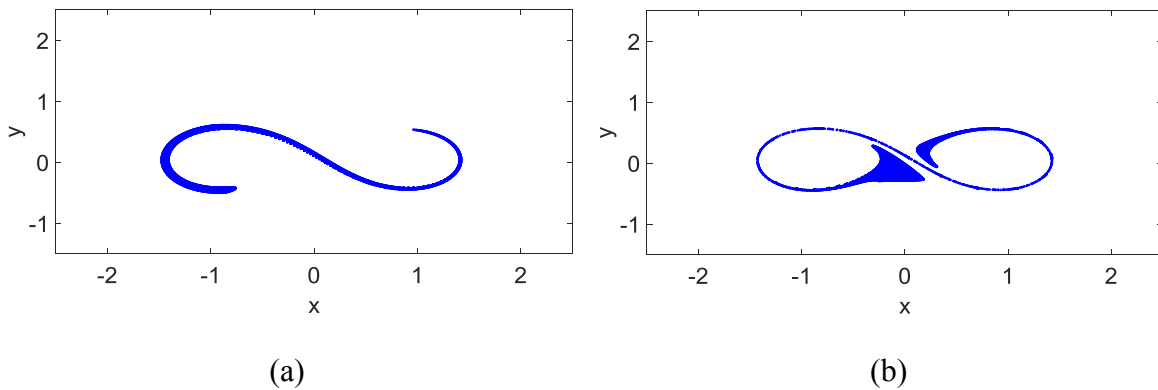


Figure 3.15 Poincaré Sections of BV flows with different flow strength: (a) $\mu_{BV} = 0.01$; (b) $\mu_{BV} = 0.15$; (c) $\mu_{BV} = 0.25$; (d) $\mu_{BV} = 0.30$; (e) $\mu_{BV} = 0.40$; (f) $\mu_{BV} = 0.50$.

To investigate chaotic advection of BV system, a square patch of particles consisting 10000 particles are released at $t = 0$. The square has a side length 0.5 and is located between two vortices with a central of $(0, 0.25)$.

When $\mu_{BV} = 0.25$ as shown in Figure 3.16, the patch begin to stretch from its initial condition to form a particle band and attracted by two vortex. Although the patch have already stirred to a very thin band roughly cover the whole area since $t = 10T$, the particles never travel into the centre area of two vortices which is shown as a chaotic mixing area in Figure 3.15(c). The limitations of particle behaviour proves that particles are trapped by the transport barriers made up by KAM tori (Aref, 1984) and do not mix efficiently even for a very long time ($t = 30T$).



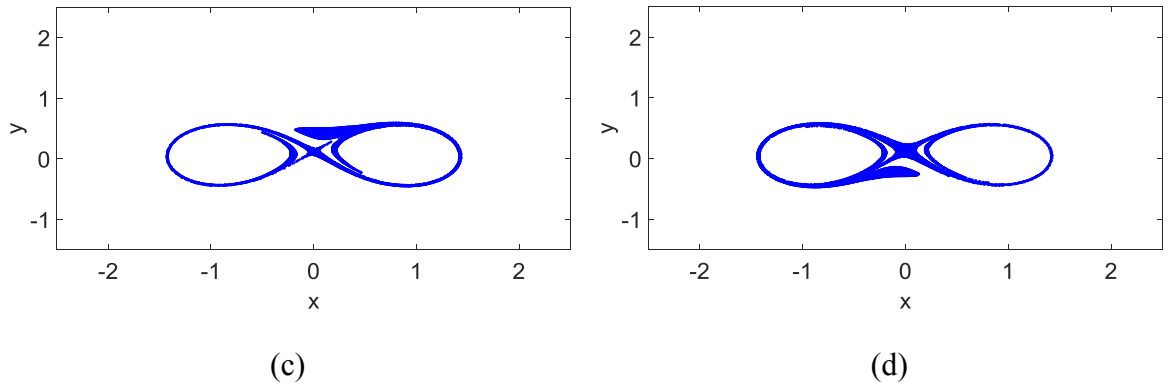


Figure 3.16 Advection of a particle patch with $\mu_{BV} = 0.25$ (a) $5T$; (b) $10T$; (c) $20T$; (d) $30T$.

The situation is quite different in Figure 3.17 where $\mu_{BV} = 0.75$. Within only first five periods, the patch wiggles insanely following the unstable manifolds of the BV system and create a very complicated structure. As μ_{BV} increases, KAM tori breaks into chains of small islands constructed by trajectories of period points and further disappeared. Without limitation of these transport barriers, particles evolve rapidly and finally wonder throughout an extended region. At $t = 30T$, almost the whole area are occupied by particles showing a high mixing properties of the system.

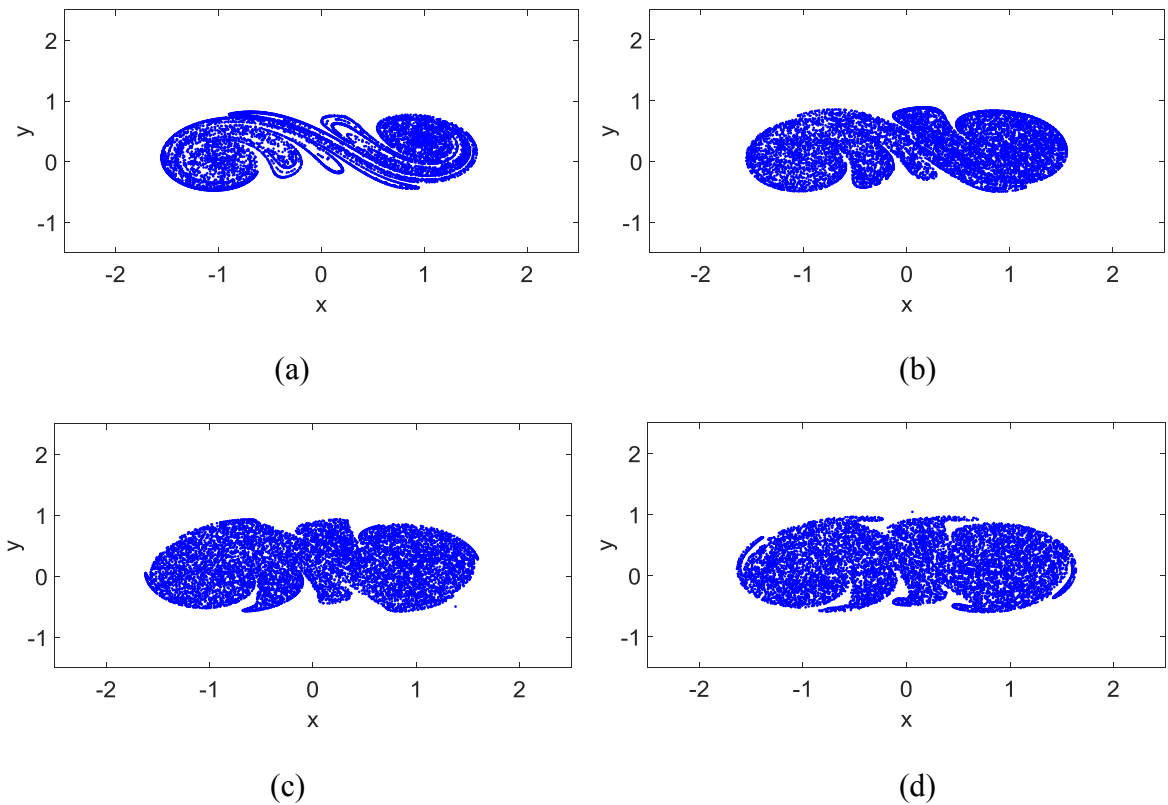


Figure 3.17 Advection of a particle patch with $\mu_{BV} = 0.75$ (a) $5T$; (b) $10T$; (c) $20T$; (d) $30T$.

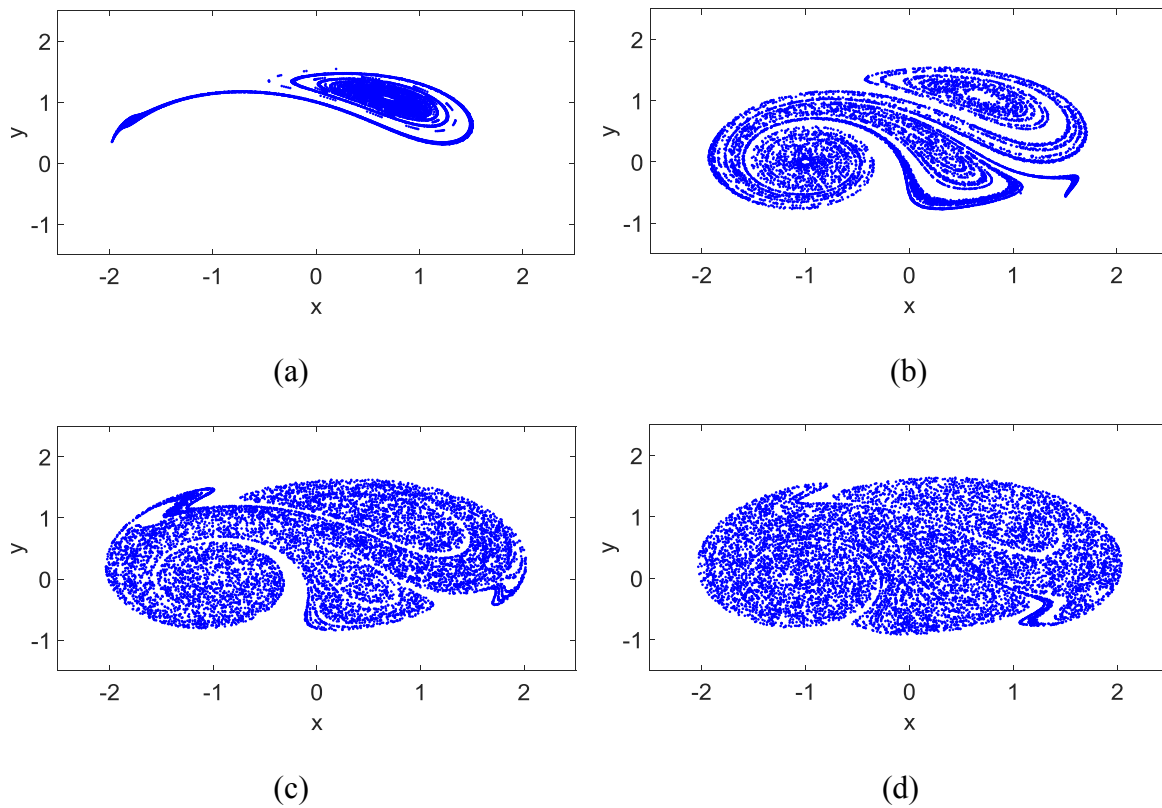


Figure 3.18 Advection of a particle patch with $\mu_{BV} = 2.25$ (a) $2T$; (b) $4T$; (c) $6T$; (d) $8T$.

Figure 3.18 illustrates the fate of same patch when a larger perturbation ($\mu_{BV} = 2.25$) is added to the system. First patch is stretched and swirled to the left and form a spiral upon the right vortex. Then particles travel to the right through a trajectories curve and create a larger spiral at the centre area of the left vortex. The rapid and complicated behaviour of particles shows a fully chaotic mixing in BV flows. Compare to the results in Figure 3.17, a bigger region is occupied by the particles which means chaotic advection in BV flows becomes more global on the influence of larger perturbations.

3.4.5 Chaotic properties of Kranenburg’s lake

In this project, particle tracking model will be used in real nature cases where no analytical solution exist. In other words, the particle tracking model should be proved to successfully deal with discretised velocity data from a numerical model (shallow water model). This is the so-called offline scheme in which flow information such as depth-averaged velocity field is obtained in advance and no velocity computation is involved during the particle tracking process. For this purpose, the particle tracking model are validated in two different solutions—analytical solution and semi-numerical solution. The ‘semi’ means that the velocity field is derived from analytical functions though it is discretised later. The process of semi-numerical solution is could be illustrated by three steps:

- A. Continuous velocity field from the analytical solution is discretized with finite resolution (Here is 420×420), which is known as the discretised analytical velocity field.
- B. The two discretised analytical velocity field corresponding to wind of two directions are outputted and then reloaded as discretised steady velocity field.
- C. The bilinear interpolation is used to interpolate the discretised steady velocity field to obtain the velocity information where the particle located in the particle tracking process.

In the analytical solution given by Kranenburg (1992), the hydrodynamics of the shallow lake is governed by a stream function ψ . And the velocity equations obtained from ψ are:

$$u = \frac{B}{h} \left(1 - \frac{x^2 + 2y^2}{R\sqrt{x^2 + y^2}}\right) \quad (3.64)$$

$$v = \frac{Bxy}{hR\sqrt{x^2 + y^2}}$$

Where B is a constant, h is the water depth of point (x, y) and R is the horizontal distance from the centre of the lake to the point. All the other parameters are identical to the previous case of wind-induced shallow lake.

To make the dynamics of the lake become a non-integrable system which are capable of chaotic behaviour, wind stress field with constant intensity change periodically in north-east and north-west directions every half T . And it is assumed that the velocity field adapts to wind stress instantaneously. Hence the whole velocity system is consisting of two steady velocity conditions governed by wind from two directions. This alternative and periodic velocity field evolution creates a sample dynamics system describing by a single parameter relating to the storm duration t_w . The parameter μ_k is defined as (Kranenburg, 1992):

$$\mu_k = \frac{\ln(H/z_0) u_*}{8\kappa R_0} \quad (3.65)$$

Poincaré section is applied to investigate complicated particles trajectories by observing several special particles at regular time intervals. Here we observe 10 particles released at x-axis at the end of each period time T . To get the Poincare section of these particles, $500T$ are needed.

Figure 3.19 shows the Poincaré section of the 10 particles released with the application of different values of μ_k . The plots shown in Figure 3.19 are symmetric because of the symmetry of the wind force and the velocity fields. It is clear that three particles—red, dark green and pink respectively in Figure 3.19(a) go through in the middle of the lake in the direction from north to south. Also they travel along the boundary of the lake and their trajectories become very complicated. Trajectories of other particles make two large islands at either side of those three trajectories. Two period-one elliptic points are located at the centre of each island, respectively. And elliptic points are surrounded by chains of higher-order periodic islands indicating the regular regions. These chains have the function of preventing the exchange between regular and chaotic area. So there are no chaotic trajectories inside the two inlands and no other colours' trajectories outside the chains. The dynamics skeleton of the mentioned particle behaviours could be explained with Figure 3.19(b) and Figure 3.19(c). The highest FTLE both in time forward and backward direction in Figure 3.19(b) and Figure 3.19(c) can be regard as the ridges of the FTLE field and these ridges are analogue to the stable and unstable manifolds of hyperbolic trajectories in dynamic systems. These stable and unstable manifolds only located around the only diameter from north to south. So the chaotic behaviour of particles only appears at a very narrow area where the stable and unstable manifolds intersects. In other words, the three particles behave chaotic only because they are initially located in the area which governed by the stable and unstable manifolds of the hyperbolic trajectories. Another important property of these manifolds is that they are the transport barriers of particles and separate the whole lake into areas with different dynamics. So particles in Figure 3.19(a) have totally different behaviour and are limited in one area forever.

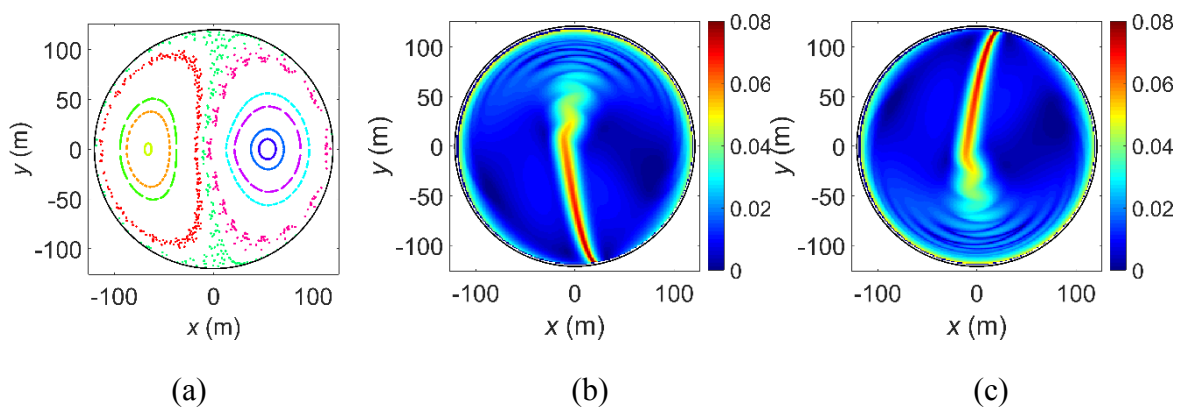


Figure 3.19 dynamics property of analytical solution when $\mu_k = 0.14$ (a) Poincaré section; (b) backward FTLE; (c) forward FTLE.

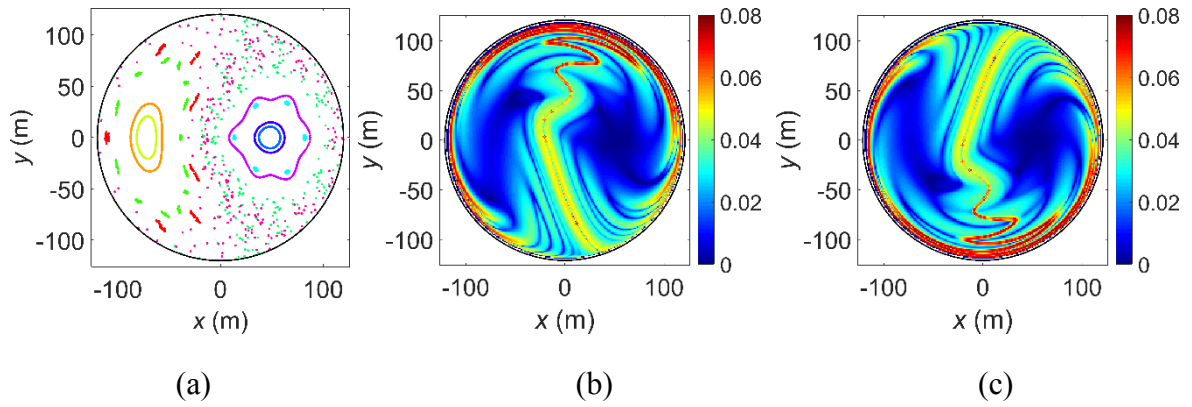


Figure 3.20 dynamics property of analytical solution when $\mu_k = 0.28$ (a) Poincaré section; (b) backward FTLE; (c) forward FTLE.

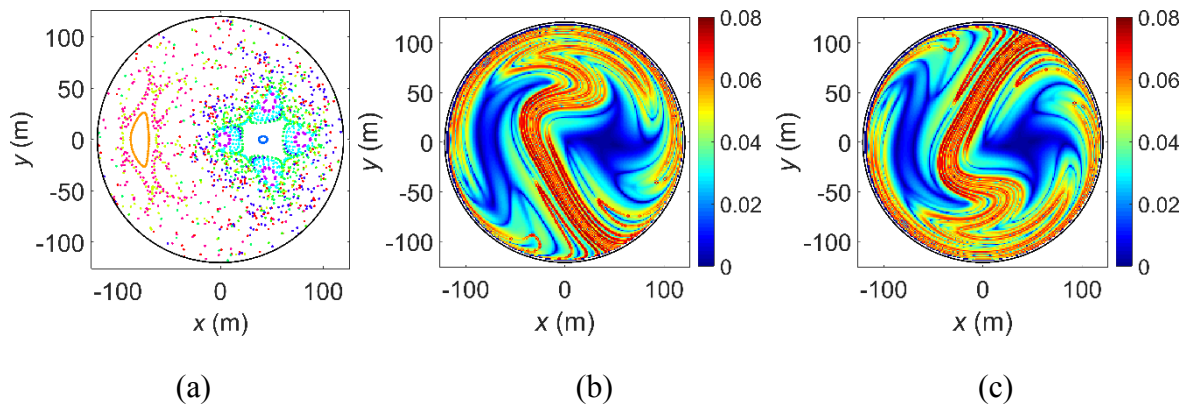


Figure 3.21 dynamics property of analytical solution when $\mu_k = 0.42$ (a) Poincaré section; (b) backward FTLE; (c) forward FTLE.

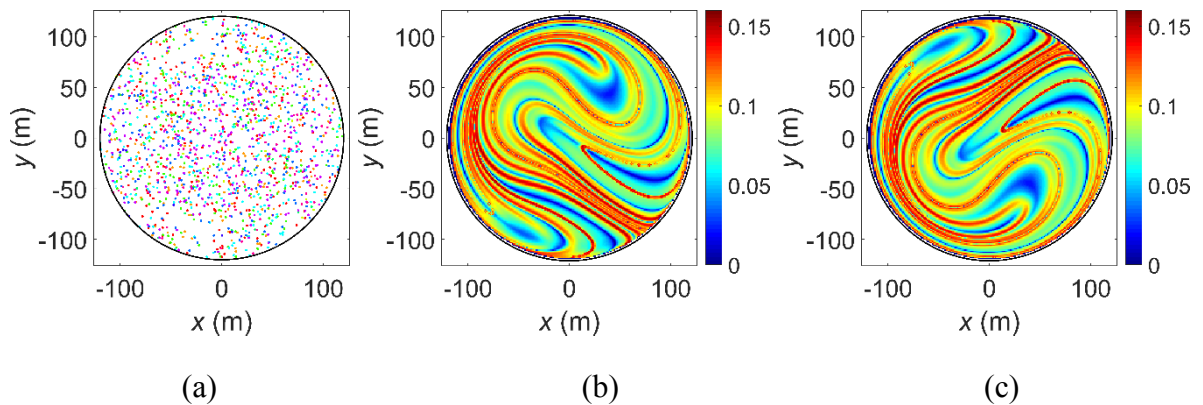


Figure 3.22 dynamics property of analytical solution when $\mu_k = 0.84$ (a) Poincaré section; (b) backward FTLE; (c) forward FTLE.

Figure 3.20 and Figure 3.21 illustrate the situation when the μ_k is equal to 0.28 and 0.42, respectively. More particles involves in chaotic behaviour and only high order period of islands still remains. FTLE field show that the filamentary structures become more complicated and they keep stretching in several special directions. More areas are controlled by the stable and unstable manifolds and the chaotic area begin to erode the regular motion area step by step.

As shown in Figure 3.22 where $\mu_k=0.84$, the period-one points are ruined. The regular areas become smaller and smaller and finally disappeared. Particles of different colours can be seen everywhere in the lake indicating that the different particles can go through freely around the lake with help of chaotic mixing and now the whole lake is well mixed. This means that the domain is fully filled with strong chaotic mixing areas. Although Poincaré sections show that the domain reaches a totally chaotic stage when μ_k is 0.84, but FTLE field tells us that there are still some weak mixing area existing which is predicated by the Kolmogorov-Arnold-Moser (KAM) theorem. The KAM theory indicates that regular regions comes into infinitely scales if the perturbation (Here is μ_k) is larger enough but these regular regions will not totally disappeared.

To investigate the different kinds of particles motion in different areas, two circles of particles are released simultaneously (each circle is consist of 5000 particles and has a radius of 1m). Here we take $\mu_k = 0.28$ for example. The blue one is centred at (-50, 0) (a weak mixing area in Figure 3.22) and the red one is centred at (0, 50) (a strong mixing area in Figure 3.22. Figure 3.23 shows the positions of the particle circles at $t = 0, 8T, 16T$.

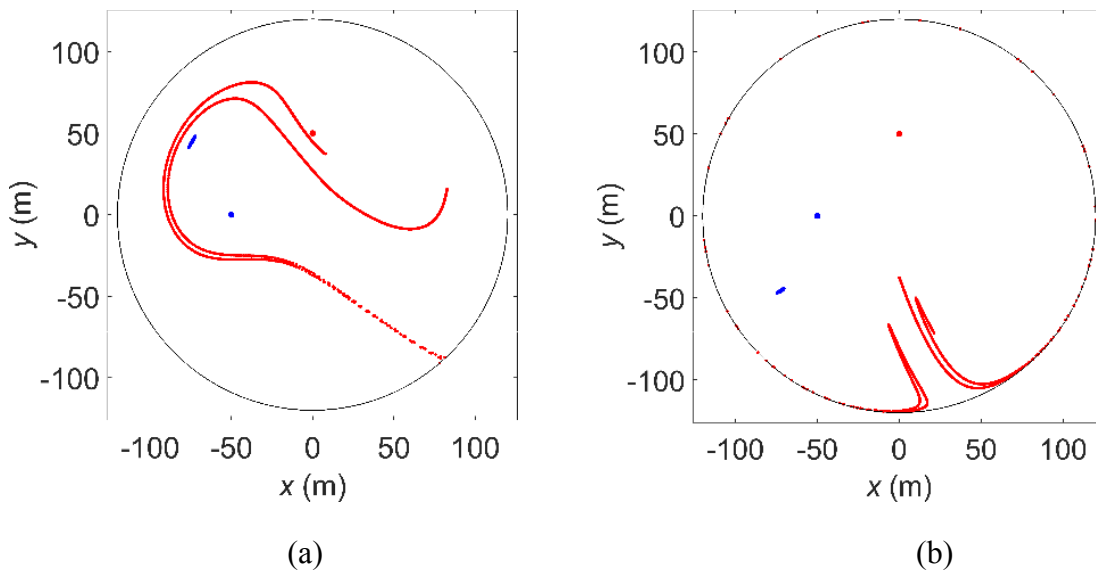


Figure 3.23 Advection of two particle circles in analytical solution (a) $8T$; (b) $16T$.

As shown in Figure 3.23, it is obvious that the blue circle deforms very slowly during $8T$ and $16T$. Though all blue particles change their positions by following the flows, they are still very close to each other. However, the red particles show absolutely different particle behaviours in the same time. At the time of $8T$, the red circle has turned to be a quite complicated patch nearly across the whole lake. That means in a high FTLE value area the mixing progress is developing very quickly and intensely and has a much stronger influence on the whole lake. The red

particles are almost everywhere where the FTLE value is high at $16T$. A very important characteristic of chaotic advection is sensitivity to initial conditions. For the purpose of comparison of the two circle patch, mean distances between initially neighbouring particles in the circle patch are calculated and the result is shown in Figure 3.24. In the red circle patch, the distance between two particles released closely each other increase exponentially with time. As the time flies, two closet particles can have a huge distance just because they are not at the same point at the beginning. This sensitivity to initial conditions indicates that chaotic advection exists where the red circle is located. This is quite different with the blue particles. Since the blue circle is at a regular region, the mean distance tends to grow extremely slowly with time.

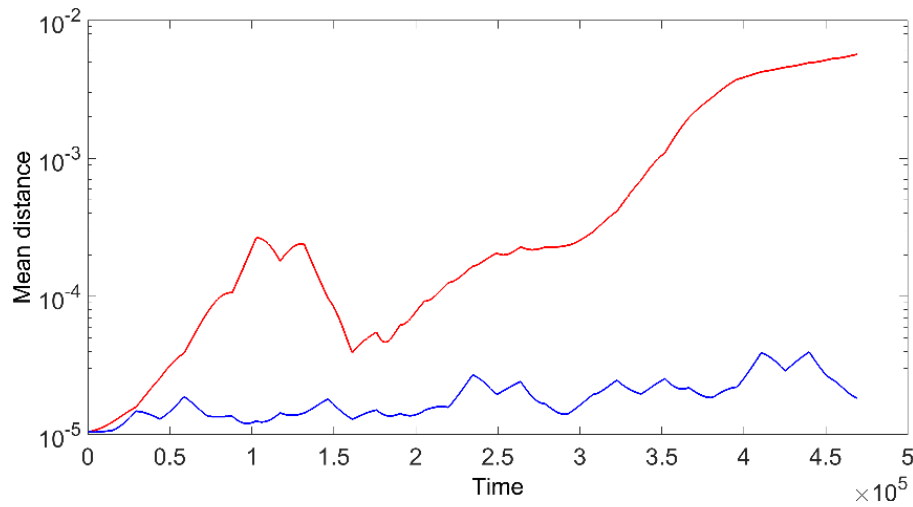


Figure 3.24 Mean distance of two particle circles in analytical solution.

Figure 3.25 to Figure 3.28 illustrate that Poincaré section and FTLE distribution obtained with the application of semi-numerical solution are in very good agreement with those obtained with analytical solution. The stable/unstable manifold are almost same which means particle tracking model have the capacity of investigating dynamic systems of real cases.

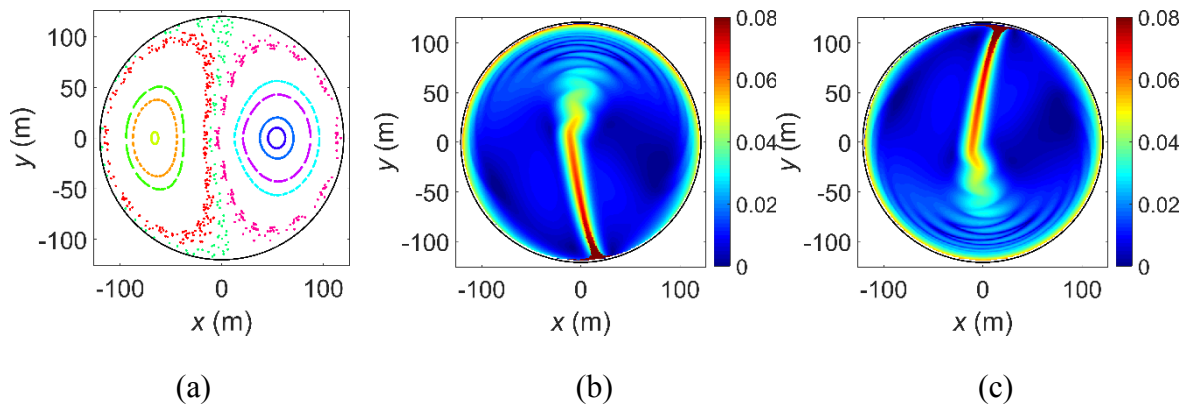


Figure 3.25 dynamics property of semi-numerical solution when $\mu_k = 0.14$ (a) Poincaré section; (b) backward FTLE; (c) forward FTLE.

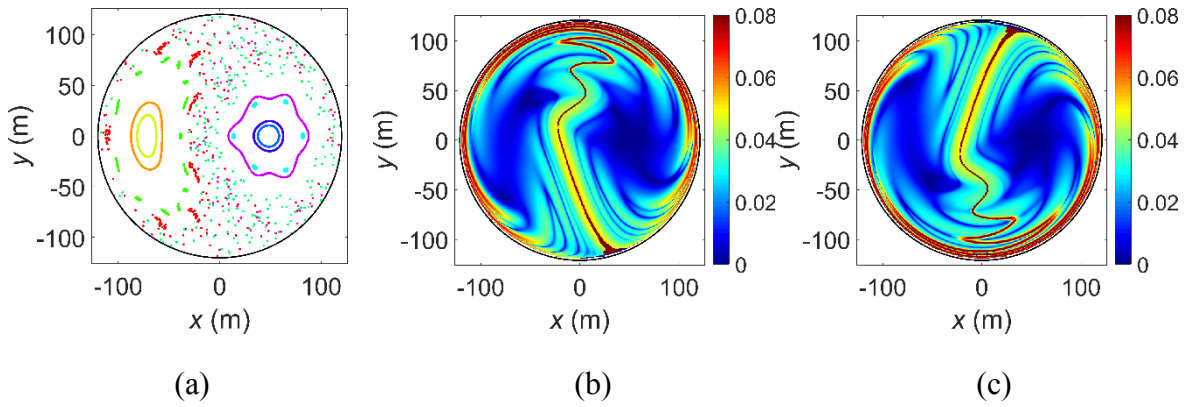


Figure 3.26 dynamics property of semi-numerical solution when $\mu_k = 0.28$ (a) Poincaré section; (b) backward FTLE; (c) forward FTLE.

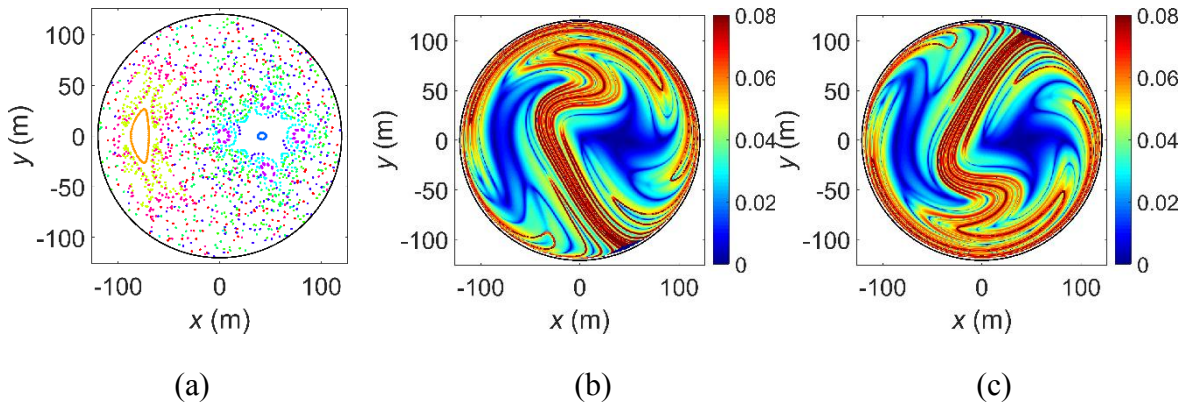


Figure 3.27 dynamics property of semi-numerical solution when $\mu_k = 0.42$ (a) Poincaré section; (b) backward FTLE; (c) forward FTLE.

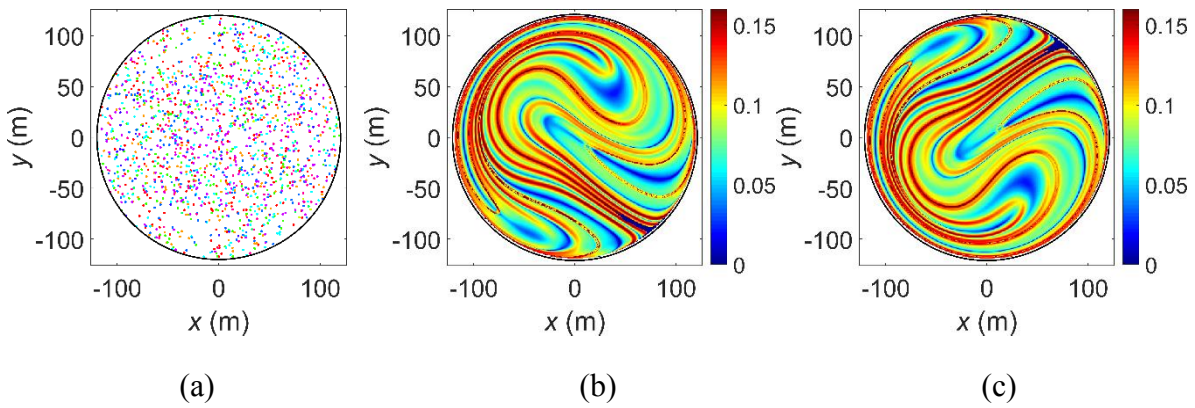


Figure 3.28 dynamics property of semi-numerical solution when $\mu_k = 0.84$ (a) Poincaré section; (b) backward FTLE; (c) forward FTLE.

3.5 Summary

This chapter has presented the main methods that are involved in this work. For the simulation of realistic environmental shallow water flows, viscosity (turbulent) terms are added properly into the shallow water equations and the corresponding shallow water model is updated. A two-

dimensional particle tracking model is developed to simulate the passive particle trajectories with the numerical velocity field obtained by the shallow water model. Dynamic systems and its relevant concepts which will be used to investigate the Lagrangian dynamics in shallow water flows are introduced. Finally, five benchmark cases are selected to validate the shallow water model and the particle tracking model.

Chapter 4. Inflows/outflow driven particle dynamics in an idealized lake

4.1 Introduction

Horizontal transport and mixing properties of an enclosed or semi-enclosed shallow flow system is not only induced by surface stress such as wind force, but also the direct surface flows such as inflows and outflows connecting to this shallow flow system. Compared to wind stress which usually directly inflicts the force to the whole enclosed shallow flow system, inflows/outflows influence more locally the flow patterns in the regions close to these inflows/outflows and then spread the momentum to the rest of domain (Kranenburg, 1992). Therefore the characteristics of transport and mixing processes induced by inflows/outflows are expected to be different from those induced by winds and should be considered when studying the Lagrangian dynamics of a semi-enclose environmental shallow flow connected to external water bodies.

The wind-induced transport and mixing properties in enclosed shallow flow systems have been studied by many researchers. Kranenburg (1992) investigated chaotic advection in a circular idealised shallow basin with analytical velocity field induced by periodic wind force. Liang *et al.* (2006a) used numerical methods to study wind-induced chaotic advection in several circular basins with more complicated bathymetry. Also Liang *et al.* (2006b) investigated the particle dynamics in a mine tailing pond with realistic bathymetry and geometry. Károlyi *et al.* (2010) showed that chaotic particle dynamics in a shallow rectangular basin could be well described by finite size Lyapunov exponents (FSLE). Lee *et al.* (2014b) simulated the wind-induced hydrodynamics Kranenburg's model lake using a two-layer shallow flow model and compare the Lagrangian dynamics in the two layers using a particle tracking method. Although nonlinear dynamic system approaches have already been developed and applied to analyse wind-induced transport and mixing processes in enclosed shallow water bodies, the corresponding transport and mixing properties triggered by inflows/outflows have received less attention. A better understanding and accurate numerical modelling of inflow/outflow-driven Lagrangian particle dynamics in bounded flows may be significant for relevant sciences and engineering applications, such as interpreting the transportation of pollutant and designing routes for transferring freshwater from alternative sources to improve the water quality of a polluted water body.

In this chapter, we focus on Lagrangian dynamics driven by inflows/outflows, without considering the influence from winds which has been intensively investigated in the literature. The results are presented in the form of FTLE and LCS distributions, trajectories of localised particle patches and trajectories of particles continuously released from external flows.

4.2 The flow fields in the idealised model lake

For the sake of simplicity and easy comparison, the bathymetry of the idealised circular lake considered herein is chosen to be the same as the one used by Kranenburg (1992) and the initial water depth h_k (indicating the bathymetry) is given as a function of radial distance from the basin centre:

$$h_k = H(1/2 + \sqrt{(1/2 - 1/2 * (r/R))}) \quad (4.1)$$

where r is the distance from the basin centre; H and R are the weighted mean water depth and radius of the lake and set to 0.5 m and 120 m, respectively. But instead of assuming an entirely enclosed water body as in Kranenburg (1992), two 8 m wide inflow channels are carefully designed and connected to the main basin at northwest and northeast direction to impose inflows while a 12 m wide outlet is attached to the south to allow outflows. The bathymetry (initial water depth) of the lake and the configuration of the inflow and outflow channels are shown in Figure 4.1.

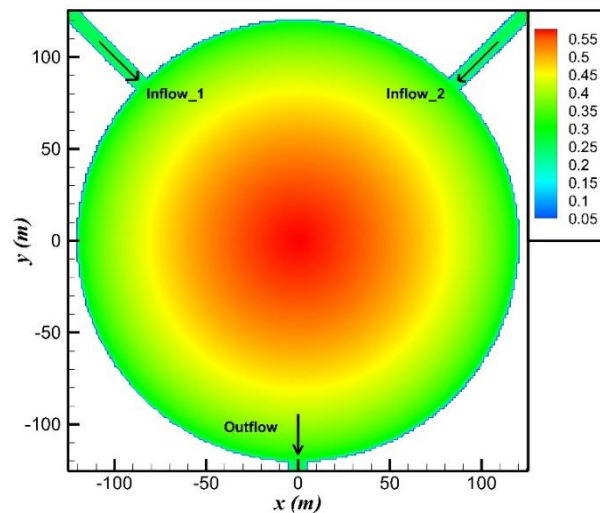


Figure 4.1 bathymetry (initial water depth) and inflow/outflow channels of the idealised lake.

The flow hydrodynamics in this idealised lake is simulated using the shallow flow model introduced in Chapter 3. The Manning coefficient n is set to be 0.025. The p_{vt} for calculating turbulent fluxes is selected to be 3.4 for a circular basin (Fischer *et al.*, 2013). The initial water

depth in the inflow/outflow channels is set to be 0.251m, to give the same water level as the ambient flow in the main water body. The inflow discharge is maintained at $20\text{m}^3/\text{s}$ during the whole simulation. The computational domain is discretised using a uniform grid with 210×210 cells to give a resolution of 1.2m. For each constant inflow, the simulation is run for 12 hours until the flow field becomes steady. The simulated steady-state circulations are presented in Figure 4.2.

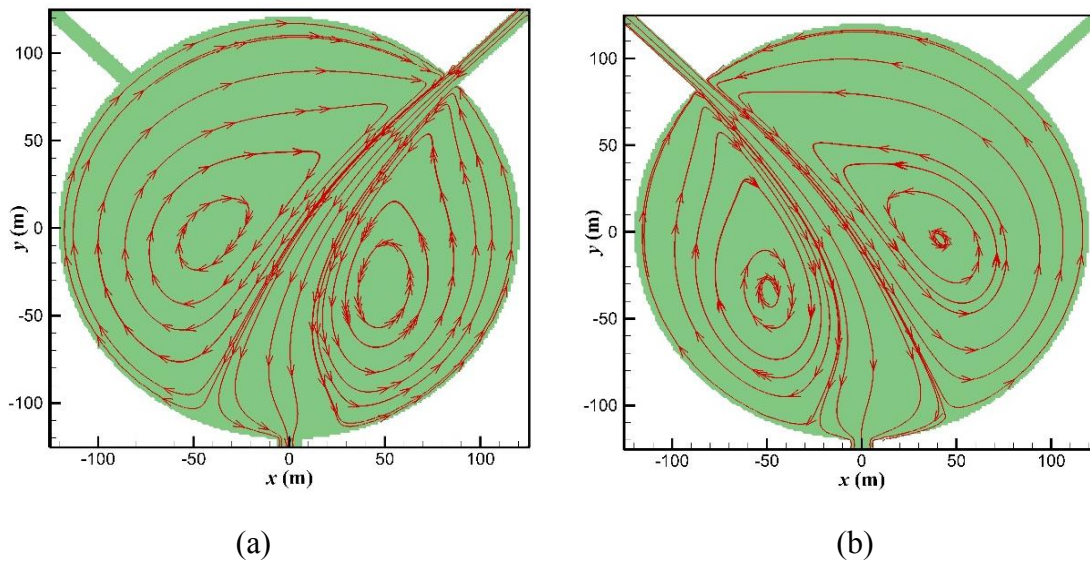


Figure 4.2 Aerial view of the steady-state streamlines caused by (a) inflow from the northeast; (b) inflow from the northwest.

Taking Figure 4.2(a) as an example, which corresponds to the flow field driven by the northeast inflow, most of the basin is occupied by two big gyres and they are separated by a streamline traced out by the main flow from inflow channel to outflow channel. The gyre system is similar to the one induced by wind stresses as presented by Kranenburg (1992) but the rotation direction of the gyres is opposite. In Kranenburg (1992) and Liang *et al.* (2006a), water velocities tend to be directed against the wind in deeper part of the lake, and with the wind in shallow areas. While in this flow-induced flow, flow in deeper part follows the inflow to the outflow and reverses back to the inflow from shallow part, as shown in Figure 4.2.

The time histories of the x -direction velocity component at four gauge points located inside the basin at $(70, 0)$, $(0, 70)$, $(-70, 0)$ and $(0, -70)$ are recorded during the simulation process and presented in Figure 4.3, showing that the velocity field become steady after about 3 hours.

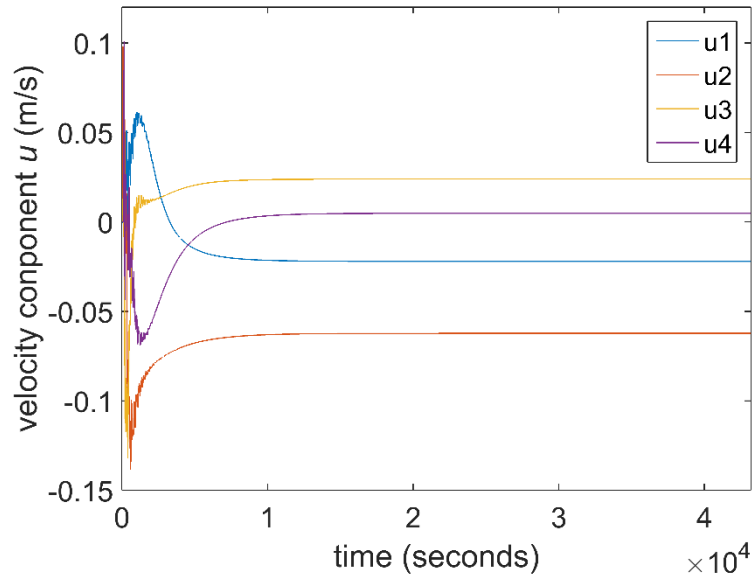


Figure 4.3 History of u of four gauge points.

4.3 Dimensionless parameter controlling particle dynamics

For particle tracking, a simple dynamic/periodic system is considered. Each inflow channel is assumed to have a gate to control whether this channel is open or closed to alternate inflow and hence the flow field in one period T . In the first half of a period, the northeast channel is open and the northwest channel is closed; in the second half of a period, a reversed situation is assumed. Also it is assumed that the flow alters instantaneously following the change of inflow conditions. These settings are identical to Kranenburg (1992) and Liang *et al.* (2006a) for the consideration of the wind-induced periodic particle dynamics.

Following Kranenburg (1992) and Liang *et al.* (2006a), this simple dynamic system may be described by a dimensionless parameter derived as:

$$\mu_i = \frac{\ln(H/z_0)}{8\kappa} \frac{Q_{in} t_f}{R_0 h w} \quad (4.2)$$

where $z_0 = 2.8$ mm is the roughness height of the bed; $\kappa = 0.4$ is the von Kármán constant; Q_{in} is the constant discharge; h is the water depth in the inflow channels; w is the width of inflow channels; t_f is the duration of the inflow which equals to half of the period T ; and R_0 is the characteristics length of the lake which is chosen to be the radius of the lake herein.

The parameter μ_i in equation (4.2) may be regarded as a dimensionless inflow duration parameter which is only related to the inflow duration t_f (half of the period). In fact μ_i may be defined as a dimensionless time duration $t_i = \ln(H/z_0) Q_{in} t / (8\kappa R_0 h w)$ and is essentially the ratio between the travel distance during the inflow duration $Q_{in} t / h w$ and the characteristics

length R_0 . μ_i provides an effective parameter to describe/control the magnitude of chaotic mixing in the idealised lake and the particle dynamics in this idealised model lake is actually controlled by the length of the inflow duration.

4.4 Lagrangian dynamics of the lake

In this section, the FTLE structures corresponding to different μ_i are calculated to show the mixing and transport properties corresponding to different inflow durations. Passive particles initially released in different locations of the lake is tracked to validate the FTLE structures and to investigate the mixing properties in different regions of the lake. Finally, passive particles representing freshwater are released from the inflow channels to quantify the occupy rate of freshwater and to investigate the effectiveness of ‘lake-flushing’ in improving water quality.

4.4.1 FTLE distribution and local particle dynamics

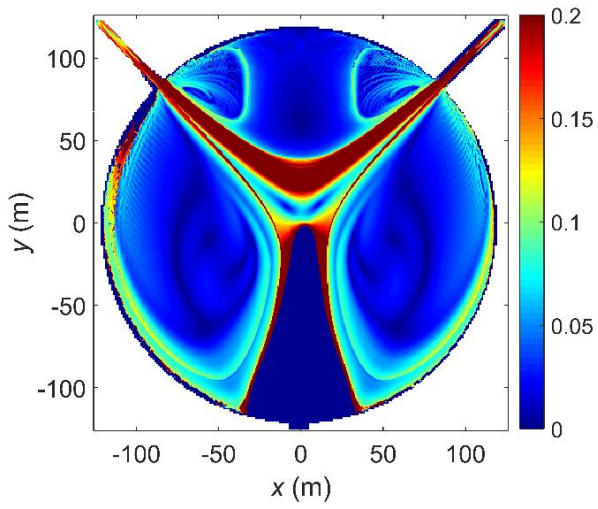
As introduced in Chapter 3, FTLE structures can be obtained by tracking particle trajectories forwards and backwards in time. Forward-tracked FTLE means that FTLE is calculated when particles are tracked in forward time direction while backward-tracked FTLE means that FTLE is calculated when particles are tracked in backward time direction. The values of FTLE fields may be regards as a function of the initial particle location \mathbf{x} and the highest values in the function trace out filamental structures approximating relevant manifolds: ridges in forward (backward) FTLE fields identify the areas of locally maximum separation (compression), approximating repelling (attracting) material surfaces or stable (unstable) manifolds of hyperbolic trajectories, which may be identified as the Lagrangian coherent structures and characterize the shallow flow dynamics from the Lagrangian point of view. Since the idealised lake represents a periodic dynamic system, the FTLE distribution and the locations of LCS change periodically, or more specifically, switch between two dynamic situations driven by two alternating inflows. If the flow is aperiodic, the FTLE distribution and locations of LCS will change over time and the FTLE computation could be repeated for a range of times (with different initial time) to obtain a time series of FTLE distribution, and consequently, a time history of LCS evolution.

To properly visualize FTLE distribution, grid with a resolution of 420×420 cells (twice the resolution of hydrodynamic grid) is used to define the initial locations of passive particles in this idealized lake. FTLE distribution is presented in an order of *minutes*⁻¹ and the range of FLTE value is normally between 0 and 0.2. Software package Matlab is used to plot the FTLE

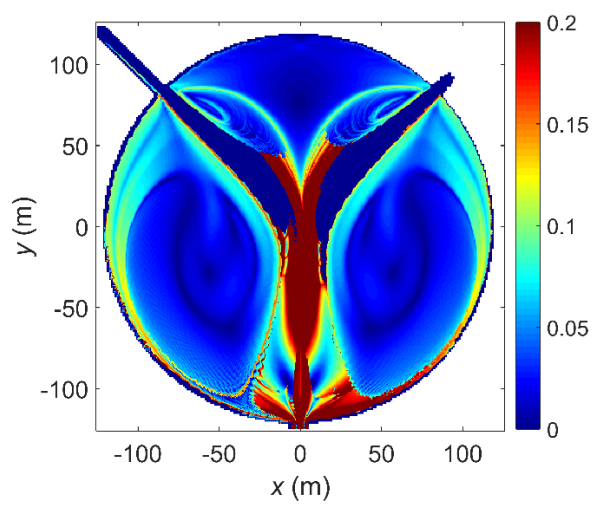
fields in the form of contour maps where LCSs are automatically filtered out by red lines (the highest values) based on the color scheme used in this work.

Theoretically, there should be no zero-FTLE (i.e., the darkest blue zone in the current colour scheme) zones in the FTLE distribution maps since the separate rate of nearby particles should not equal to zero. The existence of zero-FTLE zones in the results as presented later in this Section is a result of escaping particles. Particles initially located in these areas run out of domain when the simulation finished and the values of FTLE in these areas cannot be obtained and are simply set to be zero. In fact, particles in these zero-FTLE zones behave vehemently and rush out of the lake in a short time.

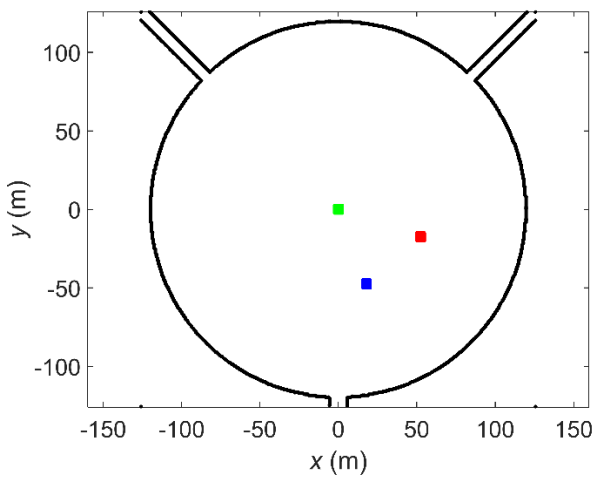
Figure 4.4(a) and Figure 4.4(b) present the FTLE distribution maps computed through forward-tracking and backward-tracking with an integration time length of $50 T$ for $\mu_i = 2.7$. It can be observed that both forward and backward FTLE distributions show nearly symmetrical patterns about a vertical axis owing to the alternating inflow forcing in the north-western and north-eastern directions. The main flow channels are covered by red colour indicating high FTLE and high separation rate, and dark blue indicating manually zero values of FTLE set for those particles being rapidly flushed out of the domain. LCSs occupy the high FTLE zones. Between these LCSs are the so-called ‘valleys’ which are marked by dark blue colour and indicate the lower values of FTLE compared with the LCSs. These valleys have poor mixing property while LCSs represent the zones with high mixing rate. There are clearly three low-mixing zones surrounded by LCSs, with the LCSs acting as separatrix restricting the transport and mixing of passive particles. Passive particles initially located in the vortex-style dark blue areas will stay inside these areas and can hardly be transported to other areas or flushed out of the domain. On the other hand, particles initially located outside these low-mixing zones may travel along those representative unstable manifolds but never move into the low-mixing zones. Therefore, the nearby particles may belong to regions of different mixing properties (LCSs or valleys) and have entirely different behaviours (well mixing or poor mixing). This essentially implies that the behaviour of a particle is highly sensitive to its initial conditions, which is a signature of chaos.



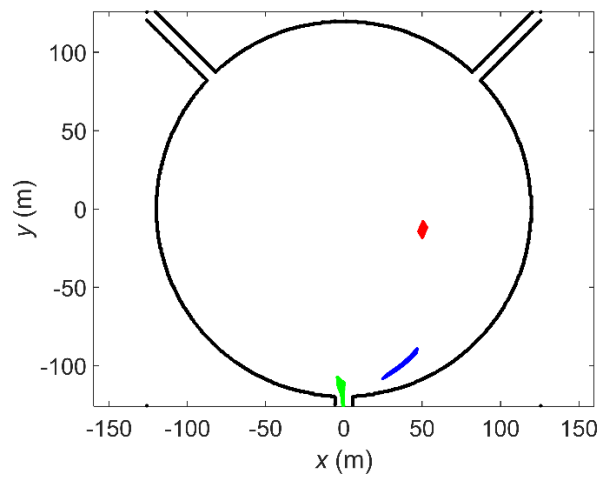
(a)



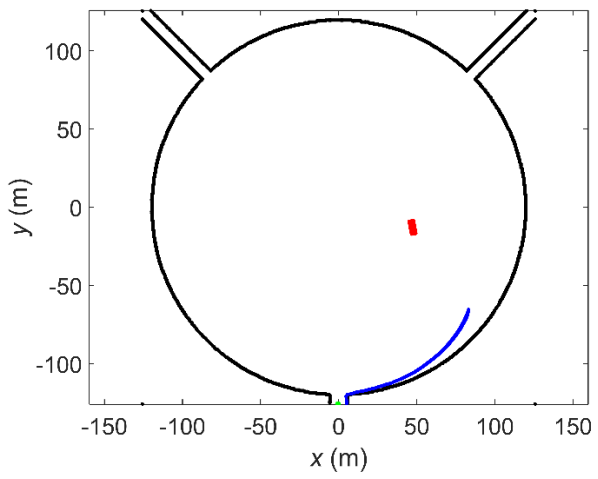
(b)



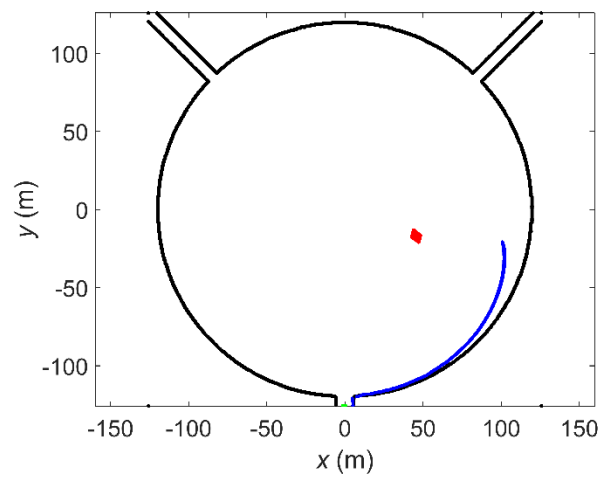
(c)



(d)



(e)



(f)

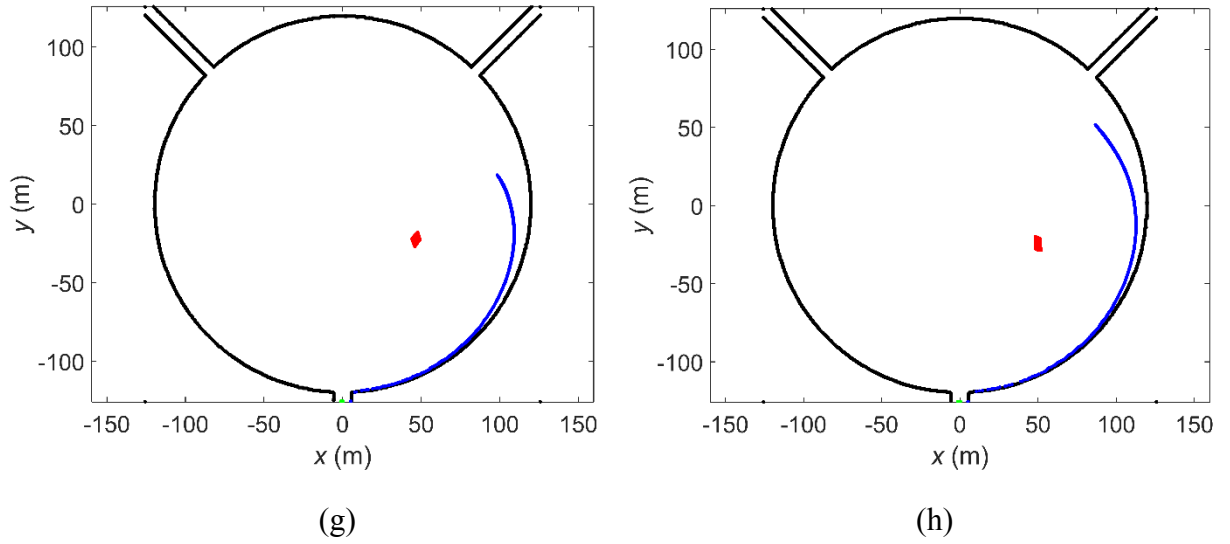
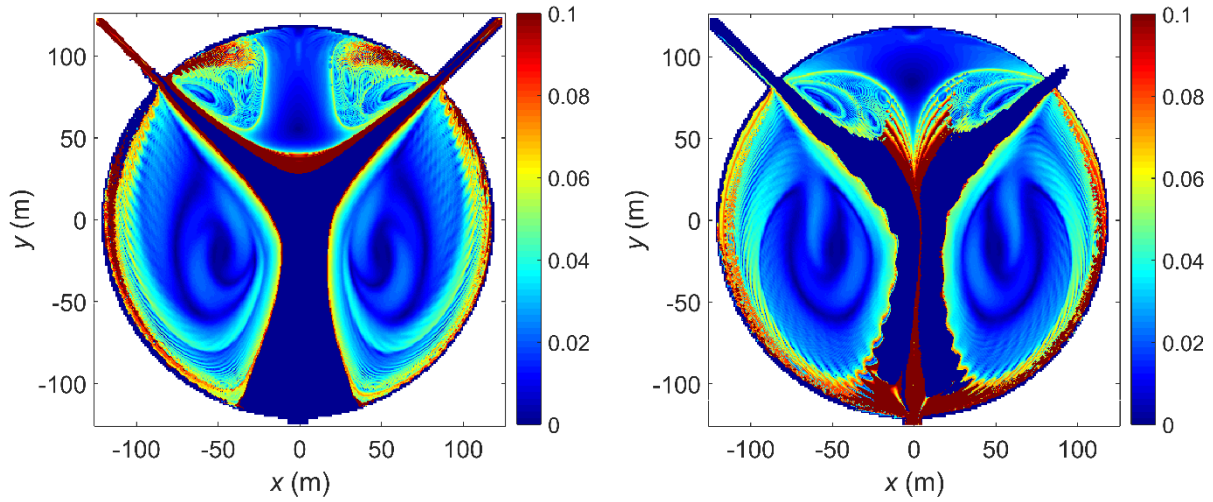


Figure 4.4 FTLE distribution and evolution of three particle patches located in different mixing zones when $\mu_i = 2.7$: (a) forward-tracked FTLE distribution; (b) backward-tracked FTLE distribution; (c) initial positions of the three particle patches; (d) snapshot of the particle patches at $t = 10T$; (e) $t = 20T$; (f) $t = 30T$; (g) $t = 40T$; (h) $t = 50T$.

To demonstrate the fact that the LCSs are invariant manifolds (or at least semi-invariant) and the lake is featured with zones of different mixing properties, three square particle patches, each with 10000 particles, are released in different mixing zones inside the lake at the starting time, as illustrated in Figure 4.4(c). The green patch is initially located in the rush-out zone, the red patch in a poor mixing zone and the blue patch on LCSs. The fate of the three particle patches is entirely different during the $50T$ of particle tracking process. The green patch, driven by the powerful inflows, moves directly southwards to the outflow channel and quickly leaves the domain, as shown in Figure 4.4(d). The red patch is located in one of the low-mixing zones and neither the shape nor position of the particles has changed much during the whole particle tracking process. The blue patch first travels to the south and is simultaneously stretched into a filament. When it reaches the domain boundary, the filament reverses its direction and travels back to north along the unstable manifolds. The mixing processes of the three patches are clearly demonstrated in Figure 4.4(c-h). The sensitive dependence to initial conditions may be indicated by the trajectories of particles in the blue patch. Overall, chaotic behaviour only exists in small areas when $\mu_i = 2.7$.

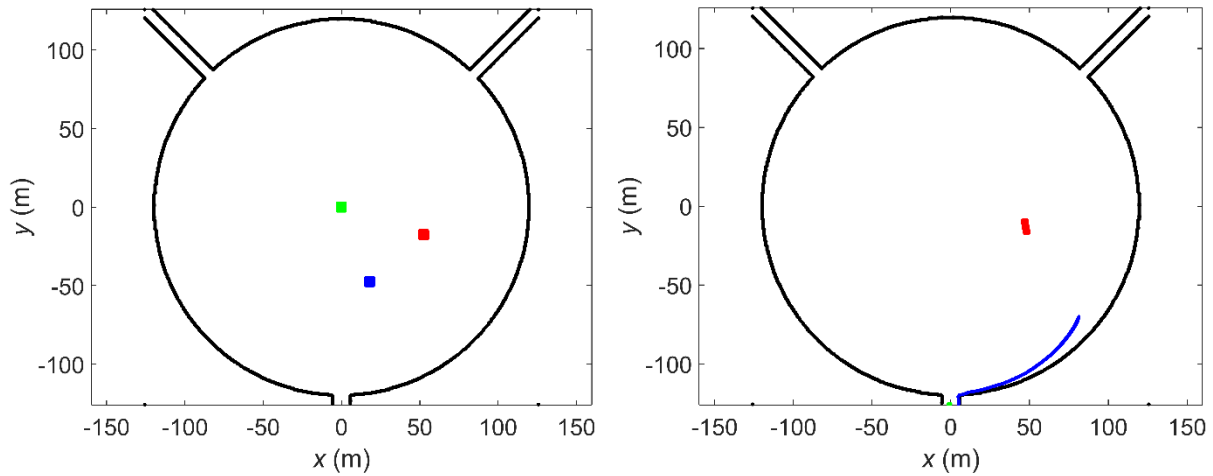
When $\mu_i = 5.4$, the FTLE distribution does not change too much compared with that obtained for $\mu_i = 2.7$. Two dark blue vortex-shape zones are detected, as shown in Figure 4.5(a) and Figure 4.5(b), which are similar to those as found in Figure 4.5(a) and Figure 4.5(c), except that the LCSs surrounding the poor mixing zone have become more tortuous for $\mu_i = 5.4$. Also, in northern part of the lake, more LCSs appear and they clearly occupy a larger region.

The dynamics of local passive particle is also similar to that of $\mu_i = 2.7$. The green patch is flushed out of the domain in a shorter time interval (less than $10T$). The red patch still shows the properties of low mixing and transport. While the blue patch, which is initially located at LCSs, becomes more active and almost traces out the full skeleton of LCSs at that region in 50 periods. It is clear that when μ_i increases, the mixing and transport properties become enhanced in some areas, especially those along the LCSs. But the whole lake is still predominantly featured with regular rather than chaotic particle motions.



(a)

(b)



(c)

(d)

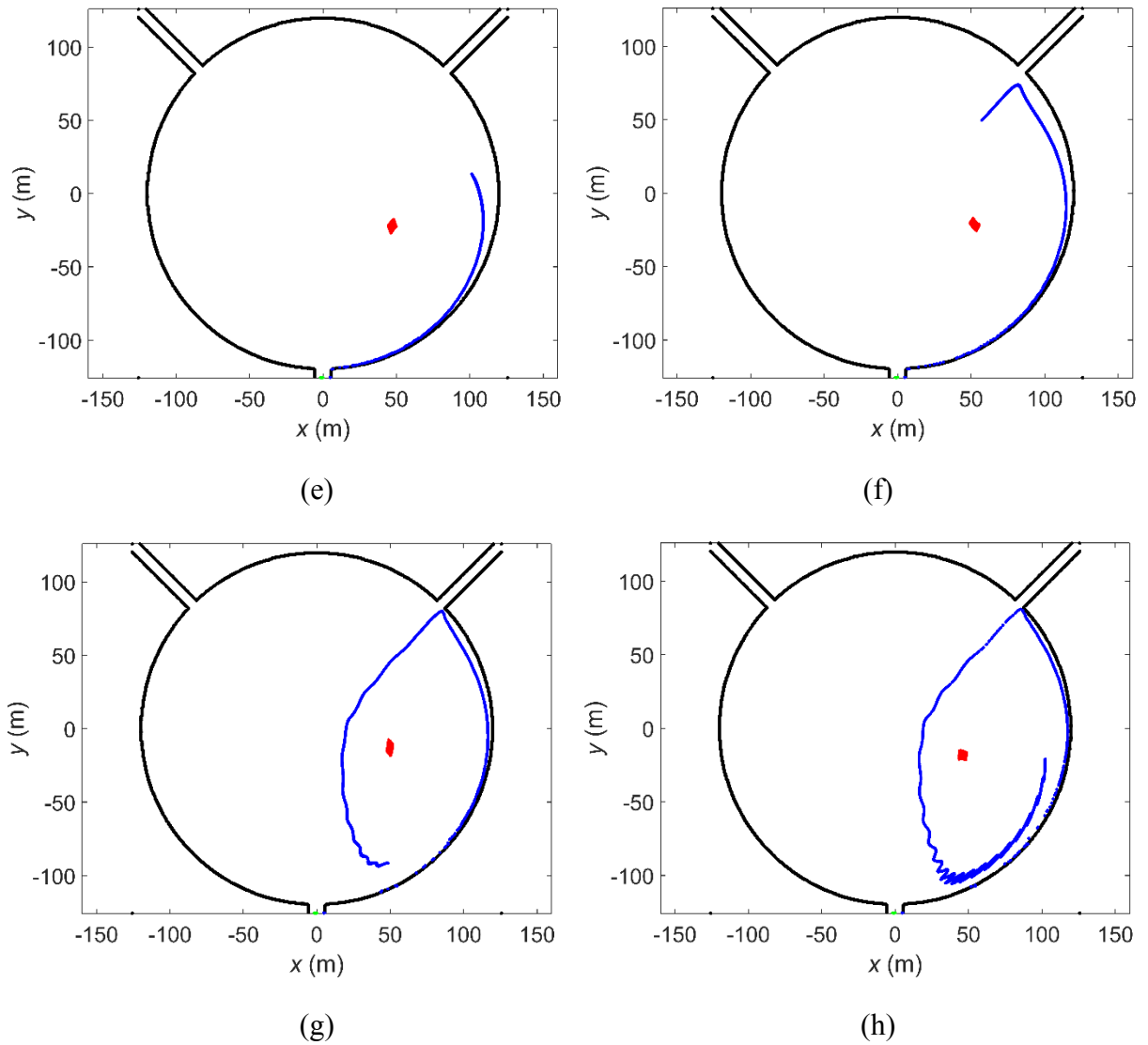
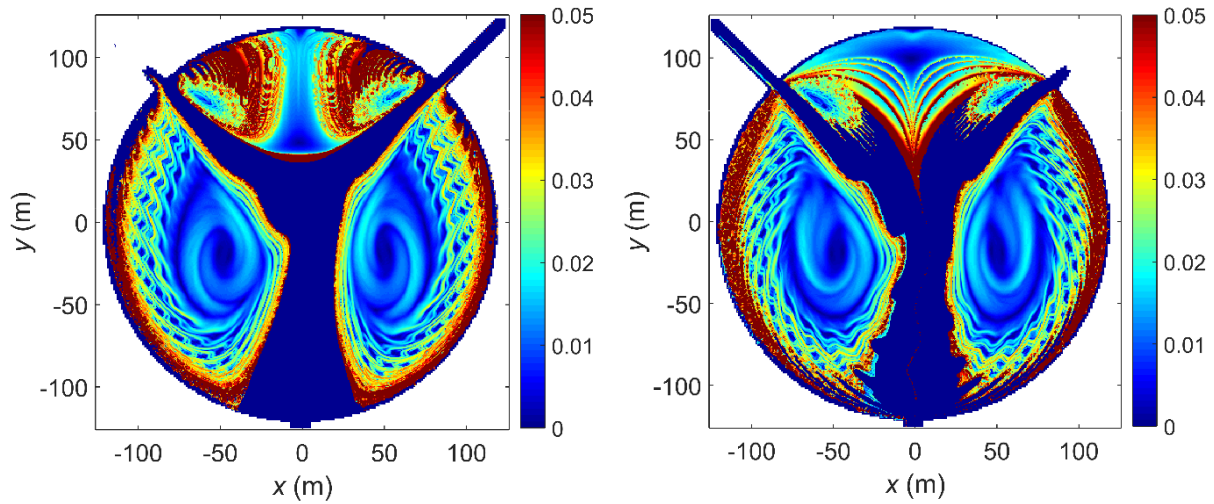


Figure 4.5 FTLE distribution and Evolution of three different particle patches with $\mu_i = 5.4$: (a) forward FTLE distribution; (b) backward FTLE distribution; (c) initial position of patches; (d) snapshot of the particle patches at $t = 10T$; (e) $t = 20T$; (f) $t = 30T$; (g) $t = 40T$; (h) $t = 50T$.

For $\mu_i = 10.8$, obvious changes to FTLE distribution have been detected compared with $\mu_i = 2.7$ and 5.4 . The LCSs that were previously only surround the low-mixing zones have begun to penetrate these zones and affect the particle dynamics inside. In Figure 4.6(a) and Figure 4.6(b), LCSs close to the centre of lake have not changed much compared to the previous situations. But the LCSs close to the boundary of the lake have extended their influence to low-mixing zones, making the whole FTLE distribution to become more complicated. The low-mixing zones shrink in size and their boundaries become unstable.

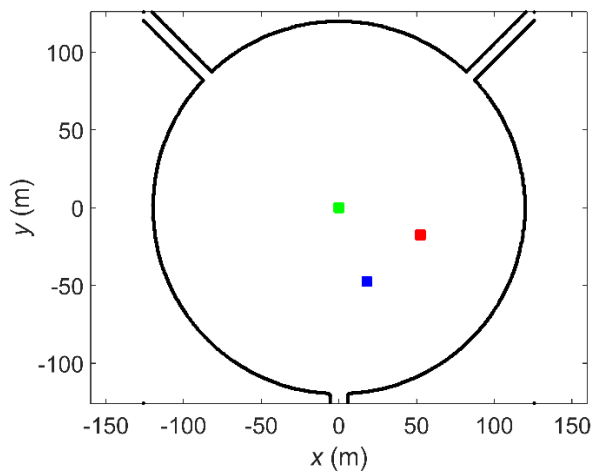
With regard to the advection of the particle patches, the behaviours of the green and red particle patches are similar to those in Figure 4.4. The blue particle patch traces out the structure of backward-tracked LCSs at the right hand side of the lake. Since the forward-tracked LCSs (stable manifolds) and backward-tracked LCSs (unstable manifolds) now interact with each

other at the boundary of low-mixing zones, chaotic mixing has been evidently created in these regions. As shown in Figure 4.6(d-h), the blue particle patch is repeatedly stretched and folded when they travel along the unstable manifolds from south to north. The stretching and folding actions have led to a complicated self-similar structure that fills the regions close to the eastern boundary of the left hand side poor mixing zone, indicating chaotic particle dynamics.

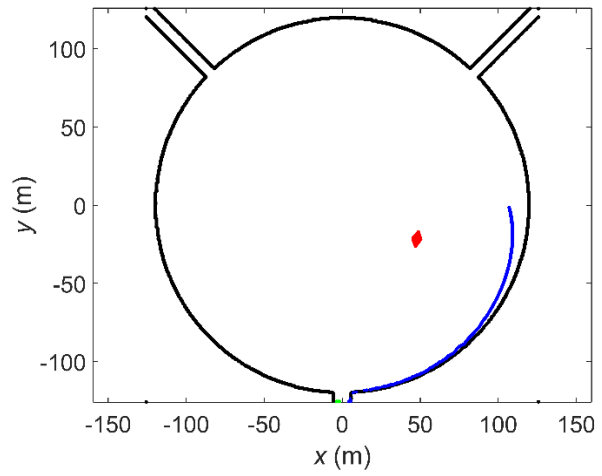


(a)

(b)



(c)



(d)

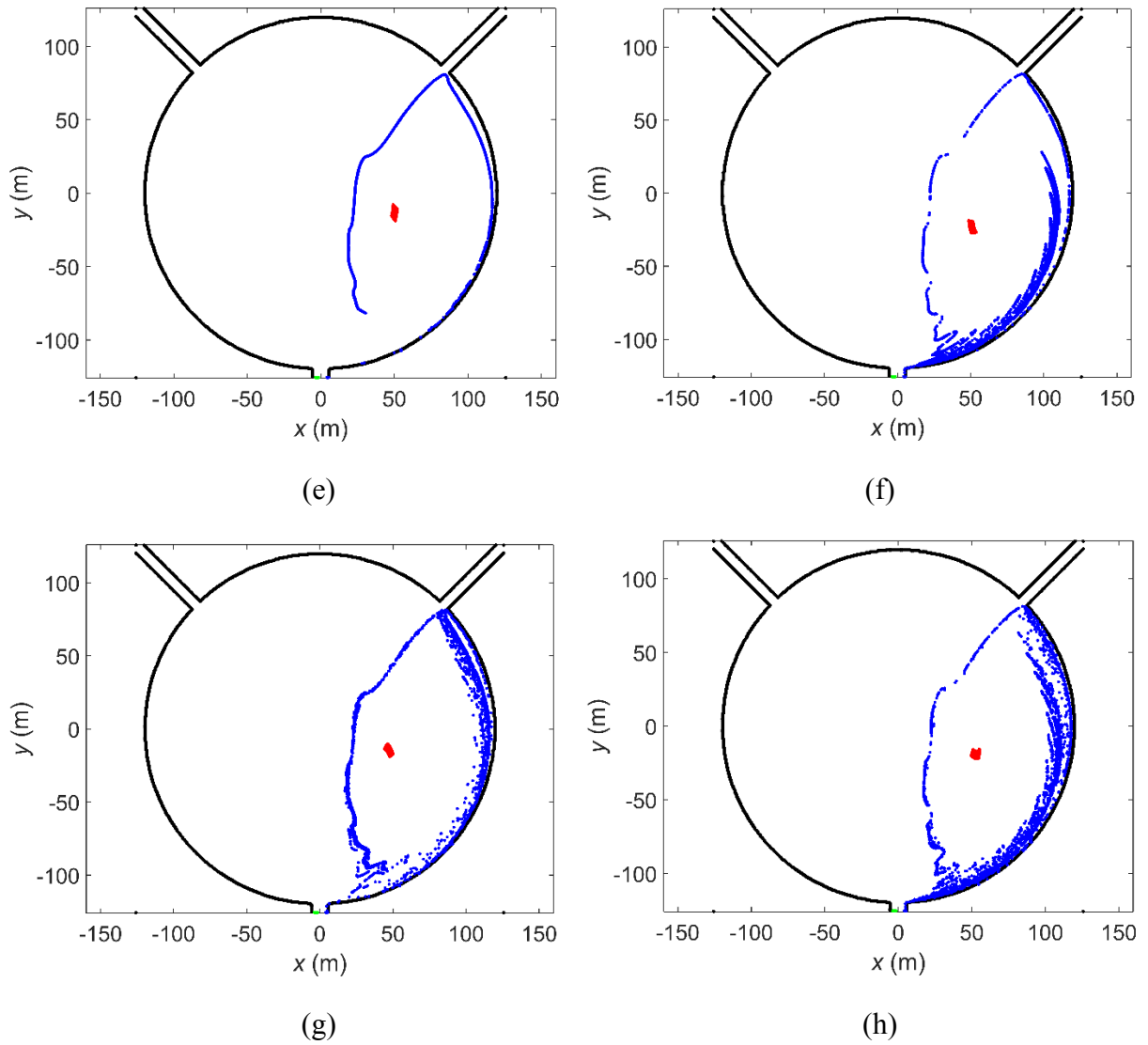
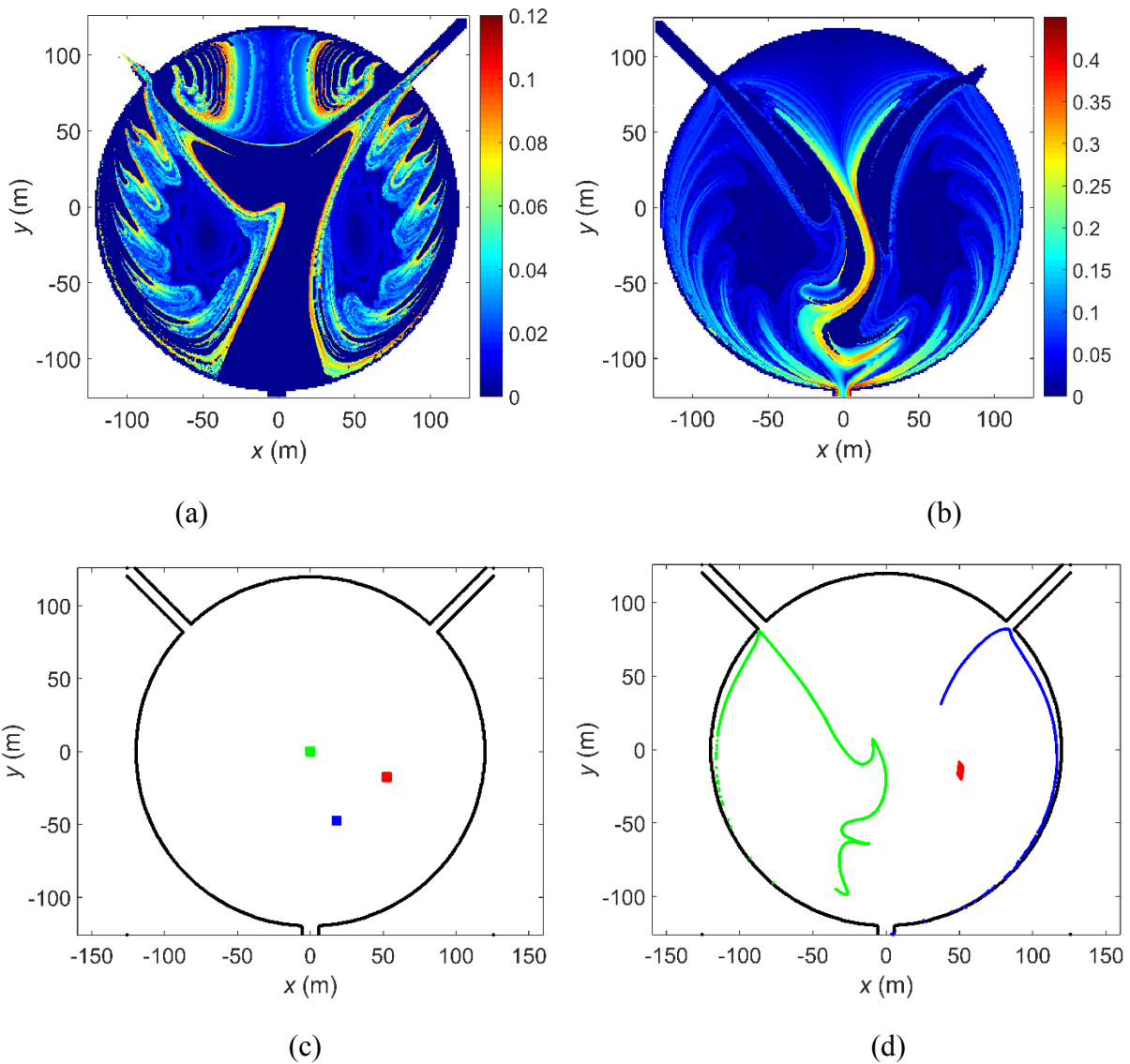


Figure 4.6 FTLE distribution and Evolution of three different particle patches with $\mu_i = 10.8$: (a) forward FTLE distribution; (b) backward FTLE distribution; (c) initial position of patches; (d) snapshot of the particle patches at $t = 10T$; (e) $t = 20T$; (f) $t = 30T$; (g) $t = 40T$; (h) $t = 50T$.

The mixing and transport properties of the lake is tremendously enhanced as μ_i further increases to $\mu_i = 21.6$, as illustrated in Figure 4.7. The two large low-mixing zones located at the left and right hand sides of the lake have essentially crushed and replaced by two vortex-shape islands. The LCSs have extended to almost all over the lake except several small poor mixing areas. The main flow path inside the lake has also been influenced. In the previous cases with lower μ_i , the main flow path features two upper branches connected to the inlet and one almost straight channel to the south connected to the outlet. Now the lower part of main channel is highly twisted, as shown in Figure 4.7(b), indicating that particles initially located in the twisted main channel may have different mixing behaviours rather than simply being flushed out of the domain.

Considering the evolution of particle patches, some particles from the green patch have been stretched into a filamentary structure within $10T$. As time elapses, the green patch rapidly traces out the complicated skeleton of unstable manifolds which have not been observed at the left hand side of the lake for lower μ_i . Meanwhile, the blue patch is observed to trace out the unstable manifolds at the right hand side of the lake. Finally in Figure 4.7(f), most area of the lake is occupied by green or blue particles, indicating more comprehensive chaotic mixing has occurred. But these particles can never travel into the low-mixing zones, for example the area where red particle patch is located. Another important point is that although green and blue particles behave chaotically, they just mix up with the congeneric particles. In another word, the green particles only mix up with other green particles and their motions are still limited at the left had side of the lake, similar to the blue particles at the right hand side.



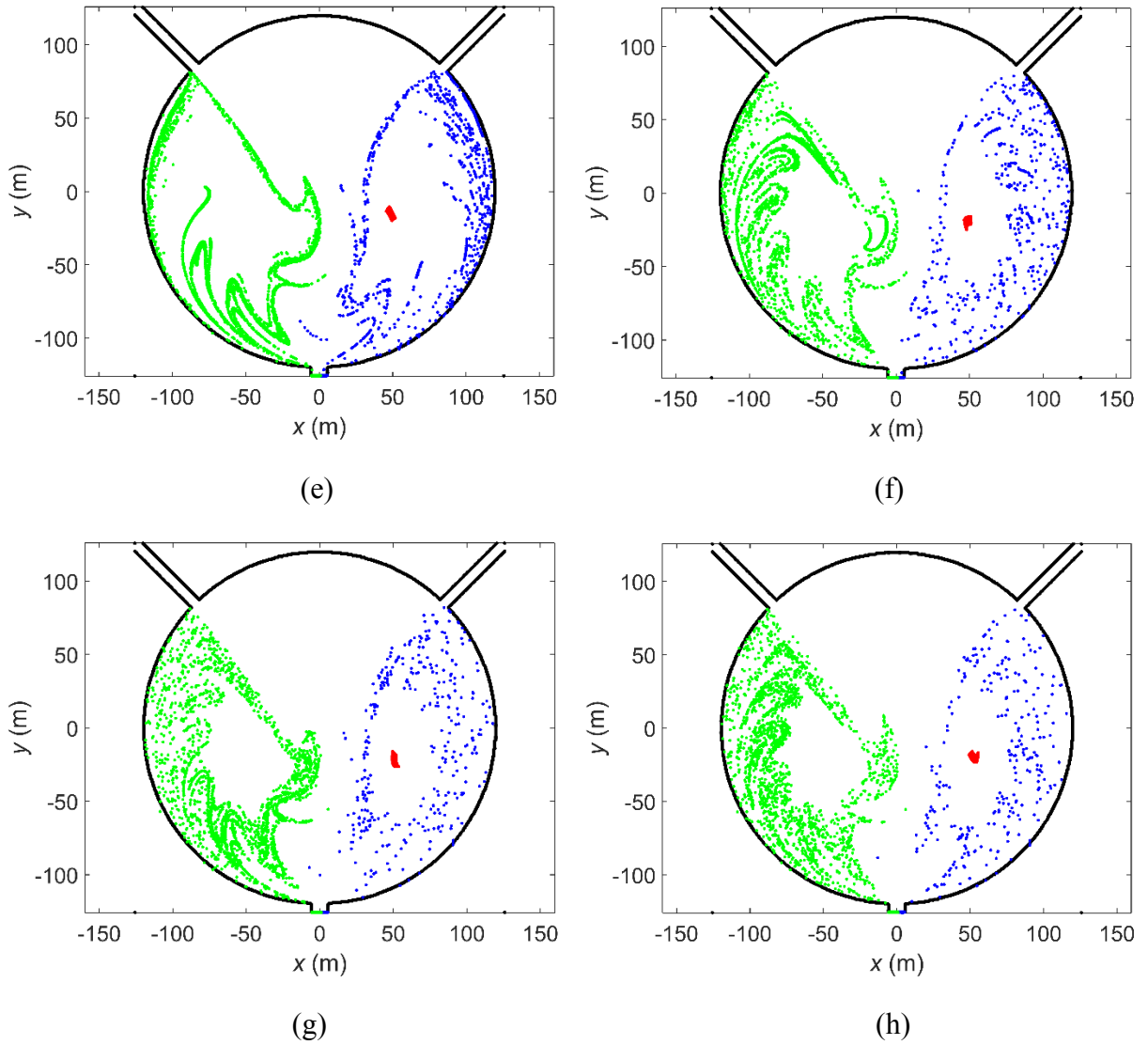
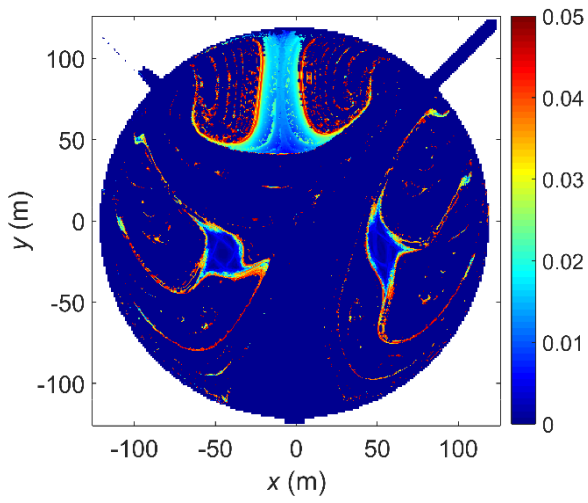
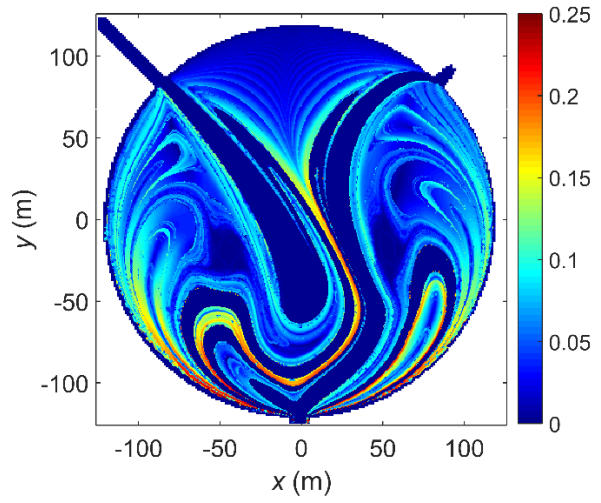


Figure 4.7 FTLE distribution and Evolution of three different particle patches with $\mu_i = 21.6$: (a) forward FTLE distribution; (b) backward FTLE distribution; (c) initial position of patches; (d) snapshot of the particle patches at $t = 10T$; (e) $t = 20T$; (f) $t = 30T$; (g) $t = 40T$; (h) $t = 50T$.

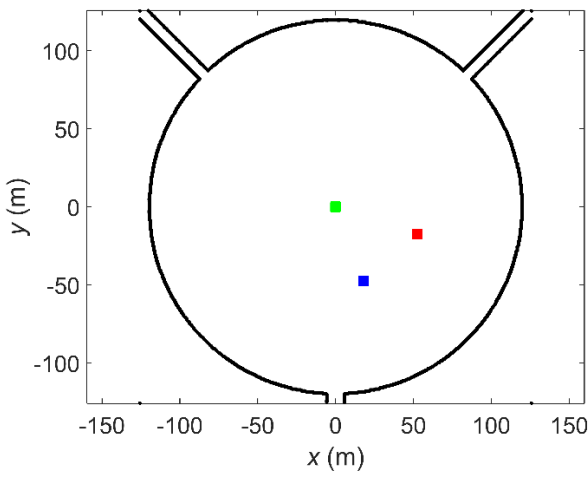
When $\mu_i = 43.2$, FTLE distributions in Figure 4.8(a) and Figure 4.8(b) are observed to have changed dramatically. Many particles used to calculate the FTLE values finally get away from the lake due to high transport and mixing dynamics, leading to large darkest blue area (representing zero FTLE values left by escaped particles). It is also noted that the FTLE distribution has totally lost its previous symmetric pattern at this high flow duration parameter ($\mu_i = 43.2$). With the increased flow duration, particles are advected over longer distances leading to larger spatial divergence, and thus there is an increased likelihood of being stretched and folded by the periodic flow field. The stirring effect of every first half-cycle becomes increasingly difficult to be offset in the second half-cycle, leading to loss of symmetry.



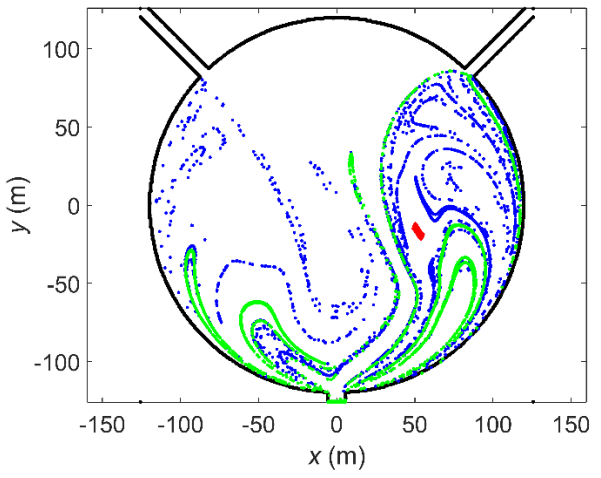
(a)



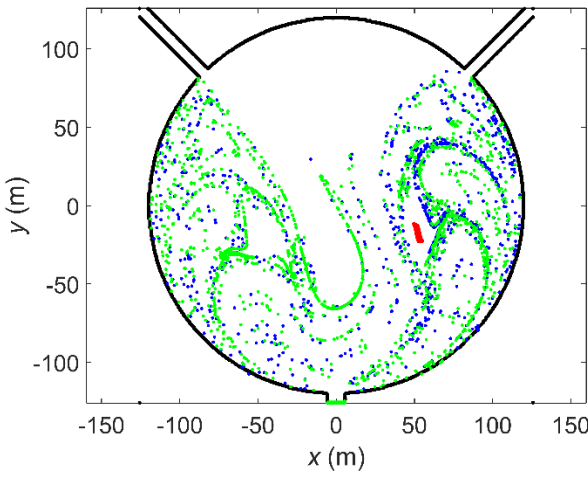
(b)



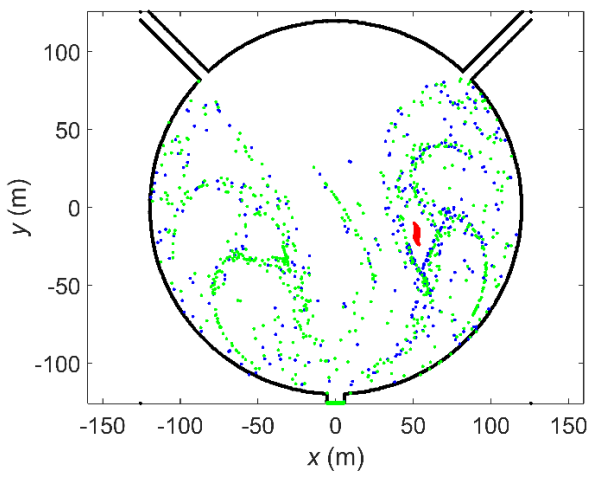
(c)



(d)



(e)



(f)

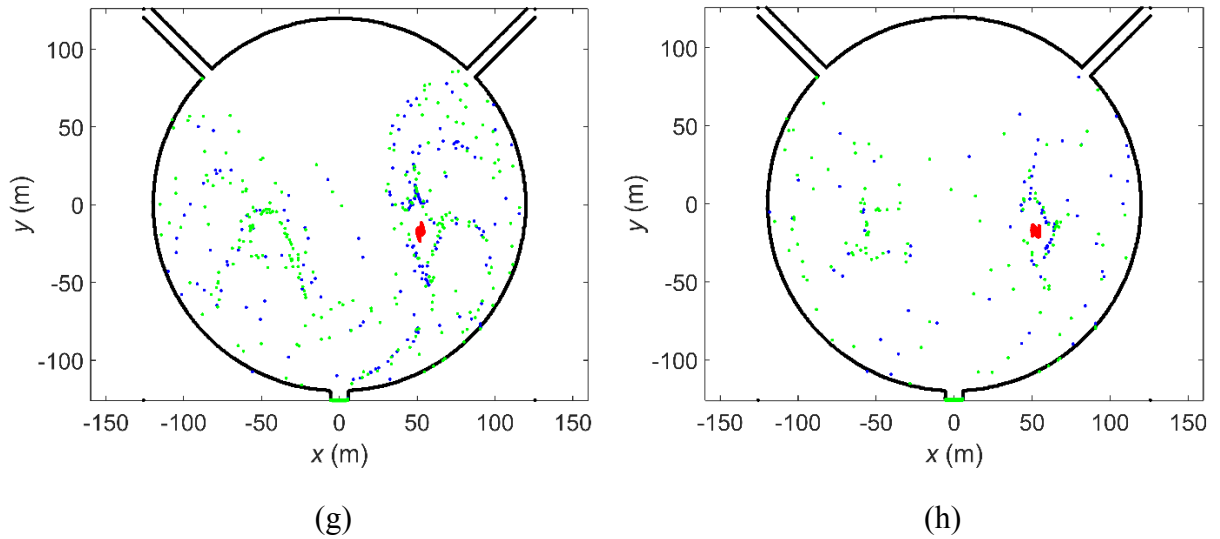
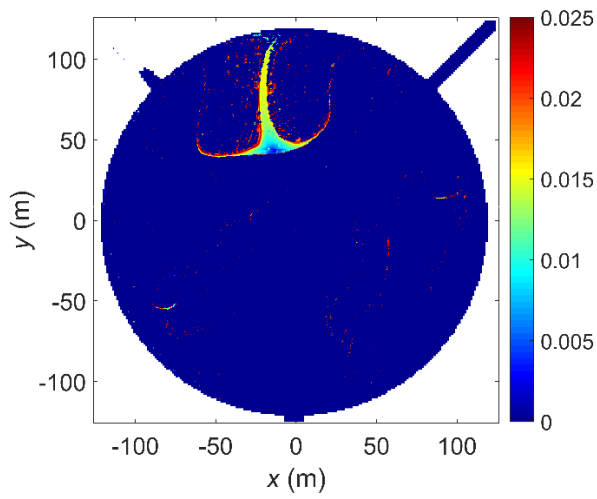


Figure 4.8 FTLE distribution and Evolution of three different particle patches with $\mu_i = 43.2$: (a) forward FTLE distribution; (b) backward FTLE distribution; (c) initial position of patches; (d) snapshot of the particle patches at $t = 10T$; (e) $t = 20T$ (f) $t = 30T$; (g) $t = 40T$; (h) $t = 50T$.

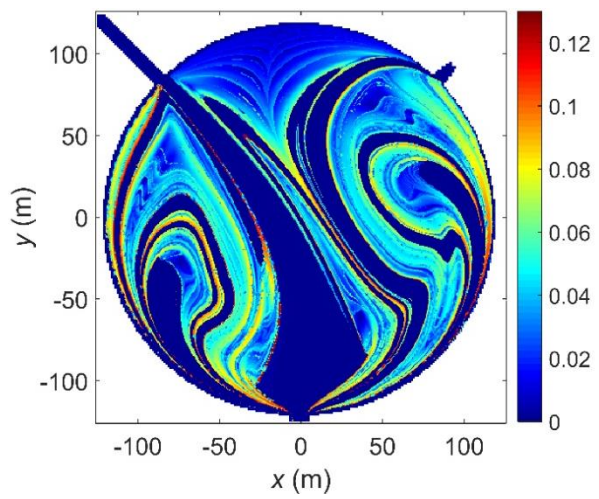
Under the current conditions, the LCSs from both sides (left and right hand sides) have begun to stretch all over the lake rather than being restricted within half of the domain, and so the particle motions have almost reached a globally chaotic mixing stage. The green and blue particle patches rapidly develop into complicated tendril-type structures under the influence of attracting LCSs (i.e. unstable manifolds) and are highly mixed with each other, as shown in Figure 4.8(d) and Figure 4.8(e). After a sufficient long time ($50T$), most of the green and blue particles have already been washed out of the lake through outflow channel, as clearly demonstrated in Figure 4.8(h). This is because the lake is not a fully closed system and there are escaping LCSs along which the particles can escape from the lake. Due to high mixing dynamics, it is easy for those chaotic particles to find these escaping LCSs and follow them to leave the lake. However, inside the whole lake, global chaotic mixing does not strictly achieve everywhere and there still exist small stagnant areas that show poor transport and mixing properties, e.g. the area where the red particle patch is located, as shown in Figure 4.8(h).

When μ_i is further increased to $\mu_i = 86.4$, the lake dynamic system now becomes fully chaotic. As shown in Figure 4.9(a), the forward-tracked FTLE distribution is no longer meaningful since almost all the particles leave the domain after $50T$ and FTLE values cannot be calculated using the current FTLE computation technique. The backward-tracked FTLE distribution (Figure 4.9(b)) shows that the LCSs have begun to fill most of the space in the whole lake and no clear unmixed areas can be detected. Particles from three different patches quickly develop into complicated fractals and finally the unstable manifolds are perfectly traced out by these particles, as demonstrated in Figure 4.9(c-d). From $t = 20T$ to $50T$, the number of particles

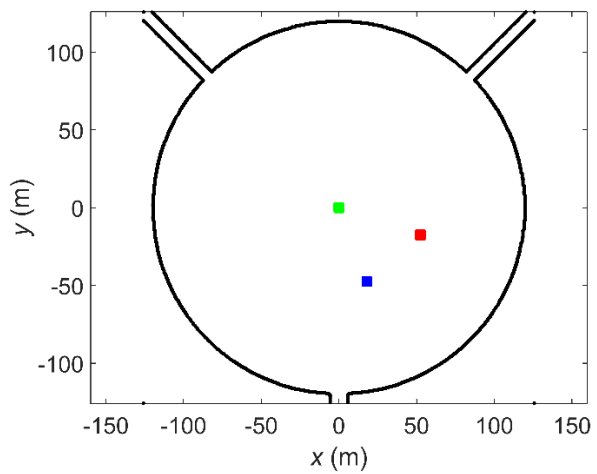
remaining in the lake quickly decreases. When it comes to $t = 50T$, there are few particles still inside the domain, which indicates that the lifetime of particles is finite in an open chaotic system.



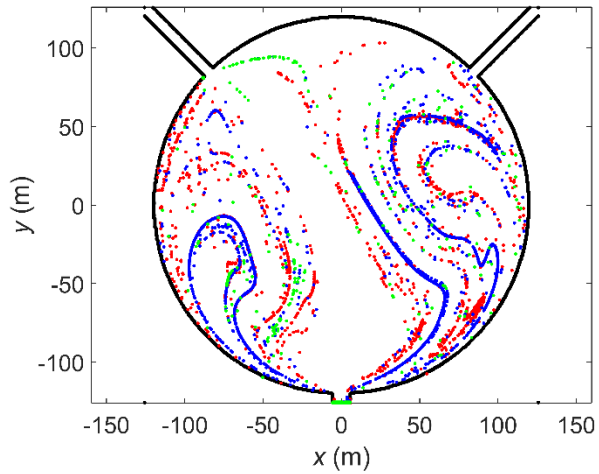
(a)



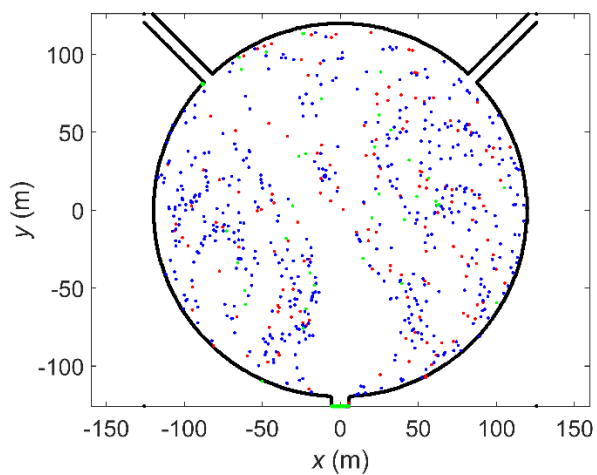
(b)



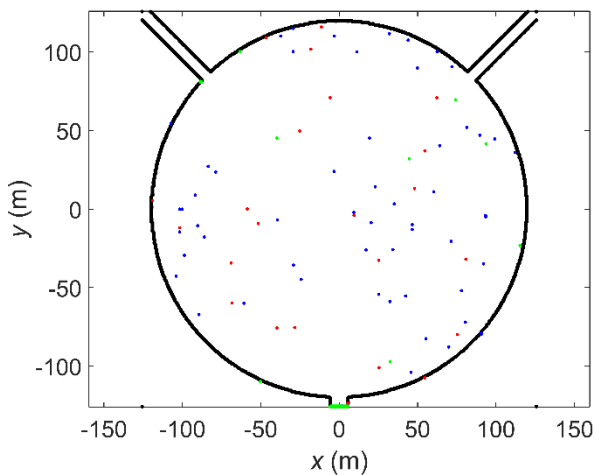
(c)



(d)



(e)



(f)

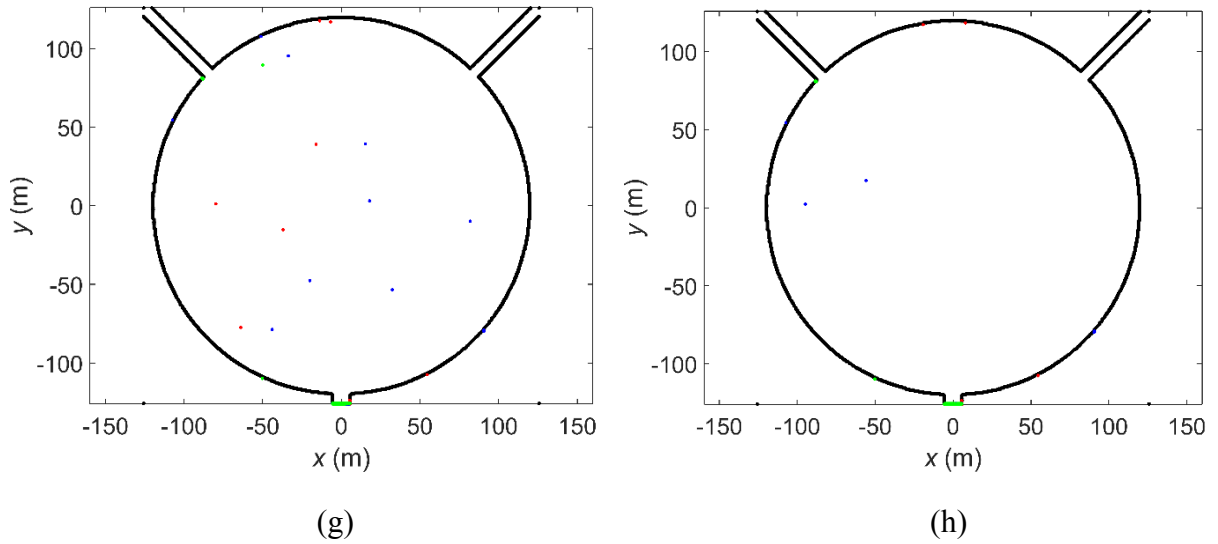


Figure 4.9 FTLE distribution and Evolution of three different particle patches with $\mu_i = 86.4$: (a) forward FTLE distribution; (b) backward FTLE distribution; (c) initial position of patches; (d) snapshot of the particle patches at $t = 10T$; (e) $t = 20T$; (f) $t = 30T$; (g) $t = 40T$; (h) $t = 50T$.

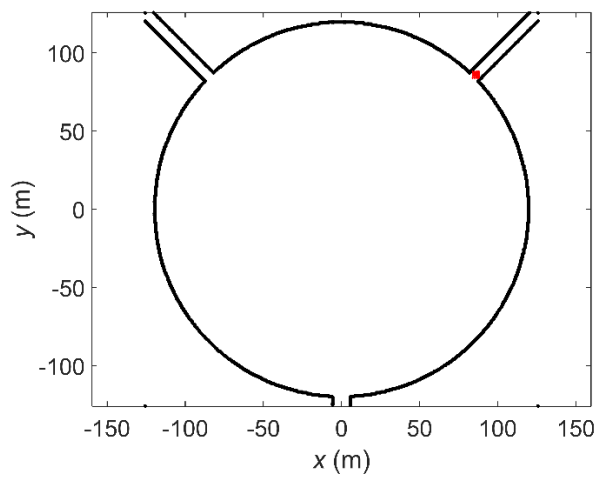
4.4.2 Continuous particle dynamics and occupy rate

In the previous section, we have investigated the Lagrangian dynamics of passive particles in the idealised model lake. We have discussed how particle patches initially located in different regions inside the lake are advected by the flow field and develop patterns of different levels of complexity under the influence of LCSs. In engineering applications, it is also important to know how the particles carried by the inflows are transported and occupy different areas in the lake. The investigation of Lagrangian behaviour of particles from outside is able to provide suitable guidance for effective engineering solutions to improve the water quality of the inflows/outflow-induced shallow water flows. In reality, the duration of inflows may be regulated using gates in inflow channels and the particle dynamics will be mainly dependent on duration and magnitude of the inflows. On the contrary, it is almost impossible to directly control the wind forces (neither the magnitude nor the duration and direction) in a natural flow system. Controlling inflows/outflows therefore provides an effective way to alter the dynamics and hence improve water quality of a (semi-)enclosed water body.

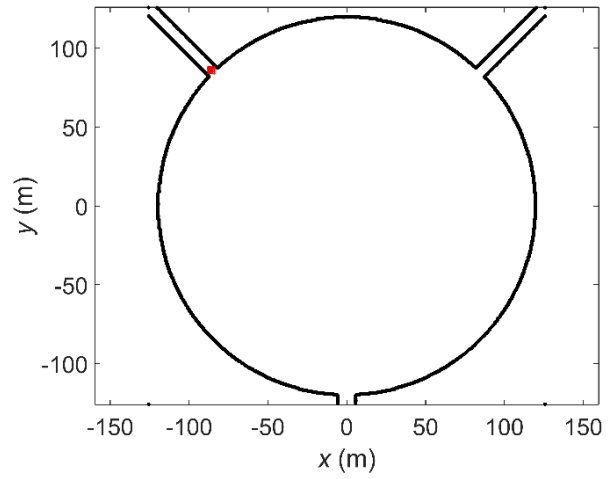
In this section, passive “freshwater” particles will be introduced into the lake through the inflows. Scenarios with six different μ_i are simulated for 50 periods and the corresponding occupy rates are calculated. The occupy rate is defined as the ratio between the area that is ever reached by passive freshwater particles during 50 periods and the total areas of the lake and may be used as an indicator of the effectiveness of the water quality improvement. The best scenario for water quality improvement may be found by analysing the relevant results.

Since continuous injection of passive particles represents freshwater from inflow channels, there are two sources of these particles corresponding to two different inflows. The shape of the patches where particles are created and carried into the lake is rectangular. Each of the patches contains 25 particles and centred at inlets of the inflow channel that is open, as shown in Figure 4.10(a-b). In each time step of the particle-tracking process, 25 new particles are created and occupy the patch in the open inflow channel and flushed into the lake.

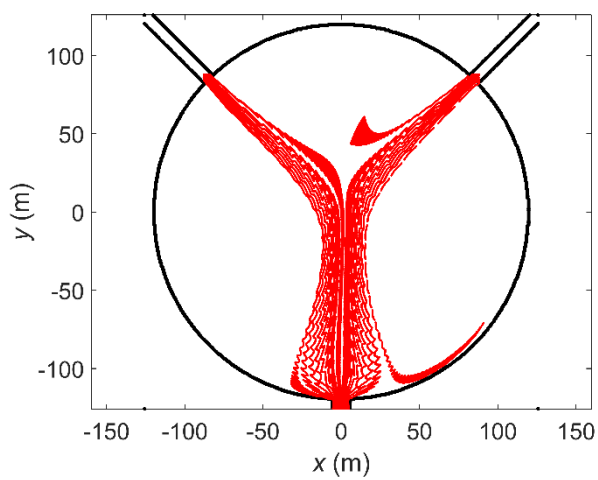
The six scenarios with different μ_i are illustrated in Figure 4.10(c-h). When $\mu_i = 2.7$, particles are first transported to the central area of the lake by the inflow currents and then moved straight to the south before leaving the lake from the outflow channel. The region of particle motions are limited by the LCSs and the “freshwater” particles just pass through the main flow channel and have no chance to mix with other parts of the lake. As μ_i increases to 5.4, some particles have begun to have a longer lifetime in the lake. These particles change their direction near the south shoreline and start to travel along the shoreline of lake from the south to the north, along the attracting LCSs (unstable manifolds) which now partly coincide with lake shoreline. For $\mu_i = 10.8$, particles have already occupied the entire main flow channel and large areas close to the south, west and east shorelines. Also the stagnant zone at northern part of lake has been partly occupied. When μ_i comes to 21.6, most parts of the lake have been occupied by freshwater particles except the two poor mixing islands and area close to the north shoreline. It is clear that the LCSs are material surface and play a significant role in water quality improvement. Due to these LCSs acting as separatrix, passive freshwater particles are not able to enter the poor mixing areas to dilute the possible pollutants or to wash the pollutants out of the lake. At $\mu_i = 43.2$, the northern zone close to the shoreline becomes reachable by the freshwater particles. Meanwhile, the two poor mixing islands become smaller and fresh water occupies most of the rest of lake. Finally for $\mu_i = 86.4$, the particle dynamics becomes chaotic and the whole lake is washed by freshwater, potentially leading to improved water quality.



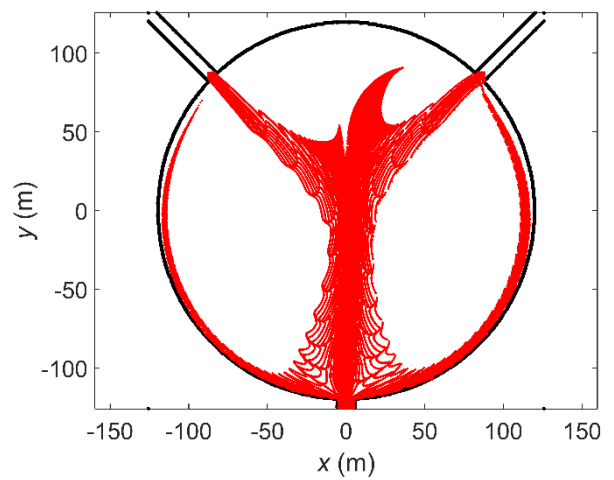
(a)



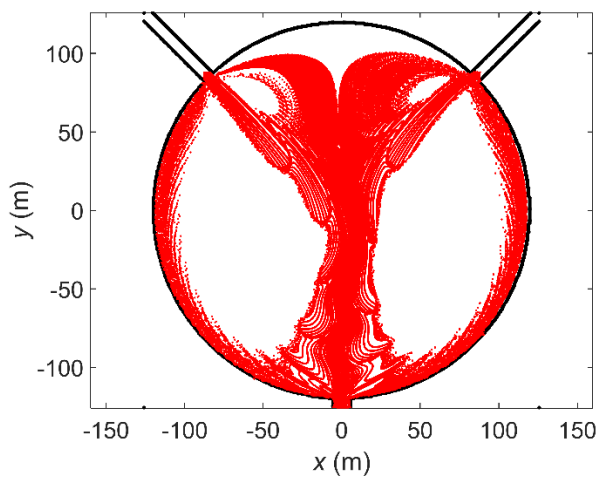
(b)



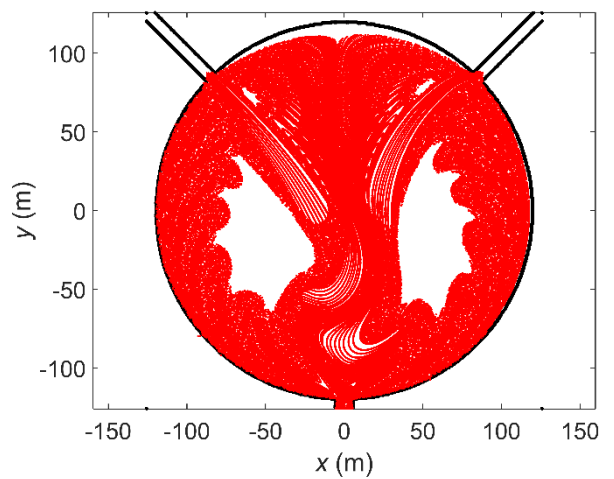
(c)



(d)



(e)



(f)

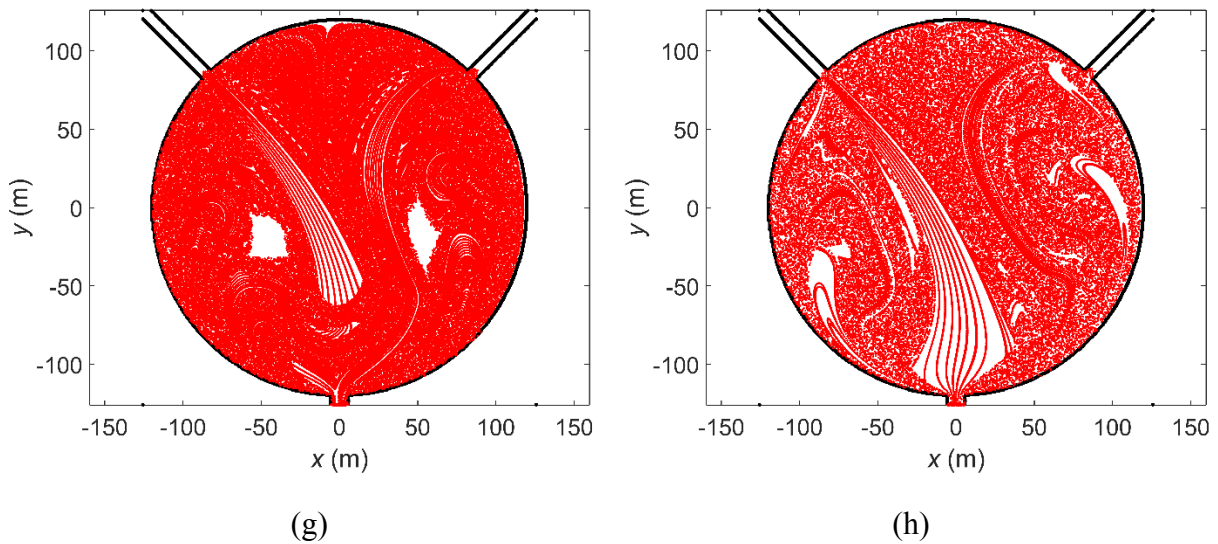


Figure 4.10 The lake area reached by continues particles from inflows with different μ_i condition (a) initial particle position in northeast inflow channel; (b) initial particle position in inflow northwest channel; (c) $\mu_i = 2.7$; (d) $\mu_i = 5.4$; (e) $\mu_i = 10.8$; (f) $\mu_i = 21.6$; (g) $\mu_i = 43.2$; (h) $\mu_i = 86.4$.

In order to quantify the effectiveness of using “freshwater” to encourage particle mixing inside the lake, occupy rate is calculated simultaneously during the particle-tracking process, which describes the percentage of the lake being washed and cleaned by the freshwater coming from outside environments. To calculate the occupy rate, the whole lake is divided into 31428 hydrodynamic cells. If one hydrodynamic cell is ever reached by a passive particle during the whole particle tracking simulation, it is marked as being occupied and the ratio between the marked and total hydrodynamic cells gives the occupy rate. Table 4.1 presents the highest occupy rates for different μ_i and the times required to achieve the corresponding highest occupy rate.

μ_i	Occupy rate (%)	Total time (s)
2.7	20.76	2000
5.4	31.47	4000
10.8	54.46	8000
21.6	87.18	16000
43.2	97.90	32000
86.4	98.96	64000

Table 4.1 The highest occupy rates for different μ_i and the times required to achieve the corresponding rates.

From the results, it is evident that, as μ_i increases, the higher occupy rate is obtained but more time is required to achieve the converged rate. The highest occupy rate among all of the simulations being considered herein is 98.96% and it is obtained when $\mu_i = 86.4$. The time required to achieve the converged occupy rate is 64,000s. When $\mu_i = 43.2$, the final converged occupy rate is 97.90% and the time for achieving this rate is only half of that for $\mu_i = 86.4$, which may be more appropriate for practical applications, considering the fact that $\mu_i = 43.2$ leads to similar converged occupy rate but only needs half of the time to achieve the rate.

4.5 Conclusions

A particle-tracking model is applied to investigate the transport and mixing property of a semi-enclosed shallow flow system induced by inflows/outflows in an idealised shallow water lake. The horizontal mixing dynamics are interpreted using FTLEs, advection of localised particle patches and particles continuously injected from the inflows.

Although the particle motions are greatly influenced by the main flow paths inside the lake influenced by inflows and outflow, which intend to transport the flow/particles directly to the downstream outlet, the dynamics of transport and mixing processes may still be very complicated. Periodic inflow/outflow-induced flow patterns are able to create a weak dynamic system that can be described by a single dimensionless parameter associated with inflow flow duration. FTLE distributions and the associated LCSs confirm that the transport and mixing property of the lake changes from regular to chaotic as the dimensionless parameter (μ_i), i.e. the dimensionless flow duration, increases. Higher mixing efficiency is achieved with higher μ_i and entirely chaotic particle dynamics is achieved when it reaches 86.4. Therefore chaotic mixing may be successfully produced by inflow/outflow induced flow patterns, comparable to those produced by periodic wind stresses. By studying the advection of localised particle patches, it is observed that particles released in a valley area of the FTLE distribution map tend to move and deform slowly, implying poor mixing; particles initially located near to LCSs can be repeatedly stretched and folded to trace out complicated filamentary structures. The analysis of the advection of continuously fed particles is able to provide guidance for engineering applications with regard to how mixing and so the water quality in such an inflow/outflow-induced shallow water flow system can be improved efficiently and economically. In this work, the scenario associated with $\mu_i = 43.2$ is considered to be more appropriate for applications as a high occupy rate 97.90% (almost 100%) can be achieved in a relatively short time.

Chapter 5. Hydrodynamic modelling of Lake Taihu

Investigation of particle dynamics in Lake Taihu requires detailed knowledge of hydrodynamics of the lake, and specifically, velocity fields are required to drive the particle-tracking model. Therefore, accurate prediction of flow hydrodynamics including velocity fields is vital for the subsequent particle-tracking simulations. The aim of this chapter is to therefore set up a lake model and evaluate its performance on reproducing flow hydrodynamics of Lake Taihu in 2005 by comparing the numerical results with field measurements or alternative numerical predictions available in the literature.

5.1 Introduction about Lake Taihu

Lake Taihu, which is located in the Yangtze River delta, is the third largest freshwater lake in China. The lake surface area was about 2,550 km² in the early 1950s but has since decreased, due to high in-lake sedimentation and expanding farming activities to change part of the lake into farm lands, to its present size of about 2,338 km² (Hu *et al.*, 2008). Lake Taihu is a typical natural shallow lake with an annual average water depth of 1.9m and a mean hydraulic retention time of 300 days (Li *et al.*, 2014). Also it is one of the world's heavily populated regions with the highest rate of economic development in the recent years. The lake provides normal water usage for several cities nearby, each occupied by millions of residents (e.g. Wuxi, Suzhou, etc.). Lake Taihu and its associated catchment only cover 0.4% of China's land area and are occupied by 3% of China's population (approximate 37 million), but the region accounts for 11% of the country's GDP (Li *et al.*, 2011a). The lake provides major resources for drinking water, fishing and tourism. However, it also serves as a waste repository for urban, agricultural and industrial sectors of the local economy bodies (Jin *et al.*, 2006). Thus, the water quality in Lake Taihu plays a critical role in supporting the regional economy and ecosystem but has degraded due to intensive human activities.

Lake Taihu is a semi-enclosed shallow water system connected to complicated river and channel networks. There are 219 tributaries or rivers connected to Lake Taihu and those located at the west or southwest of the lake are generally defined as upstream while those located at the east or southeast are usually considered as downstream (Hu *et al.*, 2006). In the flooding season (spring and summer), water flows into the lake from the west or southwest tributaries, travels through the lake to east and finally pours into the Yangtze river (Li *et al.*, 2011a).

Lake Taihu is located in a subtropical region that is strongly influenced by monsoons and wind is a key driving force of the hydrodynamic processes. Wind direction changes with seasons,

with prevailing wind from the southeast in the summer to winds from northwest in the winter. The average wind speed is 3.5 – 5 m/s (Hu *et al.*, 2006).

Due to its vast size and highly complex hydrodynamic and ecological characteristics in different regions, Lake Tai is usually divided into eight sub-regions: Zhushan Bay, Meiliang Bay, Gonghu Bay, Northwest Zone, Southwest Zone, Central Zone, East Epigeal Zone and Dongtaihu Bay (Hu *et al.*, 2008). The southeast part of the lake has significantly better water quality than the northwest regions due to the locations of the influent and effluent rivers (Qin, 2008). The northwest regions, including Meiliang Bay, Zhushan Bay, Northwest Zone and Southwest Zone, suffer from frequent algal blooms and serious eutrophication (Xu *et al.*, 2010).

5.2 Eutrophication of Lake Taihu

Eutrophication is an ecological process, by which a water body acquires a high concentration of nutrients, especially phosphates and nitrates. These nutrients typically promote explosive growth of water plants and algae. As these organisms die and decompose, the decomposition process consumes the dissolved oxygen in water body, thereby creating a hypoxia environment. The hypoxia environment leads to the death of more species, such as fishes, contributing further to eutrophication and causing a severe reduction in water quality and biodiversity. Eutrophication is a natural, slow-aging process in water bodies, particular in lakes, but human activities may accelerate this process (Le *et al.*, 2010; Chislock *et al.*, 2013).

Eutrophication in Lake Taihu is associated with blue-green algal blooms (Chen *et al.*, 2003b; Qin *et al.*, 2007; Paerl *et al.*, 2011). Algal blooms may be triggered by the following conditions: 1) the nutrient level is high, particularly when the phosphorus and nitrogen are sufficient for the algae population to rapidly grow; 2) the transport process of water flux is low and water body is lack of mixing; and 3) the weather patterns, especially warm temperature in the summer, are stable for a long time.

With the rapid economic development and population growth, more pollutants have been discharged into the Lake Taihu, resulting in serious water pollution and accelerating eutrophication over the past three decades (Qin *et al.*, 2007; Qin *et al.*, 2010). During this period, the lake has changed from a mesotrophic, diatom-dominated lake to a hyper-eutrophic, cyanobacteria-dominated system (Paerl *et al.*, 2011) and the area of the lake affected by harmful algal blooms has been continuously increased (Zhu *et al.*, 2008). Before 2000, algal blooms mainly occurred in several northern bays that are close to main cities and part of the western

lake area. Then they had spread to the whole western lake area, involving half of the lake by 2007. Now algae blooms appear regularly and frequently throughout most of the lake, especially in summer time, and the duration of algae blooming has also become longer (Chen *et al.*, 2003b; Dong *et al.*, 2008). In particular, the notorious 2007 blue-green algae outbreak event resulted in a series of environmental, economic and societal problems, including a threat to potable water supplies for approximately 10 million consumers (Guo, 2007). Therefore, there is an urgent need for a better understanding of the mixing and transport dynamics of Lake Taihu, and effective engineering solutions to dilute the pollution and improve water quality.

5.3 Fresh water transfer and possible routes

To enhance water exchange and alleviate eutrophication in Lake Tai, different inter-basin water diversion projects have been implemented or planned to flush pollutants out of Lake Taihu by transporting freshwater from the Yangtze River or other watercourses.

In this work, four different routes are considered to transfer water to dilute the pollutions and mitigate the influence of eutrophication. Two routes (Wangyu Route and Xingou Route) have already been applied as an emergency countermeasure to improve the water quality and the other two routes (Xinmeng Route and Fuchun Route) are still in the stage of discussion.

Route Wangyu, which was implemented in winter-spring 2002, transfers freshwater from Yangtze River into Lake Taihu through Wangyu River at the northeast of the lake. Freshwater transferred from this route has been proved to have positive environmental effects on decreasing the concentration of phytoplankton and total nitrogen in some sub-areas (Meiliang Bay, Gonghu Bay and Northwest Zone) (Jia *et al.*, 2008). Route Xingou is considered as a supplement to the Wangyu Route to improve water quality of northern lake region, especially the Meiliang Bay that is highly polluted by industrial and daily life contaminants from Wuxi City. This route was implemented in 2004 together with the installation of two pump stations named Meiliang and Xingou in Meiliang Bay. Li *et al.* (2013b) proved that this route combined with Route Wangyu is able to provide an integrated engineering solution to enhance water transport and exchange capacity in Meiliang Bay.

Though Route Wangyu and Route Xingou show positive effects on temporal water quality improvement at the northern part of the lake (mainly in Gonghu Bay and Meiliang Bay), water transfer from these two routes does not have any significant influence on water quality of northwest and western areas, especially in the Zhushan Bay (Li *et al.*, 2013b). Hence, a new transfer route is required for the western region as part of the water transfer plan. Route

Xinmeng has been designed to introduce freshwater from Yangtze River via Xinmeng River to mitigate the pollution situation in these areas. Route Xinmeng can directly introduce freshwater into Zhushan Bay and then transfer freshwater to wash the western areas. Finally, the last route, Changxing Route, is planned to transfer freshwater via Changxing River to improve the water quality of southwestern part of the lake.

Although these routes are designed to improve water quality of the Lake by transferring ‘clean’ water into the highly polluted and eutrophic areas and flushing the pollutants to avoid algae blooms, their performance may be difficult to be evaluated directly due to the complicated hydrodynamic and ecological situations of the lake. Traditional methods of environmental assessment, which usually analyses relevant environmental factors, such as the concentration of phytoplankton, etc., using ecological models (Hu *et al.*, 2010; Zhai *et al.*, 2010), cannot directly link the change of water quality with the sources (i.e. how fresh water transferred from different routes contributes to the improvement of water quality) and hence are not applicable here to give an informative evaluation of the aforementioned water transfer projects. The change of the environmental factors may be due to a variety of reasons, for example, the change of local temperature or the duration of sunshine. Therefore, this chapter aims to set up a lake model to simulate the hydrodynamic of Lake Taihu to support analysis of particle dynamics in the next chapter to evaluate the performance of these transferred routes.

5.4 The lake model

The lake model is constructed to simulate the hydrodynamic of Lake Taihu for 2005. In the model, a rectangular domain of 67 km × 68.625 km covering the entire Lake Taihu is considered as the computational domain, with the Lake as shown in Figure 5.1. Measurements in terms of water level are available for the current study from four gauge stations as marked by the black triangles in Figure 5.1, three stations (Dapukou station, Jiapu station and Xiaomeikou station) located nearshore and one (Xishan station) near the center. The daily measurements of water level for the whole year of 2005 at the four gauge stations are used herein to calibrate the hydrodynamic lake model.

Input datasets for model setup include wind, inflow discharge, water level of outflow and Digital Elevation Model (DEM). A constant wind speed is reasonable to represent the annual wind speed in Lake Taihu (James *et al.*, 2009). Hence an average wind speed of 5m/s is used to represent applied in the lake model and the corresponding magnitude of wind stress is assumed to be a constant, 0.044N/m², and is uniformly distributed all over the surface area of

Lake. Since Lake Taihu is located in a monsoon region, wind direction is monthly changed. For winter time, including January, November and December, wind direction is northwest (NW); for spring and summer time, including February, March, May, June, July and August, wind comes from southeast (SE); for April, wind direction is east (E); for September and October, wind direction is northwest (NW) (Li *et al.*, 2013a). It should be noted that, in the model, the wind direction changes linearly during the year.



Figure 5.1 Computational domain, gauge stations and inflow/outflow locations.

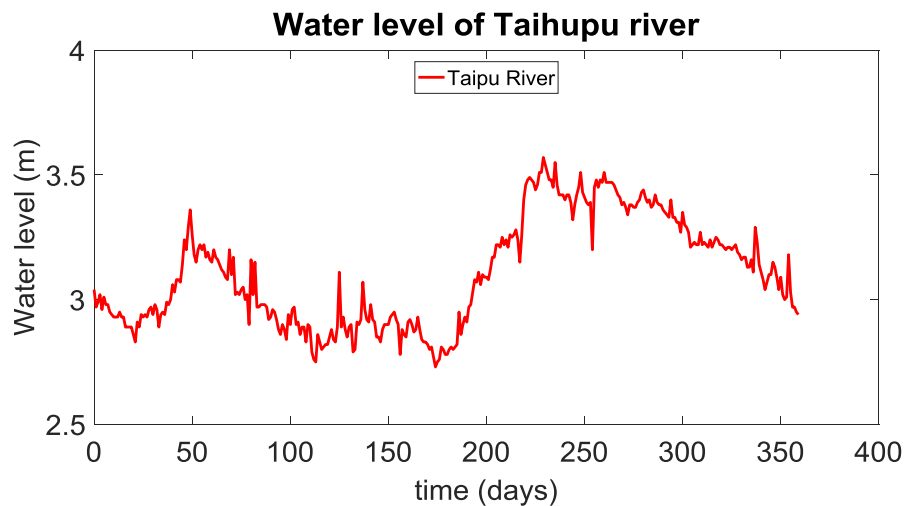
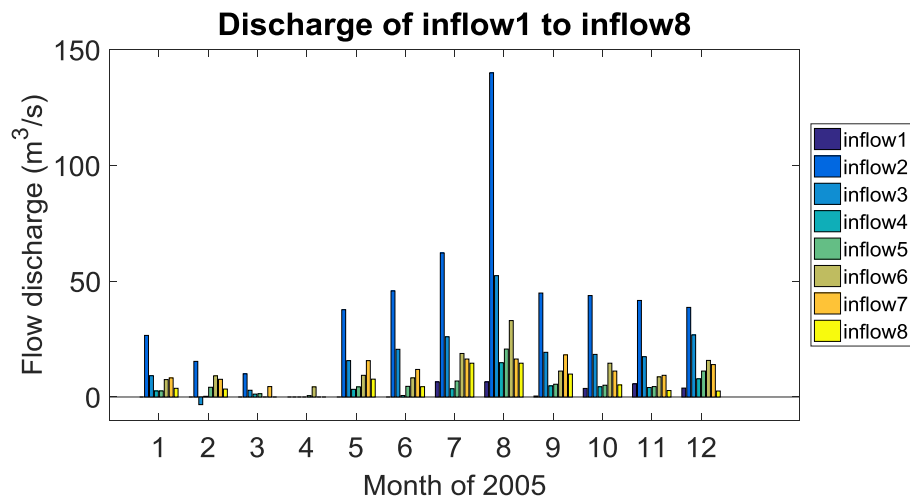


Figure 5.2 Annual time history of the water level in the Taipu River outlet.

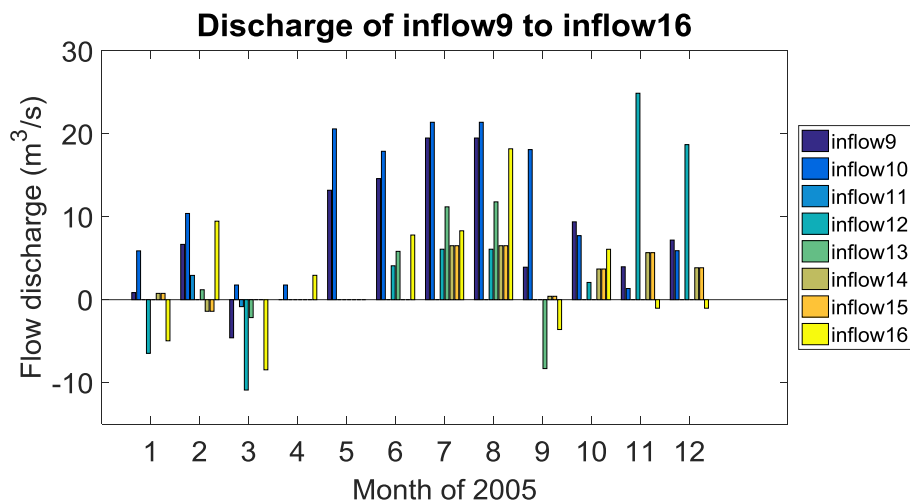
The inflow/outflow river system is simplified to 34 main rivers and channels, as marked by green, red and orange circles in Figure 5.1, with the red circle representing Wangyu River (inflow) and the orange circle being the Taipu River (outflow). Monthly varying inflow

discharges are imposed in these inflow/outflow points to provide boundary conditions. The outflow boundaries are specified with water level and Figure 5.2 presents the annual time history of water level at Taipu River.

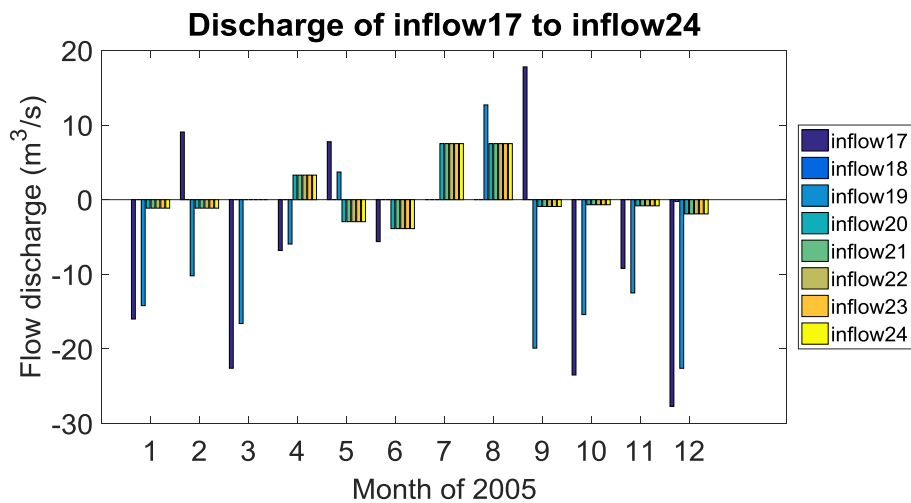
For the inflows, the 33 tributaries including the main inflow through Wangyu River are treated as point sources because the width (less than 50m) of most of the river entrances is smaller than the grid size (i.e. 62.5m, 125m and 250m as used in the simulations). The effect of the inflow/outflow on the overall lake hydrodynamics is insignificant compared with the influence from the wind stress (Qin, 2008), and the means used to impose these inflow and outflow boundary conditions does not have any major effect on the simulation results. Figure 5.3 presents the monthly-changed discharge for the 33 inflow channels. Most of tributaries receive inflows from outside throughout the whole year while a small numbers of channels have reversed flows, indicating these channels essentially draw water from the Lake.



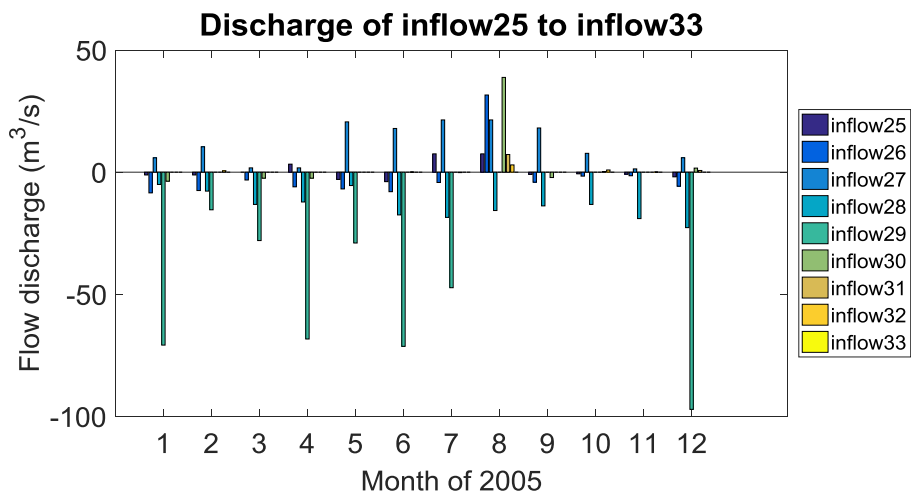
(a)



(b)



(c)



(d)

Figure 5.3 Monthly-changed discharge of the 33 inflow channels surrounding Lake Taihu.

The bathymetry is also required in setting up the shallow water model for simulation of lake hydrodynamics. The original bathymetric data was provided as 8793 discrete points dotted all over the lake as shown in Figure 5.4(a). These points contain the elevation of bottom topography. These discrete bathymetric data are transformed into raster based elevation model, referred to as digital elevation model (DEM) from now on, using ArcGIS, which can be directly used in the shallow water model. The transformed DEM is shown in Figure 5.4(b). To analyze the grid convergence of numerical simulations and determine the appropriate grid resolution as required to resolve the hydrodynamic processes in Lake Taihu, three grids of different resolutions are used, i.e. $250\text{m} \times 250\text{m}$, $125\text{m} \times 125\text{m}$ and $62.5\text{m} \times 62.5\text{m}$. The numerical results obtained at different resolutions are presented and discussed in next section.

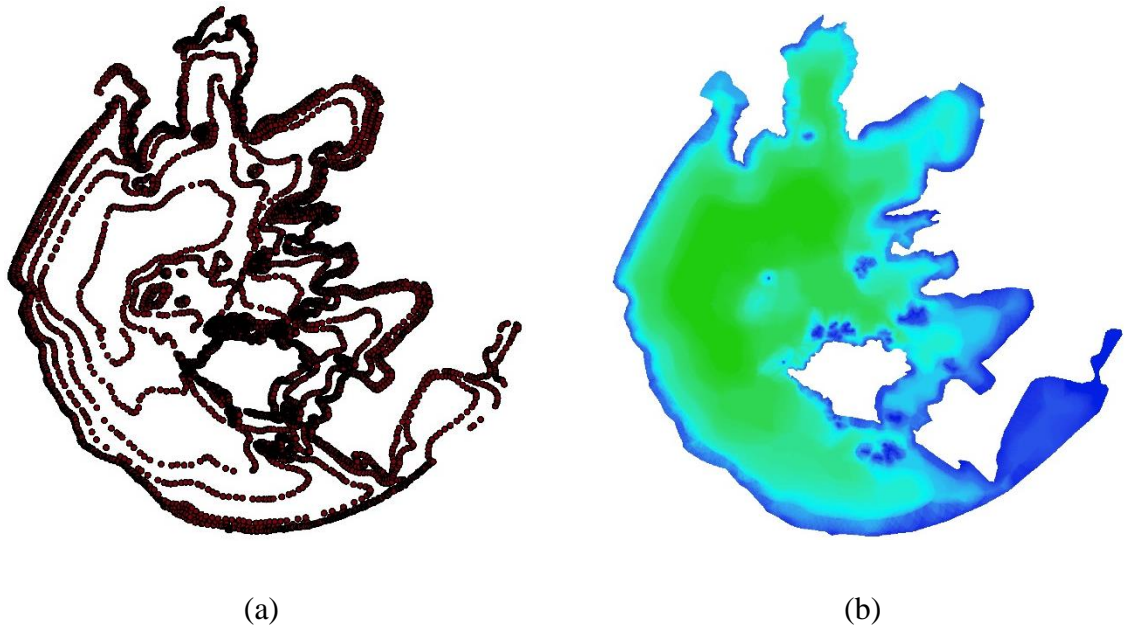


Figure 5.4 Bathymetry of computational domain: (a) original discrete point data; (b) transferred DEM at $125\text{m} \times 125\text{m}$.

5.5 Model calibration and result discussion

In the section, the two-dimensional hydrodynamic model introduced in the previous chapter is set up, calibrated and tested for simulating the flow hydrodynamics in Lake Taihu.

5.5.1 Model calibration and validation

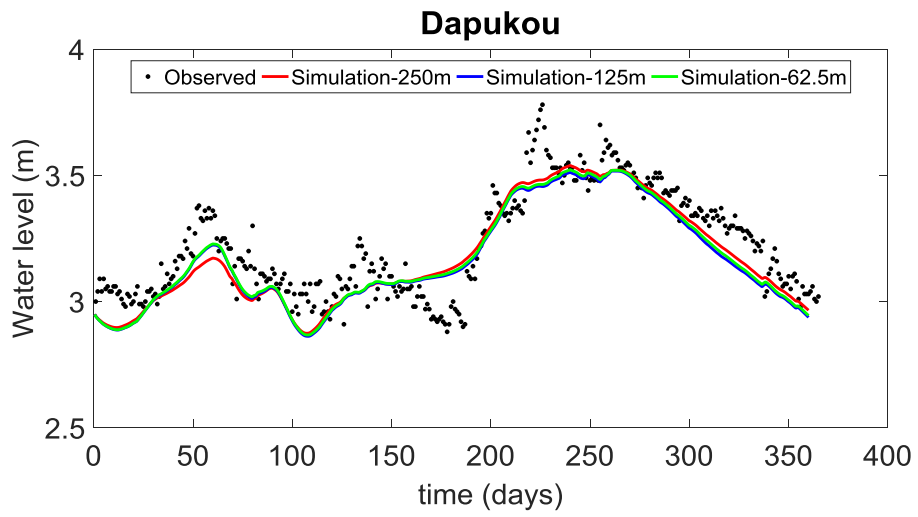
In the shallow water model adopted in the current study, two parameters, the Manning coefficient and the eddy viscosity coefficient, are required to be determined first through model calibration. Because these two parameters have an obvious effect on flow pattern distribution. Model calibration is carried out by comparing the numerical results with field measurements of annual histories of water level at four gauge points. The final parameters chosen for the rest of the simulations are Manning coefficient $n = 0.025 \text{ s/m}^{1/3}$ that is constant over the entire domain and eddy viscosity parameter equal to 3.4. During all of the simulations, slip boundary conditions are assumed along the lateral boundaries.

Figure 5.5 shows the annual time histories of water level at the four gauge stations computed with the final calibrated parameters in comparison with the measured data. The numerical results as well as the measured histories of water level present a very similar trend at all four stations. The water level reaches its peak value in the summer (approximate the 230th day of the year) and then decreases continuously during autumn and winter. This may be due to the seasonal change of discharge patterns of the inflow/outflow rivers connected to the lake.

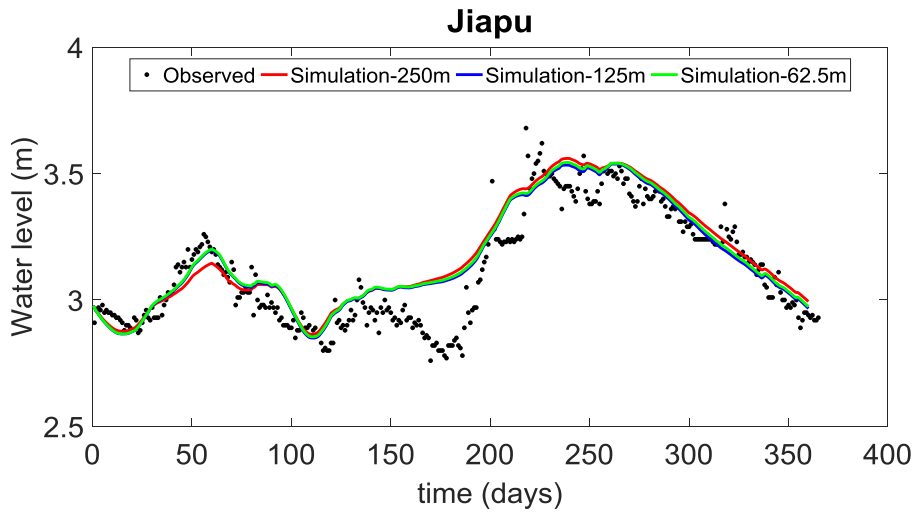
Particular, the surrounding catchment experiences a wet season over the summer with substantial rainfall, which is reflected in the increased inflows during the summer months, leading to increased water in the lake. Inflow discharge and subsequently lake level decrease when it comes the dry autumn and winter months. Due to the low flows, some tributaries even have reversed flow direction and drain the lake.

The numerical results agreed reasonably well with the observed data. However, obvious difference between the predicted and measured water level is observed in the spring and summer time. This may be a result of using inaccurate wind data because wind has a great influence on water level. The averaged wind data used to drive the shallow water model is collected from the weather station of Taihu Laboratory for Lake Ecosystem Research in Meiliang bay near the land, underestimating the actual wind force over the lake. Spring and summer is the monsoon period when wind speed sometimes is larger than the averaged wind speed. This makes the influence of underestimate of actual wind force more obvious. While in autumn and winter, the actual wind speed is relatively small and the difference between measured wind speed and real wind speed is small (James *et al.*, 2009). So the predicted water level fits better with the measurements in these two seasons.

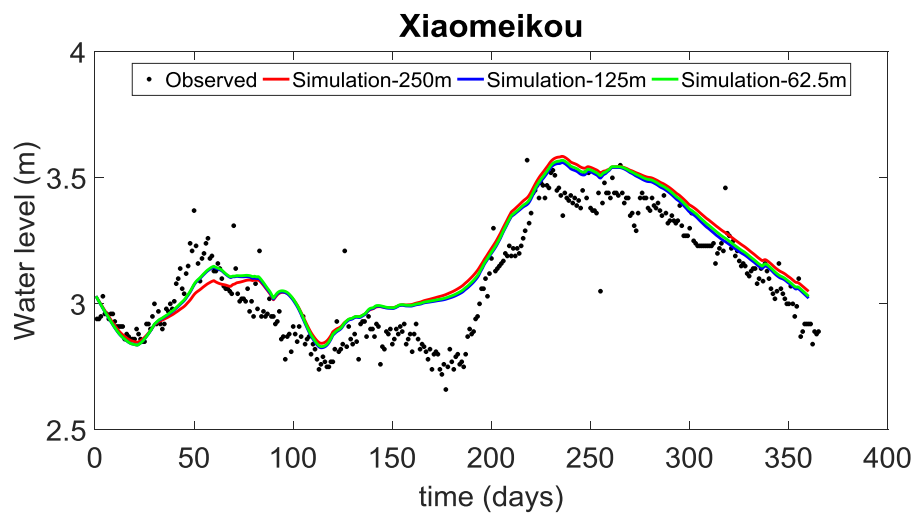
Also presented in Figure 5.5 are the numerical results obtained from simulations at three different resolutions. It is evident that all three simulations produce similar results, with the results obtained on the $250\text{m} \times 250\text{m}$ diverge slightly further from the other two simulations. This indicates that the lake simulations could be performed with two successively finer grids (125m and 62.5m). So the grid convergence is achieved. Considering both of the computational efficiency and accuracy of numerical simulations, the grid with $125\text{m} \times 125\text{m}$ cells is selected to predict the final flow field of Lake Taihu, which will be used by the particle-tracking model in the next chapter to analyse particle dynamics.



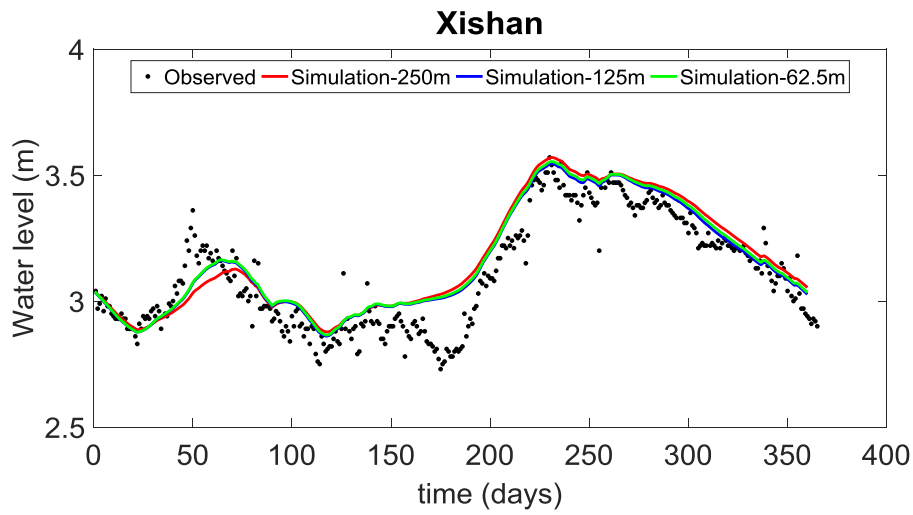
(a)



(b)



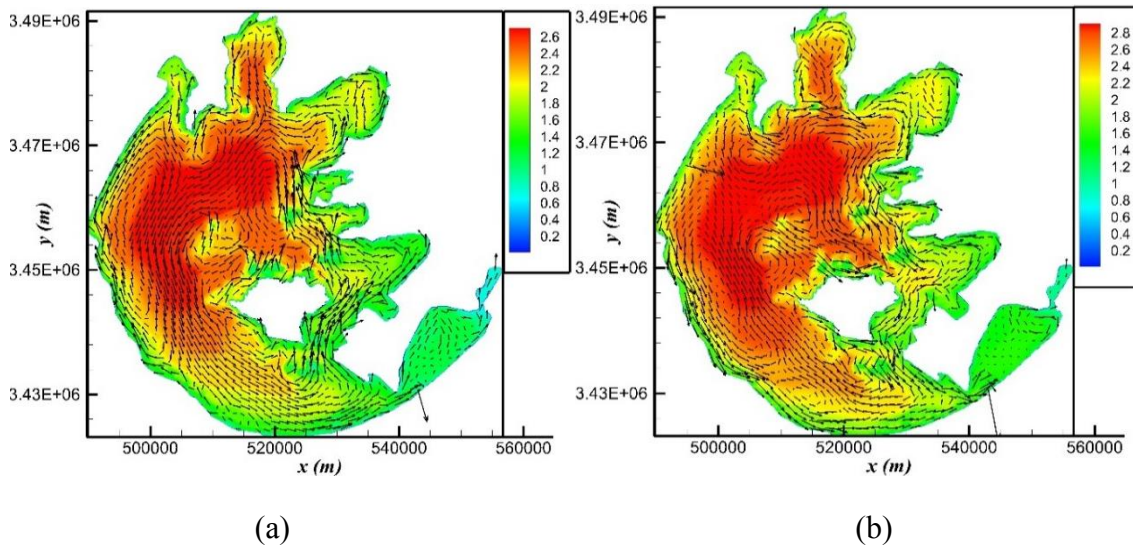
(c)



(d)

Figure 5.5 Annual time histories of water level at the four gauge stations: (a) Dapukou station; (b) Jiapu station; (c) Xiaomeikou station; (d) Xishan station.

In order to further validate the numerical results, the predicted velocity field is compared with alternative results available in the literature. Figure 5.6(a)&(b) presents the velocity fields on two different days (i.e. 14th March and 19th August 2005) predicted by the current model.



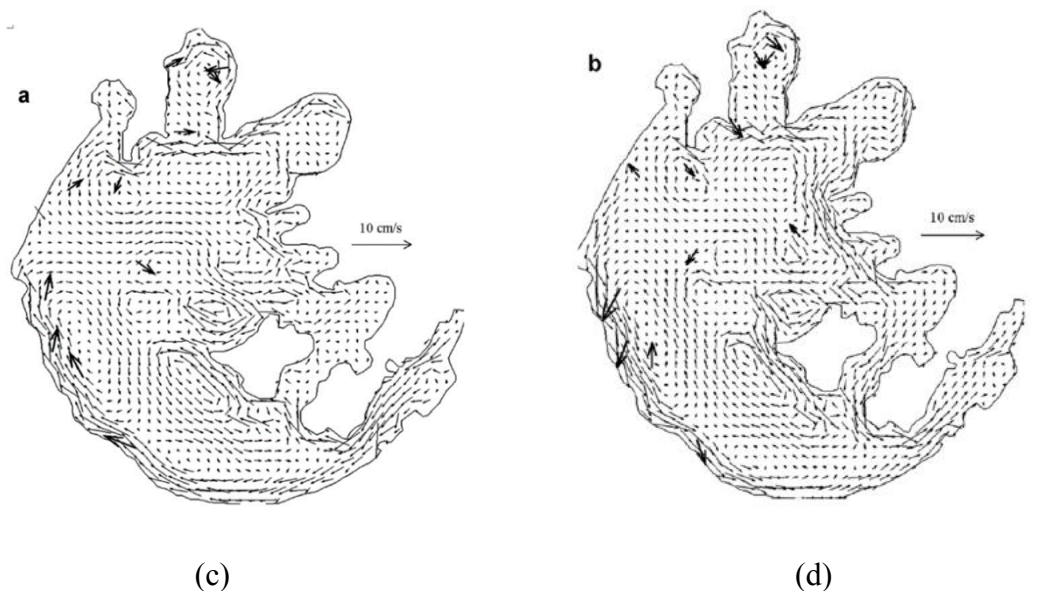


Figure 5.6 Predicted flow fields of Lake Taihu at two different days: (a) Current predicted velocity field on 14th March 2005; (b) Current predicted velocity field on 19th August 2005; (c) Predicted velocity field and point-based velocities on 14th March 2005 (from Li *et al.* (2011b)); (d) Predicted velocity field and point-based velocities on 19th August 2005 (from Li *et al.* (2011b)).

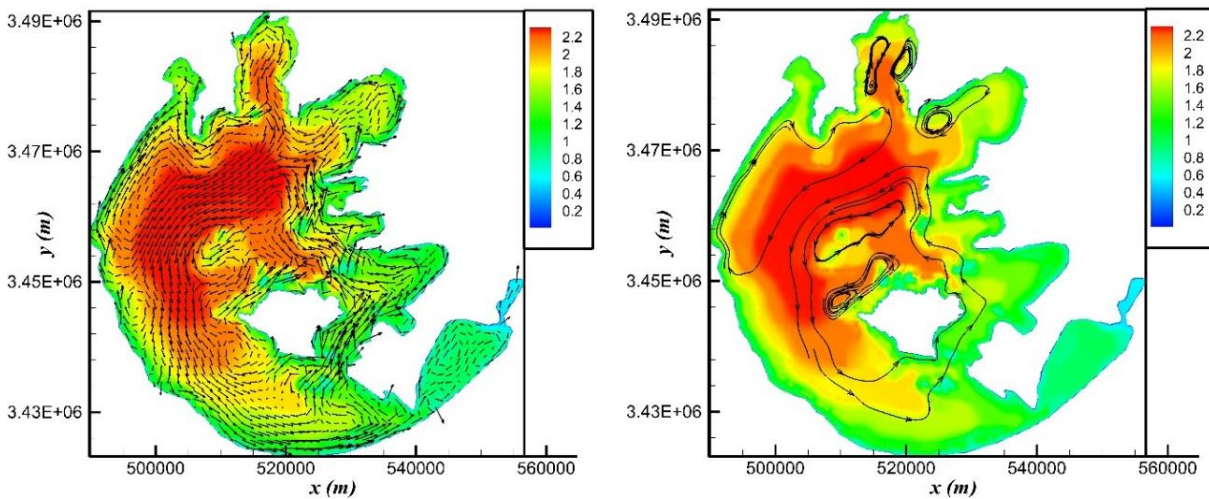
On both days, large velocities develop at the western coast of lake due to relatively straightened boundary geometry. On the other hand, the flow velocities become small, leading to almost stagnant water in those relatively enclosed bays, e.g. Meiliang Bay, Gonghu Bay and Dongtaihu Bay, irrelevant to the change of wind direction. These flow features have been correctly captured by the current model as observed. Specifically for the predicted velocity on 14th March, a major clockwise flow circulation and an anticlockwise circulation have developed respectively in the western part and around Xishan Island. Water moves to the north along east and west coasts and flows to south through centre. On 19th August, due to the change of wind direction, a reversed flow field is predicted. The current predicted velocity fields are found to agreed closely with those obtained by (Li *et al.*, 2011b) using a different numerical model, as shown in Figure 5.6(c)&(d) for either of the days. On Li *et al.*'s numerical velocity fields, point-based observed velocities are also plotted with large bold arrows.

Figure 5.6 still shows some difference between the numerical results and the literature finding. This may be caused by the different grid resolution. The grid resolution used by Li is 750m \times 750m while the grid resolution used in this thesis is 125m \times 125m. The dimension of hydrodynamics models used may also influence the results. Compared to the proposed 2D shallow water model, the 3D model (EFDC) used by Li produce different flow patterns in some narrow regions where the vertical process may not be ignored.

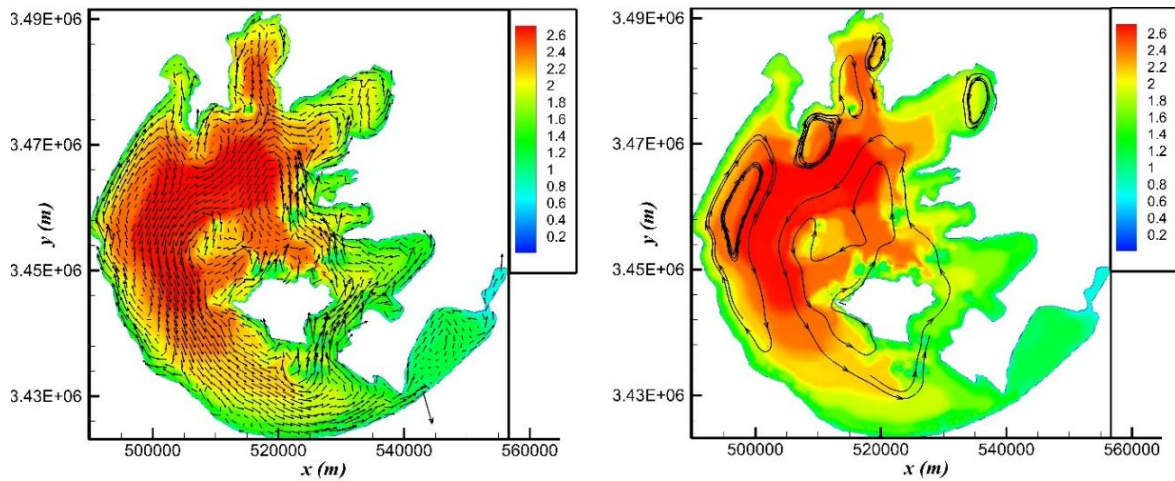
5.5.2 Wind-induced velocity fields at different seasons

As mentioned above, the hydrodynamics of Lake Taihu is mainly driven by prevailing northwesterly monsoon winds in the winter and southeasterly monsoon winds in the summer. Spring is dominated by easterly winds and autumn is characterized by northeasterly winds. These time-varying wind forcing conditions have been used to drive the shallow water model and predict the flow circulations in the lake and the predicted velocity fields at different seasons are shown in Figure 5.7 and Figure 5.8, which will be used to drive the particle-tracking model in the next chapter.

Following the prevailing NW winds in the winter, two large circulations and several smaller circulations are created, as shown in Figure 5.7(a). The big anticlockwise circulation surrounding Xishan Island is located in the central area of the lake. Water is transported from NW to SE through along the western part of the lake and returns to north through east part. Another large clockwise circulation is located at the north of the previous circulation. Meiliang Bay has been divided into two parts from the east-west direction by two local circulations. When the wind direction change to east in spring, the corresponding flow field is shown in Figure 5.7(b). The big anticlockwise circulation remains with similar shape and location but the clockwise circulation has been pushed to western part by the east winds. The circulation located in the west of Meiliang bay has begun to move southwards and connect with another circulation outside the bay.



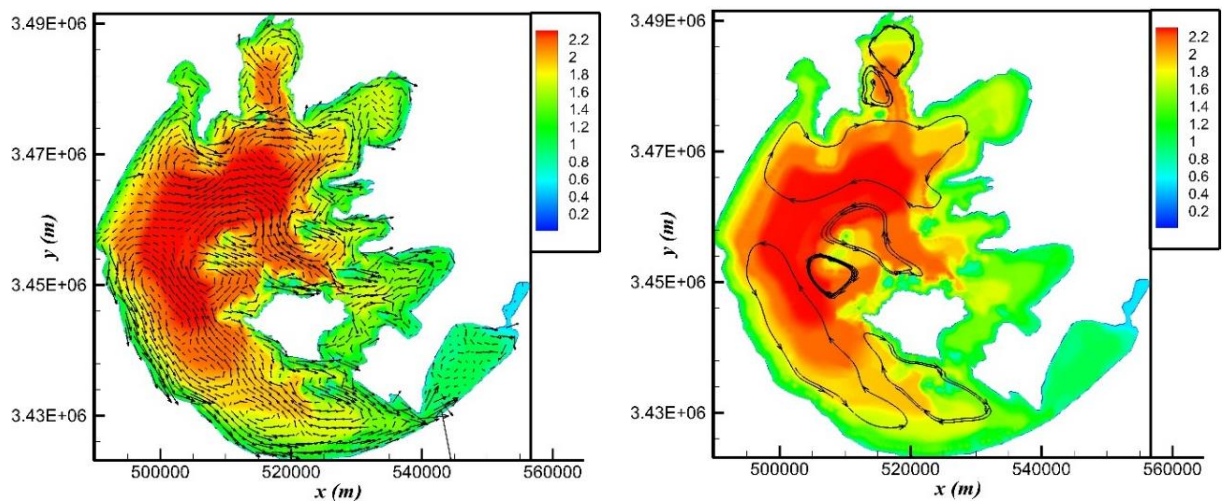
(a)



(b)

Figure 5.7 Numerical velocity fields and corresponding streamlines in: (a) winter; (b) spring.

In early summer, following the change of the wind direction, the big anticlockwise circulation that occupied the central area of the lake has already split and replaced by smaller local circulations, as shown in Figure 5.8(a). The flow in Meiliang bay is divided into two circulations in north-south direction due to the influence of SE winds. When it comes to the late summer, the SE winds continue to influence the flow hydrodynamics in the lake. Water is transported from SE to NW through the central area and returns back along the west and east coasts, as indicated in Figure 5.8(b). Finally in the autumn, the big circulation which was surrounding the Xishan Island appears again but its direction has switched to clockwise, as shown in Figure 5.8(c). Under the influence of the NE winds, the water in the Meiliang Bay has been forced out of the bay and moved to southwest and a northern circulation exists in the region covering the Meiliang Bay and West zone.



(a)

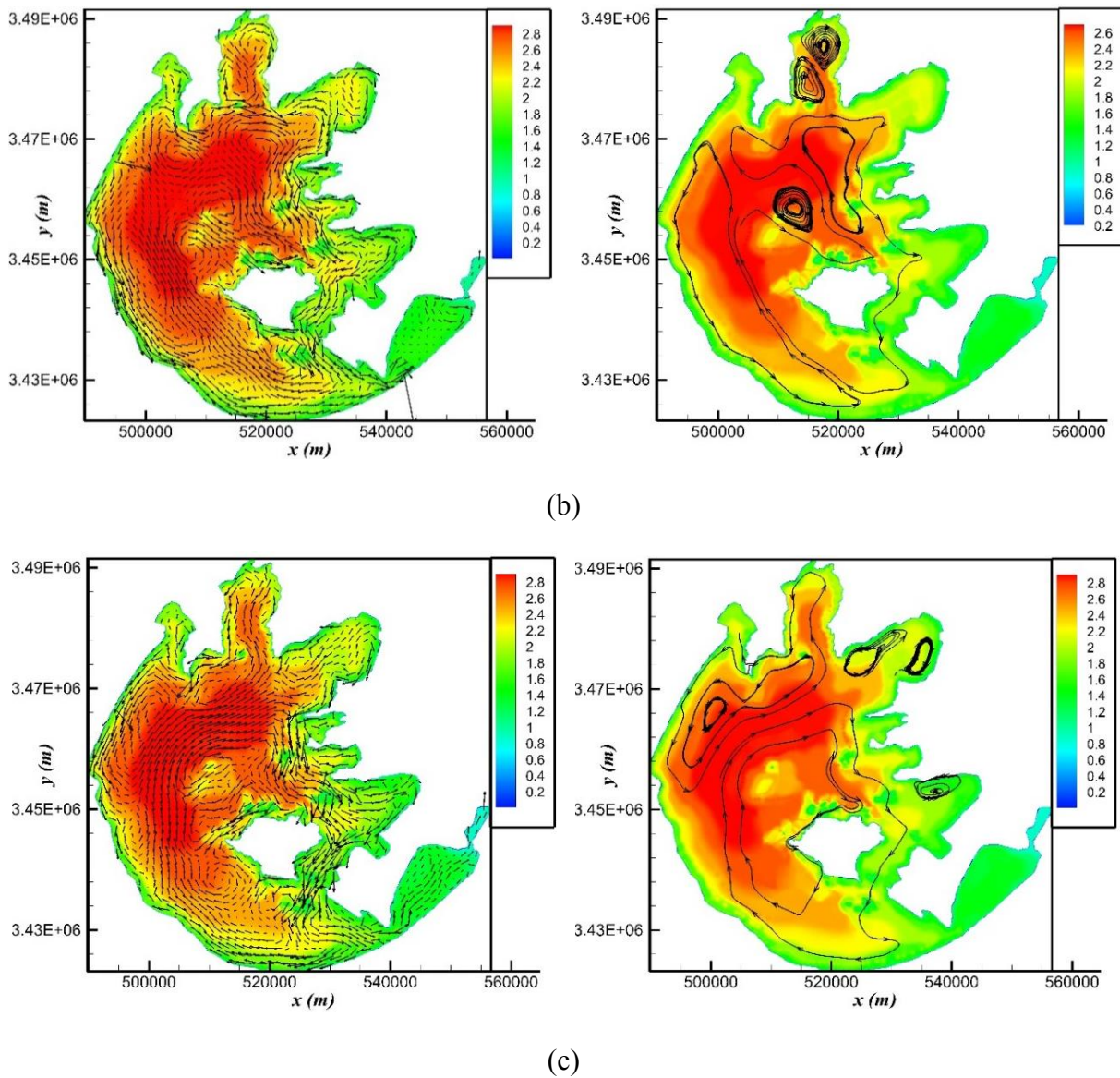


Figure 5.8 Numerical velocity fields and corresponding streamlines in (a) early-summer; (b) late-summer; (c) autumn.

5.6 Conclusions

In this chapter, a lake model has been set up to simulate the annual Lake Taihu hydrodynamics. Wind stress, inflow discharges and outflow water level observed in 2005 are used as the boundary conditions to drive the hydrodynamic model.

The model is first calibrated to determine the key model parameters by comparing the simulated water levels with observations available for four gauge stations. Simulations have also been carried out with different grid resolutions. It is found that the simulation results are not very sensitive to the grid resolution and a computational grid consisting of 536×549 cells is for the final simulation, compromising the model accuracy and efficiency. The final simulated velocity

fields are compared with alternative numerical results available in the literature and good agreement is achieved, further validating the current numerical results.

Finally further investigation has been conducted to discuss the effect of varying wind direction on lake hydrodynamics by demonstrating the seasonal change of the wind-driven flow field. It is clear that wind direction has a great influence on the distribution of the lake circulations. Circulating flows appear or disappear following the change of the wind field. In the winter when the NW winds are dominant, large circulations are observed in the central of the lake; while in the summer when the SE winds are prevailing, the large circulations essentially split into smaller ones. The predicted annual flow field will be used in the next chapter to drive the particle-tracking model and investigate the Lagrangian particle dynamics in the next chapter.

Chapter 6. Particle dynamics of Lake Taihu

The study of transport and mixing in natural (semi-)enclosed shallow flows is of major interest because of their economic and ecological importance. Due to the associated complex topography, geometry and highly variable driving forces (e.g. wind stresses), the flow dynamics in the natural (semi-)enclosed shallow environments remains poorly understood. Traditional Eulerian descriptions, such as Eulerian velocity field which is obtained by solving the dynamics governing equations or through field measurements, are not sufficient to provide insight of the complex dynamics because transport and mixing of fluid is inherently a Lagrangian process which is unstable owing to its sensitivity with respect to initial conditions. Recent developments of nonlinear dynamic theory shows that Lagrangian coherent structure (LCS) are robust features of Lagrangian fluid motion in aperiodic environmental flows. LCS uncover special surfaces of fluid trajectories that organize the flow and provide a sketch of transport and mixing property, when Lagrangian chaos impedes a meaningful direct comparison of single tracer trajectories (Schuster and Grigoriev, 2012). In this chapter the transport and mixing properties of a large natural shallow lake, Lake Taihu, will be studied using Lagrangian techniques.

6.1 Introduction of particle dynamics

In order to investigate the particle dynamics and evaluate water transfer applications in Lake Taihu for different seasons, the velocity fields are stored at time steps of 86400s (one day) for the particle trajectory calculations, and for the whole hydrodynamic simulation process, 360 velocity fields are obtained to represent the annual velocity distribution of Lake Taihu (Due to the reason of wind data pollution, the velocity fields of five days are removed). These velocity fields will be used as inputs in the particle tracking model. Then the advection Equations are integrated by a fourth-order Runge–Kutta scheme using the velocity fields obtained by bilinear spatial interpolation within the grid cells and by linear interpolation between the stored time levels.

In the particle tracking model, Lagrangian methods including FTLE and passive particle tracking are used to investigate the transport and mixing dynamics of the lake and calculate the occupy rate of transformed water to the whole lake and four heavy polluted sub-areas including zhushan Bay, Meiliang Bay, Gonghu Bay and Northwest Zone respectively. In this study, two kinds of route scenarios are simulated: single route scenarios and combined route scenarios. For single route scenarios, relative fresh water are only transferred into Lake Tai

from one selected route and these scenarios are able to analysis how the water quality of the whole lake and heavy pullulated sub-areas are influenced by a single-route water transfer engineering solution; for combined route scenarios, different kinds of route combination including two route combination and three route combination are tested and these scenarios could be used to study how to maximize the benefits for improving water quality of the whole lake and heavy pullulated sub-areas with minimum economical cost and environmental impact. In our project, the most appropriate water transferred route scenarios (no matter single route scenarios or combined route scenarios) are assessed by using the calculation of occupy rate mentioned in Chapter 4 and Lagrangian particle tracking with the application of shallow water model and particle tracking model.

6.2 FTLE distribution of Lake Tai

Now the FTLE-LCS method, achieved by the application of particle tracking model, will be used to study the transport and mixing property of Lake Taihu, in particular to identify the transport barriers in the lake.

6.2.1 FTLE parameter setting

The application of FTLE algorithm to the simulated velocity fields requires to set up relevant parameters to identify the structures of transport and mixing clearly and efficiently. With the scale of structures to be observed and with the characteristics of the velocity field, a suitable combination of these parameters should be decided.

The first parameter should be considered is the integration time. Because FTLE distribution uncover the transport and mixing properties of fluid over a certain duration. When computing FTLE, an integration time should be chosen properly. For the study of Lake Taihu, a period of 30 days, which is shown in Figure 6.1(c), is chosen as the flexible integration time for FTLE computation. The values of these LCSs are in order of 0.05-0.2 $hours^{-1}$. Though it seems to be quite long compared to our idealized case and other researcher's case, the length of time is still feasible because the magnitude of main flow speed in Lake Taihu is too small (centimeter-level per second) compared to the huge area of the lake (approximate 2338 km^2). So a long-time advection process is required to let the flow features have a chance to emerge, but not so long that most artificial tracers have already leave the considered domain and make the calculation of the deformation gradient uncorrelated. Generally speaking, LCS can shrink, grow, appear and disappear with the selection of integration time.

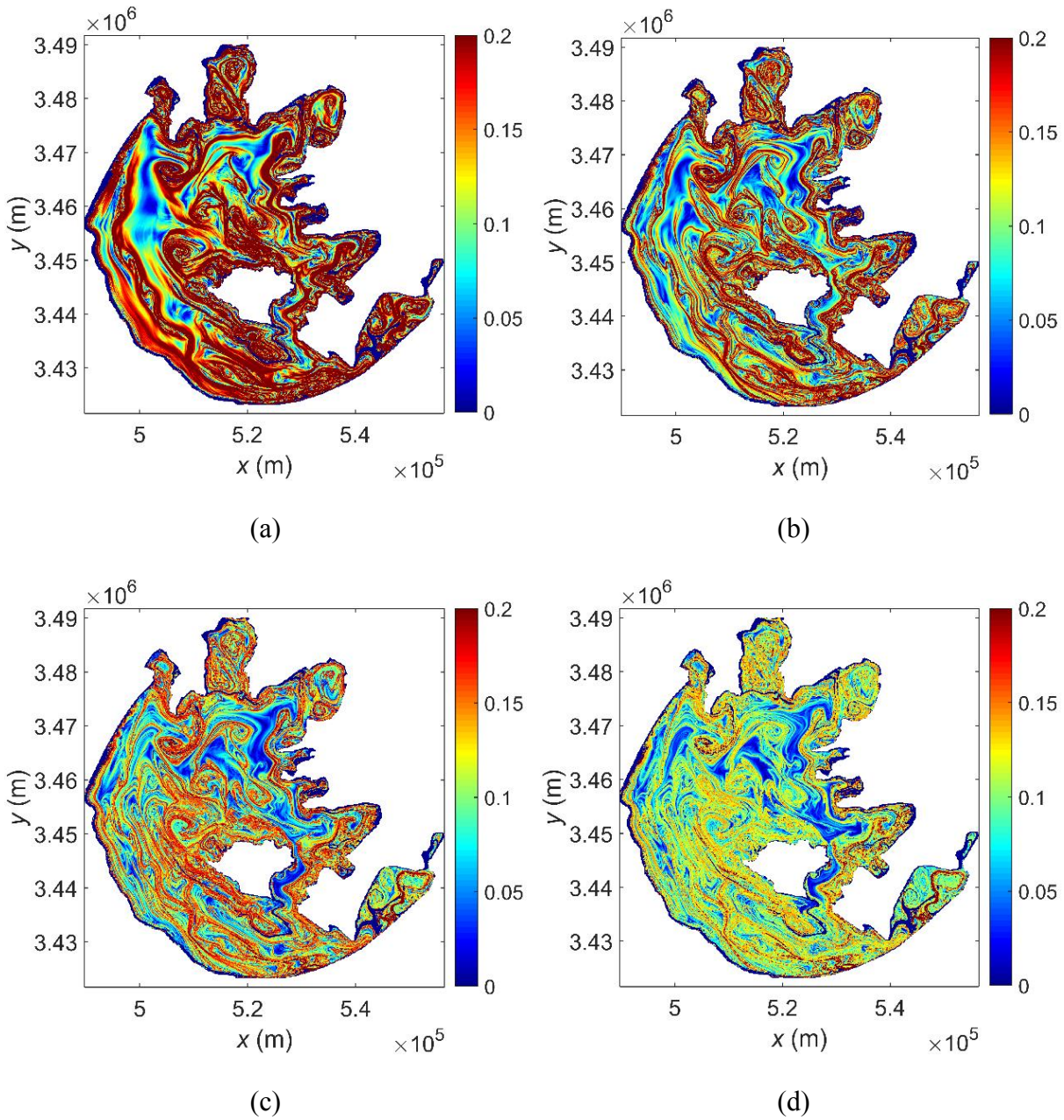


Figure 6.1 FTLE distribution in Lake Taihu with integration time: (a) 10 days; (b) 20 days; (c) 30 days; (d) 40 days.

As illustrated by Figure 6.1, FTLE distribution tends to sharpen along LCS and the exposed length of LCS tends to grow as integration time is initially increased; the exposed position of a particular LCS in the FTLE distribution is typically not sensitive to changes in integration time. In other words, if the start time of the FTLE computation is fixed, the identified position of LCS will remain fixed.

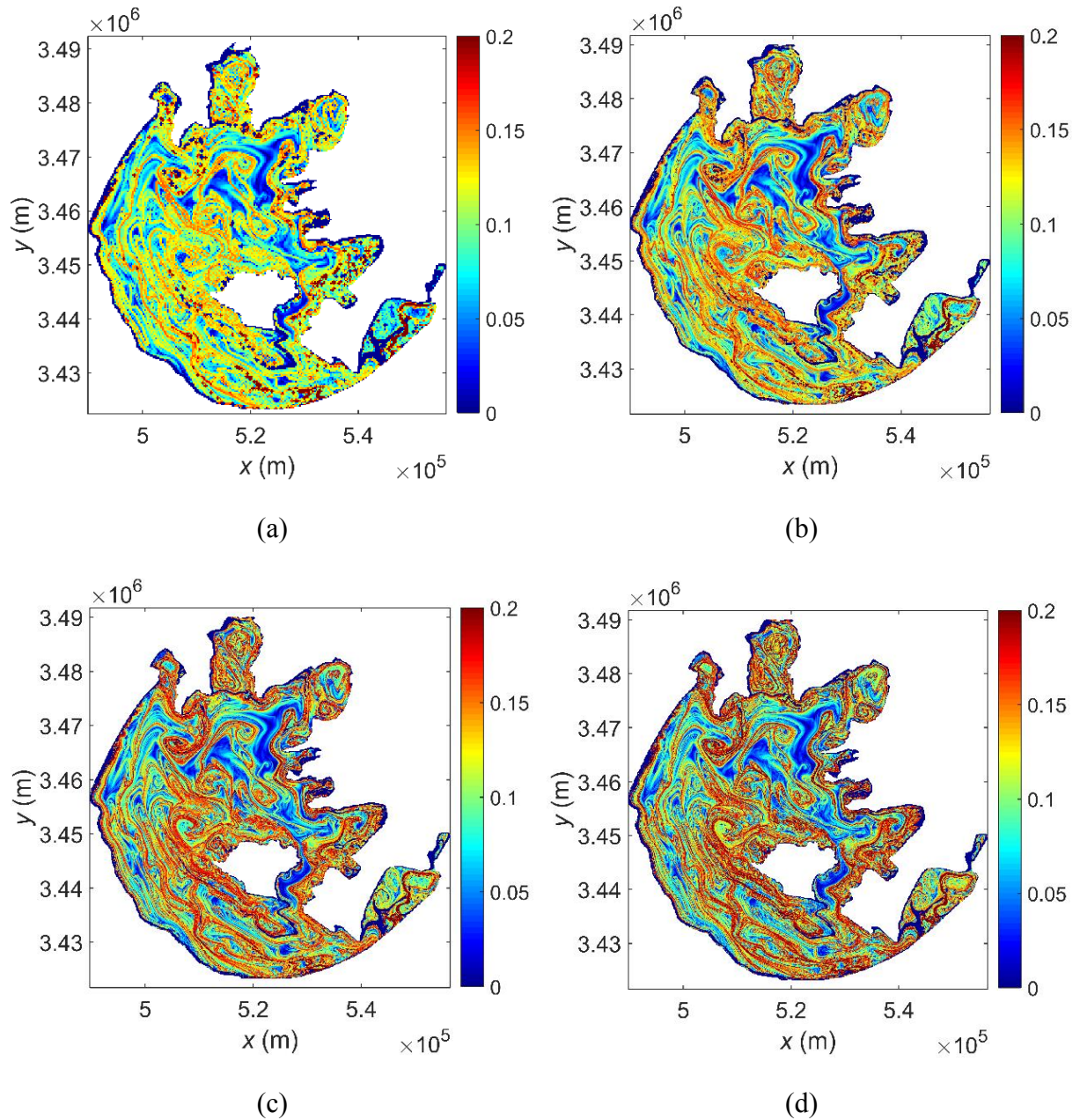


Figure 6.2 FTLE distribution in Lake Taihu with different grid size: (a) grid size of 250m; (b) grid size of 125m; (c) grid size of 62.5m; (d) grid size of 31.25m.

The second parameter is the resolution of particle grid. In Figure 6.2, time backward FTLE field of same period (From 15th March day to 15th April) are obtained at different resolutions. As the resolution gets finer (smaller particle grid), more dynamical structures are revealed and filaments get thinner. It is remarkable, however, that the large-scale structures are not much affected by the changing resolution: they are just sharper or more blurred, but maintaining the same shape and locations. If the grid spacing is too large, then neighboring grid points can span multiple LCS, or portions of the same LCS, and results become uncorrelated with any particular LCS. More generally, as the grid spacing decreases, LCS detection is improved; however, computational cost may increase. FTLE particle grid could be more resolved than the velocity

grid used to drive computations. Certainly, two points starting inside the same element of the velocity mesh are not expected to have the same dynamics. Indeed, for example, it is certainly possible for more than one LCS to lie between velocity grid points. In this study, the resolution of FTLE mesh (1072×1098) is selected twice as much as that of velocity mesh (536×549). Because compared to the results in Figure 6.2(a) and (b) whose FTLE resolution are 268×274 and 546×549 respectively, Figure 6.2(c) shows a satisfactory property of visualization of FTLE distribution. Also, a higher resolution (2144×2196) which costs more computational time does not have an obvious improvement as shown in Figure 6.2(d).

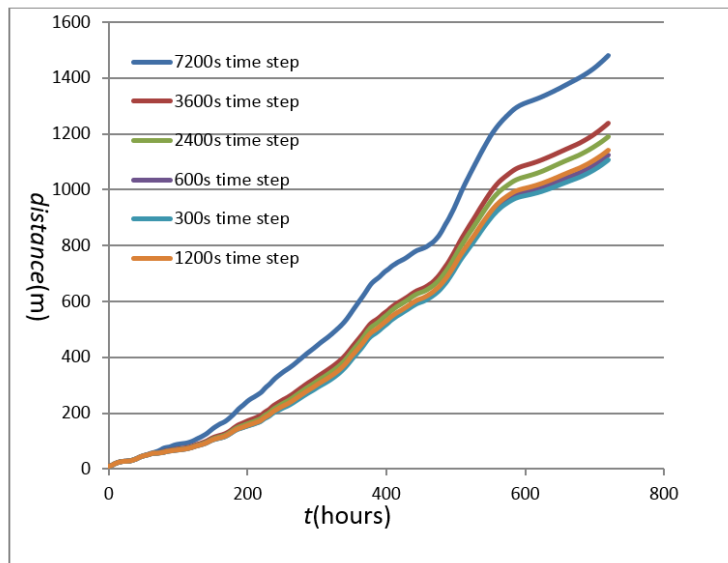


Figure 6.3 Average distance of neighboring particles during simulation progress with different particle tracking time steps.

The third parameter is the time step for particle tracking process when FTLE is calculated. Shallow water model and particle tracking have separately time step during the simulation, which are represented by respectively. The time step for shallow water model is evaluated by a subroutine based on the CFL method. The time step for particle tracking should be considered from the accuracy of results and the efficient of calculation. It is obvious that the smaller the particle time step is, the more accurate the results will be. But small particle time step means huge time spending on particle tracking process may cause inefficient simulation. Since the velocity of particles are obtained by interpolating the velocity value of four grids around the target particle, particle time step could be limited as less than 10000s. Otherwise in a single time step a particle may run out of the area in which its velocity is determined. Figure 6.3 illustrates the average distance of neighboring particles during simulation progress with different particle-tracking time steps. It is clear that if the particle time step is more than 1200s, the average distance of neighboring particles increase. Large time steps obviously influence the

accuracy of particle tracking results. While both the result of 600s and 1200s time step have a good agreement with the result of 300s time step. By considering the accuracy and efficiency, particle time step is chosen to be 1200s for all particle tracking simulation in Lake Taihu in the following contents.

6.2.2 FTLE distribution of Lake Taihu in different months

Figure 6.4 to Figure 6.11 show a sequence of snapshots of FTLE distribution of every 30 days from 15th January to December 15th day in 2005, obtained from particles advection with simulated velocity fields given by the shallow water model. The integration time is 259200s (30 days) and the particle resolution is 1072×1098. The time step in the particle tracking model is selected to be 1200s constantly.

In these sequence images, ridges are represented by red lines which indicates the largest value in local area. In time-forward simulations, the largest value indicates the highest separation rate and ridges reveal the repelling LCSs which approximates stable manifolds of hyperbolic moving points; while in time-backward simulations the largest value indicates the highest converge rate and ridges reveal the attracting LCSs which approximates unstable manifolds of hyperbolic moving points. Since LCS could be regarded as stable and unstable manifolds, they cannot be crossed by particle trajectories. LCS strongly constrain and determine fluid motion and organize the transport processes in Lake Taihu. LCS ranging from the small scales to the ones typical of mesoscale vortices are clearly identified in every period.

Due to wind force influence on the hydrodynamics of Lake Taihu, the FTLE distribution evolve aperiodically during the 300 days of consideration and this indicates that the transport and mixing property of Lake Taihu changes with time. From 15th January to 15th March as shown in Figure 6.4 and Figure 6.5, large vortex-shape LCS obviously could be found in Gongu Bay, Meiliang Bay, central areas of the lake and West Zone. In the core of these vortices one has low values of FTLE (i.e., low dispersion rates); on the contrary, the largest values of the FTLE could always be found in the outer part of vortices, where the stretching of the fluid parcels is particularly important, and in lines indicating robust transport barriers. So particles initially inside these vortex-shape LCS will have relatively lazy behavior and could not escape from vortices, while particles initially outside these vortex-shape will be attracted and travel along the outer LCS of these vortices, but never enter these vortices. The appearance of vortex-shape LCS is a signal of low transport and mixing property of local place where these LCS exist.

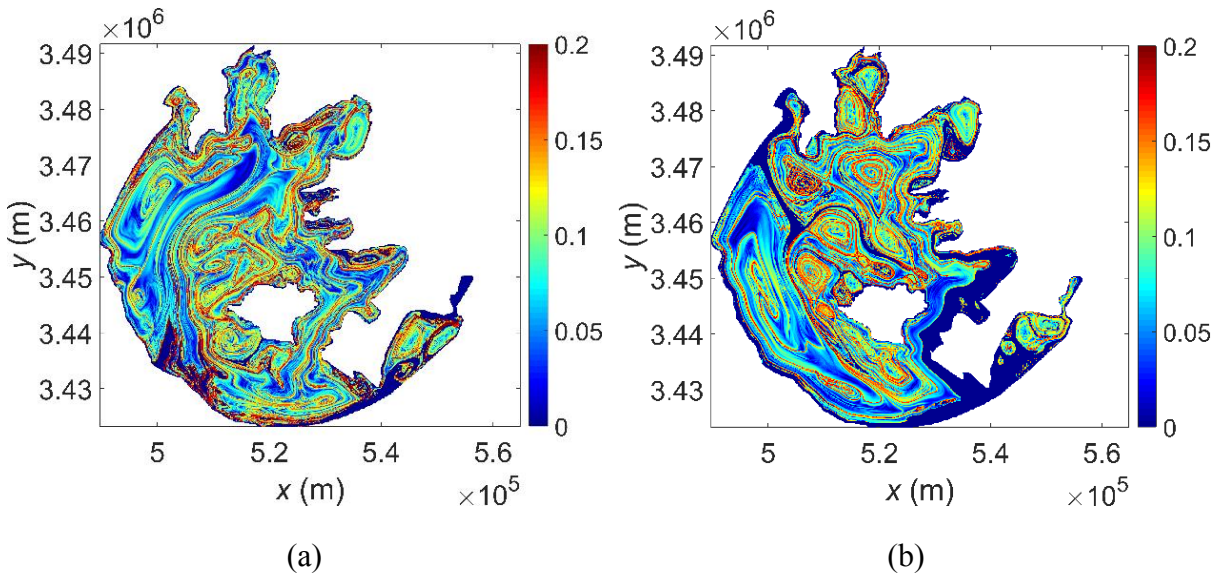


Figure 6.4 FTLE distribution of Lake Taihu for 15th January to 15th February: (a) Forward FTLE; (b) Backward FTLE.

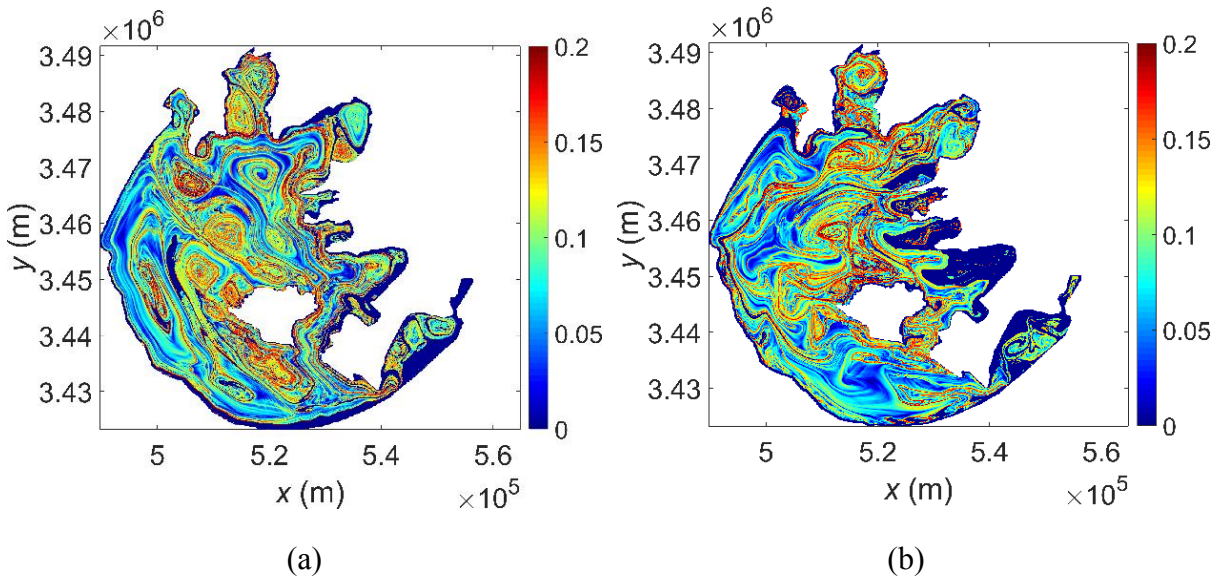


Figure 6.5 FTLE distribution of Lake Taihu for 15th February to 15th March: (a) Forward FTLE; (b) Backward FTLE.

FTLE distributions from 15th March to 15th May which is time of spring are shown in Figure 6.6 and Figure 6.7. Most vortex-shape LCS break out and more complicated spatial structures are created. Especially in the period from 15th March to 15th April, filamentary-shape LCS (red lines) are so intensive and almost distribute at every area of the lake. There are a lot of It is clear that the transport and mixing property of Lake Taihu is very strong in this period.

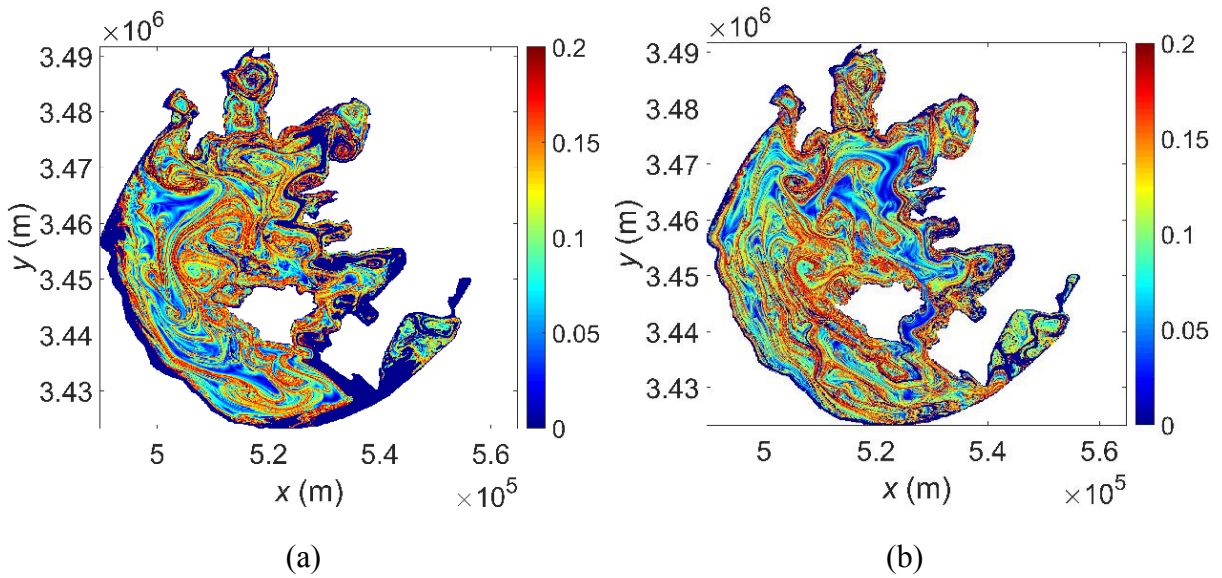


Figure 6.6 FTLE distribution of Lake Taihu for 15th March to 15th April: (a) Forward FTLE; (b) Backward FTLE.

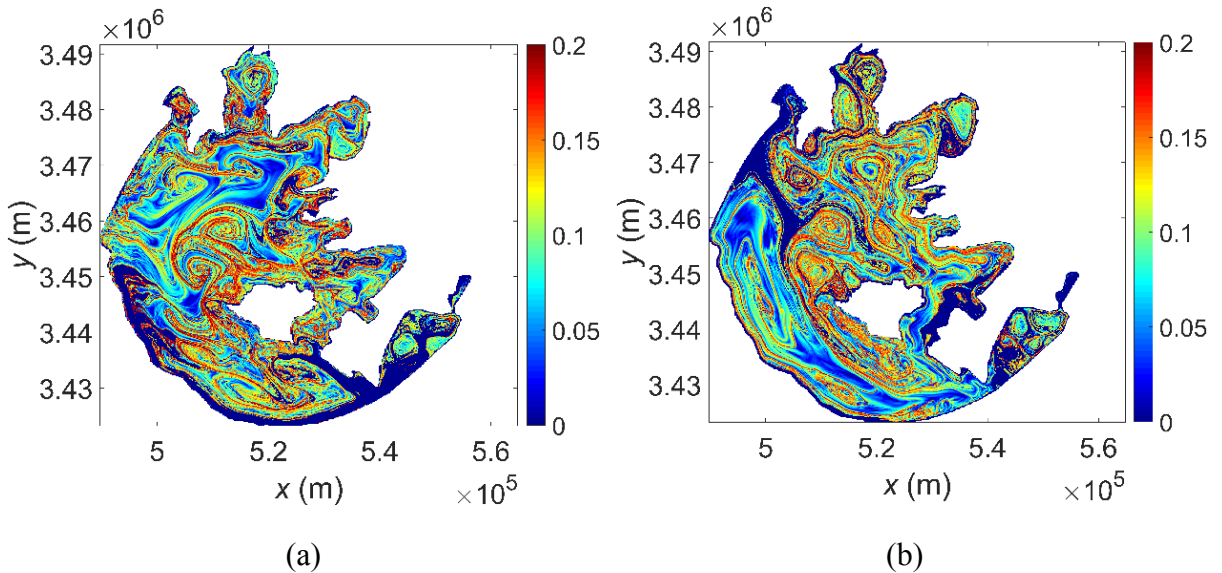


Figure 6.7 FTLE distribution of Lake Taihu for 15th March to 15th April: (a) Forward FTLE; (b) Backward FTLE.

When it comes to the period of 15th May to 15th July in Figure 6.8, it is obvious that the whole lake is separated into several areas by these LCS. Flow transport and exchange between these areas are absolutely hindered due to the barrier property of LCS. This may explain why the water quality of Lake Taihu decrease in this period: dead zones are formed and pollutants gain the opportunity to assemble and react.

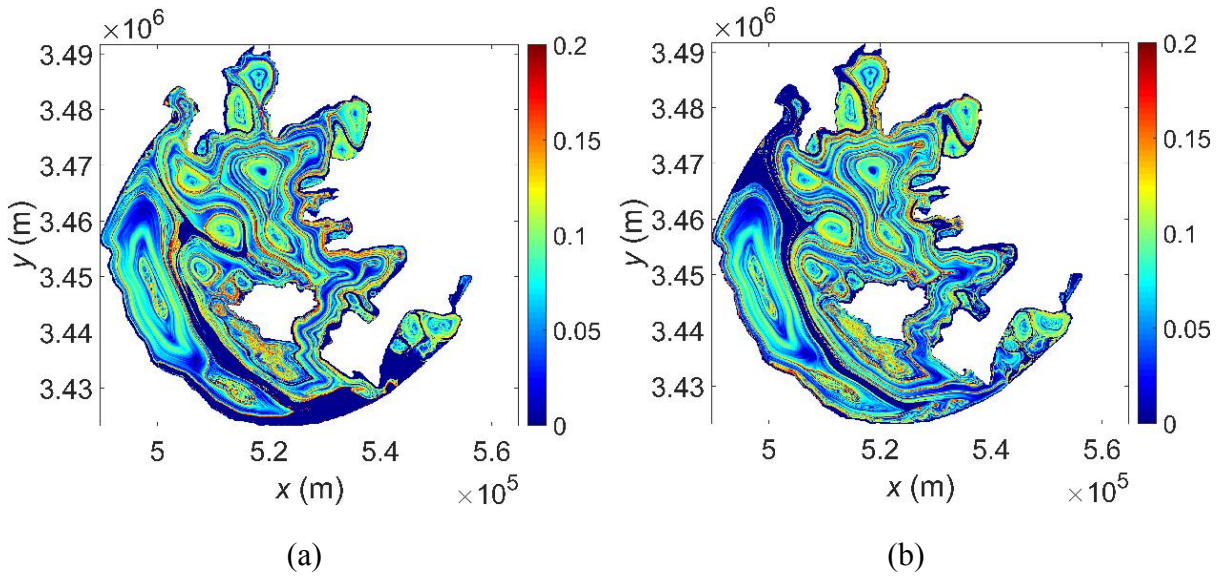


Figure 6.8 FTLE distribution of Lake Taihu for 15th May to 15th June: (a) Forward FTLE; (b) Backward FTLE.

From 15th July to 15th September, vortex-shape LCS disappear and the lake is governed by filamentary-shape LCS again as shown in Figure 6.9 and Figure 6.10. We know the transport and mixing are enhanced at the late summer time and this will be suitable time to apply engineering projects such as water transfer to dilute pollutants and refresh the whole lake. These engineering projects will be further discussed and evaluated in the section of continues Lagrangian dynamics.

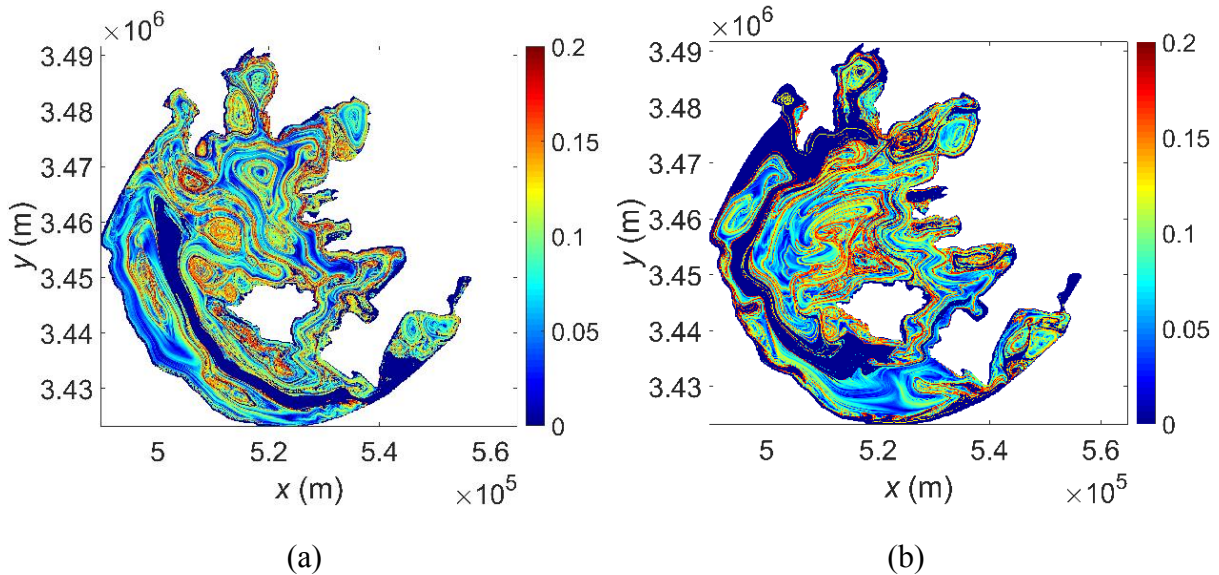


Figure 6.9 FTLE distribution of Lake Taihu for 15th July to 15th August: (a) Forward FTLE; (b) Backward FTLE.

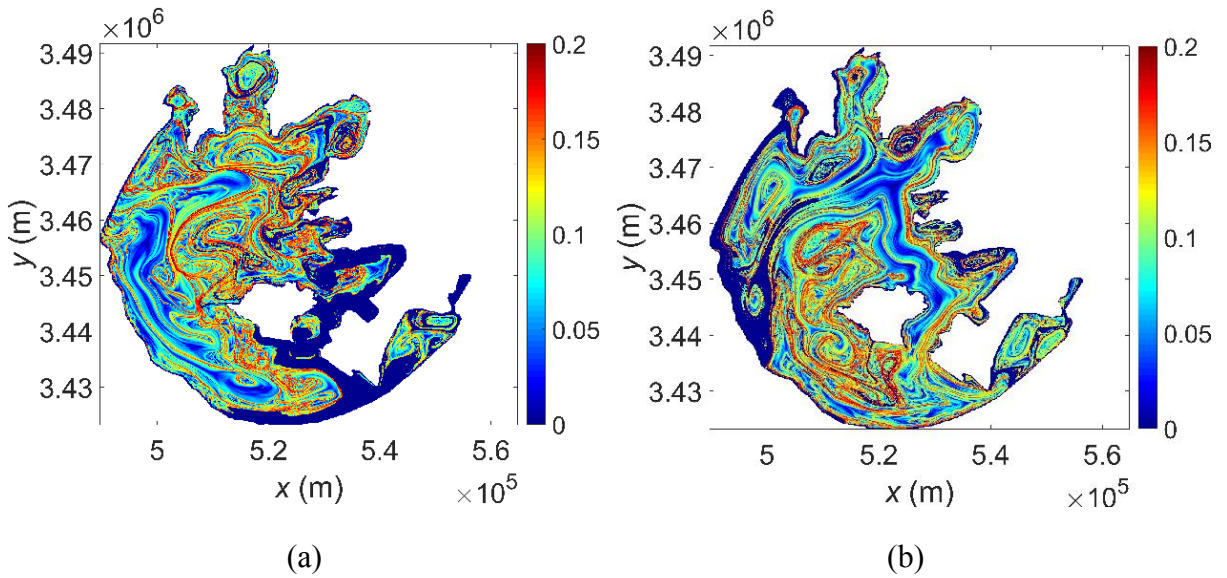


Figure 6.10 FTLE distribution of Lake Taihu for 15th August to 15th September: (a) Forward FTLE; (b) Backward FTLE.

Finally for autumn period which is from 15th September day to 15th November as shown in Figure 6.11, the situation is quite similar with that of early summer. The lake is occupied by vortex-shape LCSs which indicate low transport and mixing properties in the lake.

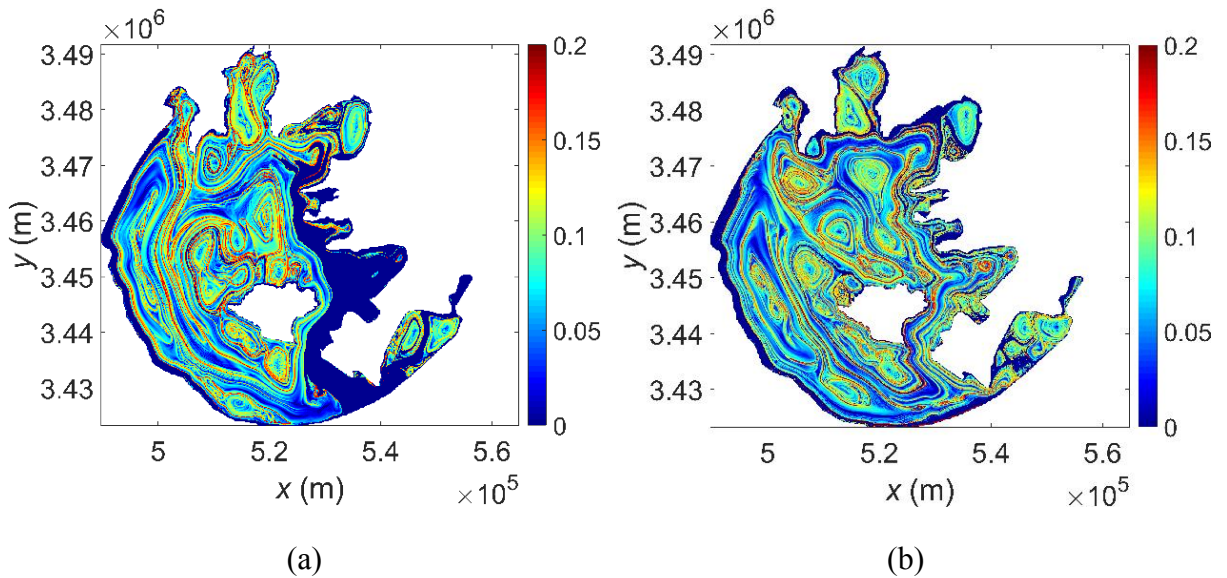


Figure 6.11 FTLE distribution of Lake Taihu for 15th September to 15th October: (a) Forward FTLE; (b) Backward FTLE.

6.3 Localized particle dynamics

In this section, the effect of LCSs on dynamics of localized passive particles which originate in Lake Taihu is studied. These particles could be recognized as pollution particles such as algae blooms, leaked oil or other pollutants which are produced locally and initially in a relatively

small area due to an environmental accident. The purpose of this study is to investigate how these local particle patches will evolve in given time intervals and evaluate the influence of these pollutions on water environment of Lake Taihu.

In aperiodic environmental flows such as flows in Lake Taihu, the evaluation of localized particle trajectories effected by LCS are highly related to time and initial positions of particles. Time-varying LCS may lead to different dynamic properties for transport and mixing of particles in different time intervals. And the heterogeneous spatial distribution of LCS in Lake Taihu indicated that particle motions are very sensitive to their initial positions.

Here localized particles will be released in two different time intervals. The length of each time interval is two months. The first interval i_{early} is from 15th May to 15th July which could be regard as early summer period and the second interval i_{late} is from 16th July to 15th September which could be regard as late summer period. The reason for choosing these two intervals is that heavy pollution especially eutrophication usually take place in summer which is approximate from May to September. Also, as shown by FTLE distribution in 6.2.2, the transport and mixing property of Lake Taihu in these two intervals are very different.

Localized particles will be released from two different areas. The initial positions of localized particle patches are shown in Figure 6.12. Two different lake areas (Gonghu Bay and West Zone) are chosen to be investigated. Rectangular patches consisting of 10000 passive particles respectively are released in both areas.

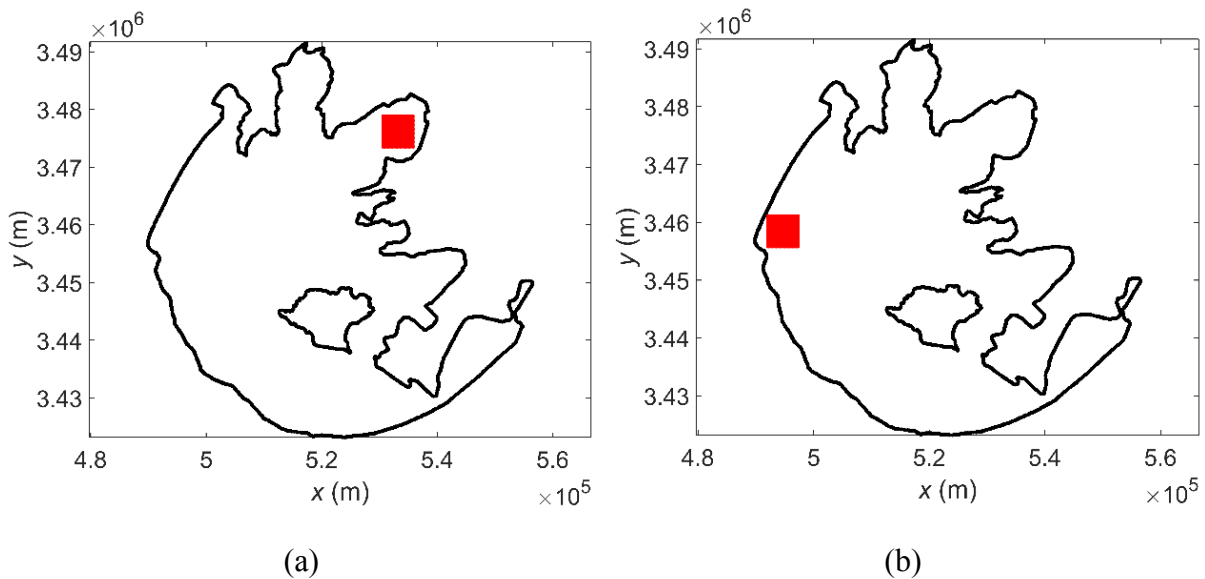
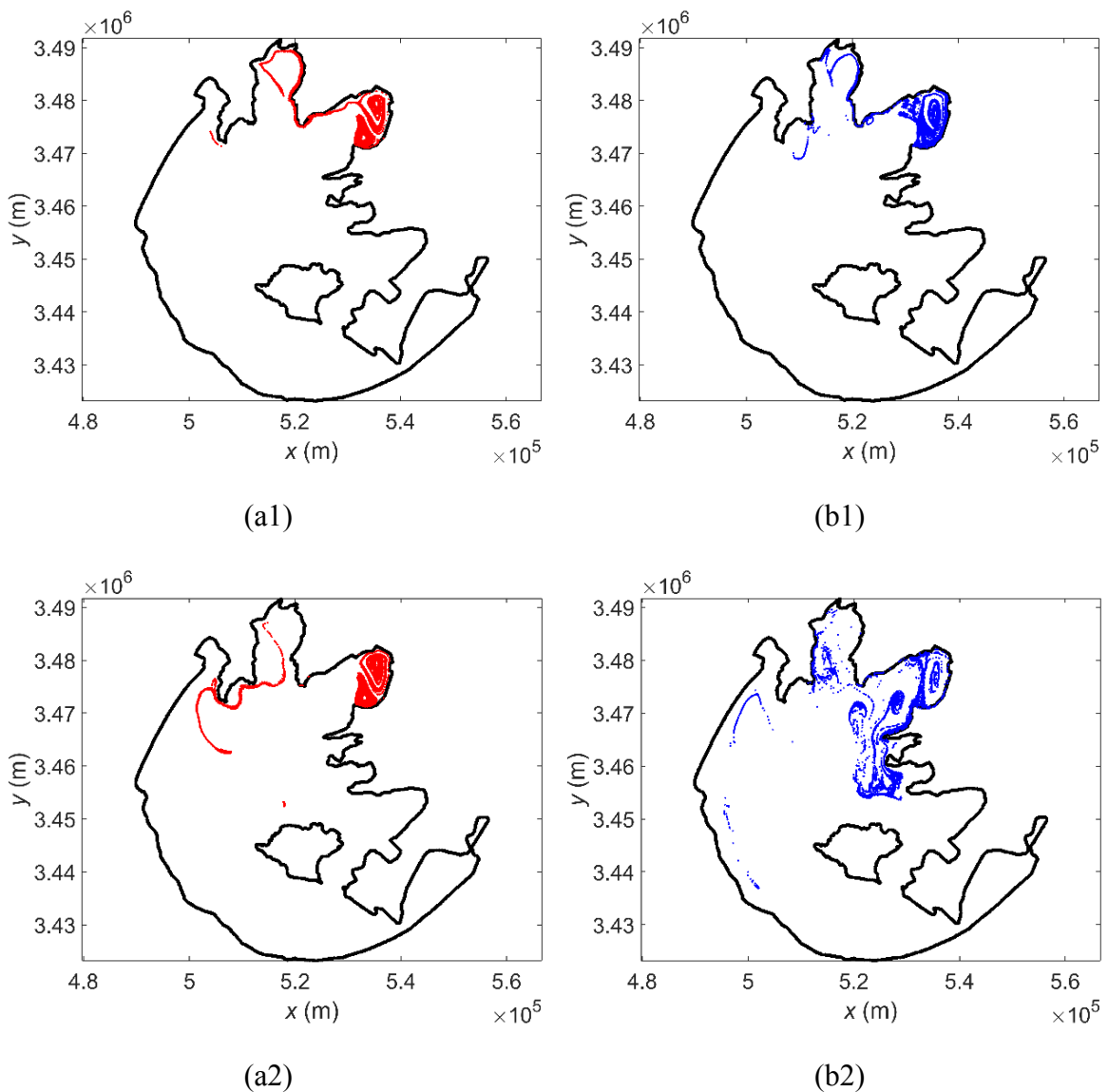


Figure 6.12 Initial positions of localized particles released in lake areas: (a) Gonghu Bay; (b) West Zone.

The trajectories of local particles initially located in Gonghu Bay are shown in Figure 6.13. For early summer period i_{early} , the particle tracking results are presented in Figure 6.13(a1-a3). Lack of flow exchange between Gonghu bay and the main lake could be observed. Most particles are roaming within two big vortexes in Gonghu Bay and are trapped there for the whole interval. Only a small number of particles successfully escape from west and travel into Meiliang Bay. This indicates that the main pollution source is limited in Gonghu Bay and the influence of this accident is local rather than global. For late summer time i_{late} , lake areas which are influenced by this environmental accident are much larger: Local particles in Gonghu Bay trace out very complicated trajectories which shows a strong transport and mixing property in north part of the lake. Meiliang Bay, West zone and east part of the lake are seriously affected by pollutants originating in Gonghu Bay. The stirring behaviours of particles at i_{late} is due to the appearance of new LCSs which break out the transport boundaries and enhance the mixing properties of the lake.



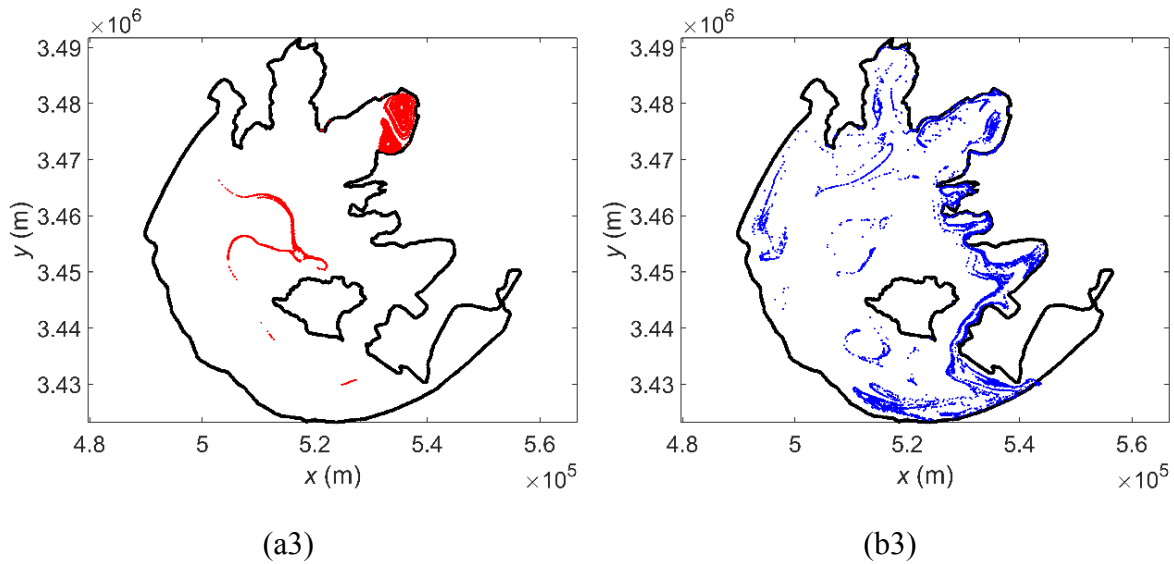


Figure 6.13 Trajectories of Local particles patch initially located in Gonghu Bay: (a1) 20 days early summer; (b1) 20days of late summer; (a2) 40days of early summer; (b2) 40days of late summer; (a3) 60days of early summer; (b3) 60days of late summer.

For the scenario of West Zone, Figure 6.14 shows that the simulation of particle trajectories in the first 20 days of two time intervals have the same evolution tendency: square patch integrally travel to southeast along the shoreline and stretch into a long and thin filamentary. When it comes to 40 days' simulation and 60 days' simulation, the situations are totally different. For i_{early} , particles reverse their direction of motions to northeast and finally trace out a large vortex. It is clear that though a pollution event occurring at an open area (West zone) instead of a semi-closed bay (Meiliang Bay or Gonghu Bay) have the ability to affect wider areas, the trajectories are still limited inside a local region due to the characteristics of Lagrangian dynamics in i_{early} . And for i_{late} , the filamentary in the first 20 days evolve into complicated trajectories at central and south of the lake.

The results of localized particle tracking indicate that the spread of passive particles regarded as contamination is efficiently and precisely described by LCS. Due to LCS's properties of time-varying and spatial heterogeneous, contaminations released with different time intervals and initial positions have radically different behaviors which could evolve into either a local or a global environment problem. LCS-based analysis promises to provide quantitative support for decisions involving coastal evacuation, intervention to protect aquatic life, and optimal deployment of resources for pollution abatement.

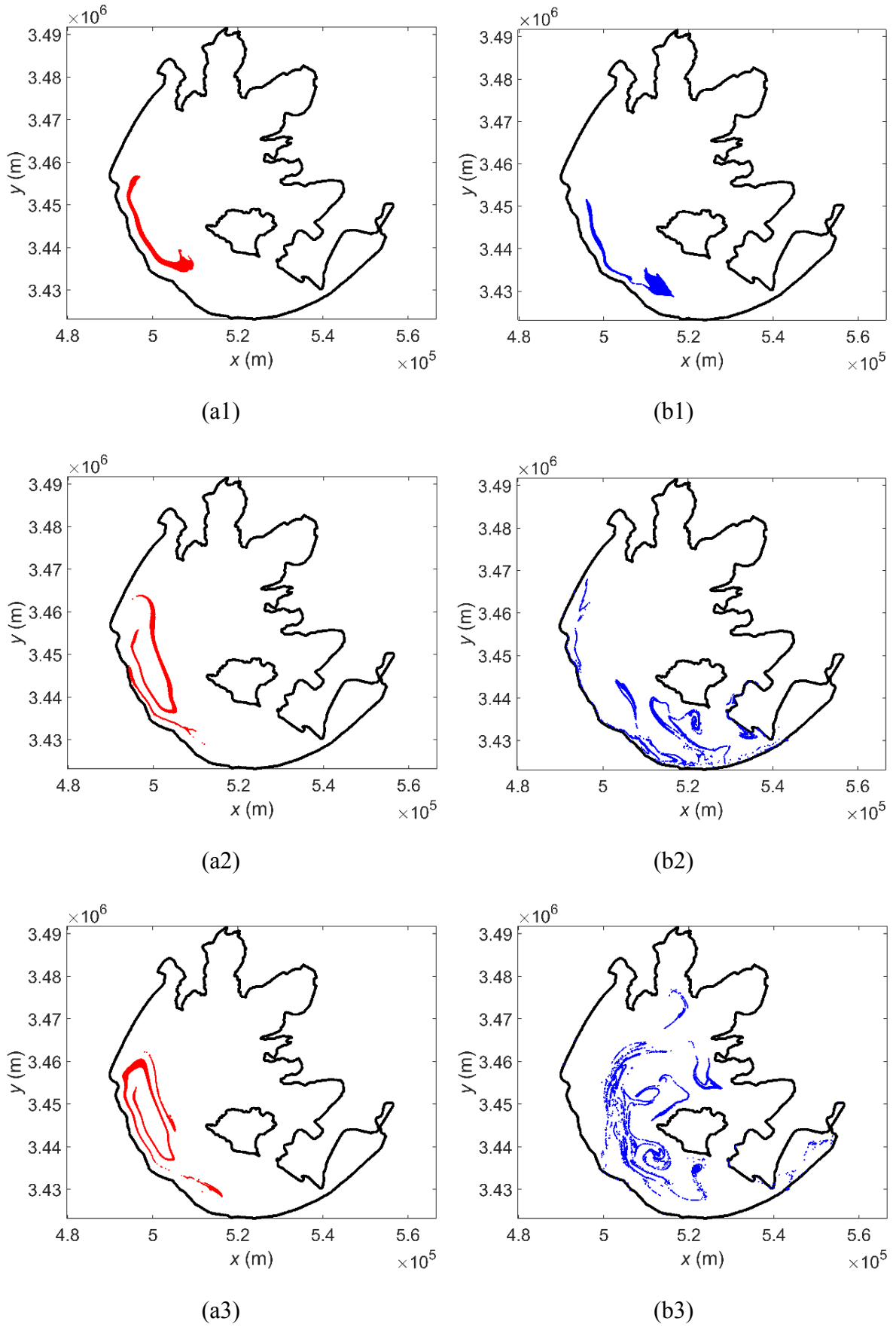


Figure 6.14 Trajectories of Local particles patch initially located in West Zone: (a1) 20days of early summer; (b1) 20days of late summer; (a2) 40days of early summer; (b2) 40days of late summer; (a3) 60days of early summer; (b3) 60days of late summer.

6.4 Continuous particle dynamics

In order to simulate the transport and mixing processes of freshwater transferred into Tai Lake from Yangzhe River through different routes, continuous particles are released at the entrance of these engineering routes. Different routes are represented by different colours. The initial positions of these particles and their corresponding colour are shown in Figure 6.15(a). For each transfer route, a rectangular particle patch consisted of twenty five particles are released at each particle time step (1200 seconds) during the particle tracking process.

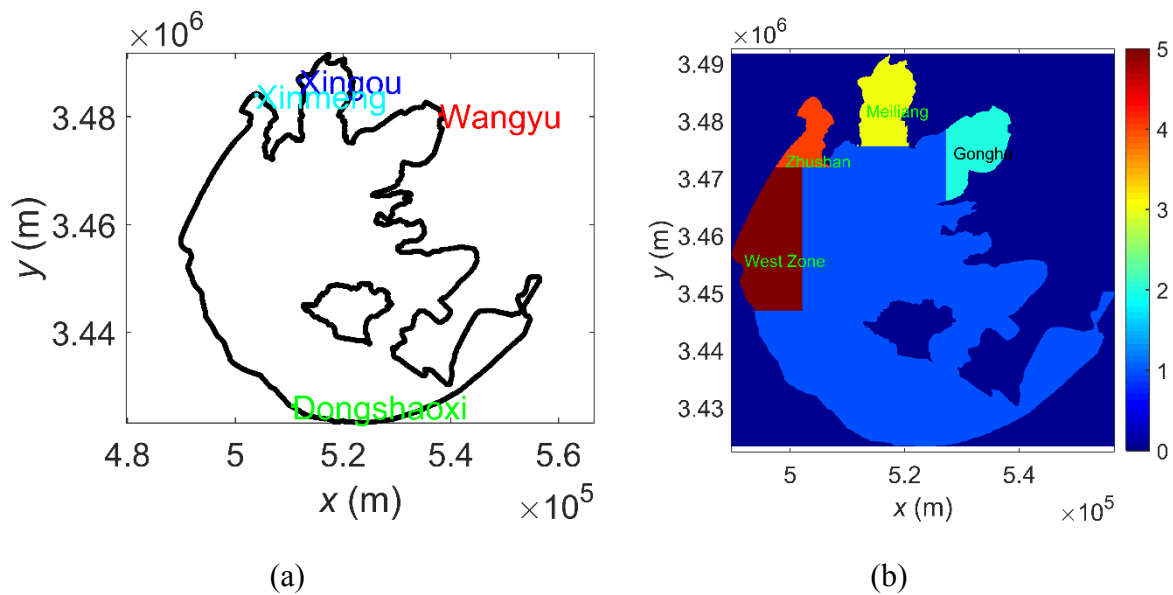


Figure 6.15 (a) locations of four routes for water transfer; (b) four highlighted areas for calculating the local occupy rates.

In the investigation of continuous particle dynamics of Lake Taihu, there are two kind of occupy rates, the global occupy rate and the local occupy rate, will be considered when the performance of one transfer route is studied. The global occupy rate of Lake Taihu is quite similar to the occupy rate of the idealized lake in last chapter. It represents how many percent of the whole lake will be achieved by freshwater from one transferred route and is considered as a factor indicating how the transferred route will affect the water quality of the whole lake system. However, the situation in Lake Taihu is more complicated and the global occupy rate is not enough to objectively evaluate the transferred route. Because there are several highlighted regions (Gonghu Bay, Meiliang Bay, Zhushan Bay and West Zone) which always involve into heavy pollution and eutrophication. Also there are a large number of human habitation along their coastal areas. Hence it is very necessary to study the change of water quality in these regions by using local occupy rate. The local occupy rate regards each highlighted region as an independent “lake” and will calculate how many percent of the independent “lake” will be

achieved by freshwater, therefore will be used to indicate how water quality are improved in these independent “lake”. The exact regions of four highlighted lake areas will be considered to calculate local occupy rates are shown in Figure 6.15(b).

The simulation of continues particles illustrates that how the transport of freshwater will be influenced by LCSs (transport barriers in the lake) and which areas could be reached and refreshed by these freshwater. By analyzing the particle tracking results of these routes and calculate occupy rate of local areas or the whole lake, we are able to evaluate the performance of these routes on water improvement and provide useful guidance for designing effective engineering solutions to remit and solve relevant water environmental problems in designated areas.

6.4.1 *The Lagrangian dynamics of particles released from Wangyu Route*

Figure 6.16 illustrates the trajectories of freshwater particles transferred from Wangyu Route in winter period. Particles representing freshwater are released at 15th January 2005 and tracked for 60 days. These particles first travel to the north and then turns the west along the shoreline. Between the period of January and February, there is an LCS structure acting as a barrier to prevent direct water exchange between Gonghu Bay and the main area. The motion of freshwater particles are obviously influenced by this LCS and suddenly change the moving direction to south instead of west. After reaching the south shoreline of Gonghu Bay, particles of freshwater begin to show two kinds of different behaviors due to their different positions: some particles travel to west, forming a vortex-shape patch, and then circle at the southwest of Gonghu Bay for quite a long time (approximate one month) before the vortex break out; while others move to east, join the later released particles and travel to the north again. These particles continue travel along shoreline of Gonghu Bay and finally comes into the area of Meiliang Bay. By 25th February, the particles have already formed a circulation that surrounding the whole Gonghu Bay and occupy the area close to the shoreline of Meiliang Bay. But there is a still vortex-shape attracting LCS in Gonghu Bay and its barrier property of transport prevent most particles to enter the central area of the bay. When it comes to 15th March, the old LCSs are destroyed and new ones are created due to the change of time-dependent velocity fields. Particles in Gonghu Bay are exported out of the bay by new attracting LCSs and particles in Meiliang Bay have already occupied the north part of the bay and continue to travel to west area of Lake Taihu.

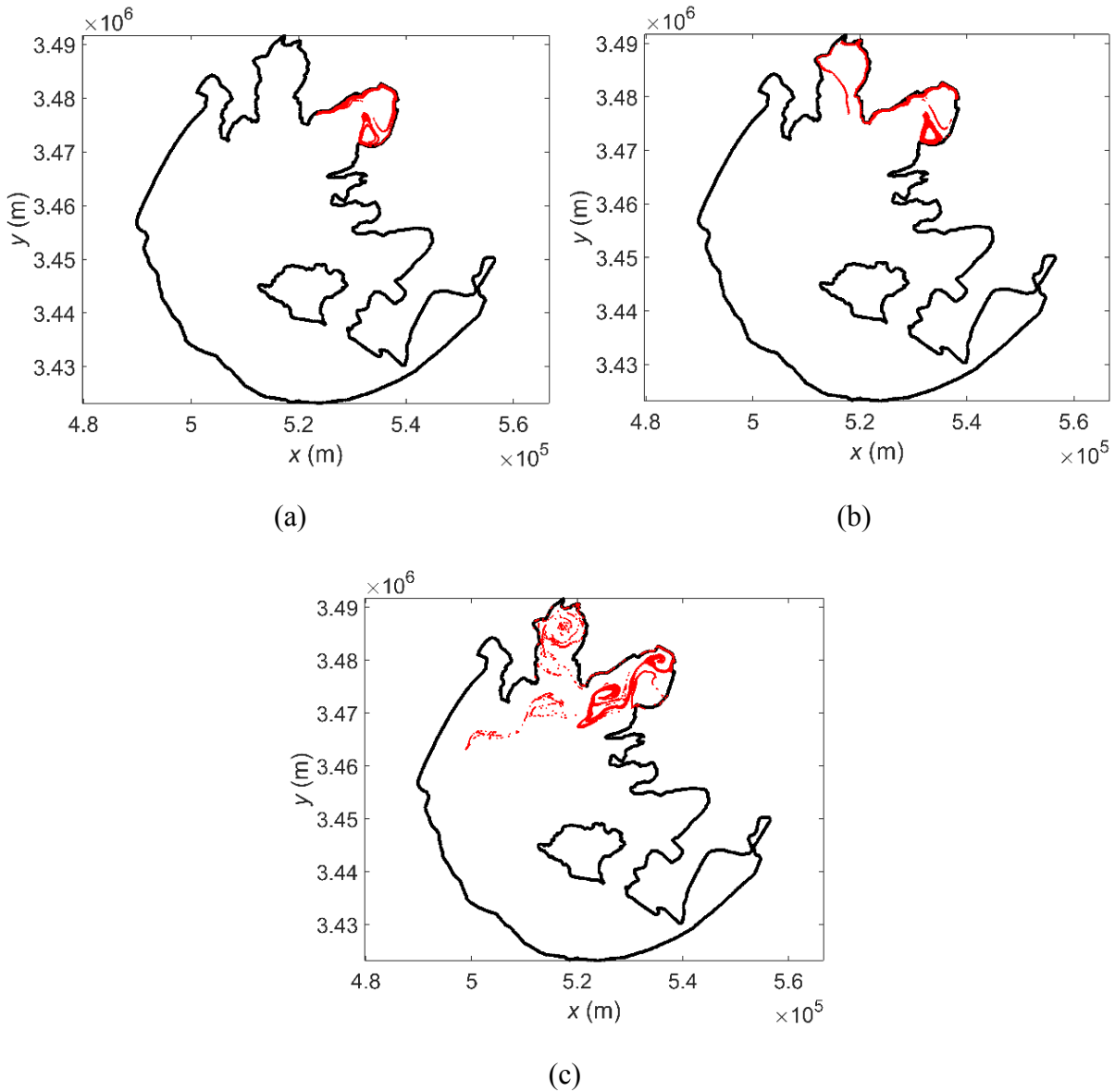


Figure 6.16 Particles continually released at Wangyu Route in winter: (a) particle trajectories on 5th February; (b) particle trajectories on 25th February; (c) particle trajectories on 15th March.

The simulation of continues particles released at Wangyu route in spring period are shown in Figure 6.17. Particles representing freshwater are released at 15th March 2005 and tracked for 60 days. There are two vortex-shape LCSs system in Gonghu Bay. A large one located at north and a small one located at south. From 15th March to 5th April, particles released at Wangyu route initially travel to both north and south along the shoreline. Then the particle travelling to north turn back to south due the influence of north vortex-shape LCS. As time flows, particles continue travel to south very rapidly and show very complicated trajectories by following the anfractuouse LCSs extending to south of Lake Tai.

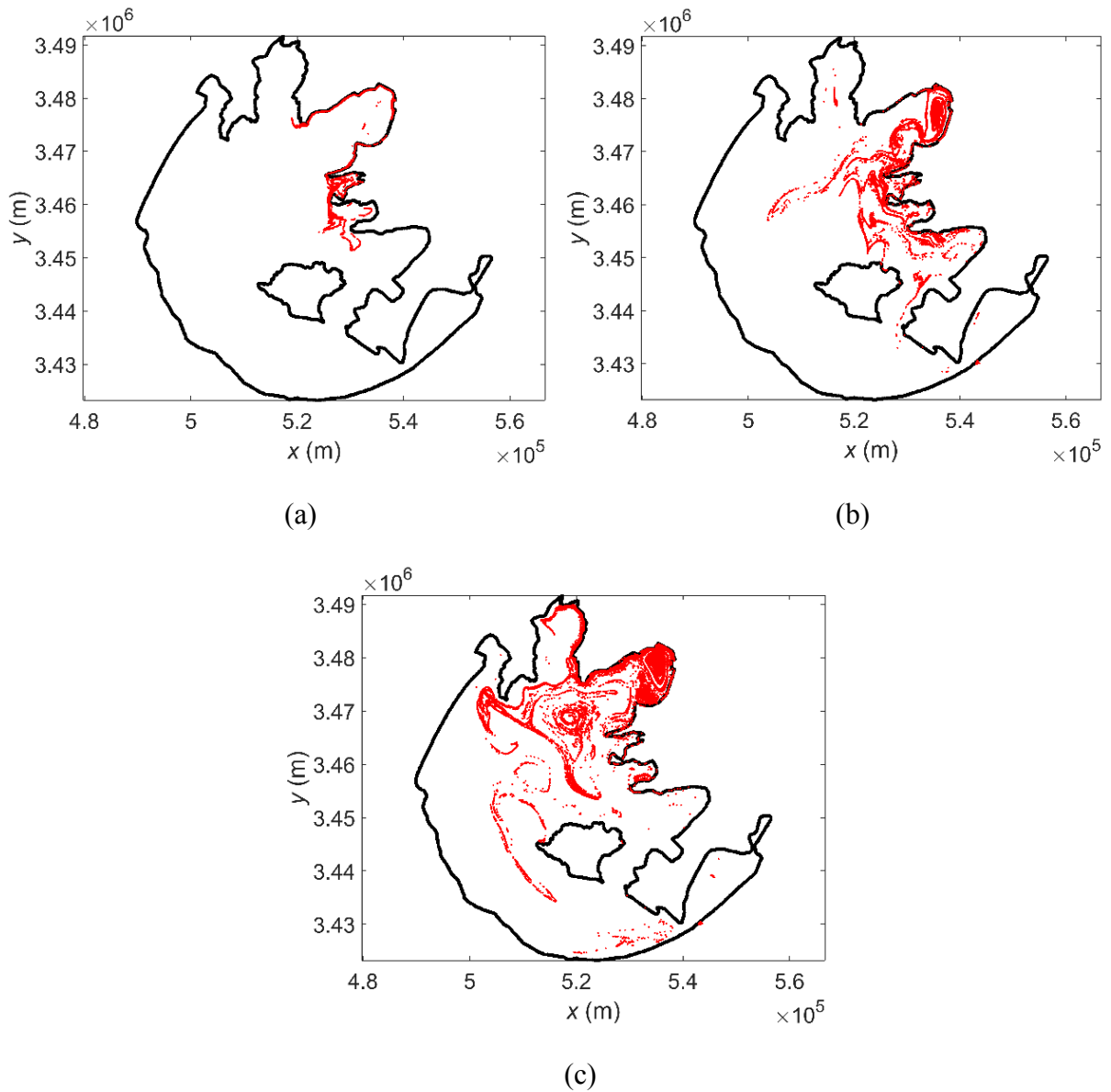


Figure 6.17 Particles continually released at Wangyu Route in spring: (a) particle trajectories on 5th April; (b) particle trajectories on 25th April; (c) particle trajectories on 15th May.

When it comes to 25th April as shown in Figure 6.17(b), most particles change their tendency of motion and begin to travel westward. After 60 days, the whole Gonghu Bay are well mixed by particles while only few particles are transferred into Meiliang Bay. Also part of central area, which is at the north of Xishan Island, are mostly occupied by particles. Stretching, folding and vortex-shape of particle lines could be clearly observed in this area. Their shape are very similar with attracting LCSs and some of them even coincide with each other. This is a strong evidence that LCSs are the key structures that govern the transport and mixing property in Lake Taihu.

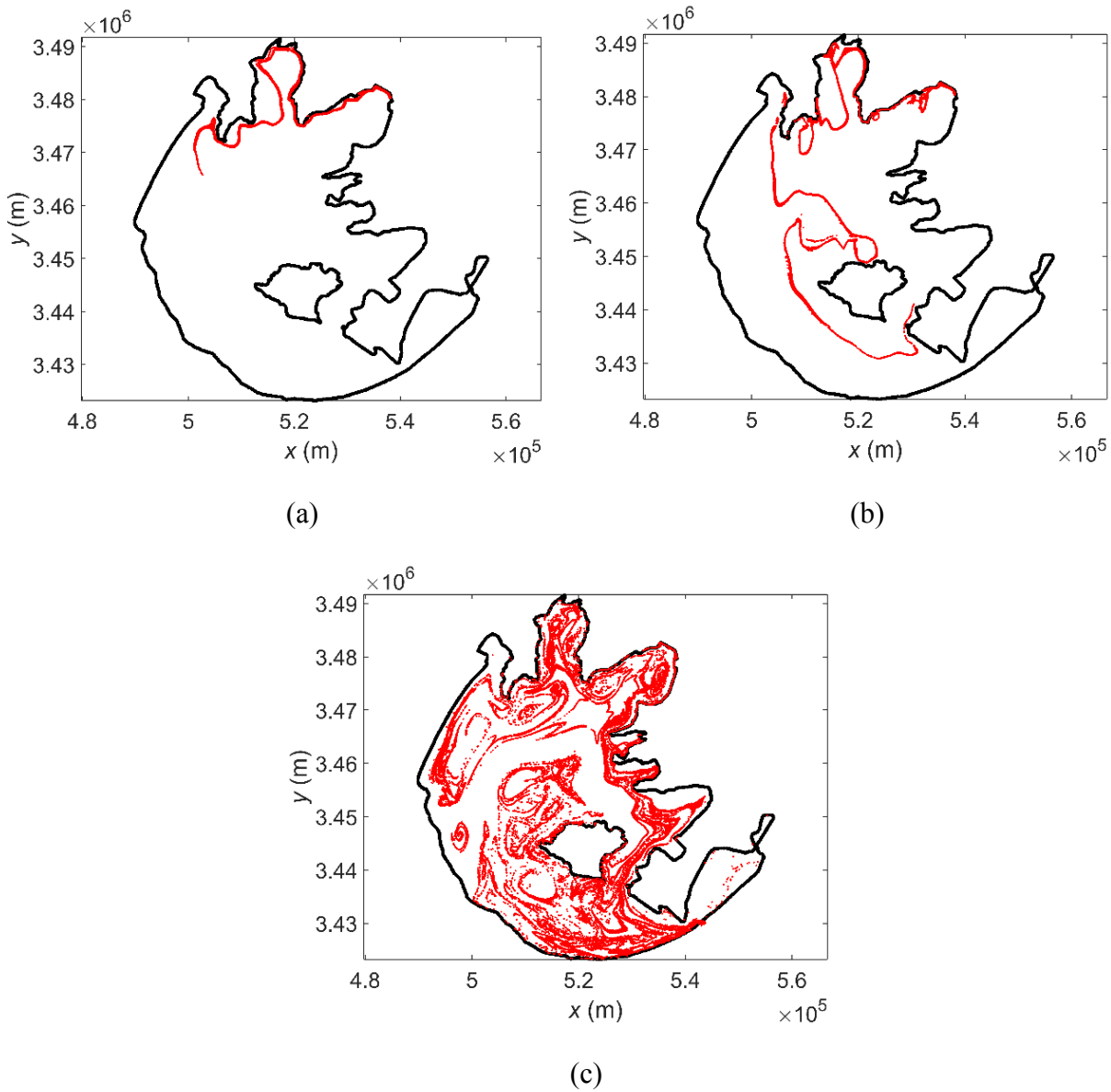


Figure 6.18 Particles continually released at Wangyu Route in summer: (a) particle trajectories on 25th June; (b) particle trajectories on 5th August; (c) particle trajectories on 15th September.

In Figure 6.18, the trajectories of particles transferred from Wangyu Route are described in summer period. Particles representing freshwater are released at 15th May 2005 and the simulation time is extended to 120 days from mid of May to mid of September. This is because Lake Taihu is located in south of China where the duration of summer is always much longer than that of other seasons. Also summer is the season when eutrophication will happen most frequently and seriously (Zhu, 2008). So we want a better view of the transport and mixing property of particles in this whole period. Particles released in Gonghu Bay directly travel to north along the shoreline and go into Meiliang Bay. In Meiliang Bay, due to the attracting characteristic of backward LCSs, particles only follow the local LCSs and trace out filamentary structures rather than spread to other areas in Meiliang Bay. Particles leave the Meiliang Bay

by traveling to northwest area of Lake Taihu but they do not enter Zhushan Bay. Then particles change the direction and begin to travel southward by stretching and folding and arrive the southeast area of Lake Taihu by 5th August as show in Figure 6.18(b). In Figure 6.18(c), particles spread extraordinary quickly and appear in most area of Lake Taihu except southwest area. Several serious polluted areas including Gonghu Bay, Meiliang Bay and West Zone are well refreshed by freshwater. But the situation of Zhushan Bay still could not be improved by this summer water-transferred engineering plan.

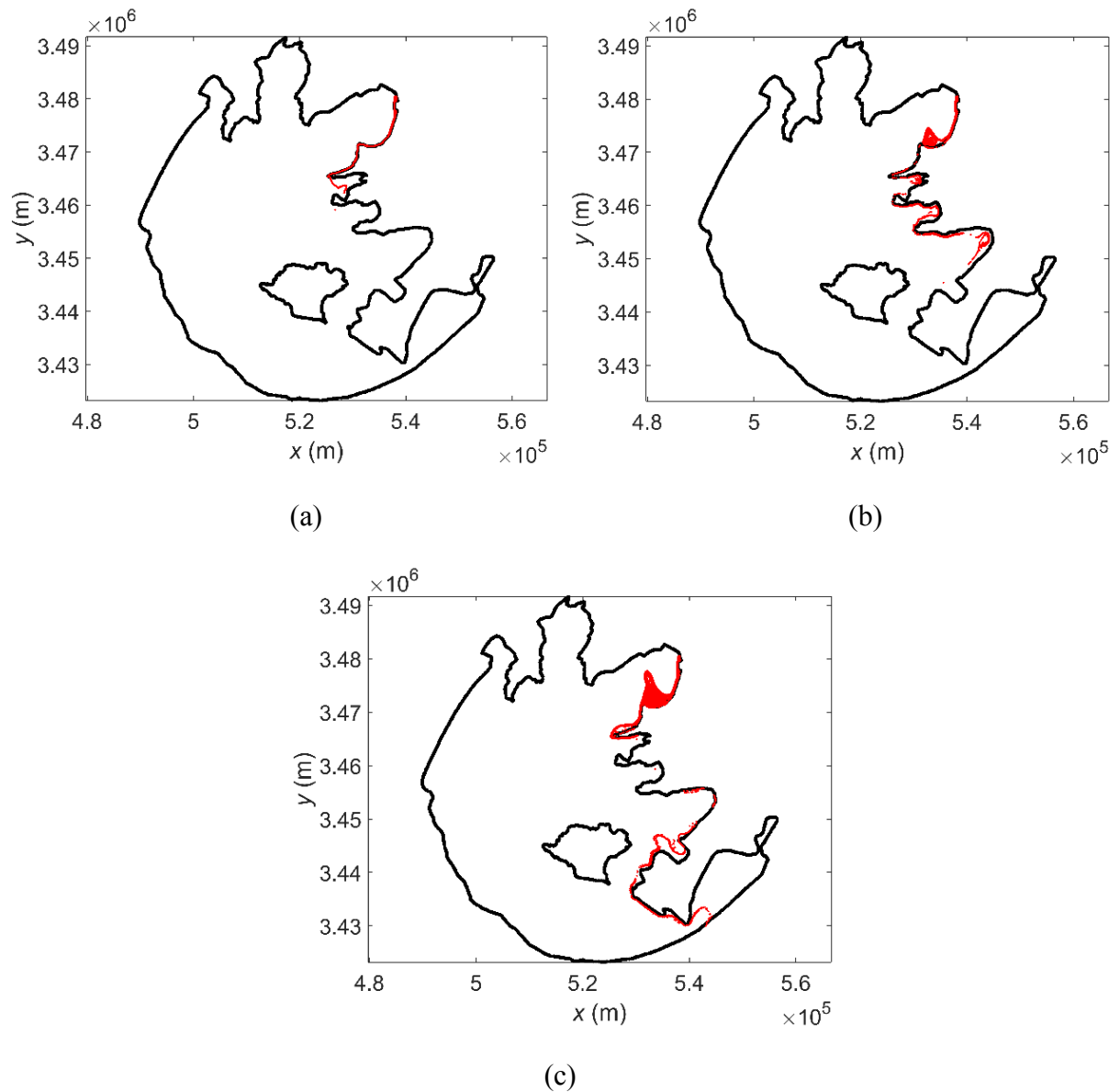


Figure 6.19 Particles continually released at Wangyu Route in autumn: (a) particle trajectories on 5th October; (b) particle trajectories on 25th October; (c) particle trajectories on 15th November.

Finally the simulation of continues particles released from Wangyu Route in autumn period are illustrated by Figure 6.19. Particles representing freshwater are released at 16th September 2005

and tracked for 60 days. After entering Lake Taihu from Wangyu River, particles go directly to south along the shoreline of Gonghu Bay. Since the LCSs field is quite simple and similar in October and November, the behavior of particles seems quite gently and stable in this period. Particles just go southward along the relatively long-existing LCSs which is lying through the east part of the lake. The simulation of particle trajectories in autumn shows that the transport and mixing is relatively low compared to other seasons. Particles just travel along east shoreline to East Epigeal Zone and Dongtaihu Bay with few material exchange other parts of the lake. Even Gonghu Bay in which particles are released could not be fully refreshed within two months.

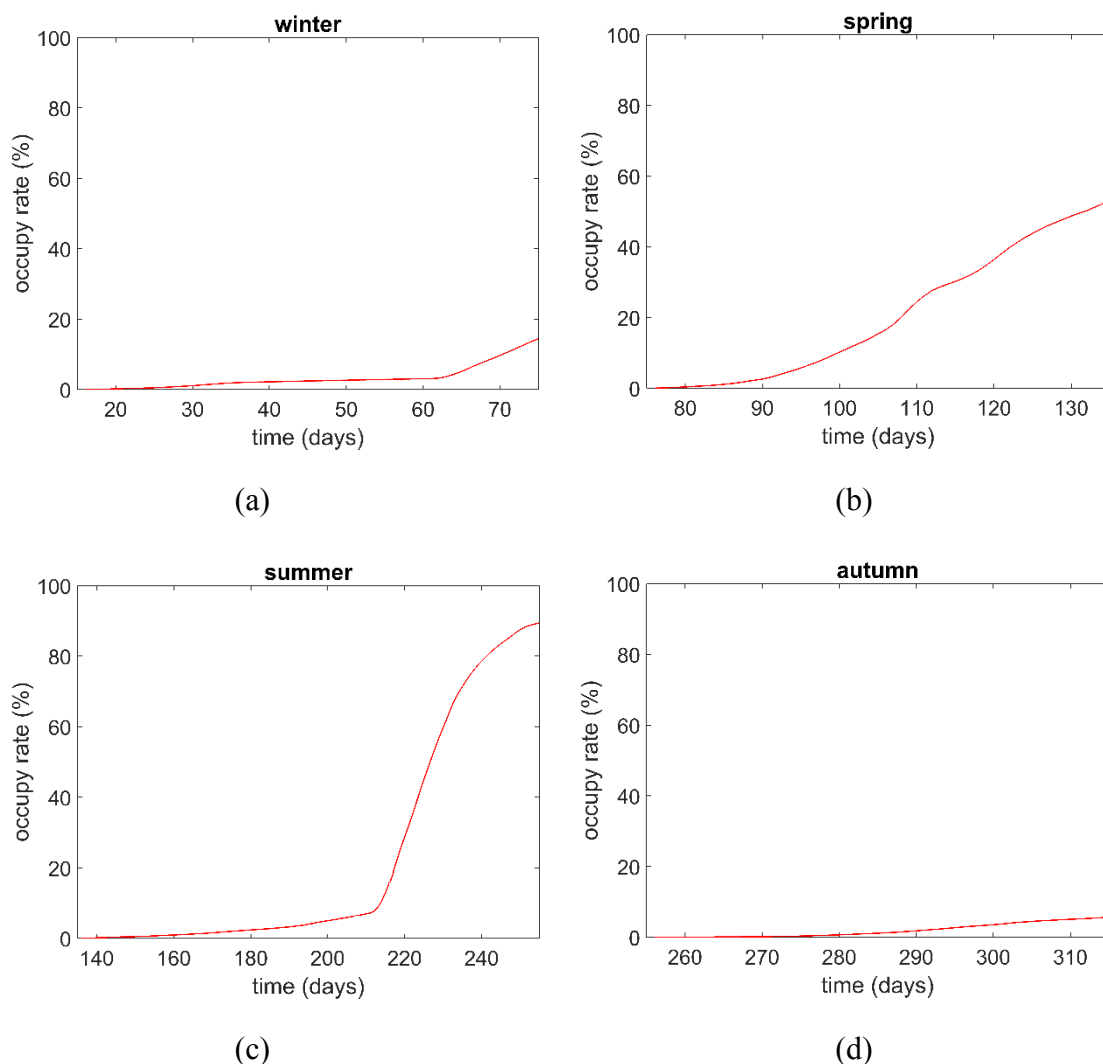


Figure 6.20 Global Occupy rate of particles released at Wangyu Route for different seasons in year 2005: (a) winter; (b) spring; (c) summer; (d) autumn.

Figure 6.20 shows the global occupy rate of particles released from Wangyu Route for different seasons in year 2005. It is clear that summer, with an occupy rate of total lake of nearly 90%, is the best season to transfer freshwater from Wangyu Route. In summer, the occupy rate

increase dramatically after the 210th day. This is because LCSs distribution in July and August shows a very strong transport and mixing property in Lake Taihu. Both forward LCSs (repelling LCSs) and backward LCSs (attracting LCSs) evolve very quickly and interact with each other more frequently during these two months. This will create more temporal hyperbolic points. These temporal hyperbolic points and their associated stable manifolds (forward LCSs) and unstable manifolds (backward LCSs) will definitely enhance the transport and mixing of passive particles.

Spring is also a considerable season for water transfer engineering at Wangyu Route if any water quality problems happens in this period. While water transfer engineering at Wangyu Route in winter and autumn should not be applied to improve water quality of the whole lake due to their low total occupy rate.

Table 6.1 shows the local occupy rate of four highly polluted sub-zones mentioned in previous paragraph. For water transfer engineering at Wangyu route, application summer is the best choice for improving water quality of all four sub-zones. Spring is the best season to improve water quality in Gonghu Bay, with an occupy rate of 99.75% in two months. Though winter application has a low occupy rate of the whole lake, the occupy rate of Gonghu Bay and Meiliang Bay is quite high. Autumn application is absolutely not suggested because of its poor performance.

	Whole lake	Lake Gonghu	Meiliang Bay	Lake Zhushan	Wester area
Winter	14.46%	85.88%	80.91%	0	1.92%
Spring	52.96%	99.75%	47.26%	27.5%	2.13%
Summer	89.44%	99.18%	97.84%	64.96%	81.56%
Autumn	5.6%	22.63%	0	0	0

Table 6.1 Local occupy rates of particles released at Wangyu Route for different season

6.4.2 *The Lagrangian dynamics of particles released from Xingou Route*

Figure 6.21 illustrates the trajectories of freshwater particles transferred from Xingou Route in winter period. In Figure 6.21(a), particles first travel to the north along the shoreline and change the direction to south suddenly at midpoint of the north shoreline. This is because there is vortex-shape LCS at the northeast of Meiliang Bay in January and it stop particles entering this

area directly from west area of Meiliang Bay. Particles evolve into two different trajectories: some particles return to north along the east shoreline of Meiliang Bay and trace out the LCS at the northeast; others begin to move to the west and trace out another vortex-shape LCS at the southwest. Then particles follow the second trajectory mentioned above gradually enter Zhushan and sequentially travel to south along a very large vortex-shape LCS as shown in Figure 6.21(b). When it comes to 15th March, large vortex-shape LCSs located at the west of the lake break out, the transport barriers separating west zone with main lake disappeared. Particles gain the opportunity to enter west zone. Also the mixing and transport property in Meiliang Bay also enhanced due to the birth of new LCSs.

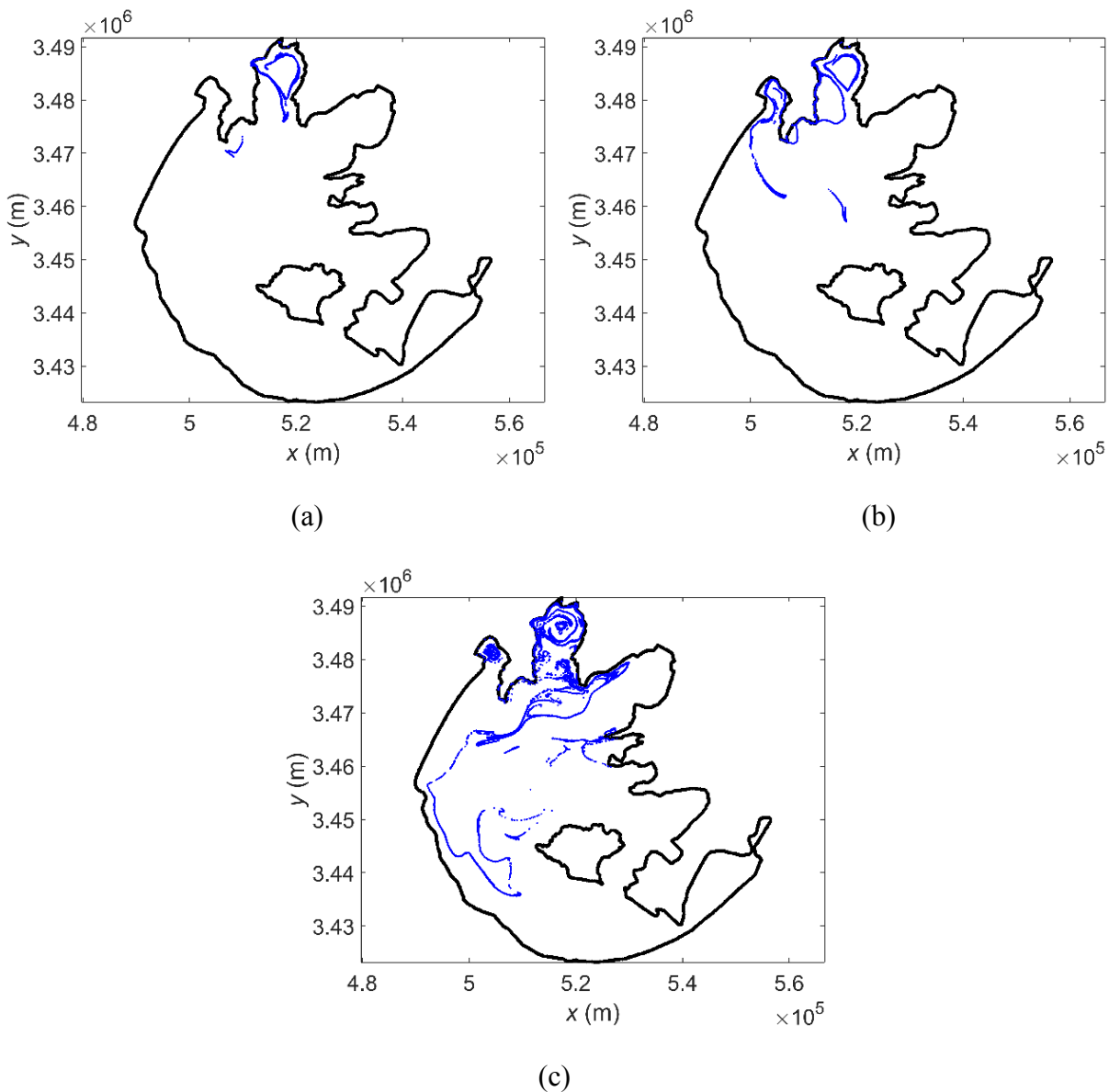


Figure 6.21 Particles continually released at Xingou Route in winter: (a) particle trajectories on 5th February; (b) particle trajectories on 25th February; (c) particle trajectories on 15th March.

The simulation of continues particles released at Xingou route in spring period are shown in Figure 6.22. By 5th April, most particles leave Meiliang Bay directly through LCSs near to east shoreline and are introduced into Zhushan Bay. At 15th May, the barrier property of LCS is very obvious to be observed: particles moving to east are refused to enter the main area of Gonghu Bay and they just circle at the external area of Gonghu Bay. Also new released particles just roam in Meiliang Bay while those early particles travel very fast and dot in most part of the lake.

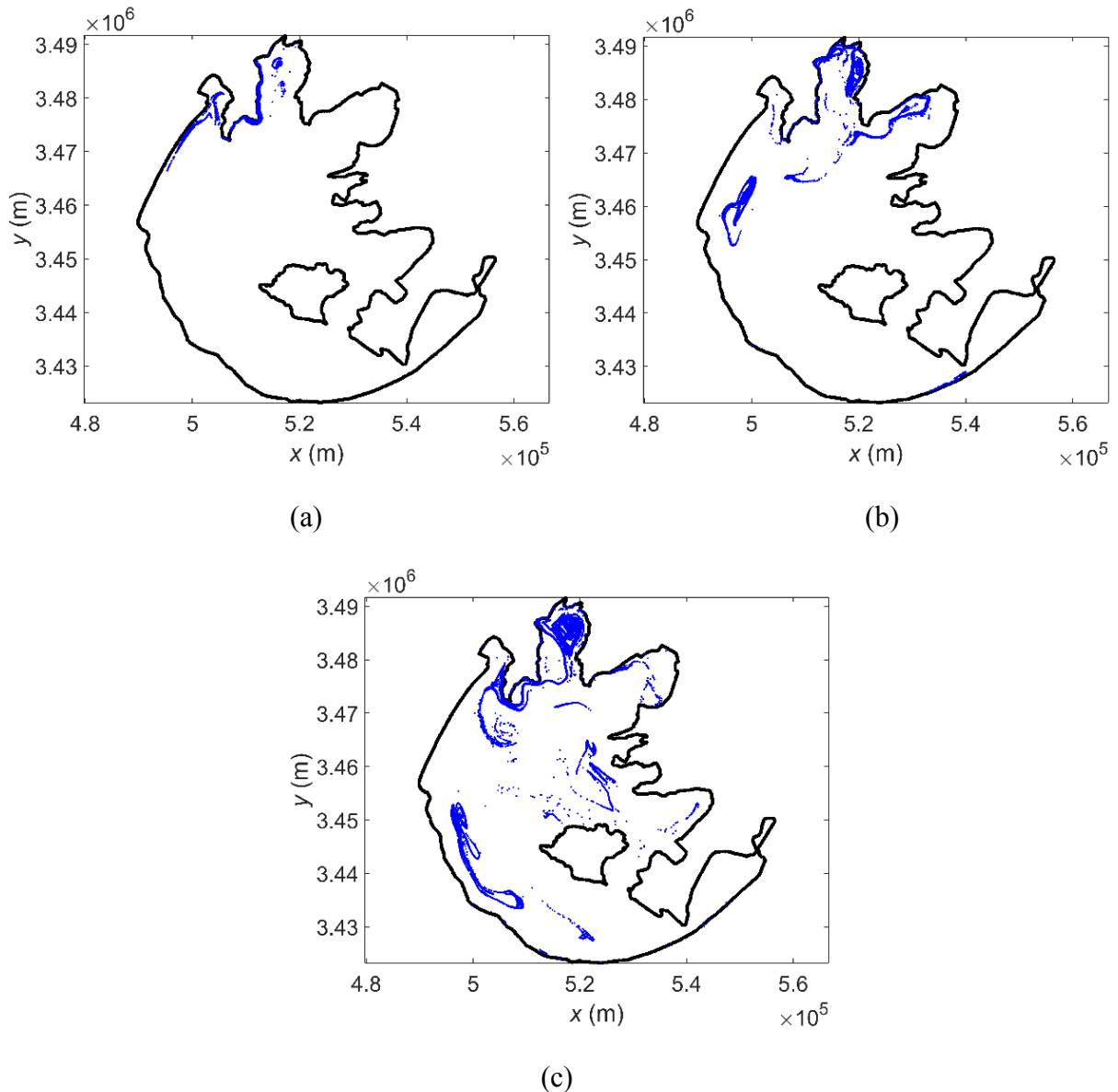


Figure 6.22 Particles continually released at Xingou Route in spring: (a) particle trajectories on 5th April; (b) particle trajectories on 25th April; (c) particle trajectories on 15th May.

The particle tracking results in Figure 6.22 show that water transfer engineering from Xingou Route at spring could only refresh northwest area of Meiliang Bay and outer area of Gonghu Bay due to the influence of LCSs. It means that this engineering solution is not helpful to

transport freshwater into northern bays and dilute water pollution in them. But freshwater could be transported to west zone in a relatively short time (approximate 30 days).

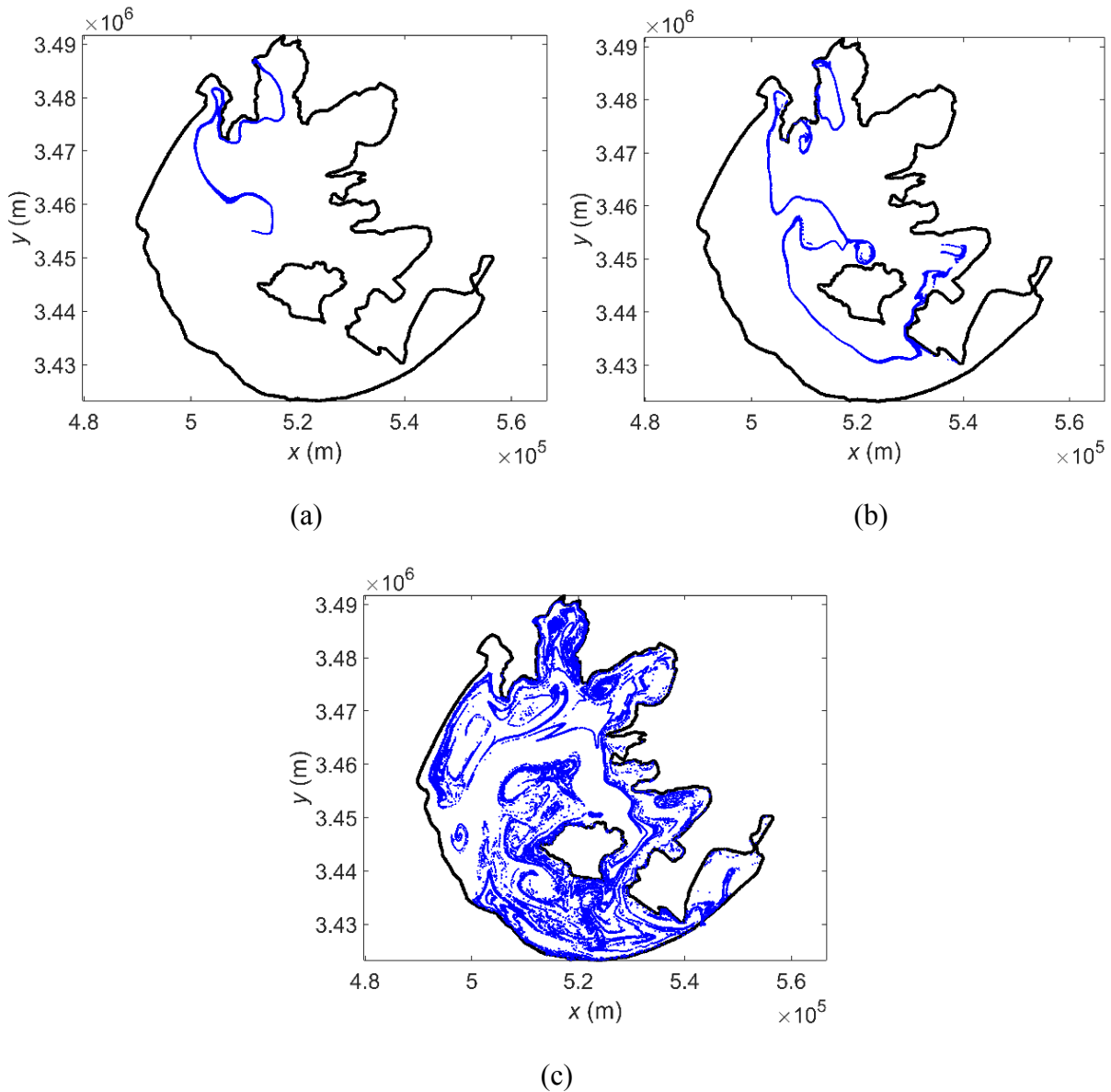


Figure 6.23 Particles continually released at Xingou Route in summer: (a) particle trajectories on 25th June; (b) particle trajectories on 5th August; (c) particle trajectories on 15th September.

In summer period (120 days) as shown in Figure 6.23, the trajectories of particles released from Xingou Route are quite similar with that of particles released from Wangyu Route. This is because both Xingou Route and Wangyu Route are at the north of Lake Tai and these particles are organized by the same northern LCSs. Particles follow the out boundary of a vortex-shape LCS system located at southwest of Meiliang Bay and travel into Zhushan Bay. Within 60 days, particles trace out a filamentary structure which is lying across the whole lake from North to South. When it comes to July and August, particles are highly mixed all around the lake. The results illustrate that water transfer plan from Xingou Route at summer are highly recommended

as a powerful engineering solution to solve water quality problems in Lake Taihu. Both the main lake and those important sub-zones including Gonghu Bay, Meiliang Bay, Zhushan Bay and west zone could be fully refreshed by clean water from Yangtze River.

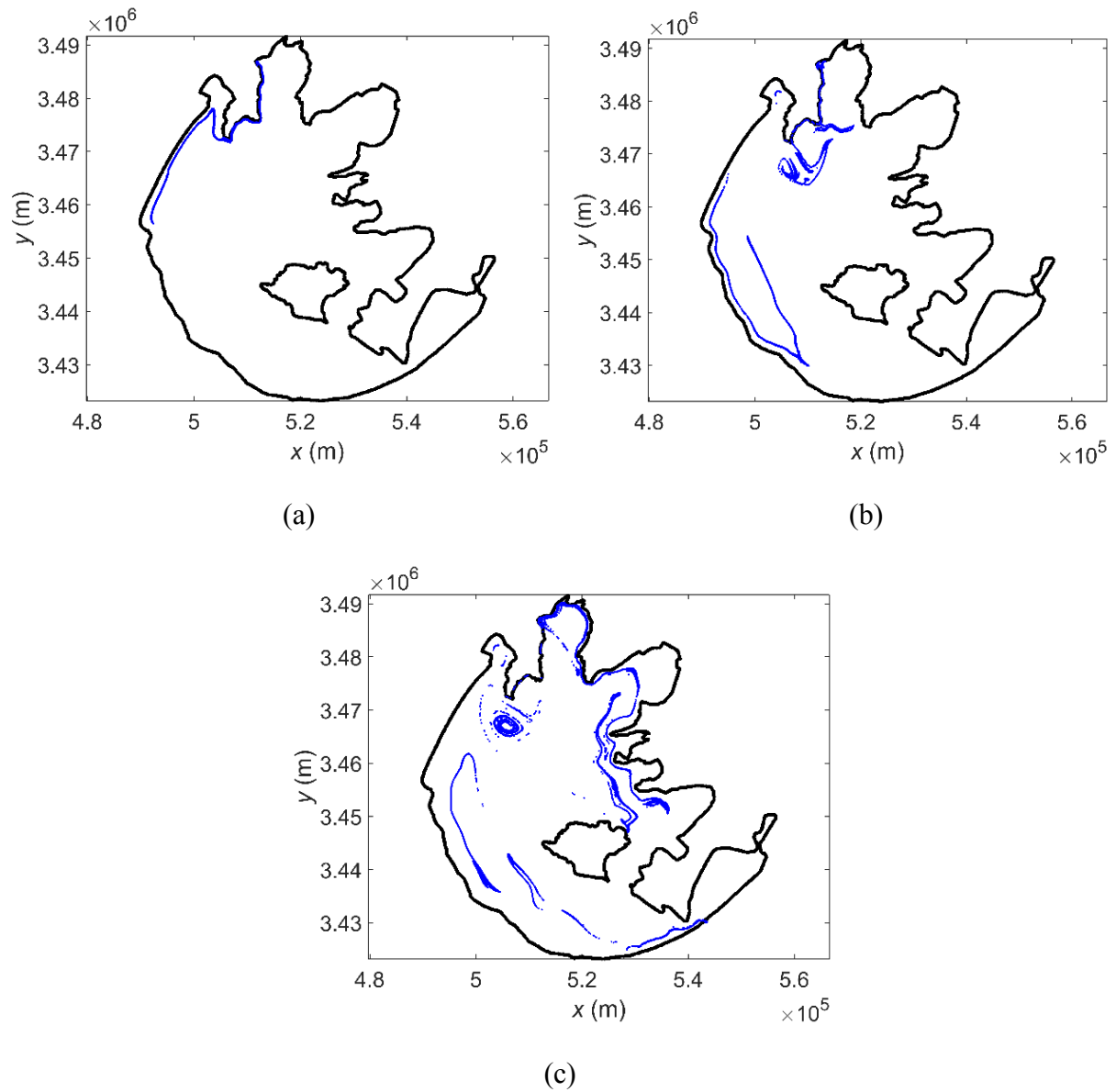


Figure 6.24 Particles continually released at Xingou Route in autumn: (a) particle trajectories on 5th October; (b) particle trajectories on 25th October; (c) particle trajectories on 15th November.

The particle trajectories in autumn are shown in Figure 6.24. In the first 20 days to 5th October, particles first travel to south along the shoreline and leave Meiliang Bay. Then particles arrive west zone of Lake Taihu and begin to follow the large vortex-shape LCSs occupying west zone and southwest area of the Lake. When it comes to 25th October, particles shows different motions. Particles reverse the direction and start to move to the north of Meiliang bay along the north and east shoreline of Meiliang Bay. After leaving Meiliang Bay from southeast area,

particles keep moving southward to East Epigeal Zone. And early particles which roam in west zone enter Dongtaihu Bay from west.

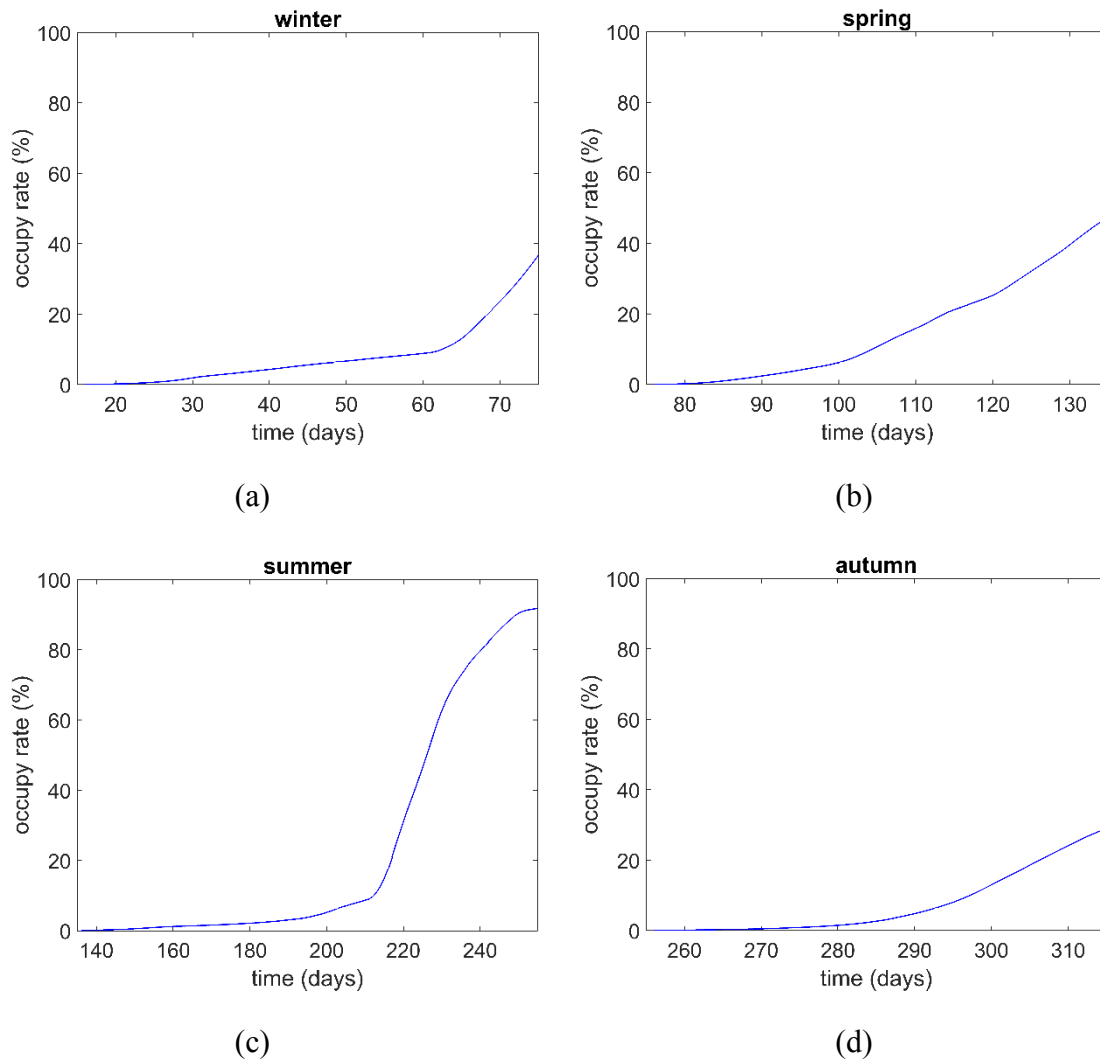


Figure 6.25 Global occupy rate of particles released at Xingou Route for different seasons in year 2005: (a) winter; (b) spring; (c) summer; (d) autumn.

Figure 6.25 shows the global occupy rate of particles released from Xingou Route for different seasons in year 2005. Again summer is the best season to apply water transfer plan from this route, with an occupy rate of more than 90 percent. For winter and spring, their occupy rate for the whole lake is quite close, both about 40 percent. While their performance to special sub-zones should be discuss in details in following paragraphs. Autumn, having a rate of approximate 30 percent, is still the worst season for this water transfer application. But compared to the result of winter application in Wangyu Route, which is less than 10 percent, the performance of Xingou route have obviously improved. So if there is any need to dilute contaminants or wash out harmful microorganisms in winter period, Xingou Route should be considered as a better plan than Wangyu Route.

Table 6.2 shows the local occupy rates of four highly polluted sub-zones mentioned in previous paragraph. Summer application have the highest occupy rate for Gonghu Bay, Meiliang Bay and West zone, with occupy rates of 85.94%, 98.23% and 81.65% respectively. For Zhushan Bay, winter application with the occupy rate of 89.44% is the best choice. One thing should be mentioned is that winter, spring and summer all have favorable performances (more than 95%) on freshwater transportation in Meiliang Bay. Since winter and spring application only spend half of time used by summer application, winter and spring are the most suitable seasons to deal with the water environmental problems which happen in Meiliang bay with the consideration of efficiency and economy.

	Whole lake	Lake Gonghu	Meiliang Bay	Lake Zhushan	Wester area
Winter	36.76%	4.05%	95.51%	89.44%	55.92%%
Spring	47.44%	46.27%	96.75%	78.63%	61.32%
Summer	91.76%	85.94%	98.23%	68.34%	81.65%
Autumn	28.99%	24.5%	28.9%	55.67%	32.91%

Table 6.2 Local occupy rates of particles released at Xingou Route for different seasons

6.4.3 The Lagrangian dynamics of particles released from Ximeng Route

Figure 6.26 illustrates the trajectories of freshwater particles transferred from Ximeng Route in winter period. Particles immediately move to the south of Zhushan Bay before leave it. The particle trajectories evolve into an anticlockwise vortex which is coincide with LCS distribution of January to February. Early particles are trapped in this vortex for quite a long time before their next motions. At 15th March., particles have almost occupied west zone and central zone. The particle tracking results shows that winter application of Ximeng Route have a positive influence on water quality improvement of Zhushan Bay and West zone.

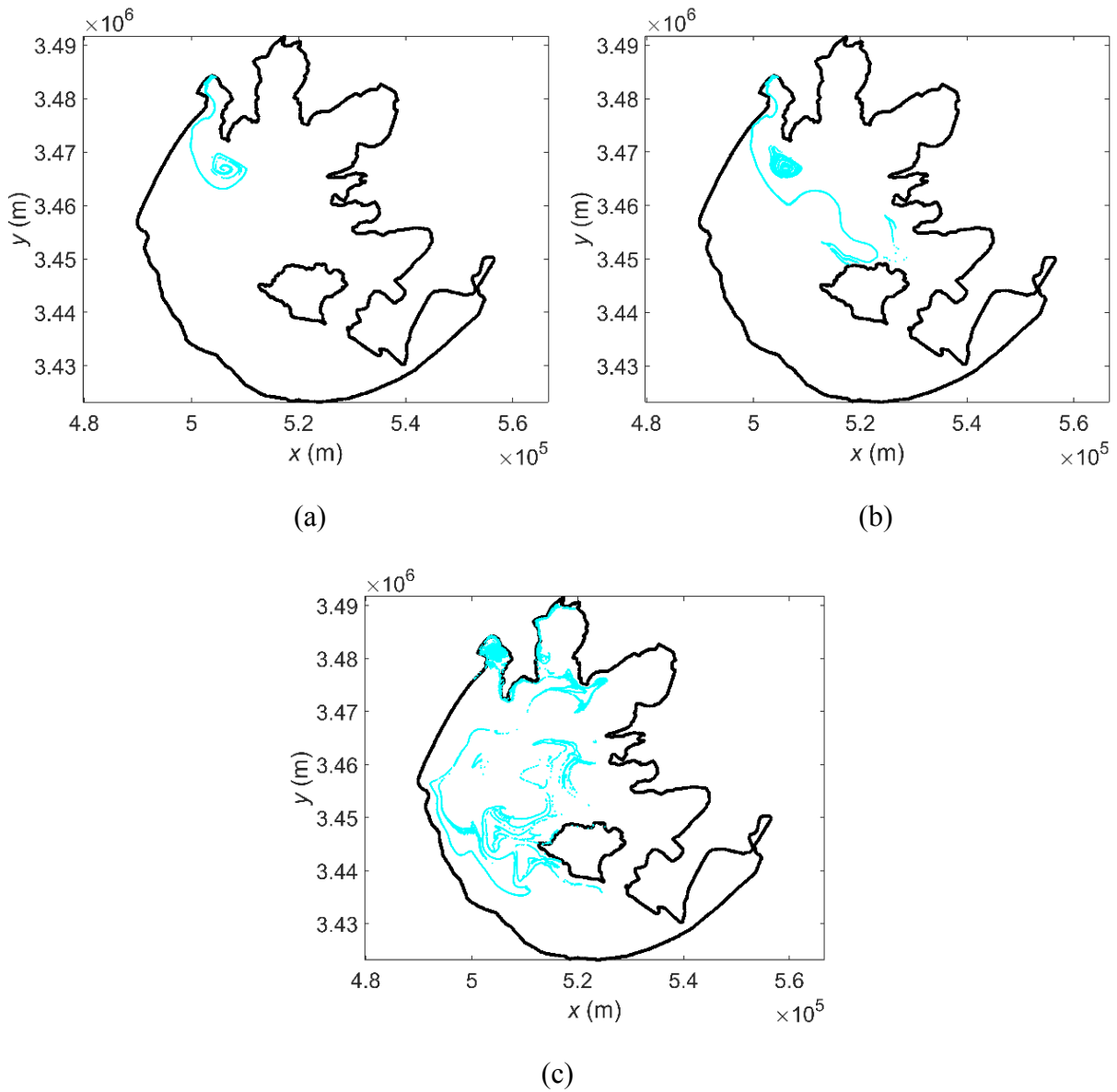


Figure 6.26 Particles continually released at Xinmeng Route in winter: (a) particle trajectories on 5th February; (b) particle trajectories on 25th February; (c) particle trajectories on 15th March.

The simulation of continues particles released at Xinmeng Route in spring period are shown in Figure 6.27. In Figure 6.27(a), particles first travel inside Zhushan Bay along the east shorelines and then travel to west of Zhushan Bay before leaving the bay. By 25th April in Figure 6.27(b), the motion of particles in Meiliang Bay is strictly limited due to the two vortex-shape LCSs systems in Meiliang Bay. These particles just roam outside of the LCSs rather than enter the main part of Meiliang Bay and a poor water exchange between Meiliang Bay and outside environment are observed. The simulation of spring application of water transfer from Xinmeng Route illustrated that only Zhushan bay could be benefited by this engineering application.

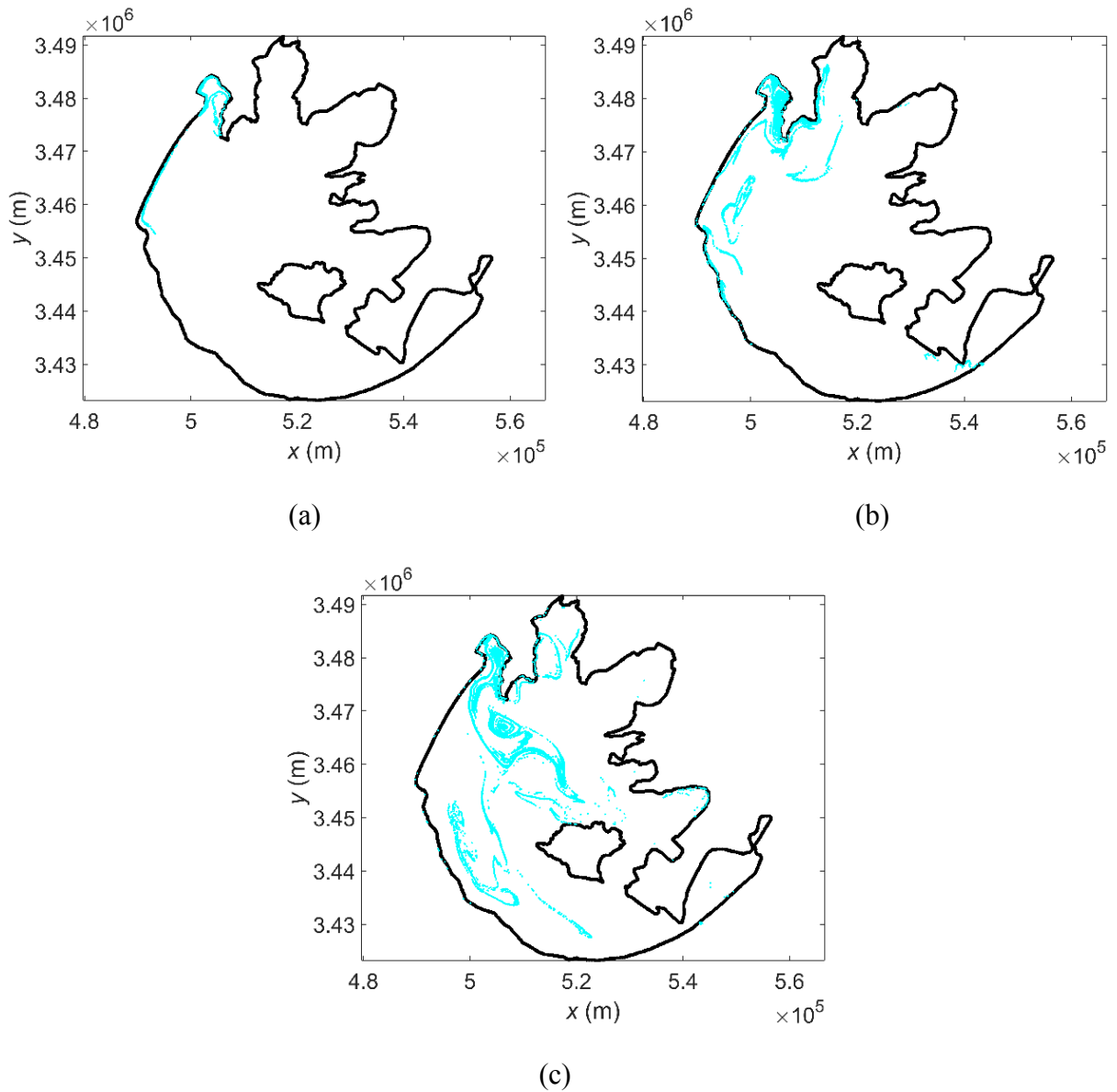


Figure 6.27 Particles continually released at Xinneng Route in spring: (a) particle trajectories on 5th April; (b) particle trajectories on 25th April; (c) particle trajectories on 15th May.

In Figure 6.28, the trajectories of particles transferred from Xinneng Route are described in summer period. From 15th May to 5th August, the behaviour of particles are quite simple: particles leave Zhushan Bay through southwest of the bay without delay and trace out a very long filamentary pattern from northwest to southeast of the lake. From 5th August to 15th September, the Lagrangian dynamics become much more complicated which have already been shown on the FTLE distribution section. This complicated dynamics dramatically enhance transport and mixing of particles all over the lake. Trajectories of LCSs-shape are detected almost anywhere in the whole lake and this proves that LCSs are the key point which dominate the fake of particles. The particle tracking simulation shows that summer application is a significant engineering solution to solve the water problems occurred in Lake Taihu.

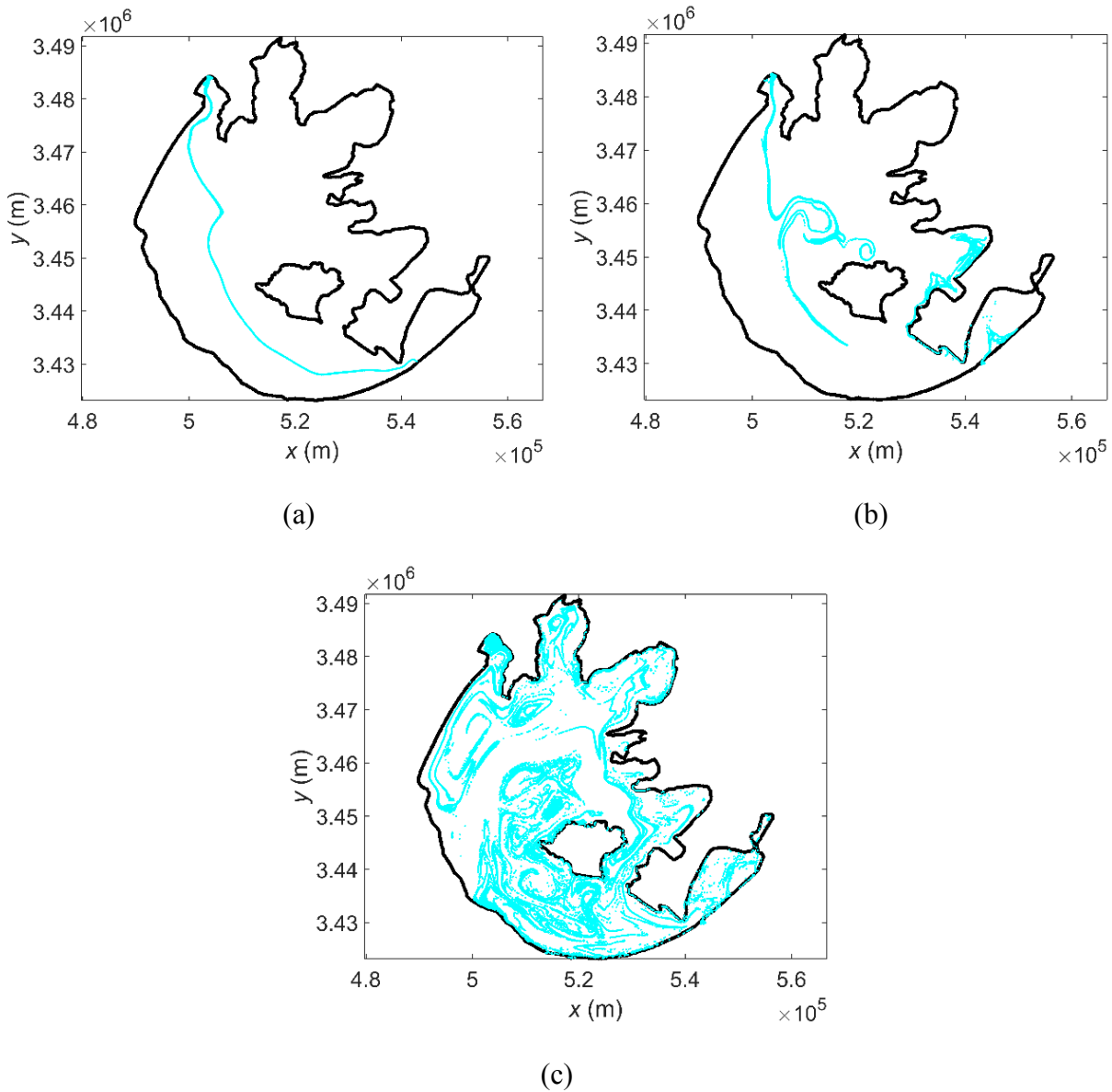


Figure 6.28 Particles continually released at Xinmeng Route in summer: (a) particle trajectories on 25th June; (b) particle trajectories on 5th August; (c) particle trajectories on 15th September.

The simulation of passive particles released from Xinmeng Route in autumn period are illustrated by Figure 6.29. Since the FTLE distribution in autumn period is mainly made up of vortex-shape LCSs which separate the whole lake into many enclosed or semi-enclosed regions, it makes particles from outside environments very difficult to enter these regions. Though particles from Xinmeng Route have the strong ability to escape from Zhushan Bay and travel around the main lake, few particles have successfully permeated into those enclosed or semi-enclosed regions such as Meiliang Bay, Gonghu bay or central zones. Transport and mixing between highlighted areas and other areas of the lake are extremely obstructed by local vortex-shape LCSs.

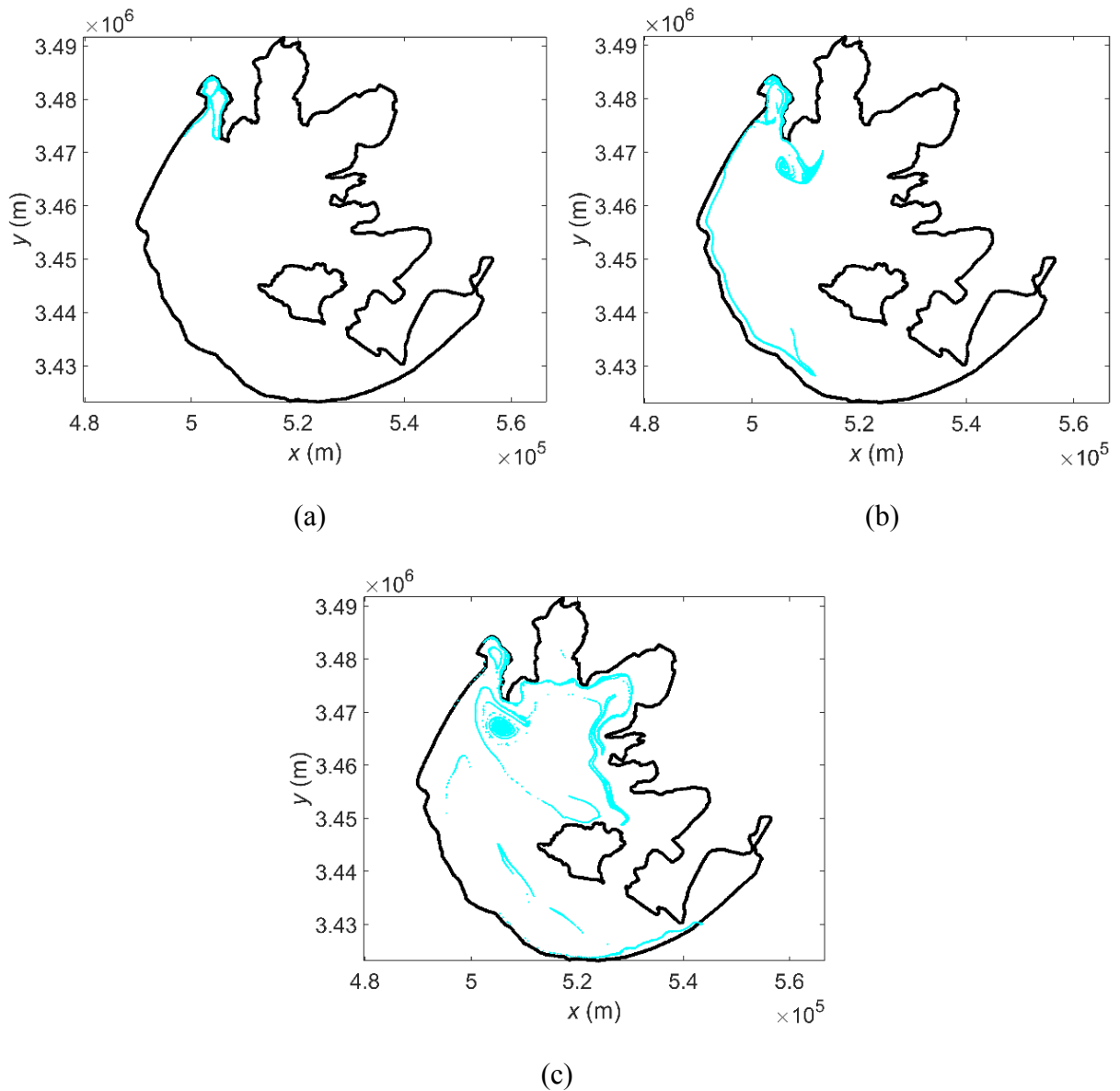


Figure 6.29 Particles continually released at Xinmeng Route in autumn: (a) particle trajectories on 5th October; (b) particle trajectories on 25th October; (c) particle trajectories on 15th November.

The global occupy rate of the whole lake by particles released from Xinmeng Route for different seasons in year 2005 are shown in Figure 6.30. The results are quite similar with that of Xingou Route. Summer is still the best time to refresh the whole lake while winter and spring have a similar occupy rate of approximate 40%. The lowest occupy rate of the whole is autumn application, with an occupy rate of about 20%.

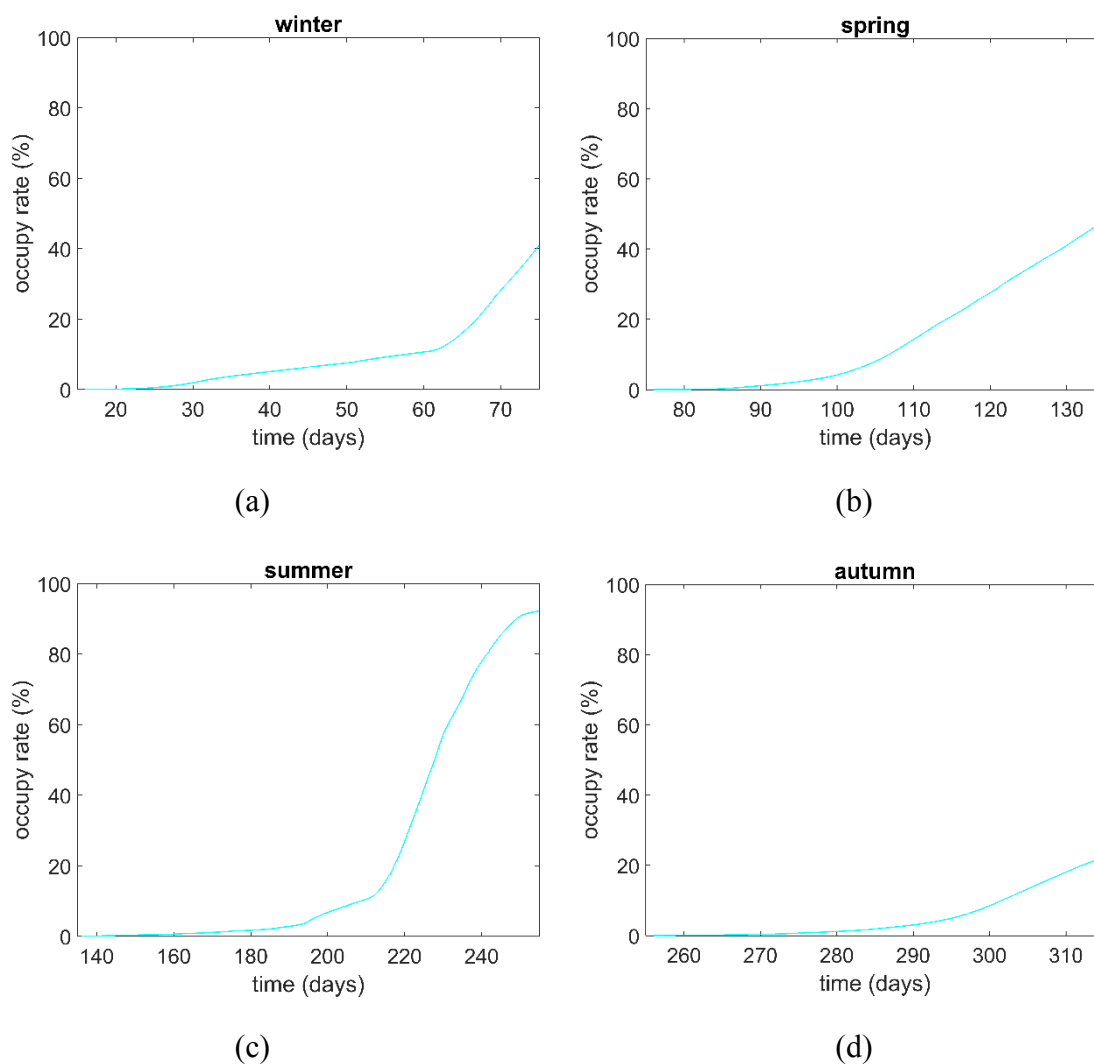


Figure 6.30 Global occupy rate of particles released at Xinmeng Route for different seasons in year 2005: (a) winter; (b) spring; (c) summer; (d) autumn.

	Whole lake	Lake Gonghu	Meiliang Bay	Lake Zhushan	Wester area
Winter	41.05%	0%	26.74%	89.26%	58.47%
Spring	48.12%	8.79%	60.43%	99.53%	94.3%
Summer	92.25%	84.84%	81.67%	91.12%	82.13%
Autumn	22.43%	19.99%	3.98%	77.09%	18.1%

Table 6.3 Local occupy rates of particles released at Xinmeng Route for different seasons

Table 6.3 shows local occupy rates of four highly polluted sub-zones: Gonghu Bay, Meiliang Bay, Zhushan Bay and West zone. For Gonghu bay and Meiliang bay, summer application having the occupy rates of 84.84% and 81.67% respectively is at priority position. Also summer is the sole option for Gonghu Bay all over the year because the maximum occupy rate of other applications on Gonghu Bay is only 19.99%. For Zhushan Bay and West zone, spring

application is the best choice, with occupy rates of 99.53% and 94.3% respectively in 60 days of application. Though winter and autumn application are not recommended for most cases, these two application still have a good performance on improving water quality of Zhushan Bay.

6.4.4 The Lagrangian dynamics of particles released from Dongshao Route

The particle tracking results in Figure 6.31 show that winter application of Dongshao Route is not a reasonable engineering application due to poor mixing and transport property of the lake in winter period. The trajectories of particles evolve into crowded patches rather than large filamentary structures which stretch and fold in different directions.

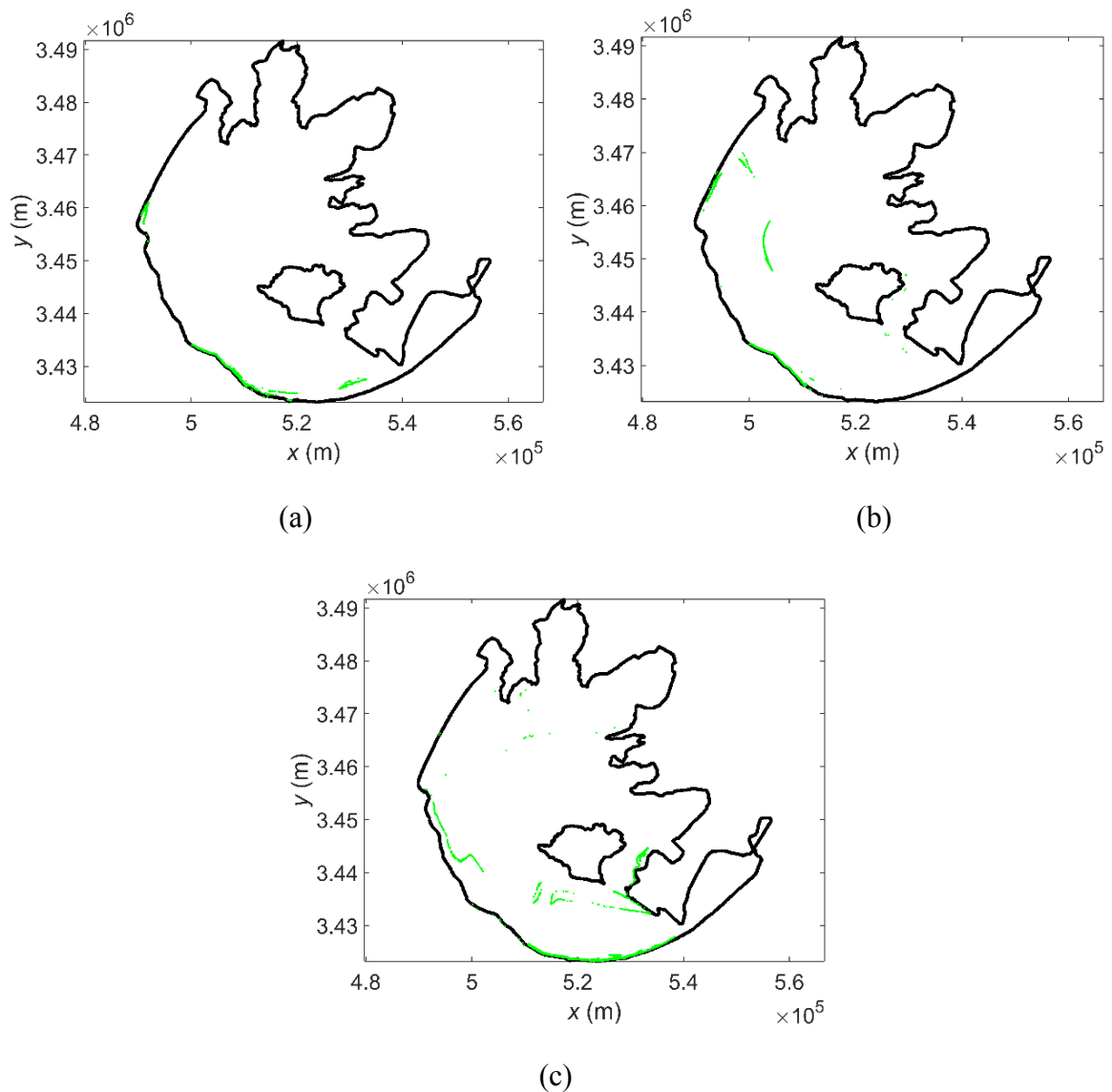


Figure 6.31 Particles continually released at Dongshao Route in winter: (a) particle trajectories on 5th February; (b) particle trajectories on 25th February; (c) particle trajectories on 15th March.

The simulation of continues particles released at Dongshao Route in spring period are shown in Figure 6.32. From 15th March to 5th April, particles just travel to north and enter West Zone by following the LCSs which are along the shoreline of the lake. During 6th April to 25th April, the mixing and exchange of water flows between southwest coastal area with central area are enhanced. Particles start to break away from shoreline and the trajectories are become complicated due to the stretching and folding processes caused by LCSs. The trajectories through East Epigeal Zone are much more sophisticated than those through West Zone which indicates that the transport and mixing property at east area is better than west area. The simulation of spring application proves that water transfer from Dongshao Route could be used to introduce freshwater to most parts of eastern area of the lake.

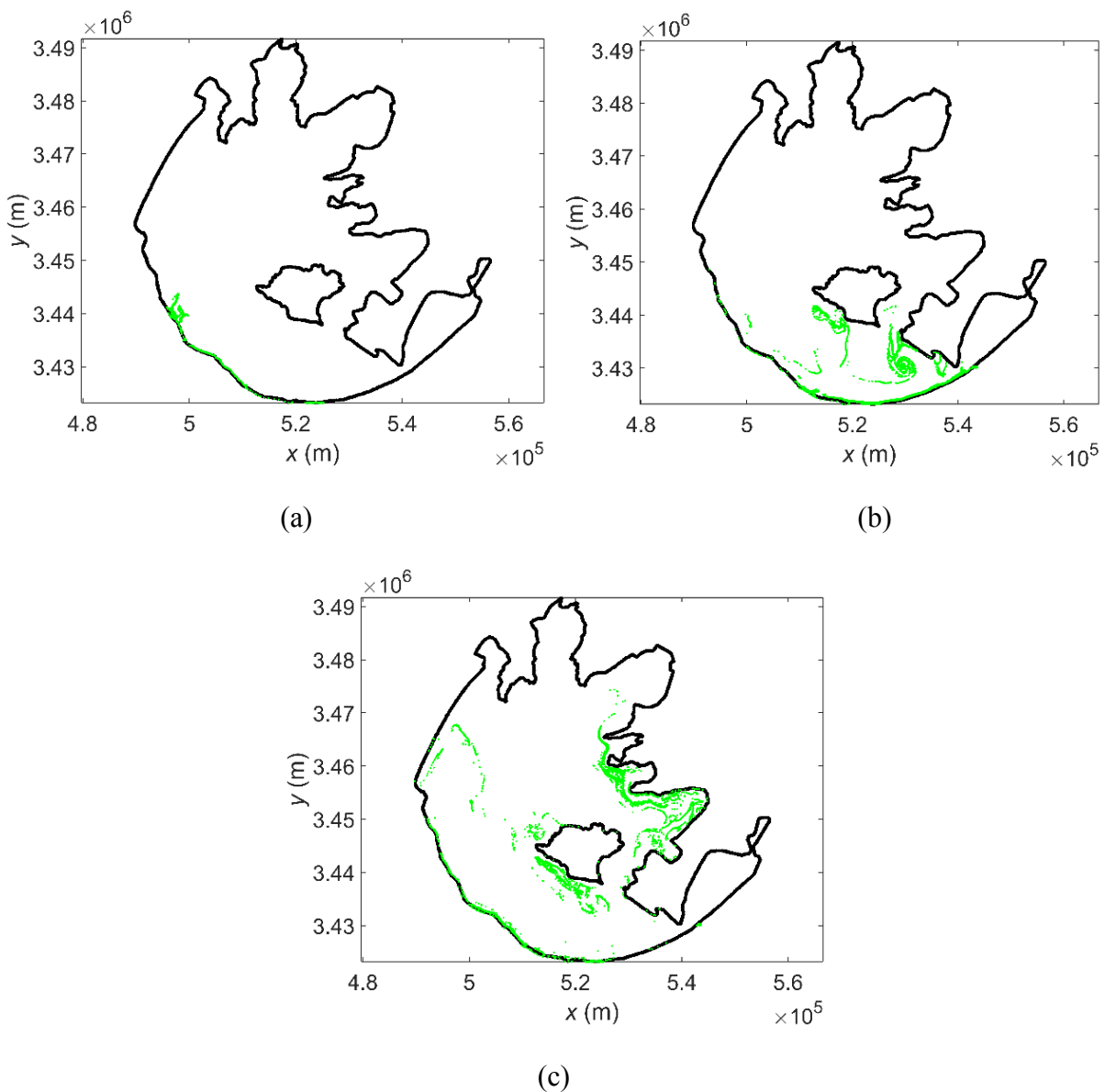


Figure 6.32 Particles continually released at Dongshao Route in spring: (a) particle trajectories on 5th April; (b) particle trajectories on 25th April; (c) particle trajectories on 15th May.

In Figure 6.33, the trajectories of particles transferred from Dongshao Route are described in summer period. Particles released from Dongshao Route go towards northwest along the shoreline of Lake Tai and be trapped for quite a long time before enter West zone as shown in Figure 6.33(a) and Figure 6.33(b). From 6th August, particles become more active and increase the speed of travel along the shoreline. Complicated trajectories could be clearly observed in West zone and north central area of the lake. Compared to spring application of Dongshao Route, summer application is more suitable and important to improve water quality of west Lake Taihu.

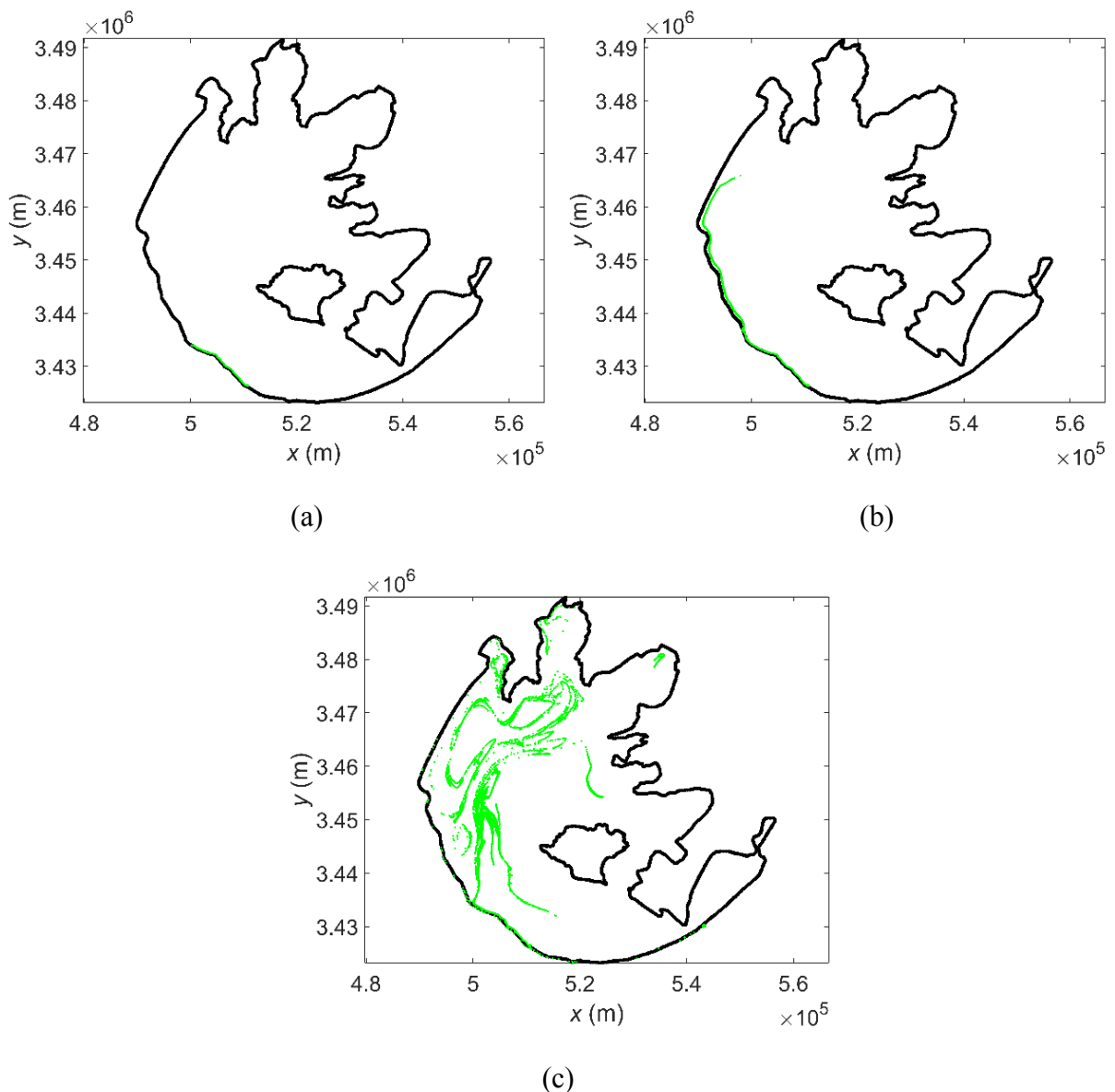


Figure 6.33 Particles continually released at Dongshao Route in summer: (a) particle trajectories on 25th June; (b) particle trajectories on 5th August; (c) particle trajectories on 15th September.

The simulation of particles released from Dongshao Route in autumn period are illustrated by Figure 6.34. Due to the existing of a large vortex-shape LCSs at southwest of the lake in autumn,

the motion of entering West Zone from southeast are forbidden and particles have to go along the outer boundary of the vortex-shape LCS to north. Particles arrive Zhushan Bay through central area of the lake and then move to northeast of the lake. Then the trajectories of particles are separated into two parts: early released particles shown complicated behaviours at northwest of the lake: some enter West Zone from north direction and some move forward to east; later released particles stop traveling to north at all and start to spread along the shoreline to southeast.

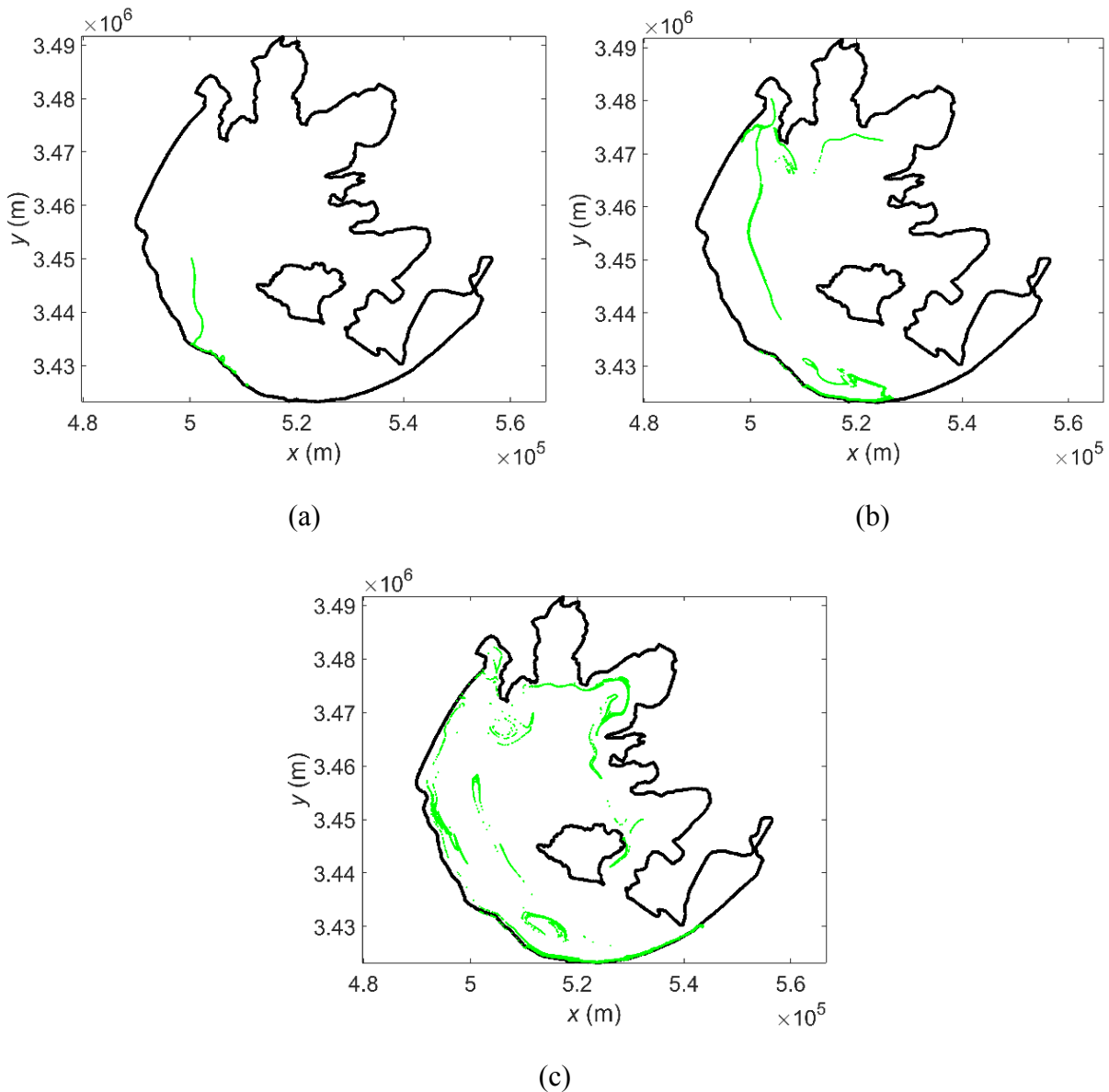


Figure 6.34 Particles continually released at Dongshao Route in autumn: (a) particle trajectories on 5th October; (b) particle trajectories on 25th October; (c) particle trajectories on 15th November.

As Dongshao Route is the only route located in the south of Lake Taihu among the four routes, autumn application of Dongshao Route seems quite important to the water environment of south part of Lake Taihu. By two months simulation, freshwater could be successfully imported to

most areas of this part: include West zone, East Epigeal Zone and Dongtaihu Bay. Although freshwater could also be introduced to north, it is very difficult for these freshwater to enter the highly polluted northern bays including Meiliang Bay and Gonghu Bay.

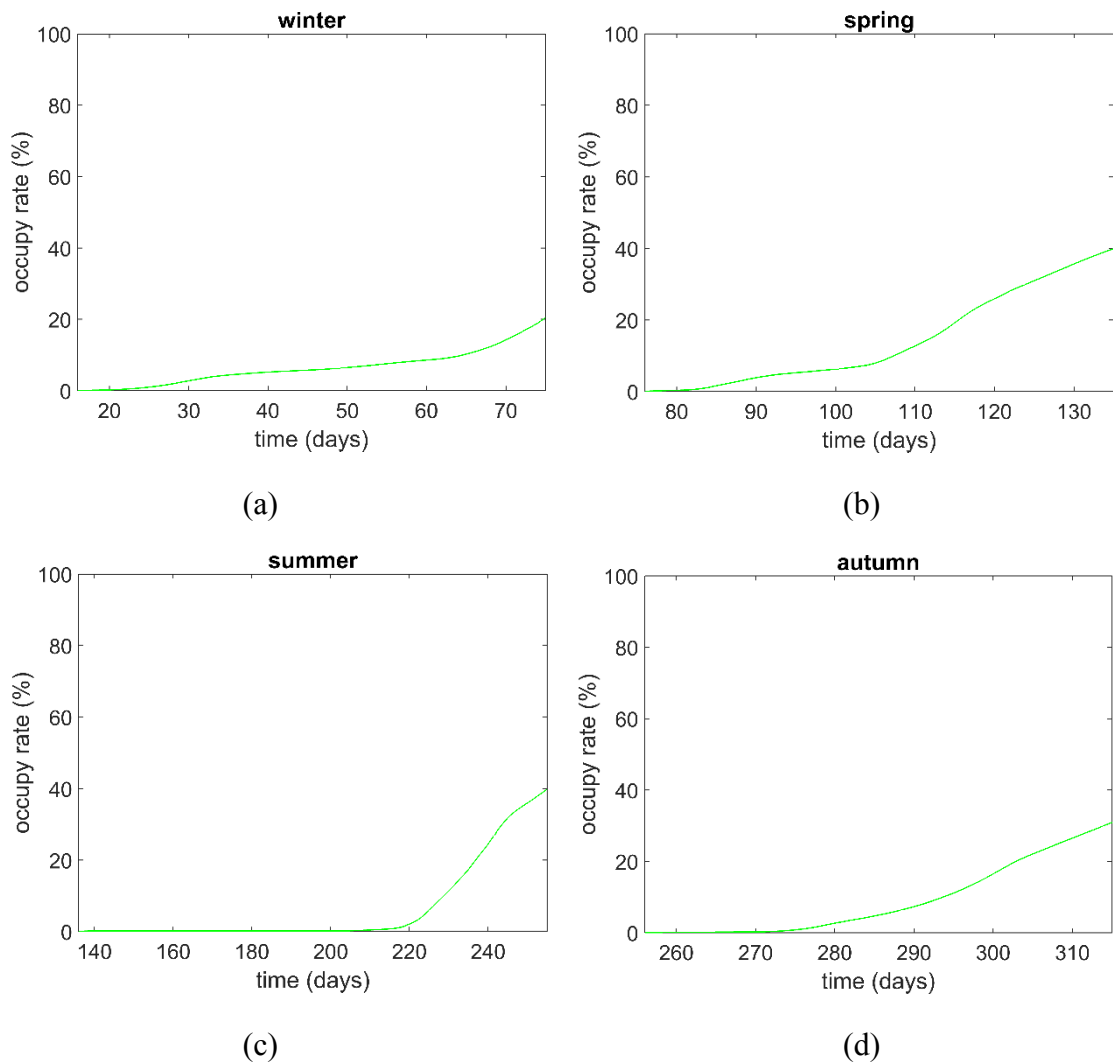


Figure 6.35 Global occupy rate of particles released at Dongshao Route for different seasons in year 2005: (a) winter; (b) spring; (c) summer; (d) autumn.

Here global occupy rate of the whole lake by particles released from Dongshao Route for different seasons in year 2005 are shown in Figure 6.35. Spring application and summer application have a similar occupy rate of about 40%, which is the highest among four seasons of year 2005. But the occupy rate of these two applications shows quite different tendency: occupy rate of spring application is keep increasing placidly all over the period; while occupy rate of summer application is almost zero in the first three months and dramatically increase after 220th day. This is because the transport and mixing property of Lake Tai is very poor in the first three months of summer 2005 and then greatly enhanced from August. This property is also indicated by FTLE distributions of those months in summer. Autumn application has the

second highest occupy rate which is approximate 30% and winter application shows the lowest occupy rate with 20%.

Table 6.4 shows the local occupy rates of four highly polluted sub-zones mentioned in previous paragraph. Since Dongshao Route is located at southwest of Lake Taihu, it is very difficult to transport freshwater to northeast part of the lake such as Gonghu Bay. Engineering applications in all four different seasons are unable to obtain satisfactory results about the local occupy rate Gonghu bay: autumn application has the highest value of only 14.06% while the values of other three season are less than 10%. For Meiliang Bay, freshwater transferred by winter, spring and autumn application could not reach this area and 38.08% area of Meiliang Bay could be refreshed by summer application. Both summer and autumn are suitable seasons to transmit freshwater into Zhushan Bay: summer application has a occupy rate of 71.21% in four months and autumn application has a occupy rate of 56.16% in two months. Finally comes to West Zone, this area is quite close to Dongshao Route and therefore it is easier to be influenced by this route compared to other northern bays. Summer application shows the highest rate of 95.65% and is followed by autumn application with the rate of 68.97%. Winter and spring application, with local occupy rate of 49.84% and 36.34% respectively, also could be acceptable choices as emergency methods to clean this area with freshwater.

	Whole lake	Lake Gonghu	Meiliang Bay	Lake Zhushan	Wester area
Winter	20.47%	0.38%	0%	10.51%	49.84%
Spring	39.98%	2.22%	0%	0%	36.34%
Summer	39.85%	9.66%	38.08%	71.21%	95.65%
Autumn	30.91%	14.06%	0.76%	56.16%	68.97%

Table 6.4 Local occupy rates of particles released at Dongshao Route for different seasons

6.4.5 Global occupy rates comparison of single route

Here global occupy rates of the whole lake by particles released from four different routes mentioned above for different seasons in year 2005 are shown together in Figure 6.36. At winter, freshwater from Xinmeng Route and Xingou Route are exchanged and transported more efficiently in the lake. Wangyu Route has the lowest occupy rate because LCSs in Gonghu Bay act as transport barriers and prevent freshwater released from Wangyu Route leaving Gonghu Bay. For spring, the results of four engineering routes are similar, with occupy rates varying

from 40% to 50%. Because of the characteristics of spring FTLE distribution, there are few LCSs that limits material exchange between bays and main body of the lake and besiege freshwater in some specific areas for quite a long time. Freshwater from every route gain the opportunity to spread in the major parts of the lake.

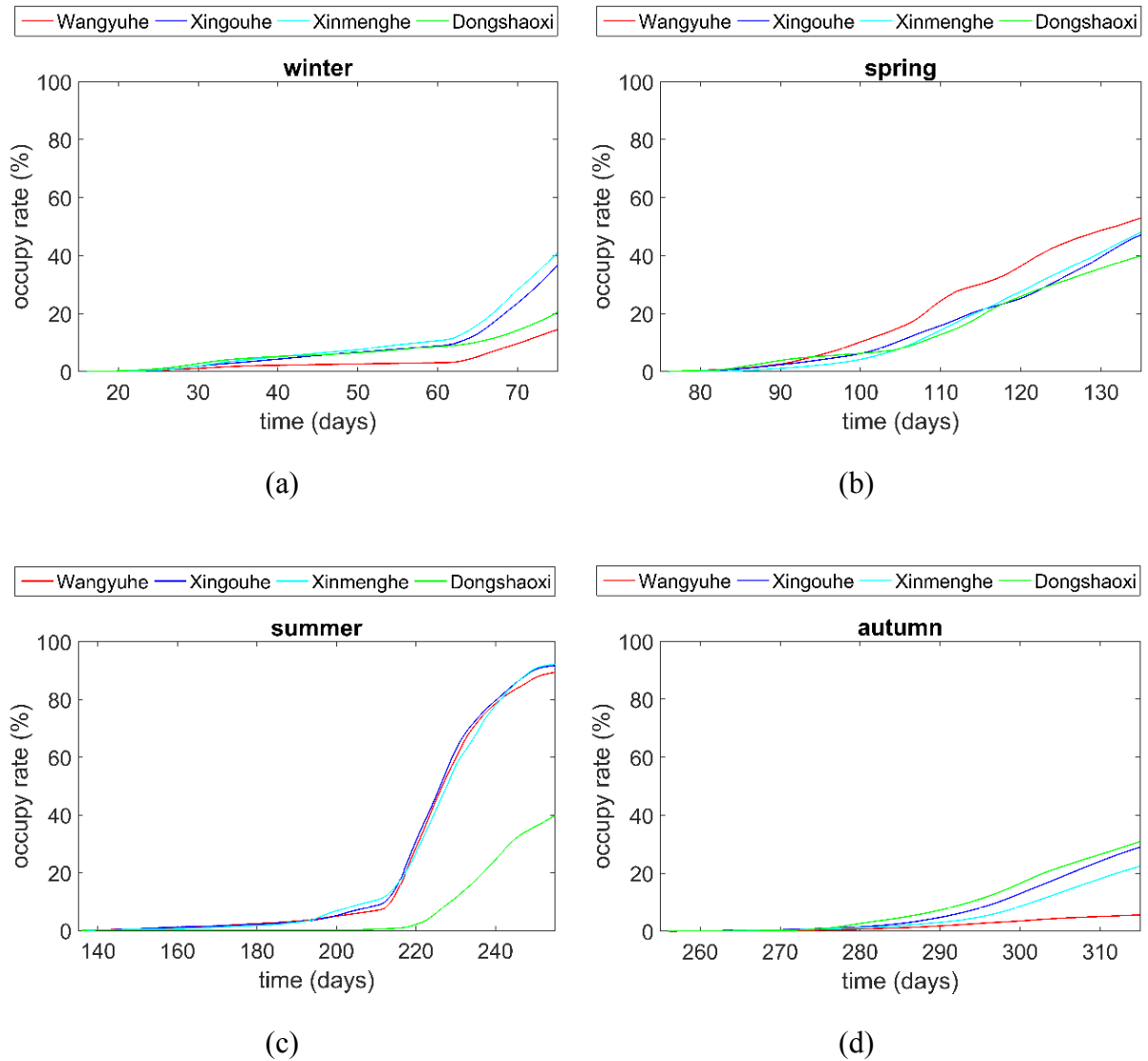


Figure 6.36 Global occupy rate of particles released at different rivers for different seasons in year 2005: (a) winter; (a) spring; (a) summer; (a) autumn.

It should be mentioned that though global occupy rates of the whole lake in spring are similar, each route has its own particular advantage to transport freshwater to special areas. For example, Wangyu Route shows an occupy rate of 99.75% to Gonghu Bay and Xingou Route owns an occupy rate of 96.75% to Meiliang Bay. About summer, the mixing and transport property of the lake is extremely excellent. Freshwater transferred by any route in northern bays has the ability to occupy more than 95% area of the lake. Due to the great contribution of transportation made by LCSs, freshwater could be successfully exported from semi-closed areas such as these

bays and be widely propagated all around lake Taihu. When it comes to autumn, more vortex-shaped LCSs appear and they form closed regions which weak the transport and mixing property of the lake. The motion of freshwater released from northern bays are seriously limited due to this reason and the occupy rates of northern routes become very low (less than 30%) in this season. The highest occupy rate is obtained by the application of Dongshao Route which is located at southwest of Lake Taihu.

6.4.6 *The Lagrangian dynamics of particles released from two routes*

Since water transfer programs are regard as emergency solutions to improve water quality efficiently when heavy pollution or eutrophication occurs, it is necessary to consider how to refresh the lake as best as we could by using these engineering routes in a given time. As discussed in our previous paragraphs, the water transfer from one single route usually have a positive influence only on some areas of the lake and it is always not enough for solving the problem of the whole domain. Hence we need to consider the applications of multiple routes. In this section, the situation of the combination of two single routes are simulated from May to August during which eutrophication caused by algae blooms most frequently appear in Lake Taihu.

Figure 6.37 illustrates the particle tracking results of six different scenarios. Because of the invariance characteristics of LCSs in a finite time interval, there are some same Lagrangian dynamics which could be observed in these scenarios. Particles released from northern bays have very similar trajectories at most areas of the lake due to the influence of LCSs. But still obvious differences between these scenarios could be found. For those multiple routes containing Wangyu Route like Figure 6.37(a-c), they have a good performance on northeast part of Lake Taihu which includes Gonghu Bay and this is because only freshwater transferred from Wangyu Route could be transported to this area. The function of Wangyu Route and Xingou Route on water transfer is almost the same in this period since their particles trajectories (red one and dark blue one) are coincide in most areas. These two routes are very efficient on improving water quality of Meiliang Bay and central areas of the lake. The advantage of multiple routes having Xinmeng Route as Figure 6.37(b), Figure 6.37(d) and Figure 6.37(f) is that more freshwater could be introduced into Zhushan Bay, East Epigeal Zone and Dongtaihu Bay. About the multiple routes with Dongshao Route like Figure 6.37(c), Figure 6.37(e) and Figure 6.37(f), they have more positive effects on West Zone and southeast area of the lake than other multiple routes.

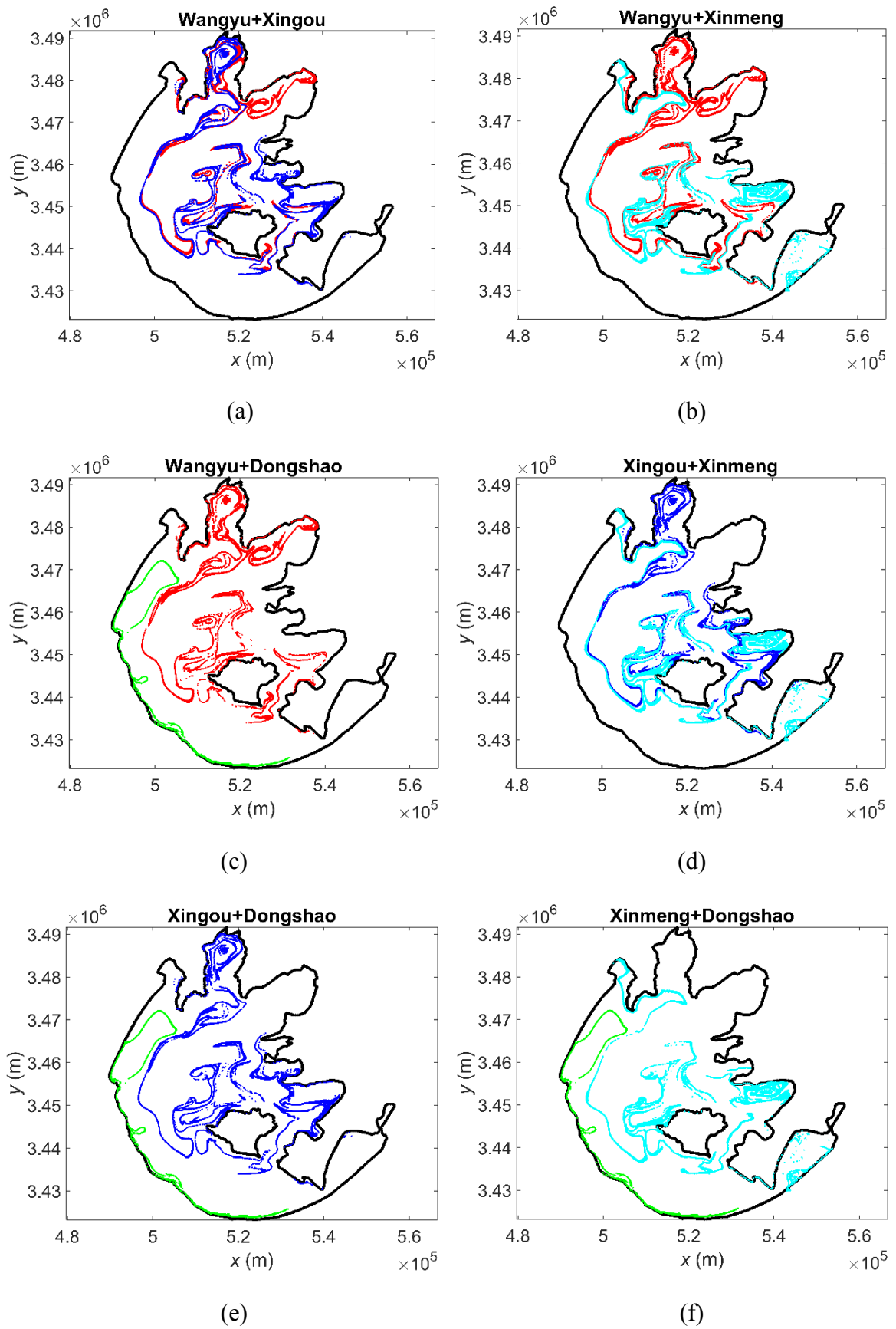


Figure 6.37 Particles released simultaneously at two different routes at early summer time (15th May to 15th July).

Compared to single route applications, the global occupy rate of multiple routes applications shown in Figure 6.38 obviously increase and the results are approximate 10% higher than that of single route. For single route applications, three northern routes (Wangyu, Xingou and Xinmeng) have very similar occupy rate of about 45% while the value of Dongshao is only 5.96%. And for multiple route applications, the results are different due to the different combinations of routes, with Wangyu-Xingou Routes having the highest occupy rate of 57.4% and Xinmeng-Dongshao Routes having the lowest occupy rate of 46.56%.

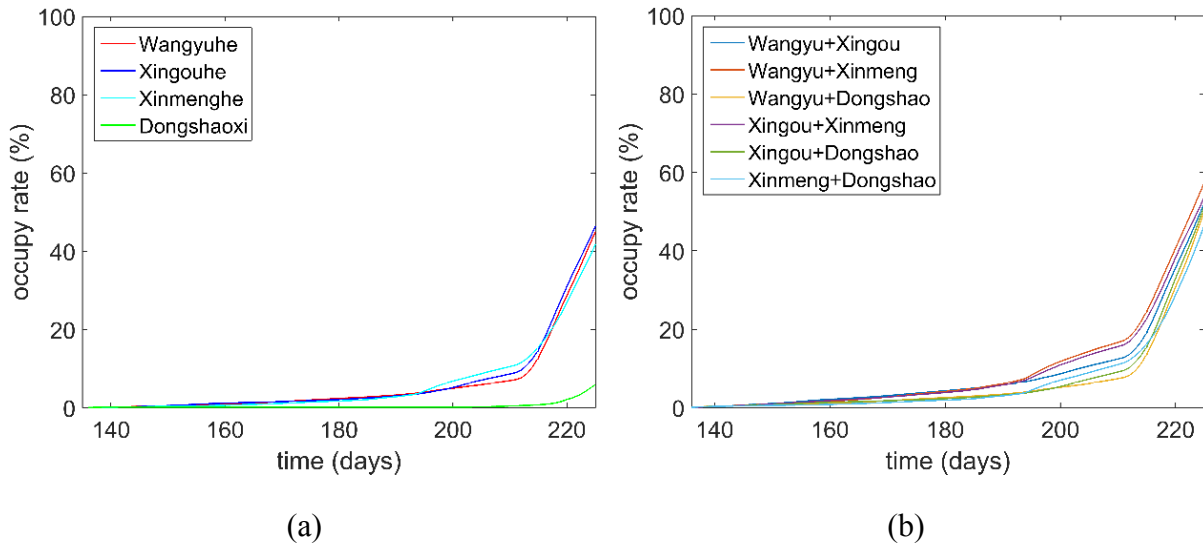


Figure 6.38 Global occupy rate with simulation time from 15th May to 15th July: (a) single route; (b) multiple routes with two routes.

The local occupy rates by combined routes are shown in Figure 6.39. For Gonghu Bay, the situation is simple: for those who have Wangyu Route, the occupy rate is 37.8%; for those who don't, the occupy rate is absolutely zero. At Meiliang bay, Wangyu-Xingou Route has the best performance of 85.03% because freshwater from either Wangyu Route or Xingou Route is well mixed in this bay; Xinmeng-Dongshao Route has the lowest occupy rate of only 5.28%. About Zhushan Bay, due to the main contribution of Xinmeng Route, both Wangyu-Xinmeng route and Xingou-have an outstanding occupy rate of more than 70% (70.02% and 70.42% respectively); And the poorest occupy rate comes from Wangyu-Dongshao Route, with a value of 36.42%. Finally comes to West Zone which majorly under the influence of Dongshao Route, the highest occupy rate of 51.03% is belong to Xinmeng-Dongshao Route, followed by Xingou-Dongshao Route (48.82%) and Wangyu-Dongshao Route (47.47%).

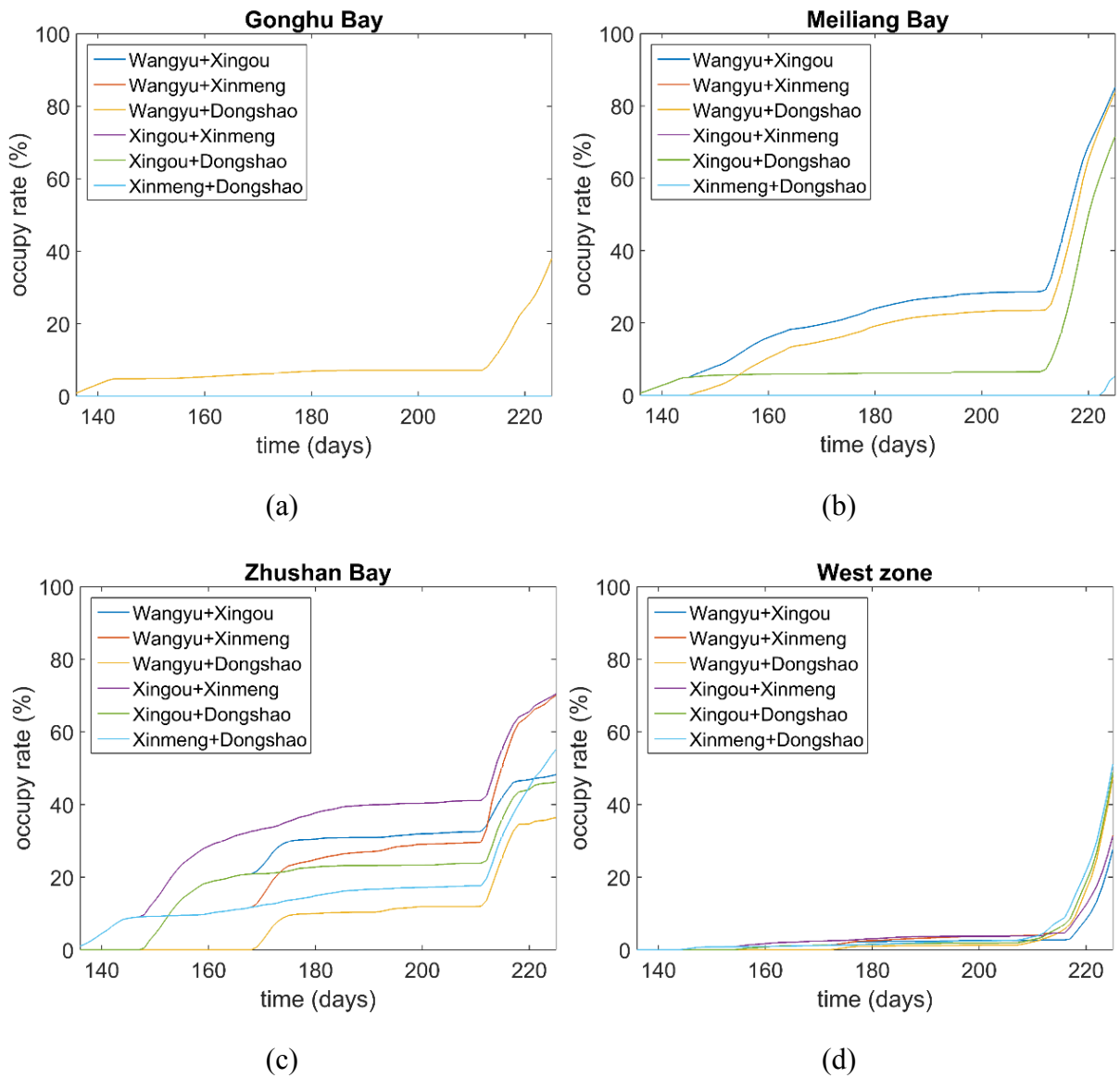


Figure 6.39 Local occupy rate of highlighted areas with simulation time from 15th May to 15th July by multiple application with two routes.

The water quality improvement of Gonghu Bay, Zhushan Bay and West Zone are highly related to unique transferred routes, they are Wangyu Route, Xinmeng Route and Dongshao Route respectively. For Meiliang bay, combination of any two northern routes (Wangyu, Xingou and Xinmeng) have an outstanding water quality improvement in Meiliang Bay since they all make great contribution for refreshing this area.

6.4.7 The Lagrangian dynamics of particles released from three routes

Simulation results of multiple routes which contain three single routes are presented in Figure 6.40. As the simulation of multiple application of two routes, particles released from three northern routes have highly coincident trajectories. This phenomenon could explain why there

is no obvious improvement of occupy rates by the application of multiple application with three routes: particles from different northern route just cover each other in same positions rather than distribute in different areas. But this kind of multiple application may have a very strong positive influence on water environment of some special areas. For example, the water quality of Meiliang Bay, central area of the lake and East Epigeal Zone are extremely improved if the multiple application is consisted of three northern bays because all of them are able to transport freshwater into these areas. So if there are any heavy pollutions or eutrophication occurring in Meiliang Bay and should be remitted as soon as possible, multiple application with three northern routes is much more effective than any other scenarios.

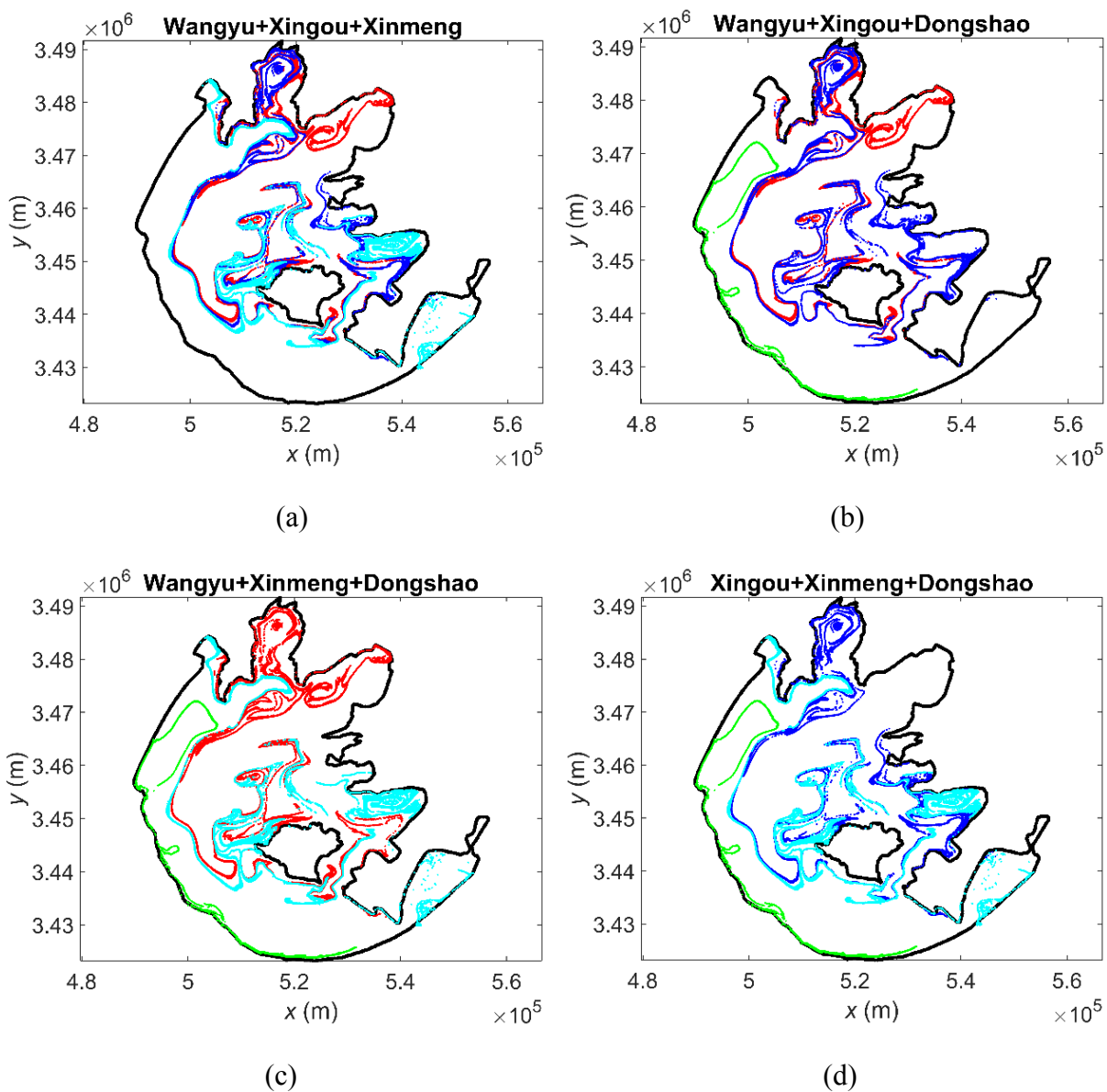


Figure 6.40 Particles released simultaneously at three different routes at early summer time (15th May to 15th July).

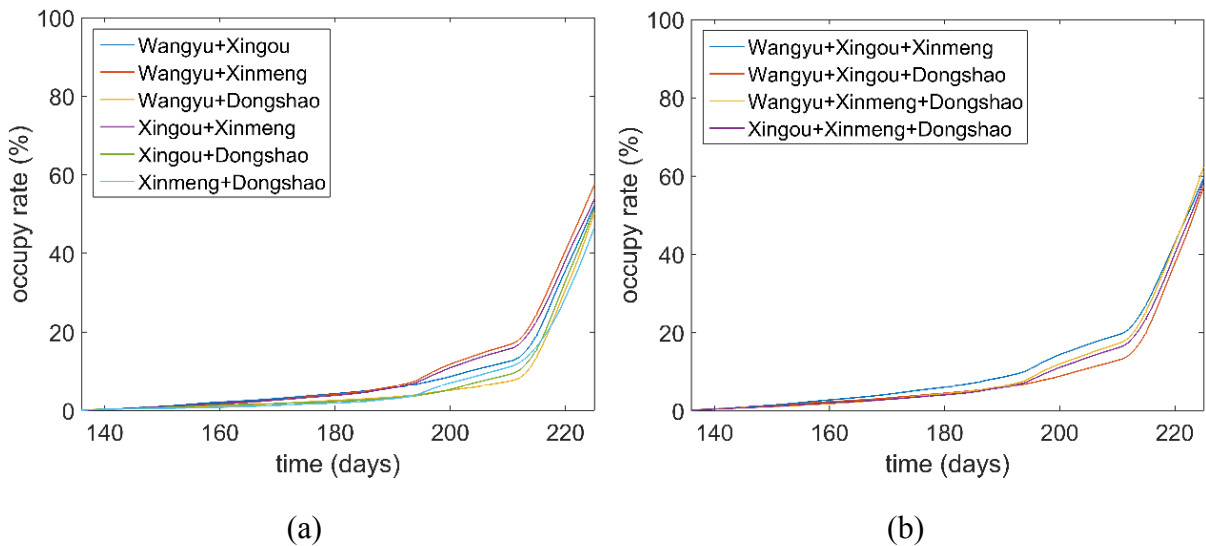


Figure 6.41 Global occupy rates with simulation time from 15th May to 15th July: (a) multiple application with two routes; (b) multiple application with three routes.

Global occupy rates by multiple routes with two routes and multiple routes with three routes are illustrated in Figure 6.41. It is clear that only slight improvements are able to be obtained by some scenarios of multiple routes with three routes. The best route combination for three routes application is the yellow line representing Wangyu-Xinmeng-Dongshao in Figure 6.41(b), with occupy rate of 62.26% which is only 4.86% higher than the best route for two routes application (Wangyu-Xinmeng). For other multiple routes of three routes, the results are almost the same as multiple routes of two routes. This indicates that in the given time intervals (from May to August) multiple applications with three routes do not have an overwhelming performance compared to multiple applications with two routes. Even though small increasement of occupy rates could be achieved by multiple applications with three routes, it is not necessary to use these applications due to their higher expenditure of money and labour force.

In Figure 6.42, it is clear that both the tendency and value of local occupy rate by using three routes applications are highly similar with those by using two routes applications. One thing should be mentioned is that more routes are involved in multiple applications, less difference they will be. Except Gonghu bay which is only influenced by Wangyu Route, the results of four scenarios on each area are close to each other.

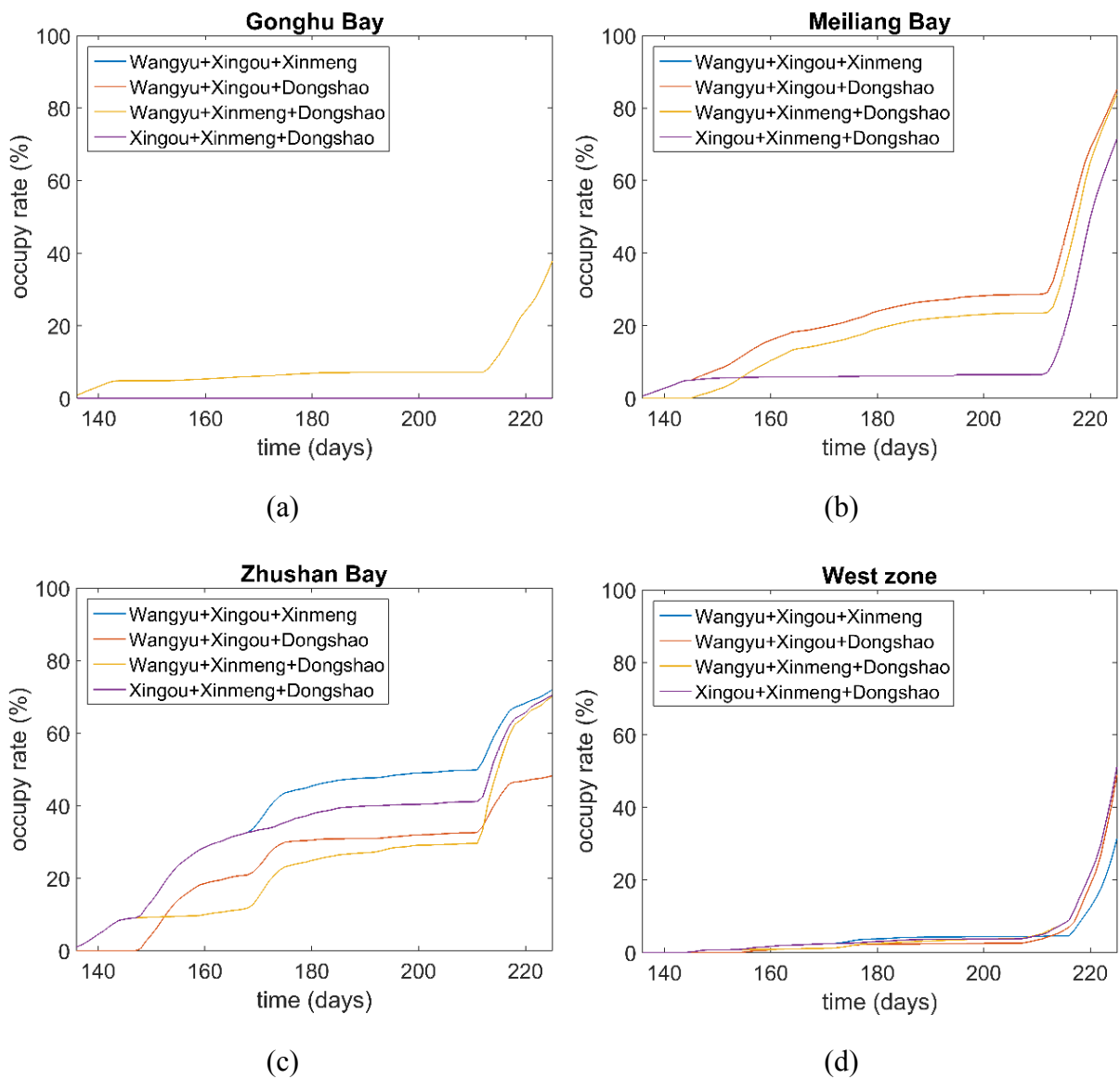


Figure 6.42 Local occupy rate of highlighted areas with simulation time from 15th May to 15th July by multiple application with three routes.

6.5 Conclusions

The investigation of transport and mixing property described by FTLE-LCSs method in Lake Taihu has been presented. Local particles tracking simulations are used to study the Lagrangian dynamic of local particle patches located in different areas of the lake and evaluate the lake areas that affected by these local particles, which could be regard as pollutants from an environmental accident. Continues particles tracking simulations are applied to assess the existing and proposed water transfer project. The main conclusions are demonstrated as:

Lake Taihu is governed by different kinds of LCS in different seasons and shows completely different kind of transport and mixing property since the Lagrangian dynamic is depended on

time. In spring and late summer period, the lake is filled with filamentary-shape LCS which indicate a strong transport and mixing property; in winter, early summer and autumn, the lake is mainly described by vortex-shape LCS which delineate the lake into different regions and prevent fluid exchange between these regions.

As the time interval and initial positions of local patch change, different particle tracking results are obtained. An environmental accident is more likely to evolve into a global problem which nearly or totally affect the water quality of whole lake in late summer time; while in early summer time, the influence of an accident is more or less limited in relatively small areas and the accident will remain as a local problem.

The performance of water transfer application is highly sensitive to the season and the location of transfer routes. Water transfer from northern routes (Wangyu Route, Xingou Route and Xinmeng Route) have the highest occupy rate of whole lake at summer and the lowest at autumn. Dongshao Route, which is located at southeast of the lake, has more average occupy rates on whole lake over the four different seasons. Generally, northern routes are more suitable for improving water quality of whole lake compared to Dongshao Route, while Dongshao Route still has the most positive effect on water quality of West Zone.

Multiple application of two routes has an obvious growth (approximate 10%) on the global occupy rate of the whole lake compared to single route application. The combination of Wangyu-Xingou routes has the best performance on water quality improvement of the whole lake with an occupy rate of 57.4%. Multiple application of three routes has similar occupy rates of the whole lake as multiple application of two routes. So the best choice to refresh the whole lake in early summer is multiple application of two routes.

The local occupy rates of four highlighted areas are extremely depend on the corresponding route that has the dominant influence on that area respectively. Multiple application of two routes or three routes do not show an outstanding performance on local occupy rates of these four areas compared to single route application. This is because though more routes are involved in multiple application, particles trajectories are almost coincide in these areas due the attracting property of LCS. Although the occupy rate of highlighted areas do not change too much by the application of multiple routes, the speed and efficiency of the refreshment are increased since more fresh water are introduced into highlighted areas by multiple applications.

Chapter 7. Conclusions and future work

An integrated fluid mixing modelling and analysis framework has been presented in this thesis, which consists of a shallow water hydrodynamic model and a particle tracking model. The framework provides a useful tool for investigating and better understanding horizontal transport and mixing processes in enclosed/semi-enclosed environmental flows. This chapter recaps those key conclusions from the previous chapters. The validation and performance of shallow water model and particle tracking model are discussed first. Then the application of the particle dynamics analysis framework to investigate the transport and mixing properties is summarized for idealized and realistic case studies as considered. Finally, possible directions for future improvement are suggested.

7.1 Conclusions

7.1.1 Full 2D Shallow water model

The 2D shallow water model used in this work has been developed and intensively tested for simulation of different large-scale shallow flows. For the semi-enclosed environmental shallow flows considered in this work, turbulence and eddies are common phenomena due to complex topographic features or highly variable boundary conditions (such as wind force). To consider the turbulent (viscous) effect on the flow hydrodynamics, an algebraic turbulent model is added to the existing shallow water model. Three benchmark test cases show that this simple turbulent model works reasonably well to reproduce the effect of viscosity in both regular and irregular domains.

It has been found that the performance of the algebraic turbulent model is sensitive to the eddy viscosity coefficient p_{vt} . In the jet-force flow case, the turbulence effect is not obvious if p_{vt} is not chosen to be large enough. When p_{vt} is increased to 3.4, the resulting shape and position of two vortices agree well with those presented by Rogers *et al.* (2001). This confirms that the algebraic turbulent model is able to simulate the effect of viscosity in an irregular domain if p_{vt} is chosen properly.

In the backward step case, the x -direction velocity components obtained from the improved shallow water model show a good agreement with results from experiment measurements and a more advanced turbulent model (k - ϵ model). However, the results from this test appear to be less sensitive to the choice of p_{vt} .

Finally in the wind-induced circular basin case, the numerical velocity profile in the radial plane that is normal to wind direction is in close agreement with the analytical solution and again is not sensitive to the choice of p_{vt} . This may indicate that, for this specific case, the wind is the dominant driving force of the flow hydrodynamics and the effect of viscosity may not be significant.

7.1.2 Particle tracking model

A Lagrangian particle tracking model is developed by solving the advection equations using a 4th-order Runge-Kutta time integration method. Bilinear interpolation is used to approximate continuous velocity field for particle tracking from the discrete numerical velocity data. The simulation of particle trajectories is combined with the calculation of FTLEs to detect LCSs and provide an exhaustive Lagrangian description of the transport dynamics for environmental shallow flows. Two benchmark cases are considered to validate the particle tracking model. In the case of blinking vortex flows, the current particle tracking model successfully reproduces the chaotic particle dynamics with results compared well with those reported in the literature (Aref, 1984; Ottino, 1989). In the case of Kranenburg's lake, the FTLE distributions and their associated LCSs show that the wind-induced oscillatory flows have a strong capability to organize the global chaotic behaviour in the lake and separate regions of different mixing dynamics, depending on the magnitude of a dimensionless parameter related to the wind duration.

7.1.3 Horizontal mixing and transport processes in an inflows/outflow-induced idealised lake

In the idealized shallow water lake, velocity fields driven by inflow/outflow boundary conditions clearly shows a periodic dynamic system that would lead to complicated transport and mixing processes. A single dimensionless flow duration parameter μ_i is introduced to control the particle dynamics. If μ_i is relatively small, the lake separates into two regions which is almost symmetric against the y axis and LCSs are detected near the ridges of regions. As the value of flow duration parameter increases, the transport and mixing properties change from regular to chaotic. Chaotic mixing first occurs at the ridges separating the two regions and gradually penetrates into inner areas of the separated low-mixing regions. High mixing efficiency is achieved in the whole lake when μ_i is increased to $\mu_i = 43.2$ and 86.4 . Under these conditions, the LCSs that separate the two low-mixing regions have totally disappeared and there appear almost no obvious transport barriers in the lake.

Particles released far away from LCSs show a weak capability of transport and mixing while those released near to the LCSs present a strong capability of transport and mixing and can travel along the LCSs. This indicated that FTLE-LCS method is useful for diagnosing areas with different mixing dynamics and predict particle motions. Particles released from two continuous sources are used to calculate freshwater occupy rate for water quality improvement. High occupy rate means that freshwater can effectively flush and refresh a large area due to enhanced mixing property.

7.1.4 Horizontal mixing and transport properties in a wind-induced natural lake

The proposed numerical framework is further applied to investigate the horizontal mixing and transport properties in Lake Taihu and evaluate the different water transfer projects based on the input data for 2005. The period for calculating FTLE distributions is set to be one month and 11 periods of FTLE distribution (each period contains a forward FTLE distribution and a backward FTLE distribution) are obtained.

The FTLE distributions show that the transport and mixing properties in Lake Taihu vary dramatically at different time of the year, largely due to the highly variable wind forcing. In winter, autumn and early summer, LCSs trace out many large-scale eddies and act as transport barriers which separate the whole into regions with different dynamic properties and prevent material exchange process between these regions, suggesting poor transport and mixing properties; while in spring and late summer, the LCSs distribute much more irregularly and break the boundaries of different regions, leading to strong transport and mixing properties in the lake.

Localized particle patches are advected to simulate the spread of contaminate (such as oil spill and outbreak of algae blooms) in Lake Taihu. The evolution process of these sudden environmental disasters are completely different due to the time intervals and initial positions of particles release. In early summer period when LCS shows poor transport and mixing properties, the effect of the local pollution event is limited within a relative small area; While in late summer period when LCS shows strong transport and mixing properties, a local pollution event has the ability to develop into a global environmental problem which affect the water quality of most parts of the lake.

Effectiveness of water transfer projects for improving water quality are simulated and evaluated by releasing particles from different sources continuously. The choice of different seasons and locations of the sources both have great influence on the performance of water transfer

applications. Wangyu Route, Xingou Route and Xinmeng Route, which are all located in the north part of the lake, have the similar tendency of global occupy rate (occupy rate for the whole lake), i.e. higher occupy rate in summer and lower occupy rate in the autumn. For the Dongshao Route located at southwest part of the lake, low global occupy rate has been calculated for all four seasons and it is therefore not suitable choice for improving the water quality in the whole lake. But this route has the advantage of effective transfer of freshwater to western part of the lake.

For global occupy rate, the performance of two-routes application and three-routes application are similar, both have an obvious growth (approximate 10%) compared to single route application. This is because every single route has its own advantage for specific areas and the combination of two different routes (especially a northern route combined with a southern route) is able to spread freshwater to a wider range than a single route does. If more routes are involved, particles trajectories from northern routes almost coincide due to the attracting property of LCS. In other words, water transferred from different northern routes finally reaches the same places. Generally speaking, a two-route scheme is enough for improving water quality for the whole lake. For local occupy rates (the occupy rate of four highlighted zones), they are extremely dependent on the corresponding route that has the dominant influence on that area particularly. Hence two-route or three-route schemes do not have an obvious advantage in terms of increasing local occupy rates of these four areas compared to single route application. But the efficiency of the lake refreshment by multiple-route schemes is higher because in the same time interval more freshwater are introduced into the highlighted areas and pollutions are diluted and washed away more quickly.

7.2 Future work

Substantial effort has been devoted to develop an integrated numerical framework to shed Lagrangian insights into fluid mixing process in environmental flows coupled with Eulerian velocity data. However, there are still a number of potential areas for future research to further improve the current framework.

7.2.1 *Diffusion effect in particle tracking process*

Diffusion is an important process for particle transport, especially in small-scale simulations where the dominance of advection is not strong. So it is recommended to include diffusion effect in the particle tracking process which is usually achieved by using a random walk technique. However, the diffusion process should be added into the particle tracking model very

carefully when it is combined with dynamical systems approaches. For many transport and mixing cases, it is important to focus on advection (deterministic motion) of particles in detail, and reveal how they separate and merge, how they are stretched and folded. Many practical transport problems are affected by this chaotic motion of fluid flows and have short time scales of the order of some eddy turnover times. For example, in the case of oil spills we are interested in its exact evolution for the following days and weeks rather than its overall mean advance as determined by the stochastic approach. If a container is lost from a ship, we want to know where it has drifted to over the last hours. Advection is the dominant process in these cases.

7.2.2 *Extraction of LCSs*

In the particle tracking model FTLE fields are calculated and then exported as the final results although LCSs are marked with high value of deformation gradient. FTLE provides a measure that enables relatively easy and robust determination of the location and strength LCSs. However, in environmental flows the FTLE fields sometimes are too complicated to interpret and it is desirable to extract the associated LCSs from FTLE fields to better understand the flow topology. What is more, reliable extraction of LCSs from FTLE fields will be crucially important in engineering applications for relevant features detection and decision making. Initial applications of the framework have been focused on demonstrating the existence and implications of these structures, which indeed is critical to this method gaining acceptance and wider use. Now that the subject has begun to become mature, LCSs are becoming part of, or have the potential to become part of, broader computational applications to support, for example, decision-making, design, transport calculations, and optimization. In this light, it is often necessary to have the ability to effectively parameterize or extract LCSs from FTLE plots.

7.2.3 *Analysis of LCSs*

The computation of LCSs in an environmental flow is typically derived from calculation of particle trajectories based on traditional Eulerian velocity field. The velocity field obtained from a shallow water model inevitably contains approximation errors (Jasak, 1996). Furthermore, since the velocity data is discrete, a bilinear interpolation method is used to derive a continuous flow field, which introduces additional deviations from the true field. The uncertainty of these data processing such as velocity data generation or interpolation on the LCS identification cannot be quantified. Indeed, local errors in the calculation of fluid trajectories will accumulate and lead to growing errors in particle positions. Because all known methods for locating LCS use particle positions, one has to contend with large errors or even spurious structures that are

artifacts of the processing techniques. Thus, it is necessary to analyse the accuracy of LCSs location or existence. This is a particularly difficult question to answer since one typically does not know the exact nature of the errors involved. Shadden (2011) provide useful approaches to study this issue and these approaches may be combined with the current framework to make the LCS results more convincing.

7.2.4 Further Applications of this numerical work

The integrated numerical framework could serve as an efficient quantitative tool in decision making, resource allocation, model validation, and scenario analysis in environmental flows. In the specific context of water transfer plan in Lake Taihu, this tool promises to provide quantitative support for decisions involving the existing and proposed water transfer projects. It could help assess the most efficient option (the ‘best’ routes and times) to introduce fresh water to the lake to maximise fluid mixing and improve water quality. This tool could be also used to forecast contamination spread in environmental flows. A real-time leaking oil forecast system could be built based on the exact mathematical results of this tool.

References

- Abd-el-Malek, M.B. and Helal, M.M. (2009) 'Application of a fractional steps method for the numerical solution of the two-dimensional modeling of the Lake Mariut', *Applied Mathematical Modelling*, 33(2), pp. 822-834.
- Ådlandsvik, B., Gundersen, A.C., Nedreaas, K.H., Stene, A. and Albert, O.T. (2004) 'Modelling the advection and diffusion of eggs and larvae of Greenland halibut (*Reinhardtius hippoglossoides*) in the north - east Arctic', *Fisheries Oceanography*, 13(6), pp. 403-415.
- Ahsan, A.K.M.Q. and Blumberg, A.F. (1999) 'Three-dimensional hydrothermal model of Onondaga Lake, New York', *Journal of Hydraulic Engineering*, 125(9), pp. 912-923.
- Ambrosetti, W., Barbanti, L., Rolla, A., Castellano, L. and Sala, N. (2012) 'Hydraulic paths and estimation of the real residence time of the water in Lago Maggiore (N. Italy): application of massless markers transported in 3D motion fields', *Journal of Limnology*, 71(1), p. 2.
- Anastasiou, K. and Chan, C.T. (1997) 'Solution of the 2D shallow water equations using the finite volume method on unstructured triangular meshes', *International Journal for Numerical Methods in Fluids*, 24(11), pp. 1225-1245.
- Anderson, E.J., Schwab, D.J. and Lang, G.A. (2010) 'Real-time hydraulic and hydrodynamic model of the St. Clair River, Lake St. Clair, Detroit River system', *Journal of Hydraulic Engineering*, 136(8), pp. 507-518.
- Andrejev, O., Soomere, T., Sokolov, A. and Myrberg, K. (2011) 'The role of the spatial resolution of a three-dimensional hydrodynamic model for marine transport risk assessment', *Oceanologia*, 53, pp. 309-334.
- Aref, H. (1984) 'Stirring by chaotic advection', *Journal of Fluid Mech.*, 143, pp. 1-21.
- Aref, H. (2002) 'The development of chaotic advection', *Physics of fluids*, 14(4), pp. 1315-1325.
- Aurell, E., Boffetta, G., Crisanti, A., Paladin, G. and Vulpiani, A. (1997) 'Predictability in the large: an extension of the concept of Lyapunov exponent', *Journal of Physics A: Mathematical and General*, 30(1), p. 1.
- Bai, X., Wang, J., Schwab, D.J., Yang, Y., Luo, L., Leshkevich, G.A. and Liu, S. (2013) 'Modeling 1993–2008 climatology of seasonal general circulation and thermal structure in the Great Lakes using FVCOM', *Ocean Modelling*, 65, pp. 40-63.
- Batchelder, H.P. (2006) 'Forward-in-Time-/Backward-in-Time-Trajectory (FITT/BITT) Modeling of Particles and Organisms in the Coastal Ocean', *Journal of Atmospheric and Oceanic Technology*, 23(5), pp. 727-741.
- Bek, M.A., Lowndes, I.S. and Hargreaves, D.M. (2010) 'The application of a validated hydrodynamic model to improve the water management of an Egyptian shallow water coastal lake', *International Environmental Modelling and Software Society (IEMSs)*.
- Beron-Vera, F.J. and Olascoaga, M.J. (2009) 'An assessment of the importance of chaotic stirring and turbulent mixing on the West Florida Shelf', *Journal of physical oceanography*, 39(7), p. 1743.

- Beron-Vera, F.J., Olascoaga, M.J., Brown, M.G., Koçak, H. and Rypina, I.I. (2010) 'Invariant-tori-like Lagrangian coherent structures in geophysical flows', *Chaos: An Interdisciplinary Journal of Nonlinear Science*, 20(1), p. 017514.
- Beron - Vera, F.J., Olascoaga, M.J. and Goni, G.J. (2008) 'Oceanic mesoscale eddies as revealed by Lagrangian coherent structures', *Geophysical Research Letters*, 35(12).
- Blumberg, A.F. and Mellor, G.L. (1987) 'A description of a three dimensional coastal ocean circulation model', *Three-dimensional coastal ocean models*, pp. 1-16.
- Blumberg, A.F. and Oey, L.-Y. (1985) 'Modeling circulation and mixing in estuaries and coastal oceans', *Advances in geophysics*, 28, pp. 525-547.
- Bonnet, M.-P., Poulin, M. and Devaux, J. (2000) 'Numerical modeling of thermal stratification in a lake reservoir. Methodology and case study', *Aquatic Sciences*, 62(2), pp. 105-124.
- Borthwick, A.G.L., Cruz León, S. and Jozsa, J. (2001) 'Adaptive quadtree model of shallow-flow hydrodynamics', *Journal of Hydraulic Research*, 39(4), pp. 413-424.
- BozorgMagham, A.E. and Ross, S.D. (2015) 'Atmospheric Lagrangian coherent structures considering unresolved turbulence and forecast uncertainty', *Communications in Nonlinear Science and Numerical Simulation*, 22(1), pp. 964-979.
- Bradford, S.F. and Sanders, B.F. (2002) 'Finite-volume model for shallow-water flooding of arbitrary topography', *Journal of Hydraulic Engineering*, 128(3), pp. 289-298.
- Branicki, M. and Wiggins, S. (2009) 'Finite-time Lagrangian transport analysis: stable and unstable manifolds of hyperbolic trajectories and finite-time Lyapunov exponents', *arXiv preprint arXiv:0908.1129*.
- Brown, S.D. (2011) 'Integrated Toolset for Water Quality Modeling in the Great Lakes', *Doctoral disseration, State University of New York at Buffalo*.
- Bussing, T.R.A. and Murman, E.M. (1988) 'Finite-volume method for the calculation of compressible chemically reacting flows', *AIAA journal*, 26(9), pp. 1070-1078.
- Castellano, L., Ambrosetti, W., Barbanti, L. and Rolla, A. (2010) 'The residence time of the water in Lago Maggiore (N. Italy): first results from an Eulerian-Lagrangian approach', *Journal of Limnology*, 69(1), pp. 15-28.
- Casulli, V. and Cattani, E. (1994) 'Stability, accuracy and efficiency of a semi-implicit method for three-dimensional shallow water flow', *Computers & Mathematics with Applications*, 27(4), pp. 99-112.
- Casulli, V. and Cheng, R.T. (1992) 'Semi implicit finite difference methods for three dimensional shallow water flow', *International Journal for numerical methods in fluids*, 15(6), pp. 629-648.
- Chaiken, J., Chevray, R., Tabor, M. and Tan, Q.M. (1986) 'Experimental study of Lagrangian turbulence in Stokes flow', pp. 165-174.
- Chansheng, H. and Croley, T.E. (2010) 'Hydrologic Resource Sheds and the US Great Lakes Applications', *Journal of Resources and Ecology*, 1(1), pp. 25-30.

Chanudet, V., Fabre, V. and van der Kaaij, T. (2012) 'Application of a three-dimensional hydrodynamic model to the Nam Theun 2 Reservoir (Lao PDR)', *Journal of Great Lakes Research*, 38(2), pp. 260-269.

Chen, C., Huang, H., Beardsley, R.C., Liu, H., Xu, Q. and Cowles, G. (2007) 'A finite volume numerical approach for coastal ocean circulation studies: Comparisons with finite difference models', *Journal of Geophysical Research: Oceans*, 112(C3).

Chen, C., Liu, H. and Beardsley, R.C. (2003a) 'An unstructured grid, finite-volume, three-dimensional, primitive equations ocean model: application to coastal ocean and estuaries', *Journal of atmospheric and oceanic technology*, 20(1), pp. 159-186.

Chen, C., Qi, J., Li, C., Beardsley, R.C., Lin, H., Walker, R. and Gates, K. (2008) 'Complexity of the flooding/drying process in an estuarine tidal - creek salt - marsh system: An application of FVCOM', *Journal of Geophysical Research: Oceans*, 113(C7).

Chen, C., Zhu, J., Kang, K., Liu, H., Ralph, E., Green, S.A. and Budd, J.W. (2002) 'Cross-frontal transport along the Keweenaw coast in Lake Superior: a Lagrangian model study', *Dynamics of atmospheres and oceans*, 36(1), pp. 83-102.

Chen, C., Zhu, J., Ralph, E., Green, S.A., Budd, J.W. and Zhang, F.Y. (2001) 'Prognostic modeling studies of the Keweenaw current in Lake Superior. Part I: Formation and evolution', *Journal of Physical Oceanography*, 31(2), pp. 379-395.

Chen, Y., Qin, B., Teubner, K. and Dokulil, M.T. (2003b) 'Long-term dynamics of phytoplankton assemblages: Microcystis-domination in Lake Taihu, a large shallow lake in China', *Journal of Plankton Research*, 25(4), pp. 445-453.

Chien, W.L., Rising, H. and Ottino, J.M. (1986) 'Laminar mixing and chaotic mixing in several cavity flows', *Journal of Fluid Mechanics*, 170, pp. 355-377.

Chislock, M.F., Doster, E., Zitomer, R.A. and Wilson, A.E. (2013) 'Eutrophication: causes, consequences, and controls in aquatic ecosystems', *Nature Education Knowledge*, 4(4), p. 10.

Chittibabu, P. and Rao, Y.R. (2012) 'Numerical simulation of storm surges in Lake Winnipeg', *Natural hazards*, 60(2), pp. 181-197.

Chung, S.W., Hipsey, M.R. and Imberger, J. (2009) 'Modelling the propagation of turbid density inflows into a stratified lake: Daecheong Reservoir, Korea', *Environmental Modelling & Software*, 24(12), pp. 1467-1482.

Courant, R., Friedrichs, K. and Lewy, H. (1967) 'On the partial difference equations of mathematical physics', *IBM Journal of Research and Development*, 11(2), pp. 215-234.

d'Ovidio, F., Fernández, V., Hernández - García, E. and López, C. (2004) 'Mixing structures in the Mediterranean Sea from finite - size Lyapunov exponents', *Geophysical Research Letters*, 31(17).

d'Ovidio, F., Isern-Fontanet, J., López, C., Hernández-García, E. and García-Ladona, E. (2009) 'Comparison between Eulerian diagnostics and finite-size Lyapunov exponents computed from altimetry in the Algerian basin', *Deep Sea Research Part I: Oceanographic Research Papers*, 56(1), pp. 15-31.

- Dabrowski, T. and Berry, A. (2009) 'Use of numerical models for determination of best sampling locations for monitoring of large lakes', *Science of the total environment*, 407(14), pp. 4207-4219.
- Deborah, C. (1996) 'Water quality assessments-A guide to use of biota, sediments and water in Environmental Monitoring', Second edition, E&FN Spon, London, UK. .
- Doglioli, A.M. and Carlotti, F. (2011) 'Lagrangian model of zooplankton dispersion: numerical schemes comparisons and parameter sensitivity tests', *Chinese Journal of Oceanology and Limnology*, 29(2), pp. 438-445.
- Dong, X., Bennion, H., Battarbee, R., Yang, X., Yang, H. and Liu, E. (2008) 'Tracking eutrophication in Taihu Lake using the diatom record: potential and problems', *Journal of Paleolimnology*, 40(1), pp. 413-429.
- Du Toit, P.C. and Marsden, J.E. (2010) 'Horseshoes in hurricanes', *Journal of Fixed Point Theory and Applications*, 7(2), pp. 351-384.
- El-Adawy, A., Negm, A.M., Elzeir, M.A., Saavedra, O.C., El-Shinnawy, I.A. and Nadaoka, K. (2013) 'Modeling the hydrodynamics and salinity of el-burullus lake (nile delta, Northern Egypt)', *J. Clean Energy Technol*, 2, pp. 157-163.
- Elçi, Ş., Work, P.A. and Hayter, E.J. (2007) 'Influence of stratification and shoreline erosion on reservoir sedimentation patterns', *Journal of Hydraulic Engineering*, 133(3), pp. 255-266.
- Eriksen, M., Lebreton, L.C.M., Carson, H.S., Thiel, M., Moore, C.J., Borerro, J.C., Galgani, F., Ryan, P.G. and Reisser, J. (2014) 'Plastic pollution in the world's oceans: more than 5 trillion plastic pieces weighing over 250,000 tons afloat at sea', *PloS one*, 9(12), p. e111913.
- Evans, P.L. and Noye, B.J. (1995) 'A model for fast oil spill trajectory prediction in shallow gulfs', *Recent advances in marine science and technology*, 94, pp. 119-130.
- Fe, J., Navarrina, F., Puertas, J., Vellando, P. and Ruiz, D. (2009) 'Experimental validation of two depth - averaged turbulence models', *International journal for numerical methods in fluids*, 60(2), pp. 177-202.
- Fiedler, F.R. and Ramirez, J.A. (2000) 'A numerical method for simulating discontinuous shallow flow over an infiltrating surface', *International journal for numerical methods in fluids*, 32(2), pp. 219-239.
- Fischer, H.B., List, J.E., Koh, C.R., Imberger, J. and Brooks, N.H. (2013) *Mixing in inland and coastal waters*. Elsevier.
- Fraccarollo, L. and Toro, E.F. (1995) 'Experimental and numerical assessment of the shallow water model for two-dimension dam-break type problems', *Journal of Hydraulic Research*, 33(6), pp. 843-863.
- Furman, A. (2008) 'Modeling coupled surface–subsurface flow processes: a review', *Vadose Zone Journal*, 7(2), pp. 741-756.
- Gal, G., Imberger, J., Zohary, T., Antenucci, J., Anis, A. and Rosenberg, T. (2003) 'Simulating the thermal dynamics of Lake Kinneret', *Ecological Modelling*, 162(1), pp. 69-86.

- Garaboa, D., Eiras-Barca, J., Huhn, F. and Perez-Muñuzuri, V. (2015) 'Atmospheric rivers as Lagrangian coherent structures', *arXiv preprint arXiv:1501.00877*.
- Gejadze, I.Y. and Monnier, J. (2007) 'On a 2D 'zoom' for the 1D shallow water model: Coupling and data assimilation', *Computer methods in applied mechanics and engineering*, 196(45), pp. 4628-4643.
- Goudsmit, G.H., Reichert, P. and Wuest, A. (1996) *Modelling of physical and bio-geochemical properties in lakes using AQUASIM*. AA Balkema.
- Gräwe, U. (2011) 'Implementation of high-order particle-tracking schemes in a water column model', *Ocean Modelling*, 36(1), pp. 80-89.
- Guizien, K., Brochier, T., Duchêne, J.C., Koh, B.S. and Marsaleix, P. (2006) 'Dispersal of *Owenia fusiformis* larvae by wind-driven currents: turbulence, swimming behaviour and mortality in a three-dimensional stochastic model', *Marine Ecology Progress Series*, 311, pp. 47-66.
- Guo, L. (2007) 'Doing battle with the green monster of Taihu Lake', *Science*, 317(5842), pp. 1166-1166.
- Hai, P.T., Masumoto, T. and Shimizu, K. (2008) 'Development of a two dimensional finite element model for inundation processes in the Tonle Sap and its environs', *Hydrological processes*, 22(9), pp. 1329-1336.
- Haidvogel, D.B., Arango, H.G., Hedstrom, K., Beckmann, A., Malanotte-Rizzoli, P. and Shchepetkin, A.F. (2000) 'Model evaluation experiments in the North Atlantic Basin: simulations in nonlinear terrain-following coordinates', *Dynamics of Atmospheres and Oceans*, 32(3), pp. 239-281.
- Haller, G. (2001) 'Distinguished material surfaces and coherent structures in three-dimensional fluid flows', *Physica D: Nonlinear Phenomena*, 149(4), pp. 248-277.
- Haller, G. (2002) 'Lagrangian coherent structures from approximate velocity data', *Physics of Fluids (1994-present)*, 14(6), pp. 1851-1861.
- Haller, G. (2011) 'A variational theory of hyperbolic Lagrangian coherent structures', *Physica D: Nonlinear Phenomena*, 240(7), pp. 574-598.
- Haller, G. and Yuan, G. (2000) 'Lagrangian coherent structures and mixing in two-dimensional turbulence', *Physica D: Nonlinear Phenomena*, 147(3), pp. 352-370.
- Hamilton, D.P. and Schladow, S.G. (1997) 'Prediction of water quality in lakes and reservoirs. Part I—Model description', *Ecological Modelling*, 96(1), pp. 91-110.
- Hamrick, J.M. (1992) *A three-dimensional environmental fluid dynamics computer code: Theoretical and computational aspects*. Virginia Institute of Marine Science, College of William and Mary.
- Han, H. and Hu, W. (2012) 'Modeling the species shift from *Potamogeton malaiianus* Miq. to *Potamogeton maackianus* A. Bennett in the experiment pond', *Ecological Modelling*, 242, pp. 10-19.

- Harten, A., Lax, P.D. and Leer, B.v. (1983) 'On upstream differencing and Godunov-type schemes for hyperbolic conservation laws', *SIAM review*, 25(1), pp. 35-61.
- He, Z., Wu, W. and Wang, S.S. (2008) 'Coupled finite-volume model for 2D surface and 3D subsurface flows', *Journal of Hydrologic Engineering*, 13(9), pp. 835-845.
- Hirsch, C. (2007) *Numerical Computation of Internal and External Flows: The Fundamentals of Computational Fluid Dynamics: The Fundamentals of Computational Fluid Dynamics*. Butterworth-Heinemann.
- Hodges, B. and Dallimore, C. (2006) 'Estuary, lake and coastal ocean model: ELCOM v2. 2 science manual', *Centre for Water Research, University of Western Australia*.
- Hodges, B.R. (2000) 'Numerical Techniques in CWR-ELCOM (code release v. 1)', *CWR Manuscript WP*, 1422.
- Hodges, B.R., Imberger, J., Saggio, A. and Winters, K.B. (2000) 'Modeling basin - scale internal waves in a stratified lake', *Limnology and oceanography*, 45(7), pp. 1603-1620.
- Hong, X. and Pang, Y. (2005) 'Calculation of concentration distribution of algae in Taihu Lake with Riemann approximate solution model', *Journal of Hohai University: Natural Sciences*, 33(1), pp. 41-44.
- Hu, K., Mingham, C.G. and Causon, D.M. (2000) 'Numerical simulation of wave overtopping of coastal structures using the non-linear shallow water equations', *Coastal Engineering*, 41(4), pp. 433-465.
- Hu, L., Hu, W., Zhai, S. and Wu, H. (2010) 'Effects on water quality following water transfer in Lake Taihu, China', *Ecological Engineering*, 36(4), pp. 471-481.
- Hu, W., Jørgensen, S.E. and Zhang, F. (2006) 'A vertical-compressed three-dimensional ecological model in Lake Taihu, China', *Ecological Modelling*, 190(3), pp. 367-398.
- Hu, W., Zhai, S., Zhu, Z. and Han, H. (2008) 'Impacts of the Yangtze River water transfer on the restoration of Lake Taihu', *Ecological Engineering*, 34(1), pp. 30-49.
- Hu, W.P., Pu, P.M. and Qin, B.Q. (1998a) 'A three-dimensional numerical simulation on the dynamics in Taihu Lake, China (II): the typical wind-driven current and its divergence', *Journal of Lake Science*, 10, pp. 26-34.
- Hu, W.P., Pu, P.M. and Qin, B.Q. (1998b) 'A Three-Dimensional Numerical Simulation on the Dynamics in Taihu Lake, China(I): the Water Level and the Current during the 9711 Typhoon Process', *Journal of Lake Sciences*, 10(4), pp. 17-25.
- Huang, H., Chen, C., Cowles, G.W., Winant, C.D., Beardsley, R.C., Hedstrom, K.S. and Haidvogel, D.B. (2008) 'FVCOM validation experiments: Comparisons with ROMS for three idealized barotropic test problems', *Journal of Geophysical Research: Oceans*, 113(C7).
- Huret, M., Runge, J., Chen, C., Cowles, G., Xu, Q. and Pringle, J. (2007) 'Dispersal modeling of fish early life stages: sensitivity with application to Atlantic cod in the western Gulf of Maine', *Marine Ecology Progress Series*, 347, pp. 261-274.

Huttula, T., Pulkkanen, M., Arkhipov, B., Leppäranta, M., Solbakov, V., Shirasawa, K. and Salonen, K. (2010) 'Modelling circulation in an ice-covered lake', *Estonian Journal of Earth Sciences*, 59(4), p. 298.

Hydraulics, W.L.D. (2006) 'Delft3D-FLOW, Simulation of multi-dimensional hydrodynamic flows and transport phenomena, including sediments', *User Manual, Delft, Holanda*.

Imberger, J. and Patterson, J.C. (1980) *Transport Models for Inland and Coastal Waters, Academic Press New York. 1981. Proceedings of a Symposium on Predictive Ability, Berkeley, California, August 18-20, 1980. p 310-361, 12 fig, 36 ref.*

James, R.T., Havens, K., Zhu, G. and Qin, B. (2009) 'Comparative analysis of nutrients, chlorophyll and transparency in two large shallow lakes (Lake Taihu, PR China and Lake Okeechobee, USA)', *Hydrobiologia*, 627(1), pp. 211-231.

Jasak, H. (1996) 'Error analysis and estimation for finite volume method with applications to fluid flow'.

Jia, S., You, Y. and Wang, R. (2008) 'Influence of water diversion from Yangtze River to Taihu Lake on nitrogen and phosphorus concentrations in different water areas', *Water Resour. Prot.*, 24(3), pp. 53-56.

Jiahu, J. and Qun, H. (1997) 'Numerical analogue of wind-driven current in East Taihu Lake by inlay-mesh model', *Oceanologia et limnologia sinica*, 4, p. 013.

Jin, K.-R., Hamrick, J.H. and Tisdale, T. (2000) 'Application of three-dimensional hydrodynamic model for Lake Okeechobee', *Journal of Hydraulic Engineering*, 126(10), pp. 758-771.

Jin, K.-R. and Ji, Z.-G. (2005) 'Application and validation of three-dimensional model in a shallow lake', *Journal of waterway, port, coastal, and ocean engineering*, 131(5), pp. 213-225.

Jin, K.-R., Ji, Z.-G. and Hamrick, J.H. (2002) 'Modeling winter circulation in Lake Okeechobee, Florida', *Journal of Waterway, Port, Coastal, and Ocean Engineering*, 128(3), pp. 114-125.

Jin, K.-R., Ji, Z.-G. and James, R.T. (2007) 'Three-dimensional water quality and SAV modeling of a large shallow lake', *Journal of Great Lakes Research*, 33(1), pp. 28-45.

Jin, X., Wang, S., Pang, Y. and Wu, F.C. (2006) 'Phosphorus fractions and the effect of pH on the phosphorus release of the sediments from different trophic areas in Taihu Lake, China', *Environmental Pollution*, 139(2), pp. 288-295.

Joseph, B. and Legras, B. (2002) 'Relation between kinematic boundaries, stirring, and barriers for the Antarctic polar vortex', *Journal of the Atmospheric Sciences*, 59(7), pp. 1198-1212.

Kaçıkoç, M. and Beyhan, M. (2014) 'Hydrodynamic and water quality modeling of Lake Eğirdir', *CLEAN–Soil, Air, Water*, 42(11), pp. 1573-1582.

Kai, E.T., Rossi, V., Sudre, J., Weimerskirch, H., Lopez, C., Hernandez-Garcia, E., Marsac, F. and Garçon, V. (2009) 'Top marine predators track Lagrangian coherent structures', *Proceedings of the National Academy of Sciences*, 106(20), pp. 8245-8250.

Kantha, L.H. and Clayson, C.A. (1994) 'An improved mixed layer model for geophysical applications', *Journal of Geophysical Research: Oceans*, 99(C12), pp. 25235-25266.

- Karagounis, I., Trösch, J. and Zamboni, F. (1993) 'A coupled physical-biochemical lake model for forecasting water quality', *Aquatic Sciences*, 55(2), pp. 87-102.
- Károlyi, G., Pattantyús-Ábrahám, M., Krámer, T., Józsa, J. and Tél, T. (2010) 'Finite-size Lyapunov exponents: A new tool for lake dynamics', *Proceedings of the Institution of Civil Engineers: Engineering and Computational Mechanics*, 163(4), pp. 251-259.
- Kelley, D.H., Allshouse, M.R. and Ouellette, N.T. (2013) 'Lagrangian coherent structures separate dynamically distinct regions in fluid flows', *Physical Review E*, 88(1), p. 013017.
- Khakhar, D.V., Rising, H. and Ottino, J.M. (1986) 'Analysis of chaotic mixing in two model systems', *Journal of Fluid Mechanics*, 172, pp. 419-451.
- Koh, T.-Y. and Legras, B. (2002) 'Hyperbolic lines and the stratospheric polar vortex', *Chaos: An Interdisciplinary Journal of Nonlinear Science*, 12(2), pp. 382-394.
- Koshel, K.V. and Prants, S.V. (2006) 'Chaotic advection in the ocean', *Physics-Uspokhi*, 49(11), pp. 1151-1178.
- Krámer, T. and Józsa, J. (2007) 'Solution-adaptivity in modelling complex shallow flows', *Computers & fluids*, 36(3), pp. 562-577.
- Kranenburg, C. (1992) 'Wind-driven chaotic advection in a shallow model lake', *Journal of Hydraulic Research*, 30(1), pp. 29-46.
- Lai, X., Jiang, J., Liang, Q. and Huang, Q. (2013) 'Large-scale hydrodynamic modeling of the middle Yangtze River Basin with complex river-lake interactions', *Journal of hydrology*, 492, pp. 228-243.
- Lapeyre, G. (2002) 'Characterization of finite-time Lyapunov exponents and vectors in two-dimensional turbulence', *Chaos: An Interdisciplinary Journal of Nonlinear Science*, 12(3), pp. 688-698.
- Laval, B. and Hodges, B.R. (2000) 'The CWR Estuary and Lake Computer Model ELCOM. User Guide', *Center for Water Research, The University of Western Australia*.
- Laval, B., Imberger, J., Hodges, B.R. and Stocker, R. (2003) 'Modeling circulation in lakes: Spatial and temporal variations', *Limnology and Oceanography*, 48(3), pp. 983-994.
- Le, C., Zha, Y., Li, Y., Sun, D., Lu, H. and Yin, B. (2010) 'Eutrophication of lake waters in China: cost, causes, and control', *Environmental Management*, 45(4), pp. 662-668.
- Lebreton, L.-M., Greer, S.D. and Borrero, J.C. (2012) 'Numerical modelling of floating debris in the world's oceans', *Marine Pollution Bulletin*, 64(3), pp. 653-661.
- Lee, W.-K., Borthwick, A.G.L. and Taylor, P.H. (2014a) 'Tracer dynamics in two-layer density-stratified estuarine flow', *Proceedings of the Institution of Civil Engineers-Engineering and Computational Mechanics*, 167(1), pp. 41-49.
- Lee, W.-K., Borthwick, A.G.L. and Taylor, P.H. (2014b) 'Wind-induced chaotic mixing in a two-layer density-stratified shallow flow', *Journal of Hydraulic Research*, 52(2), pp. 219-227.
- Lekien, F. and Leonard, N. (2004) 'Dynamically consistent Lagrangian coherent structures', *Experimental chaos*, 742, pp. 132-139.

León, L.F., Lam, D.C.L., Schertzer, W.M., Swayne, D.A. and Imberger, J. (2007) 'Towards coupling a 3D hydrodynamic lake model with the Canadian regional climate model: simulation on Great Slave Lake', *Environmental Modelling & Software*, 22(6), pp. 787-796.

Leon, L.F., Smith, R.E.H., Hipsey, M.R., Bocaniov, S.A., Higgins, S.N., Hecky, R.E., Antenucci, J.P., Imberger, J.A. and Guildford, S.J. (2011) 'Application of a 3D hydrodynamic–biological model for seasonal and spatial dynamics of water quality and phytoplankton in Lake Erie', *Journal of Great Lakes Research*, 37(1), pp. 41-53.

LEONG, C.W. and Ottino, J.M. (1989) 'Experiments on mixing due to chaotic advection in a cavity', *Fluid Mech.*, 209, pp. 463-499.

Lesser, G.R., Roelvink, J.A., Van Kester, J. and Stelling, G.S. (2004) 'Development and validation of a three-dimensional morphological model', *Coastal engineering*, 51(8), pp. 883-915.

Li, Y., Acharya, K., Stone, M.C., Yu, Z., Young, M.H., Shafer, D.S., Zhu, J., Gray, K., Stone, A. and Fan, L. (2011a) 'Spatiotemporal patterns in nutrient loads, nutrient concentrations, and algal biomass in Lake Taihu, China', *Lake and Reservoir Management*, 27(4), pp. 298-309.

Li, Y., Acharya, K. and Yu, Z. (2011b) 'Modeling impacts of Yangtze River water transfer on water ages in Lake Taihu, China', *Ecological Engineering*, 37(2), pp. 325-334.

Li, Y., Acharya, K. and Yu, Z.B. (2011c) 'Modeling impacts of Yangtze River water transfer on water ages in Lake Taihu', *China*, 37(2), pp. 325-334.

Li, Y. and Pang, Y. (2004) 'Nested grid-based numerical simulation of wind-induced current of Meiliang Lake and Gonghu Lake in the Taihu Lake [J]', *Water Resources Protection*, 2, p. 006.

Li, Y., Pang, Y. and Luo, L. (2009) 'Experimental and numerical study on the transfer process of suspended matter in the interaction of wave and current in Taihu Lake', *Advances in Water Science*, 5, p. 018.

Li, Y., Pang, Y. and Tian, N. (2004) 'Simulation Study of Artificial Neutral Network on Ecosystem of Taihu Lake [J]', *Environmental Science and Technology*, 2, p. 018.

Li, Y., Tang, C., Wang, C., Anim, D.O., Yu, Z. and Acharya, K. (2013a) 'Improved Yangtze River Diversions: Are they helping to solve algal bloom problems in Lake Taihu, China?', *Ecological engineering*, 51, pp. 104-116.

Li, Y., Tang, C., Wang, C., Tian, W., Pan, B., Hua, L., Lau, J., Yu, Z. and Acharya, K. (2013b) 'Assessing and modeling impacts of different inter-basin water transfer routes on Lake Taihu and the Yangtze River, China', *Ecological engineering*, 60, pp. 399-413.

Li, Y., Tang, C.Y., Yu, Z.B. and Acharya, K. (2014) 'Correlations between algae and water quality: factors driving eutrophication in Lake Taihu, China', *International Journal of Environmental Science and Technology*, 11(1), pp. 169-182.

Li, Z., Chen, Q. and Xu, Q. (2015) 'Modeling algae dynamics in Meiliang Bay of Taihu Lake and parameter sensitivity analysis', *Journal of Hydro-environment Research*, 9(2), pp. 216-225.

Liang, Q. and Borthwick, A.G.L. (2009) 'Adaptive quadtree simulation of shallow flows with wet–dry fronts over complex topography', *Computers & Fluids*, 38(2), pp. 221-234.

- Liang, Q., Borthwick, A.G.L. and Taylor, P.H. (2006a) 'Wind-induced chaotic advection in shallow flow geometries. Part I: Circular basins', *Journal of Hydraulic Research*, 44(2), pp. 170-79.
- Liang, Q., Borthwick, A.G.L. and Taylor, P.H. (2006b) 'Wind-induced chaotic advection in shallow flow geometries. Part II: Non-circular basins', *Journal of Hydraulic Research*, 44(2), pp. 180-188.
- Liang, Q. and Marche, F. (2009) 'Numerical resolution of well-balanced shallow water equations with complex source terms', *Advances in water resources*, 32(6), pp. 873-884.
- Liang, R.J. and Zhong, J.H. (1994) 'A three dimensional numerical simulation of wind driven water current in Taihu Lake', *Journal of Lake Science*, 4, p. 001.
- Liu, Q.J. (1993) *The data simulation of wind driven flow in Meiliang gulf of Lake Taihu*. Master's thesis, Nanjing Institute of Geography and Limnology, Chinese Academy of Sciences.
- Liu, W., Chen, W. and Hsu, M. (2011) 'Using a three-dimensional particle-tracking model to estimate the residence time and age of water in a tidal estuary', *Computers & geosciences*, 37(8), pp. 1148-1161.
- Ma, S. and Cai, Q. (1997) 'Numerical study on the distribution of TP in Taihu Lake and the impact from the lake current', *J. Lake Sci*, 9(4), pp. 325-330.
- Ma, S. and Cai, Q. (1999) 'An upwinding finite element numerical model for TP distribution in shallow lakes and its application to Lake Taihu', *Res. Environ. Sci.*, 12(5), pp. 56-59.
- Ma, X., Wang, L., Wu, H., Li, N., Ma, L., Zeng, C., Zhou, Y. and Yang, J. (2015) 'Impact of Yangtze River Water Transfer on the Water Quality of the Lixia River Watershed, China', *PLoS one*, 10(4), p. e0119720.
- Mancho, A.M., Small, D. and Wiggins, S. (2006) 'A tutorial on dynamical systems concepts applied to Lagrangian transport in oceanic flows defined as finite time data sets: Theoretical and computational issues', *Physics Reports*, 437(3), pp. 55-124.
- Mao, J., Chen, Q. and Chen, Y. (2008) 'Three-dimensional eutrophication model and application to Taihu Lake, China', *Journal of Environmental Sciences*, 20(3), pp. 278-284.
- Marchesiello, P., McWilliams, J.C. and Shchepetkin, A. (2003) 'Equilibrium structure and dynamics of the California Current System', *Journal of Physical Oceanography*, 33(4), pp. 753-783.
- Marin, J. and Monnier, J. (2009) 'Superposition of local zoom models and simultaneous calibration for 1D–2D shallow water flows', *Mathematics and Computers in Simulation*, 80(3), pp. 547-560.
- Martin, C., Frenette, J.-J. and Morin, J. (2005) 'Changes in the spectral and chemical properties of a water mass passing through extensive macrophyte beds in a large fluvial lake (Lake Saint-Pierre, Québec, Canada)', *Aquatic sciences*, 67(2), pp. 196-209.
- Mathur, M., Haller, G., Peacock, T., Ruppert-Felsot, J.E. and Swinney, H.L. (2007) 'Uncovering the Lagrangian skeleton of turbulence', *Physical Review Letters*, 98(14), p. 144502.

- Mellor, G.L. and Yamada, T. (1982) 'Development of a turbulence closure model for geophysical fluid problems', *Reviews of Geophysics*, 20(4), pp. 851-875.
- Miglio, E., Perotto, S. and Saleri, F. (2005) 'Model coupling techniques for free-surface flow problems: Part I', *Nonlinear Analysis: Theory, Methods & Applications*, 63(5), pp. e1885-e1896.
- Millet, B. and Guelorget, O. (1994) 'Spatial and seasonal variability in the relationships between benthic communities and physical environment in a lagoon ecosystem', *Marine ecology progress series. Oldendorf*, 108(1), pp. 161-174.
- Millet, B., Robert, C., Grillas, P., Coughlan, C. and Banas, D. (2010) 'Numerical modelling of vertical suspended solids concentrations and irradiance in a turbid shallow system (Vaccares, Se France)', *Hydrobiologia*, 638(1), pp. 161-179.
- Miyake, Y., Kimura, S., Kawamura, T., Kitagawa, T., Hara, M. and Hoshikawa, H. (2010) 'Estimating larval supply of Ezo abalone *Haliotis discus hannai* in a small bay using a coupled particle-tracking and hydrodynamic model: insights into the establishment of harvest refugia', *Fisheries Science*, 76(4), pp. 561-570.
- Ohshima, K.I. and Simizu, D. (2008) 'Particle tracking experiments on a model of the Okhotsk Sea: toward oil spill simulation', *Journal of Oceanography*, 64(1), pp. 103-114.
- Olascoaga, M.J., Beron - Vera, F.J., Haller, G., Trinanes, J., Iskandarani, M., Coelho, E.F., Haus, B.K., Huntley, H.S., Jacobs, G. and Kirwan, A.D. (2013) 'Drifter motion in the Gulf of Mexico constrained by altimetric Lagrangian coherent structures', *Geophysical Research Letters*, 40(23), pp. 6171-6175.
- Olascoaga, M.J. and Haller, G. (2012) 'Forecasting sudden changes in environmental pollution patterns', *Proceedings of the National Academy of Sciences*, 109(13), pp. 4738-4743.
- Omlin, M., Reichert, P. and Forster, R. (2001) 'Biogeochemical model of Lake Zürich: model equations and results', *Ecological modelling*, 141(1), pp. 77-103.
- Ottino, J.M. (1989) *The kinematics of mixing: stretching, chaos, and transport*. Cambridge university press.
- Paerl, H.W., Xu, H., McCarthy, M.J., Zhu, G., Qin, B., Li, Y. and Gardner, W.S. (2011) 'Controlling harmful cyanobacterial blooms in a hyper-eutrophic lake (Lake Taihu, China): the need for a dual nutrient (N & P) management strategy', *Water Research*, 45(5), pp. 1973-1983.
- Pang, Y., Li, Y. and Luo, L. (2006) 'Study on the simulation of transparency of Lake Taihu under different hydrodynamic conditions', *Science in China Series D*, 49(1), pp. 162-175.
- Pang, Y., Pu, P.M., Gao, G. and Wang, Q.Q. (1994) 'Numerical simulations and their verification with uniform wind stress in Taihu Lake', *Transaction of Oceanology and Limnology*, 4, pp. 9-15.
- Pang, Y., Zhuang, W., Han, T., Li, Y.P. and Zhai, J.B. (2008) 'Experiment and model simulation of suspended solids in Taihu Lake under wind-wave disturbance', *Huanjing Kexue*, 29(10), pp. 2743-2748.
- Park, K., Jung, H.-S., Kim, H.-S. and Ahn, S.-M. (2005) 'Three-dimensional hydrodynamic-eutrophication model (HEM-3D): application to Kwang-Yang Bay, Korea', *Marine Environmental Research*, 60(2), pp. 171-193.

- Pattantyús-Ábrahám, M., Tél, T., Krámer, T. and Józsa, J. (2008) 'Mixing properties of a shallow basin due to wind-induced chaotic flow', *Advances in Water Resources*, 31(3), pp. 525-534.
- Peng, J. and Peterson, R. (2012) 'Attracting structures in volcanic ash transport', *Atmospheric environment*, 48, pp. 230-239.
- Postma, L., van Beek, J.K.L., Boogaard, H.F.P. and Stelling, G.S. (2013) 'Consistent and efficient particle tracking on curvilinear grids for environmental problems', *International Journal for Numerical Methods in Fluids*, 71(10), pp. 1226-1237.
- Press, W., Teukolsky, S., Vetterling, W. and Flannery, B. (1992) 'Numerical Recipes in Fortran 77: The Art of Scientific Computing, 933 pp'. Cambridge Univ. Press, New York.
- Qin, B. (2008) *Lake Taihu, China: dynamics and environmental change*. Springer Science & Business Media.
- Qin, B., Xu, P., Wu, Q., Luo, L. and Zhang, Y. (2007) 'Environmental issues of lake Taihu, China', *Hydrobiologia*, 581(1), pp. 3-14.
- Qin, B., Zhu, G., Gao, G., Zhang, Y., Li, W., Paerl, H.W. and Carmichael, W.W. (2010) 'A drinking water crisis in Lake Taihu, China: linkage to climatic variability and lake management', *Environmental management*, 45(1), pp. 105-112.
- Raben, S.G., Ross, S.D. and Vlachos, P.P. (2013) 'Demonstration of Experimental Three Dimensional Finite Time Lyapunov Exponents with Inertial Particles', *arXiv preprint arXiv:1309.3180*.
- Razmi, A.M., Barry, D.A., Lemmin, U., Bonvin, F., Kohn, T. and Bakhtyar, R. (2014) 'Direct effects of dominant winds on residence and travel times in the wide and open lacustrine embayment: Vidy Bay (Lake Geneva, Switzerland)', *Aquatic sciences*, 76(1), pp. 59-71.
- Riley, M.J. and Stefan, H.G. (1988) 'MINLAKE: A dynamic lake water quality simulation model', *Ecological Modelling*, 43(3), pp. 155-182.
- Rogers, B.D., Fujihara, M. and Borthwick, A.G.L. (2001) 'Adaptive Q-tree Godunov-type scheme for shallow water equations', *International Journal for Numerical Methods in Fluids*, 35, pp. 247-280.
- Romero, J.R. and Imberger, J. (2003) 'Effect of a flood underflow on reservoir water quality: Data and three-dimensional modeling', *Archiv für Hydrobiologie*, 157(1), pp. 1-25.
- Rufeng, N. (1997) 'Study on System Dynamics Model for Developing the Fishery Resources in Lakes', *Shandong Fisheries*, p. 01.
- Saatdjian, E. and Leprevost, J.C. (1998) 'Chaotic heat transfer in a periodic two-dimensional flow', *Physics of Fluids*, 10(8), p. 2102.
- Sanderson, B.G. (2008) 'Circulation and the nutrient budget in Myall Lakes', *Hydrobiologia*, 608(1), pp. 3-20.
- Sanmiguel-Rojas, E., Ortega-Casanova, J., del Pino, C. and Fernandez-Feria, R. (2005) 'A Cartesian grid finite-difference method for 2D incompressible viscous flows in irregular geometries', *Journal of Computational Physics*, 204(1), pp. 302-318.

Schimmelpfennig, S., Kirillin, G., Engelhardt, C. and Nützmann, G. (2012) 'Effects of wind-driven circulation on river intrusion in Lake Tegel: modeling study with projection on transport of pollutants', *Environmental fluid mechanics*, 12(4), pp. 321-339.

Schuster, H.G. and Grigoriev, R. (2012) *Transport and Mixing in Laminar Flows: From Microfluidics to Oceanic Currents*. John Wiley & Sons.

Schwab, D.J. and Beletsky, D. (2003) 'Relative effects of wind stress curl, topography, and stratification on large - scale circulation in Lake Michigan', *Journal of Geophysical Research: Oceans*, 108(C2).

Shadden, S.C. (2011) 'Lagrangian coherent structures', *Transport and Mixing in Laminar Flows: From Microfluidics to Oceanic Currents*, pp. 59-89.

Shadden, S.C., Dabiri, J.O. and Marsden, J.E. (2006) 'Lagrangian analysis of fluid transport in empirical vortex ring flows', *Physics of Fluids (1994-present)*, 18(4), p. 047105.

Shadden, S.C., Lekien, F. and Marsden, J.E. (2005) 'Definition and properties of Lagrangian coherent structures from finite-time Lyapunov exponents in two-dimensional aperiodic flows', *Physica D: Nonlinear Phenomena*, 212(3), pp. 271-304.

Shadden, S.C., Lekien, F., Paduan, J.D., Chavez, F.P. and Marsden, J.E. (2009) 'The correlation between surface drifters and coherent structures based on high-frequency radar data in Monterey Bay', *Deep Sea Research Part II: Topical Studies in Oceanography*, 56(3), pp. 161-172.

Shore, J.A. (2009) 'Modelling the circulation and exchange of Kingston Basin and Lake Ontario with FVCOM', *Ocean Modelling*, 30(2), pp. 106-114.

Shrestha, P.L. (1996) 'An integrated model suite for sediment and pollutant transport in shallow lakes', *Advances in Engineering Software*, 27(3), pp. 201-212.

Simons, R.D., Siegel, D.A. and Brown, K.S. (2013) 'Model sensitivity and robustness in the estimation of larval transport: A study of particle tracking parameters', *Journal of Marine Systems*, 119, pp. 19-29.

Smith, S.D. (1988) 'Coefficients for sea surface wind stress, heat flux, and wind profiles as a function of wind speed and temperature', *Journal of Geophysical Research: Oceans*, 93(C12), pp. 15467-15472.

Solomon, T.H., Weeks, E.R. and Swinney, H.L. (1994) 'Chaotic advection in a two-dimensional flow: Lévy flights and anomalous diffusion', *Physica D: Nonlinear Phenomena*, 76(1), pp. 70-84.

Song, Y., Semazzi, F.H.M., Xie, L. and Ogallo, L.J. (2004) 'A coupled regional climate model for the Lake Victoria basin of East Africa', *International Journal of Climatology*, 24(1), pp. 57-75.

Song, Z.Y., Li, R.J. and Xue, H.C. (2003) 'A Quasi-3D Numerical Simulation of Storm surge Currents in Taihu Lake', *Transactions of Oceanology and Limnology*, (1; NUMB 95), pp. 7-12.

Soomere, T., Andrejev, O., Myrberg, K. and Sokolov, A. (2011) 'The use of Lagrangian trajectories for the identification of the environmentally safe fairways', *Marine pollution bulletin*, 62(7), pp. 1410-1420.

- Spaulding, M.L. and Mendelsohn, D.L. (1999) 'WQMAP: An integrated three-dimensional hydrodynamic and water quality model system for estuarine and coastal applications', *Marine Technology Society Journal*, 33(3), pp. 38-54.
- Steinebach, G., Rademacher, S., Rentrop, P. and Schulz, M. (2004) 'Mechanisms of coupling in river flow simulation systems', *Journal of Computational and Applied Mathematics*, 168(1), pp. 459-470.
- Swanson, P.D. and Ottino, J.M. (1990) 'A comparative computational and experimental study of chaotic mixing of viscous fluids', *Journal of Fluid Mechanics*, 213, pp. 227-249.
- Tallapragada, P., Ross, S.D. and Schmale Iii, D.G. (2011) 'Lagrangian coherent structures are associated with fluctuations in airborne microbial populations', *Chaos: An Interdisciplinary Journal of Nonlinear Science*, 21(3), p. 033122.
- Tang, L., Wang, P. and Yao, Q. (2011a) 'Three-dimensional numerical simulation of current, waves and sediment transport in Taihu Lake [J]', *Water Resources Protection*, 27(2), pp. 1-5.
- Tang, W., Chan, P.W. and Haller, G. (2011b) 'Lagrangian coherent structure analysis of terminal winds detected by lidar. Part I: Turbulence structures', *Journal of Applied Meteorology and Climatology*, 50(2), pp. 325-338.
- Thompson, A., Guo, Y. and Moin, S. (2008) 'Uncertainty analysis of a two-dimensional hydrodynamic model', *Journal of Great Lakes Research*, 34(3), pp. 472-484.
- Thygesen, U.H. (2011) 'How to reverse time in stochastic particle tracking models', *Journal of Marine Systems*, 88(2), pp. 159-168.
- Toro, E.F. (2001) *Shock-capturing methods for free-surface shallow flows*. Wiley.
- Tsanis, I.K. and Saied, U. (2007) 'A wind-driven hydrodynamic and pollutant transport model', *Global nest. The international journal*, 9(2), pp. 117-131.
- Twigt, D.J., De Goede, E.D., Zijl, F., Schwanenberg, D. and Chiu, A.Y.W. (2009) 'Coupled 1D–3D hydrodynamic modelling, with application to the Pearl River Delta', *Ocean Dynamics*, 59(6), p. 1077.
- Van, C.P., de Brye, B., Deleersnijder, E., Hoitink, A.J.F., Sassi, M., Spinewine, B., Hidayat, H. and Soares-Frazaõ, S. (2016) 'Simulations of the flow in the Mahakam river–lake–delta system, Indonesia', *Environmental Fluid Mechanics*, 16(3), pp. 603-633.
- Visser, A.W. (1997) 'Using random walk models to simulate the vertical distribution of particles in a turbulent water column', *Marine Ecology Progress Series*, 158, pp. 275-281.
- Voth, G.A., Haller, G. and Gollub, J.P. (2002) 'Experimental measurements of stretching fields in fluid mixing', *Physical review letters*, 88(25), p. 254501.
- Voth, G.A. and Saint, T.C. (2003) 'mixing rates and symmetry breaking in 2D chaotic flow', *Physics of fluids*, 15.
- Wang, H.Z., Song, Z.R. and Xue, H.C. (2001) 'A Quasi-3D numerical model of Wind-Driven current in Taihu Lake considering the variation of vertical coefficient of Eddy Viscosity', *Journal of lake Sciences*, 13(3).

- Wang, J., Shen, Y. and Guo, Y. (2010) 'Seasonal circulation and influence factors of the Bohai Sea: a numerical study based on Lagrangian particle tracking method', *Ocean dynamics*, 60(6), pp. 1581-1596.
- Wang, Q.Q. (1987) 'A numerical simulation of wind-driven circulation in Taihu Lake', *Journal of Hohai University*, 15(suppl 2), pp. 11-17.
- Wang, Q.Q., Jiang, J.H. and Pu, P.M. (1992) 'Numerical simulations and their verifications with one station data of wind-driven surge and currents in Taihu Lake', *Journal of Lake Sciences*, 4, pp. 1-7.
- Wang, Z.-Y., Chen, Y.-c., Zhu, D.-j. and Liu, Z.-w. (2011) '1 D-2 D coupled hydrodynamic simulation model of river-lake system', *Advances in Water Science*, 22(4), pp. 516-522.
- Weiping, H., Jørgensen, S.E., Fabing, Z., Yonggen, C., Zhixin, H. and Longyuan, Y. (2011) 'A model on the carbon cycling in Lake Taihu, China', *Ecological modelling*, 222(16), pp. 2973-2991.
- Weitbrecht, V., Uijttewaal, W. and Jirka, G.H. (2004) '2-D particle tracking to determine transport characteristics in rivers with dead zones', *Shallow flows*, pp. 477-484.
- Wiggins, S. (1992) *Chaotic Transport in Dynamical Systems*, Springer, New York.
- Wiggins, S. (2013a) *Chaotic transport in dynamical systems*. Springer Science & Business Media.
- Wiggins, S. (2013b) *Normally hyperbolic invariant manifolds in dynamical systems*. Springer Science & Business Media.
- Wilcox, D.C. (1998) *Turbulence modeling for CFD*. DCW industries La Canada, CA.
- Willis, J. (2011) 'Modelling swimming aquatic animals in hydrodynamic models', *Ecological Modelling*, 222(23), pp. 3869-3887.
- Wu, J. and Pu, P.M. (1989) 'Numerical simulations of the hydrodynamics of Taihu Lake by using the irregular-grid finite difference model', *Memoirs of Nanjing Institute of Geography and Limnology Academia Sinica. Beijing, Science Press*, pp. 1-13.
- Xu, H., Paerl, H.W., Qin, B., Zhu, G. and Gao, G. (2010) 'Nitrogen and phosphorus inputs control phytoplankton growth in eutrophic Lake Taihu, China', *Limnology and Oceanography*, 55(1), p. 420.
- Xu, X. and Liu, Q. (2009) 'Numerical study on the characteristics of wind-induced current in Taihu Lake', *Chinese Journal of Hydrodynamics*, 24(4), pp. 512-518.
- Zhai, S., Hu, W. and Zhu, Z. (2010) 'Ecological impacts of water transfers on Lake Taihu from the Yangtze River, China', *Ecological Engineering*, 36(4), pp. 406-420.
- Zhou, J., Zeng, C. and Wang, L. (2009) 'Influence of wind drag coefficient on wind-driven flow simulation', *Journal of Hydrodynamics (Ser. A)*, 4, p. 009.
- Zhu, G. (2008) 'Eutrophic status and causing factors for a large, shallow and subtropical Lake Taihu, China', *Journal of Lake Sciences*, 1, p. 005.

Zhu, G., Wang, F., Gao, G. and Zhang, Y. (2008) 'Variability of phosphorus concentration in large, shallow and eutrophic Lake Taihu, China', *Water Environment Research*, 80(9), pp. 832-839.

Zhu, S., Shi, F., Zhu, J. and Ding, P. (2001) 'Numerical study on residual current and its impact on mass transport in the Hangzhou Bay and the Changjiang Estuary. I. A 3-D joint model of the Hangzhou Bay and the Changjiang Estuary', *Acta oceanologica sinica*, 20(1), pp. 1-13.

Zhu, Y.C. and Cai, Q.M. (1998a) 'Studies on the three-dimensional hydrodynamic model for Meliang Bay, Taihu II. The Diffusion of Nutrient Salt Under the Action of Three-Dimensional Currents', *Oceanol. Limnol. Sin.*, 2, p. 008.

Zhu, Y.C. and Cai, Q.M. (1998b) 'Studies on the three-dimensional hydrodynamic model for Meliang Bay, Taihu, Model description and results interpretation', *Oceanol. Limnol. Sin.*, 29(1), pp. 169-174.